

Synthetic Receptors Based on Hydrogen-Bonded Assemblies

Jessica M.C.A. Kerckhoffs

2003

Ph.D. thesis
University of Twente



Twente University Press

Also available in print:
<http://www.tup.utwente.nl/>

**SYNTHETIC RECEPTORS BASED
ON HYDROGEN-BONDED ASSEMBLIES**



This research was supported by the Technology Foundation STW, applied science division of NWO and the technology program of the Ministry of Economic Affairs, grant number TST 4624.



Twente University **Press**

Publisher:

Twente University Press, P.O. Box 217, 7500 AE Enschede, The Netherlands

www.tup.utwente.nl

Print: Océ Facility Services, Enschede

© J.M.C.A. Kerckhoffs, Enschede, 2003

No part of this work may be reproduced by print, photocopy or any other means without the permission in writing from the publisher.

ISBN 90-365-1894-6

SYNTHETIC RECEPTORS BASED ON HYDROGEN-BONDED ASSEMBLIES

PROEFSCHRIFT

ter verkrijging van
de graad van doctor aan de Universiteit Twente,
op gezag van de rector magnificus,
prof. dr. F.A. van Vught,
volgens besluit van het College voor Promoties
in het openbaar te verdedigen
op vrijdag 11 april 2003 te 13.15 uur

door

Jessica Maria Catharina Antonia Kerckhoffs

geboren op 13 december 1974
te Breda

Dit proefschrift is goedgekeurd door:

Promotor Prof. dr. ir. D.N. Reinhoudt

Assistent-promotor Dr. M. Crego-Calama

Contents

Chapter 1

General Introduction	1
-----------------------------------	----------

Chapter 2

Synthesis of Artificial Receptors	5
2.1 Nature as an Inspiration: Antibodies.....	6
2.2 Covalent Artificial Receptors.....	7
2.3 Self-Assembled Artificial Receptors.....	11
2.3.1 Metal Coordination and Ionic Interactions.....	12
2.3.2 Hydrogen-Bonded Assemblies.....	14
2.3.2.1 Rosettes.....	16
2.4 Combinatorial Chemistry for the Preparation of Artificial Receptors.....	19
2.4.1 “Classical” Combinatorial Chemistry.....	20
2.4.2 Dynamic Combinatorial Chemistry.....	23
2.4.2.1 DCC with Receptors Based on Reversible Covalent Interactions.....	26
2.4.2.2 DCC with Receptors Based on Noncovalent Interactions.....	30
2.5 Conclusions and Outlook.....	34
2.6 References.....	35

Chapter 3

Self-Assembly of Polar Functionalities using Hydrogen-Bonded Rosette

Assemblies	47
3.1 Introduction.....	48
3.2 Formation of Double Rosette Assemblies.....	49
3.3 Characterization of Double Rosette Assemblies.....	51
3.4 Results and Discussion.....	52
3.4.1 Functionalization of Double Rosette Assemblies.....	52
3.4.2 Synthesis and Characterization of the Assemblies with Polar Functionalities.....	53
3.4.3 Thermodynamic Stability.....	55

3.5 Conclusions.....	60
3.6 Experimental Section.....	61
3.7 References.....	66

Chapter 4

Self-Assembly of Amino Acid and Peptide Functions on a Noncovalent Platform...69

4.1 Introduction.....	70
4.2 Results and Discussion.....	71
4.2.1 Single Amino Acid Functionalized Calix[4]arene Dimelamines 2	71
4.2.2 Formation and Stability of Assemblies of Amino Acid Functionalized Calix[4]arene Dimelamines 3 and 4	74
4.2.2.1 Synthesis and Characterization of Double Rosette Assemblies.....	75
4.2.2.2 Chiral Induction and Thermodynamic Stability.....	80
4.2.3 Peptide Functionalized Calix[4]arene Dimelamines 5	83
4.3 Conclusions.....	86
4.4 Experimental Section.....	87
4.5 References.....	109
Appendix.....	111

Chapter 5

Complexation of Phenolic Guests by *Endo*- and *Exo*-Hydrogen-Bonded

Receptors.....	113
5.1 Introduction.....	114
5.2 Results and Discussion.....	115
5.2.1 Synthesis of Double- and Tetra-rosette Assemblies.....	116
5.2.2 Complexation Studies with <i>Exo</i> -Receptors.....	117
5.2.3 Complexation Studies with <i>Endo</i> -Receptors.....	123
5.2.4 Selectivity Studies with <i>Exo</i> - and <i>Endo</i> -Receptors.....	128
5.3 Conclusions.....	131
5.4 Experimental Section.....	132
5.5 References.....	133
Appendix.....	139

Chapter 6

Self-Organization of Guest Molecules in Self-Assembled Capsules: Artificial

Viruses.....	141
6.1 Introduction.....	142
6.2 Results and Discussion.....	143
6.2.1 Synthesis and Formation of Double Rosette Assembly.....	143
6.2.2 Encapsulation of Alizarin (2a) by $1\mathbf{a}_3\bullet(\text{DEB})_6$	144
6.2.3 Symmetry of the Complex $1\mathbf{a}_3\bullet(\text{DEB})_6\bullet 2\mathbf{a}_3$	147
6.2.4 Detailed Studies on the Encapsulation of Alizarin (2a) by $1\mathbf{a}_3\bullet(\text{DEB})_6$	152
6.2.5 Selectivity Studies with Receptor $1\mathbf{a}_3\bullet(\text{DEB})_6$	155
6.2.6 Stability Studies with Complex $1\mathbf{a}_3\bullet(\text{DEB})_6\bullet 2\mathbf{a}_3$	157
6.2.7 X-Ray Crystal Structure of $1\mathbf{a}_3\bullet(\text{DEB})_6\bullet 2\mathbf{a}_3$	158
6.2.8 Release of Alizarin (2a) from the Complex $1\mathbf{a}_3\bullet(\text{DEB})_6\bullet 2\mathbf{a}_3$	159
6.2.9 Encapsulation of Alizarin (2a) by TetraRosette $4_3\bullet(\text{DEB})_{12}$	161
6.3 Conclusions.....	164
6.4 Experimental Section.....	164
6.5 References.....	167

Chapter 7

Towards Artificial Antibodies: Small Dynamic Combinatorial Libraries.....169

7.1 Introduction.....	170
7.2 Results and Discussion.....	171
7.2.1 Small Dynamic Combinatorial Libraries of Hydrogen-Bonded Receptors...171	
7.2.1.1 Dynamic Libraries from Functionalized Double Rosettes.....	173
7.2.1.2 Selective Noncovalent Synthesis by Receptor $1\mathbf{a}_3\bullet(\text{DEB})_6$ in a “Virtual Library” of Self-Assembled Guest Trimers 2_3	186
7.2.2 Complexation of Alizarin 2a by Chiral Assemblies $R\text{-}3\mathbf{a}_3\bullet(\text{DEB})_6$ and $S\text{-}3\mathbf{b}_3\bullet(\text{DEB})_6$	189
7.2.1.1 Dynamic Libraries from Chiral Rosettes $R\text{-}3\mathbf{a}_3\bullet(\text{DEB})_6$ and $S\text{-}3\mathbf{b}_3\bullet(\text{DEB})_6$	196
7.3 Conclusions and Outlook.....	197
7.4 Experimental Section.....	198
7.5 References.....	200

Summary.....	203
Samenvatting.....	207
Dankwoord.....	211
Curriculum Vitae.....	215

Chapter 1

General Introduction

Biological systems generate and modify their structures with startling efficiency. Natural receptors such as antibodies provide the perfect example, with four different peptidic chains (two heavy (H) and two light (L) chains) that are held together mainly by noncovalent interactions, reinforced by covalent disulfide bonds.¹ An assortment of the heavy and light chains and random genetic recombinant processes select the best antibody for the recognition of a particular antigen.

Recognition studies with synthetic molecules were pioneered by Pedersen,² Cram³, and Lehn⁴ in the early 1970s, for which they were awarded the Nobel Prize in 1987. This chemistry of intermolecular binding was coined by Lehn⁴ as *Supramolecular Chemistry*. Initially, supramolecular chemistry⁵ only dealt with the synthesis of artificial receptors for cations, anions, and small molecules. The recognition of the small guests relied on more or less preorganized molecular receptors. One step further was the design of assemblies that undergo self-organization by the self-assembly of their components.⁶ Only recently,⁷ the combination of self-assembly and molecular recognition led to the *noncovalent* synthesis of receptor molecules, i.e. aggregates prepared by self-assembly that recognize other guest molecules. Typical examples are the hydrogen-bonded capsules reported by Rebek,⁸ the molecular boxes of Fujita,⁹ and the rosettes developed by Reinhoudt.¹⁰

Nowadays, the strategy in supramolecular chemistry is changing from rational design to combinatorial chemistry, which is similar to the “trial-and-error” approach that nature uses for the synthesis of antibodies. Combinatorial chemistry, first reported in the early 1980s,¹¹ is the science of concurrently synthesizing and testing new substances in large numbers rather than sequentially, resulting in faster discovery of interesting lead molecules for varied purposes such as receptors, drugs and catalysts. These libraries consist

of large, static collections of discrete molecules synthesized by the methodologies of molecular chemistry.¹²

Recently, the combination of combinatorial and supramolecular chemistry has led to the new research field of dynamic combinatorial chemistry.¹³ This chemistry is based on two main themes, *viz.* *self-assembly* in the preparation of the library members and *molecular recognition* in the interaction of these members with the target molecule.¹⁴ The library is referred to as dynamic, because its components are formed by the reversible combination (*covalent* or *noncovalent*) of building blocks under thermodynamic control.

Thus, taking advantage of the acquired knowledge through the last 25-30 years in the field of supramolecular chemistry and with antibodies as a source of inspiration, the research described in this thesis aims at the generation of dynamic combinatorial libraries of self-assembled receptors held together by hydrogen bonds.

Chapter 2 starts with a brief literature overview about the covalent and noncovalent synthesis of artificial receptors using a rational design approach. The last part of this chapter reviews the synthesis of artificial receptor molecules using “classical” (static) and dynamic combinatorial chemistry.

Chapters 3 and 4 deal with the introduction of polar functionalities such as amides, ureas, and amino acids (short peptides) on hydrogen-bonded platforms. The thermodynamic stability of these hydrogen-bonded assemblies is studied in detail.

Chapter 5 describes the complexation of small phenol derivatives by self-assembled receptors. These hydrogen-bonded assemblies function as *endo*- and *exo*-receptors, depending on the position of the binding sites, which can be oriented towards the interior or the exterior of the assembly, respectively.

Chapter 6 reports on the highly organized encapsulation of a hydrogen-bonded trimer by a self-assembled receptor. The structure of the complex is studied by ¹H NMR spectroscopy and is confirmed by X-ray crystallography.

Finally, Chapter 7 describes the generation of small dynamic combinatorial libraries based on hydrogen-bonded assemblies. The amplification of the concentration of the best binder in the dynamic library upon addition of a guest molecule is studied in detail by ¹H NMR spectroscopy.

References

- ¹ Benjami, E.; Sunshine, G.; Leskowitz, S. *Immunology, A Short Course*, 3rd ed. Wiley, New York, **1996**.
- ² Pedersen, C.-J. *Angew. Chem. Int. Ed. Engl.* **1988**, *27*, 1021-1027.
- ³ Cram, D.J. *Angew. Chem. Int. Ed. Engl.* **1988**, *27*, 1009-1020.
- ⁴ Lehn, J.-M. *Angew. Chem. Int. Ed. Engl.* **1988**, *27*, 89-112.
- ⁵ a) Lehn, J.-M. *Supramolecular Chemistry: Concepts and Perspectives*, VCH, Weinheim, **1995**; b) Atwood, J.L.; Davies, J.E.D.; MacNicol, D.D.; Vögtle, F. *Comprehensive Supramolecular Chemistry, Vol 1,10*, Pergamon, Oxford, **1996**; c) Schneider, H.-J.; Yatsimirsky, A. *Principles and Methods in Supramolecular Chemistry*, Wiley, Chichester, **2000**.
- ⁶ Lehn, J.-M. *Angew. Chem. Int. Ed. Engl.* **1990**, *29*, 1304-1319.
- ⁷ Philp, D.; Stoddart, J.F. *Angew. Chem. Int. Ed. Engl.* **1996**, *35*, 1154-1196.
- ⁸ Heinz, T.; Rudkevich, D.M.; Rebek Jr., J. *Nature* **1998**, *394*, 764-766.
- ⁹ Takeda, N.; Umemoto, K.; Yamaguchi, K.; Fujita, M. *Nature* **1999**, *398*, 794-799.
- ¹⁰ Vreekamp, R.H.; van Duynhoven, J.P.M.; Hubert, M.; Reinhoudt, D.N. *Angew. Chem. Int. Ed. Engl.* **1996**, *35*, 1215-1218.
- ¹¹ Furka, A. Notarised report No. 36237, Hungary, **1982** on *Studies on Possibilities of Systematic Searching for Pharmaceutically Useful Peptides*.
- ¹² a) Gordon, E.M.; Barrett, R.W.; Dower, W.J.; Fodor, S.P.A.; Gallop, M.A. *J. Med. Chem.* **1994**, *37*, 1385-1401; b) Terrett, N.K.; Gardner, M.; Gordon, D.W.; Kobylecki, R.J.; Steele, J. *Tetrahedron* **1995**, *51*, 8135-8173; c) Balkenhohl, F.; von dem Bussche-Hünnefeld, C.; Lansky, A.; Zechel, C. *Angew. Chem. Int. Ed. Engl.* **1996**, *35*, 2288-2337; d) Ganesan, *Drug Discovery Today* **2002**, *7*, 47-55.
- ¹³ a) Ramström, O.; Lehn, J.-M. *Nature Reviews, Drug Discovery*, **2002**, *1*, 26-36; b) Rowan, S.J.; Cantrill, S.J.; Cousins, G.R.L.; Sanders, J.K.M.; Stoddart, J.F. *Angew. Chem. Int. Ed.* **2002**, *41*, 898-952; c) Otto, S.; Furlan, R.L.E.; Sanders, J.K.M. *Curr. Opin. Chem. Biol.* **2002**, *6*, 321-327; d) Lehn, J.-M.; Eliseev, A.E. *Science* **2001**, *291*, 2331-2332.
- ¹⁴ Lehn, J.-M. *Chem. Eur. J.* **1999**, *5*, 2455-2463.

Chapter 2

Synthesis of Artificial Receptors

A brief literature overview is given about the different aspects and developments in the field of covalent and noncovalent artificial receptors. Examples of the most representative covalently synthesized receptor molecules, such as calix[4]arenes, crown ethers, and molecular tweezers, are described. The description of the synthesis of noncovalent receptors by various interactions, such as metal coordination, ionic interactions, and especially hydrogen bonds are explained in more detail; prominent attention is given to the rosette motif. Furthermore, some general features of the “classical” and dynamic combinatorial libraries for the preparation of artificial receptors are reported, with special attention for peptidic libraries. In “classical” combinatorial chemistry, libraries are synthesized via non-reversible covalent synthesis, and are therefore static. In contrast, dynamic combinatorial libraries are synthesized by reversible covalent or noncovalent synthesis. The main advantage of the dynamic combinatorial libraries over the “classical” combinatorial libraries is the templation ability of the added guest.

2.1 Nature as an Inspiration: Antibodies

One of the most fascinating groups of natural receptors are the antibodies, which are proteins formed in response to immunization. They are characterized by their extraordinarily high binding affinity and selectivity for a target molecule known as an antigen.¹ These qualities make the antibodies a great inspiration for the generation of artificial receptors by the simple combination of different building blocks able to adjust the appropriate binding sites around the guest molecules.

The analysis of the structure of the antibody molecules began in 1959. Porter² found that the immunoglobulin molecule (the antibody) consists of three fragments of about equal size. Two fragments are referred to as Fab (fragment antigen binding) fragments and a third fragment is called Fc (fragment-crystallizable). The Fab fragments both possess one individual binding site. The Fc fragment is responsible for the biological functions of the antibody molecule after the antigen has been bound to the Fab part of the molecule. At the same time Edelman³ discovered that by treatment with mercaptoethanol (a reagent that breaks S-S bonds) the antibody fell apart into four chains; two identical light (L) chains and two identical heavy (H) chains. These four polypeptide chains are held together by a number of disulfide bonds (schematic representation, Figure 2.1). Each antibody molecule has two identical binding sites.

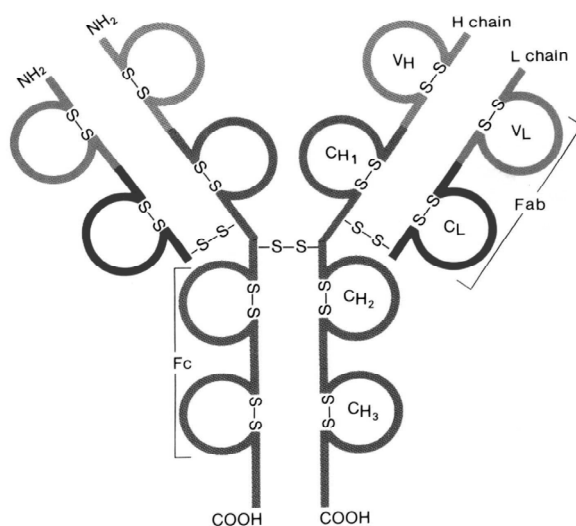


Figure 2.1. Schematic representation of an antibody.⁴

The diversity in the antibody is obtained by, among other things, random genetic recombinant processes which generate variation in the monomer sequence of the polypeptide chains (built from the set of 20 natural amino acids) and by the random assortment of the heavy and the light chains. Due to these diversity generation processes an almost unlimited number of different antibodies can be produced. Subsequent screening for a particular antigen binding affinity selects the best binding receptors from all the possible receptors, and further optimization over several cycles finally produces the best binder.

In the interaction between the antibody and the antigen there are no covalent bonds involved. The most important interactions are van der Waals forces, electrostatic forces and hydrophobic forces.

2.2 Covalent Artificial Receptors⁵

In general, the term host describes the ability of a molecular species to bind a guest with preference over all others and with greater strength than commonly found as the result of unspecific molecular interactions.⁶ Cram's "preorganization"⁷ is often used as a model to define structural features associated with an effective receptor, i.e. the substrate has to fit both sterically and electronically, and the thermodynamic driving force for the binding should be appropriate for the solvent used.

Different host classifications can be made, for example based on their type of interaction, i.e. hydrogen bonding, π - π interaction, solvophobic and electrostatic interaction of the host and the guest. In this section the classification of covalently synthesized receptor molecules is based on similarities in the shape (geometry) of the host that is involved in the interaction with the guest molecule or the scaffold used to bring the functional groups together.

Cyclodextrins⁸ were the first molecules that were recognized and studied for the purpose of binding organic molecules. They are cyclic oligosaccharides consisting of α -1,4-linked D-(+)-glucopyranose units. The hydrophobic cavity of the cyclodextrins makes them particularly good hosts for hydrophobic organic molecules in water.

A second class studied intensively are the crown ethers. Crown ethers are used as receptors for cations, anions, and neutral species.⁹ The complexation of ammonium containing guest molecules within crown ethers has been studied extensively.¹⁰ Schneider

et al.¹¹ reported the synthesis of an artificial receptor containing an 18-crown-6 ether and a peralkylammonium group for binding of the peptide *N*- and *C*-terminus, respectively. A length-selectivity for the recognition of the peptides was observed.

Another class of molecules studied widely are the calix[*n*]arenes.¹² These molecules are synthesized by condensation of phenols and aldehydes and exhibit enhanced cation- π interactions due to the preorganization of their core of aromatic units. For example, Ungaro *et al.*¹³ reported the selective recognition of *N,N,N*-trimethylanilinium (TMA), benzyltrimethylammonium (BTMA), and *p*-nitro-benzyltrimethylammonium (BTMAN) cations by conformationally (cone) immobilized calix[4]arene **1a** and **1b** (Figure 2.2). Calix[4]arene **1a** selectively binds TMA by its $N(\text{CH}_3)_3$ group, while calix[4]arene **1b** includes TMA by its aromatic ring. Receptor **1a** also binds BTMA and BTMAN by their $N(\text{CH}_3)_3$ groups. Receptor **1b**, however, selectively binds BTMAN via its $N(\text{CH}_3)_3$ group, while no binding selectivity is observed for BTMA. In addition to the recognition of cations,¹⁴ the calix[*n*]arenes are also used in the recognition of anions¹⁵ and neutral molecules.¹⁶

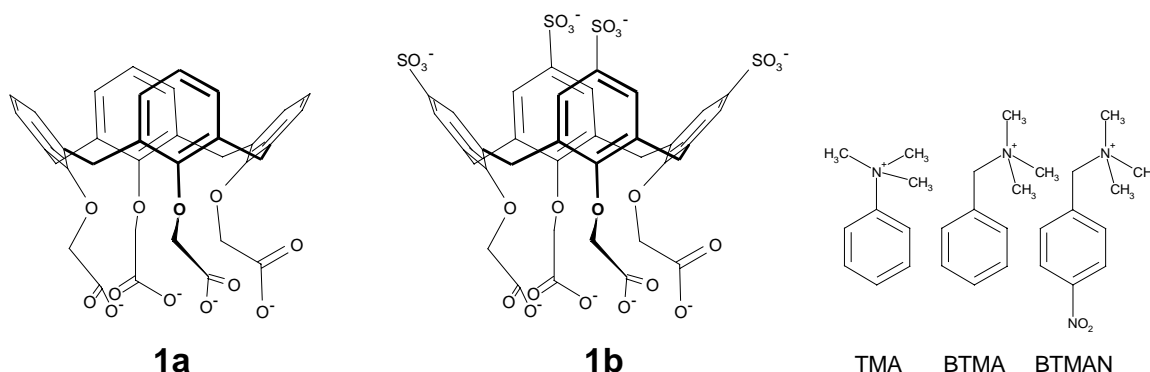


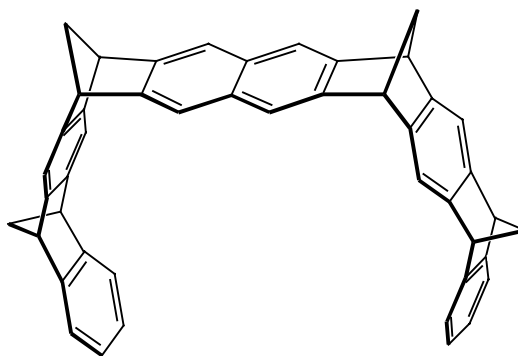
Figure 2.2. Calix[4]arene **1a** and **1b** used for the selective recognition of tetraalkylammonium ions TMA, BTMA, and BTMAN.

Ungaro and Reinhoudt¹⁷ synthesized another receptor molecule that is based on calix[*n*]arenes but combined this recognition group with a second function *viz.* crown ethers. They reported the complexation of various alkali picrates by 1,3-*alternate* calix[4]arenecrown-5 conformers. A $\log K_a$ of 9.83 for K^+ in CHCl_3 saturated with H_2O at 295 K was obtained. The observed K^+ / Na^+ selectivity was higher than that observed for valinomycin (active natural compound used to obtain K^+ / Na^+ selectivity).

Molecular tweezers are also used as host molecules. In the beginning, the term molecular tweezers referred to molecules that could complex guests by π -sandwiching.¹⁸

Nowadays, also molecules containing a "headgroup" or "hinge" bearing two side arms which provide binding interactions with the guest are referred to as tweezers.¹⁹ Klärner *et al.*²⁰ reported the binding of electron-deficient aromatic and aliphatic substrates, such as 1,4-dinitrobenzene and *p*-benzoquinone, by molecular tweezers such as **2** (Figure 2.3). Shinkai and co-workers²¹ constructed a highly selective "sugar tweezer" which has μ -oxobis[porphyrinatoiron(III)] as a basic platform and boronic acids as sugar-binding sites. A binding constant of $1.5 \times 10^5 \text{ M}^{-1}$ for glucose in water was obtained.

Similar host molecules are the clefts and clips. Nolte and co-workers²² studied the complexation of dihydroxybenzene derivatives by propanediurea-based molecular clips. A binding constant of $2.4 \times 10^6 \text{ M}^{-1}$ was found for 5-cyanoresorcinol.



2

Figure 2.3. Example of molecular tweezer used for complexation of electron-deficient aromatic guests.

Molecular containers²³ are host molecules that are characterized by the ability to completely encapsulate guest molecules. For example, hemicarcerands²⁴ encase and liberate guests at elevated temperatures but form stable hemicarceplexes at ambient temperature. Sherman and co-workers²⁵ studied the template effect (of guest molecules) on the formation of a tetramethylene-bridged hemicarceplex. Other examples of container molecules are cryptands,²⁶ cryptophanes,²⁷ and carceplexes (complexes that bind their guests irreversibly).²⁸

In addition to the classification based on shape, another way to classify receptor molecules is based on the generic type of guests that are complexed. Due to the importance of amino acids and peptides for the objective of the research described in this thesis, only receptors that complex these guests are presented. A large number of receptor

molecules for amino acids and peptides have been developed.²⁹ Kilburn et al.³⁰ reported the acyclic thiourea derivative **3** (Figure 2.4), which is capable of binding *N*-protected amino acid carboxylate salts. A good discrimination between the different amino acids was observed (*e.g.* >30:1 selectivity for *N*-Ac-*L*-Trp-CO₂⁻ over *N*-Ac-*L*-Ser-CO₂⁻), but only a moderate enantioselectivity was seen, with a general preference for *L*-amino acids.

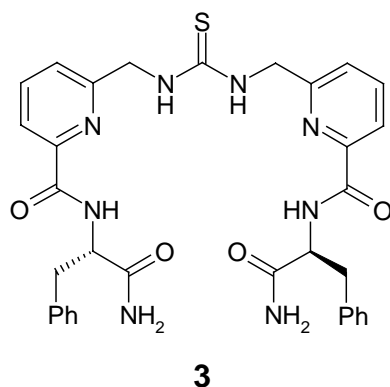


Figure 2.4. Acyclic thiourea derivative **3** for the binding of *N*-protected amino acid carboxylate salts.

Still and co-workers³¹ reported the synthesis of receptor **4** (Figure 2.5). Selectivity of this receptor for amides of *L*-valine and *L*-phenylglycine, based on the steric requirements of their sidechains, was reported. Furthermore an enantioselectivity of 99 % for *L*-amino acids was observed.

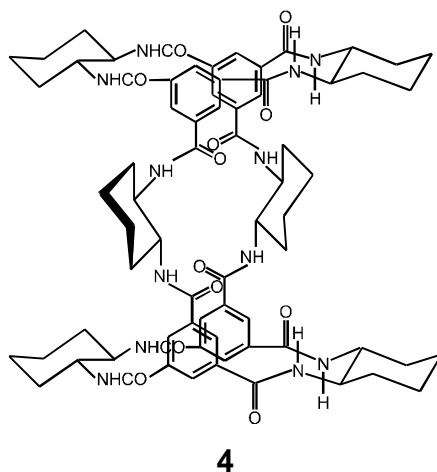


Figure 2.5. Synthetic receptor **4** for the recognition of amino acids and peptides designed by Still et al.

In the search for receptor molecules that bind a particular peptide sequence, glycopeptide antibiotics were investigated intensively.³² The antibacterial activity of glycopeptide antibiotics of the vancomycin group (Figure 2.6a) probably results mainly

from the binding to a *D*-Ala-*D*-Ala unit located at the terminus of the bacterial cell wall precursor, resulting in inhibition of the cell wall growth, and finally to lysis. Due to resistance of bacteria against this class of antibiotics, synthetic analogues are needed.³³ Calix[4]arenes bridged across the upper rim with diethylenetriamine connected via amides in the cone conformation, such as **5** (Figure 2.6), showed an antimicrobial activity only slightly inferior to vancomycin.³⁴ A $\log K_a$ significantly higher than 4.0 was estimated for the binding of *N*-acetyl-*D*-Ala-*D*-Ala to **5** in chloroform.³⁵ Many other vancomycin mimics and analogues have also been reported (see also Section 2.4.1).³⁶

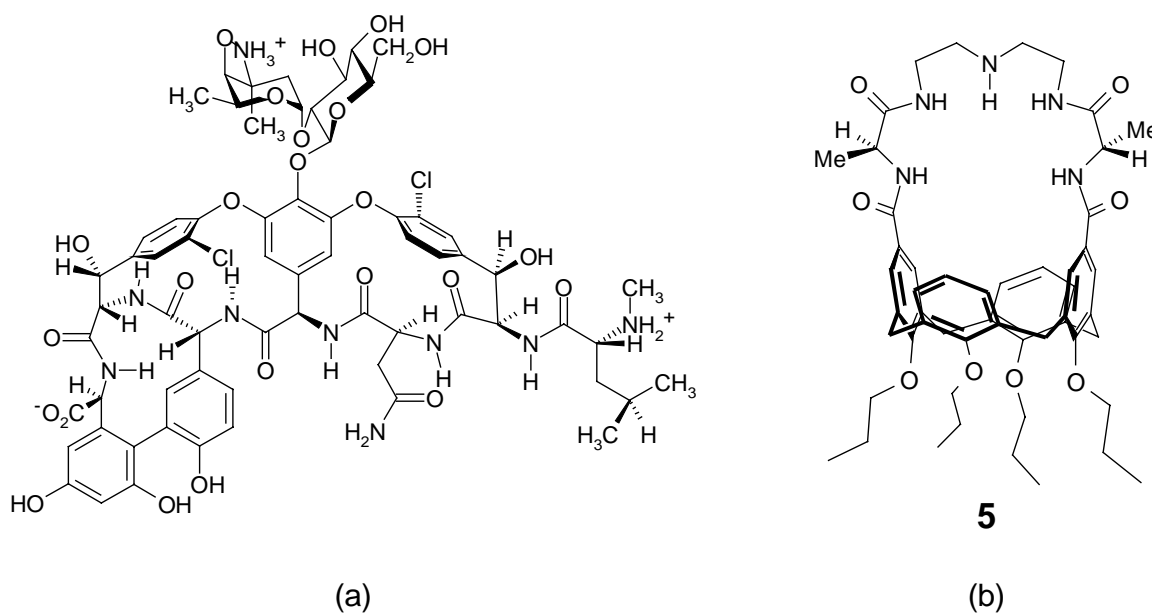


Figure 2.6. (a) Chemical structure of vancomycin and (b) upper rim bridged calix[4]arene **5**.

2.3 Self-Assembled Artificial Receptors

Until a number of years ago, artificial receptor molecules were only synthesized by a *covalent* approach. Although this approach has led to the synthesis of impressive chemical structures, as has been shown in the previous section, it has severe limitations in terms of time requirements and product yields.³⁷ The *noncovalent* approach, in which nanoscale self-assembled aggregates are formed under thermodynamically controlled conditions, is an attractive alternative for the synthesis of artificial receptor molecules. The main differences between covalent and noncovalent synthesis are summarized in Table 2.1.

Table 2.1. Main differences between noncovalent and covalent synthesis.

Characteristics	Noncovalent	Covalent
Building block	Molecule	Atom
Target	Assembly	Molecule
Bond type	Metal coordination, ionic, hydrophobic, hydrogen bond	Covalent
Bond energy	2 – 20 kcal/mol	35 – 135 kcal/mol
ΔG° assembly/ molecule	$\Delta H^\circ \sim T\Delta S^\circ$	$\Delta H^\circ \gg T\Delta S^\circ$
Kinetic stability	Low (dynamic structures)	High

Table 2.1 shows the different types of interactions that can be used for the self-assembly of molecular receptors. The most important are metal coordination, hydrogen bonding, and ionic and hydrophobic interactions.³⁸ The potential of self-assembly for the preparation of supramolecular receptors depends on the identification of noncovalent structural motifs whose enthalpic driving force for self-assembly is sufficient to overcome the unfavorable entropic consequences associated with the aggregation of several components into a single supramolecular entity.³⁷

2.3.1 Metal Coordination and Ionic Interactions

In general, metal coordination can be used to assemble flexible ligands around the coordination sphere of a metal ion. There are many examples of supramolecular aggregates built up by metal coordination.³⁹ A typical example is the spontaneous formation of a 2D lattice consisting of 9 pyridylporphyrin units held together by 12 palladium(II) ions.⁴⁰ In this section, only metal coordination used for the noncovalent synthesis of molecular containers is discussed. As already mentioned in Section 2.2, molecular containers or capsules are receptors that completely surround guest molecules.^{23,41} Dalcanale and co-workers⁴² reported the self-assembly of several tetracyano functionalized cavitands (**6**) by transition metals with a square planar coordination, such as Pd(II) and Pt(II) in CH_2Cl_2 , CHCl_3 , and acetone (Figure 2.7). They found that four structural parameters are important for the control of cage self-assembly: (i) an angle close to 90° between the chelating ligand (L-M-L, see Figure 2.7), (ii) the use of Pd or Pt as metal centers, (iii) the use of weakly coordinating counterions, and (iv) preorganization of the tetradentate cavitand ligand.⁴³ The assembly process is entropically

driven; furthermore, selectivity in anion encapsulation for BF_4^- over CF_3SO_3^- and PF_6^- at 300 K was observed.

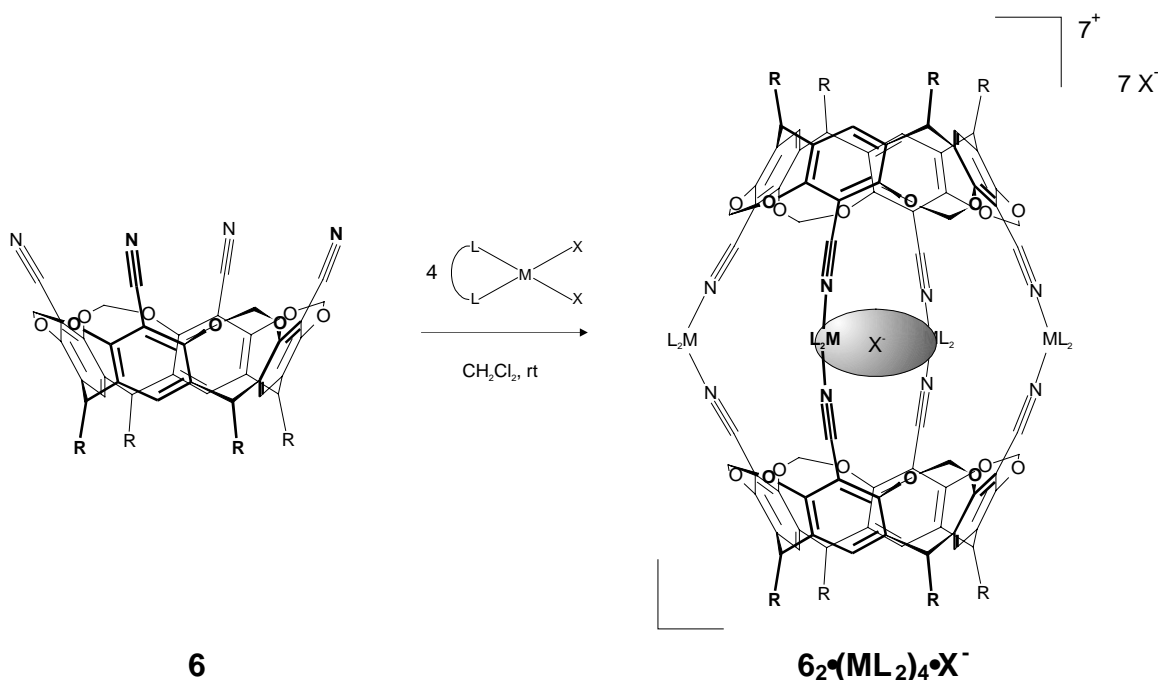


Figure 2.7. Formation of cavitand-based coordination cage 6.

Fujita et al.⁴⁴ showed the formation of a hexahedral coordination capsule by linking planar organic compounds through metal coordination, a concept that is called molecular paneling. The capsule is capable of complexing small guest molecules, such as CBr_4 , CH_2Br_2 , and CHCl_3 by the formation of hydrophobic interactions. Many other examples of capsule formation by metal ions have been reported.⁴⁵

Additionally, ionic interactions can be used to form molecular containers.⁴⁶ Some ionic capsules are able to encapsulate small guest molecules, as was reported by Reinhoudt and co-workers.⁴⁷ The capsule was formed by self-assembly of different tetraamidinium calix[4]arenes and tetrasulfonato calix[4]arene in MeOH/H₂O mixtures. The capsules are capable of binding acetylcholine, tetramethylammonium, and *N*-methylquinuclidinium cations. The same group⁴⁸ has also reported the recognition of 4-methylpyridine and 1-methylimidazole by cage-like assemblies of anionic calix[4]arenes and cationic porphyrins.

2.3.2 Hydrogen-Bonded Assemblies

A large variety of hydrogen bond motifs are described in literature.⁴⁹ Well known are the three sets of hydrogen-bonded base pairs adenine and thymine, adenine and uracil, and guanine and cytosine found in nature (DNA and RNA). Synthetic nucleotide analogues are therefore studied intensively.⁵⁰ Not only “dimers” but also higher oligomers⁵¹ and miscellaneous motifs⁵² have been investigated. One such example is an oligomer arranged in a two-dimensional lattice in which six trimesic (benzene-1,3,5-tricarboxylic) acid units form a cyclic hexamer.⁵³

In this section only hydrogen-bonded assemblies that were prepared for the purpose of complexing guest molecules will be discussed. There are different types of hydrogen-bonded receptors and among them, the ones most studied are capsules.⁵⁴ The capsules found in literature can be divided into different classes (Figure 2.8) as detailed below.

(a) Capsules synthesized from two complementary building blocks; for example two resorcarenes substituted with either four hydroxyl or four carbonyl functionalities.⁵⁵ Rebek and co-workers⁵⁶ reported many examples of this type of hydrogen bond directed capsule formation. Calix[4]arene functionalized with secondary ureas at the upper rim forms a dimeric capsule by the creation of 16 hydrogen bonds in the presence of an appropriate guest molecule.⁵⁷ Different functional groups were connected to the distal urea nitrogen atom.^{54c,58} The calixarene-based capsules containing charged guests were characterized by electrospray ionization mass spectroscopy.⁵⁹ Extended cavities, with calix[4]arenes⁶⁰ and cavitands,⁶¹ have been prepared in a similar way.

(b) The so-called “tennis ball” type of capsules, obtained by the dimerization of two molecules of two glycoluril moieties⁶² connected via a spacer.⁶³

(c) Capsules related to the “tennis ball” type of capsules reported by Rebek et al.,⁶⁴ are formed from four fragments containing both a sulfamide and glycoluril moiety.

(d) Assemblies formed from two equally functionalized building blocks that are connected to each other by “connector” molecules.⁶⁵

Most of the reported studies with hydrogen-bonded motifs are performed in apolar solvents because of the instability of these capsules in polar solvents. However, recently, hydrogen-bonded capsules were reported that are stable in polar media.⁶⁶

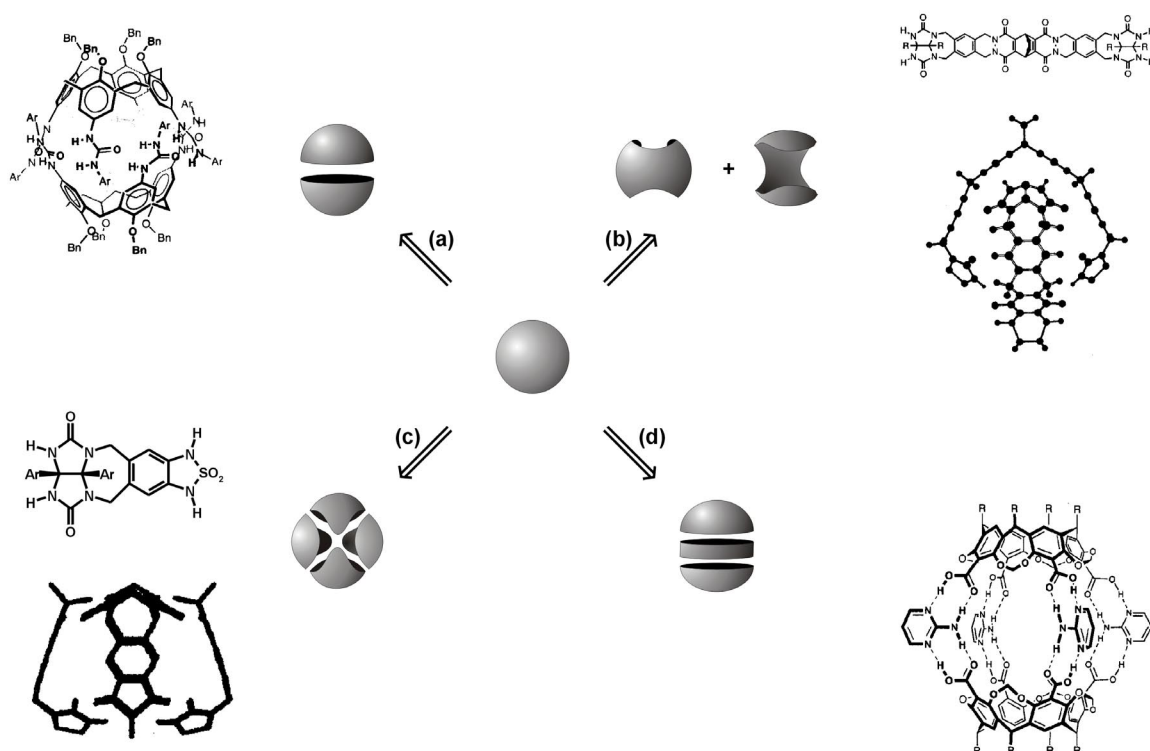


Figure 2.8. Different strategies for the synthesis of hydrogen-bonded capsules.

Hydrogen bonding is also used in the formation of motifs that are not capsules. For example, Davis et al. showed that the G-quartet, a macrocycle comprised of four hydrogen-bonded guanosine units,⁶⁷ is formed by self-association of lipophilic nucleosides in the presence of metal ions in nonpolar solvents.⁶⁸ With metal picrate salts D_4 -symmetric hexadecamers of guanosine units are formed in the solid state (Figure 2.9).⁶⁹ Two metal ions (M^{2+}) are complexed between two G-quartets and four anions (picrate) are complexed by formation of four hydrogen bonds with the NH amino protons of the two “inner” G-quartets.

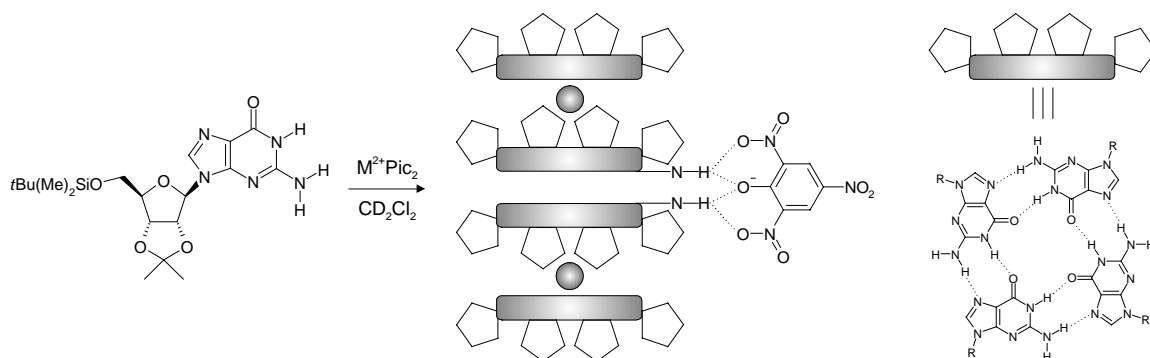


Figure 2.9. A lipophilic G-quadruplex that binds ion pairs.

Rissanen et al.⁷⁰ reported the self-assembly of aminopyridine substituted anthracene derivatives into 1- and 2-dimensional multicompartmental arrays by the formation of a hydrogen-bonded network. The arrays are capable of forming clathrate-type inclusion entities with guest molecules, such as nitrobenzene and perchloroethylene.

2.3.2.1 Rosettes

In the research presented in this thesis, the rosette motif that is formed by hydrogen bonds between isocyanuric acids and melamines is used as the platform for the synthesis of artificial receptors. Therefore, this rosette motif is discussed in more detail.

The three orthogonal ADA (Acceptor-Donor-Acceptor) hydrogen bonding arrays of isocyanuric acid (CA) are mutually complementary to the three DAD hydrogen bonding arrays of melamine (M). Mixing both compounds in a 1:1 ratio leads to an infinite 2D lattice of alternating CA and M molecules held together by hydrogen bonds (Figure 2.10).⁷¹ In this 2D lattice three different submotifs can be identified, the infinite *linear* and *crinkled* tapes, and the finite cyclic *rosette* motif. The cyclic rosette motif is the only motif that has a defined shape and size, and was therefore studied in more detail.

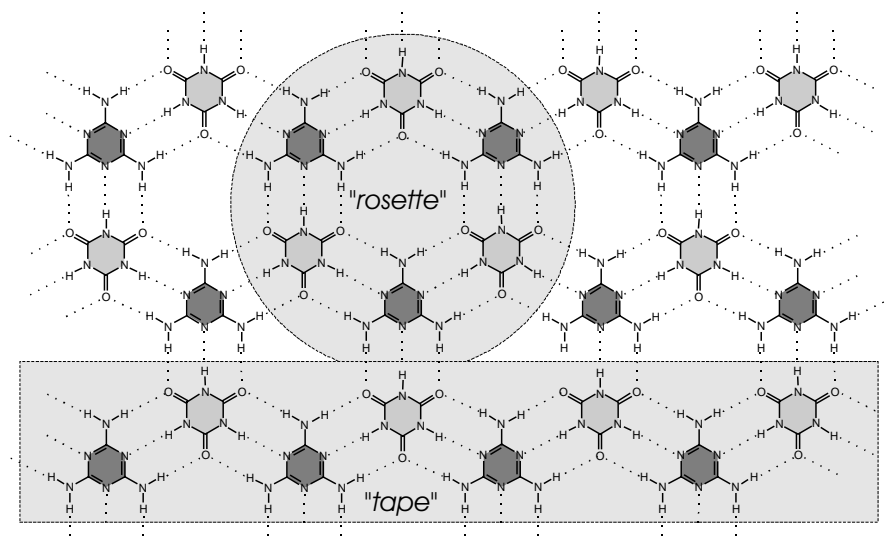


Figure 2.10. 2D lattice of alternating CA and M molecules held together by hydrogen bonds. In light grey isocyanuric acid (CA) and in dark grey melamine (M).

Whitesides⁷² and Lehn⁷³ identified the complementary hydrogen bonding in the melamine-cyanuric acid lattice and the selective synthesis of the cyclic rosette motif. In 1990, Whitesides⁷² and co-workers showed that through preorganization of three

melamine units, by connecting them covalently through a central “hub”, the rosette structure could be formed selectively (Figure 2.11a). The formation of the rosette was favored on entropic grounds. In 1994, the same group⁷⁴ showed that components with smaller substituents do not form well-defined rosettes. This was an indication that molecular steric interactions around the periphery (peripheral crowding) of the rosette might be used to selectively obtain cyclic rosette structures (Figure 2.11b). The evidence for this peripheral crowding concept came from crystal structures. In these studies it was assumed that the solid state data reflect the thermodynamic equilibrium in solution and that the solubility of the tapes is much lower than that of the rosettes in apolar solvents. These two assumptions are in a contradiction, since the first one is only valid when both solubilities are comparable. Recent model calculations carried out in the group of Reinhoudt⁷⁵ showed that it is indeed possible to promote rosette formation over tape formation by steric repulsion in the linear tapes, but the effect is not as large as previously thought. The model further showed that the ratio of tape to rosette was mainly determined by two thermodynamic parameters, i.e. the association constant between a melamine and a cyanurate/barbiturate and the formation constant for the rosette from the linear hexamer.

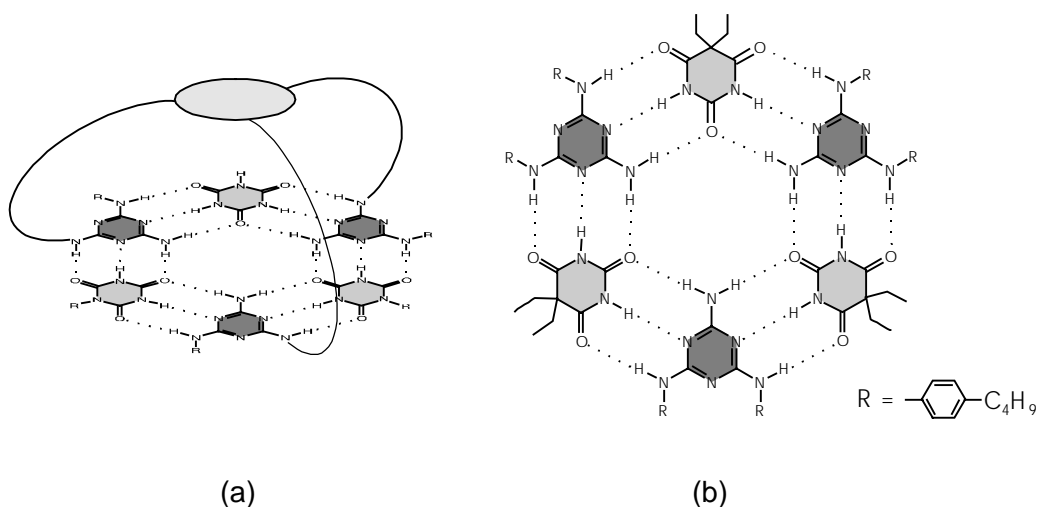


Figure 2.11. Selective rosette formation by (a) covalent preorganization and (b) peripheral crowding.

While these assemblies exhibit a high thermodynamic stability, they are kinetically labile. There is a continuous exchange of the individual components between the assemblies. This exchange process is responsible for the self-correcting ability of these assemblies. The exchange rate in these hydrogen-bonded assemblies is strongly dependent on the number of hydrogen bonds that have to be broken. As a result of this

kinetic instability, dynamic combinatorial libraries of these assemblies can be obtained by mixing the appropriate number of components under thermodynamically controlled conditions (Section 2.4.2).

As an extension of the rosette motif, Reinhoudt et al.⁷⁶ showed that calix[4]arene, diametrically substituted with two melamine units at the upper rim forms the double rosette assemblies in the presence of two equivalents of 5,5-diethylbarbuturic acid (DEB) (see also Section 3.2 and 3.3). The double rosettes could be extended to tetra-, hexa-, and octarosettes by connecting calix[4]arene dimelamine units covalently via a flexible linker (Figure 2.12).⁷⁷ These assemblies have a high thermodynamic stability due to the formation of 36 (double rosette), 72 (tetrarosette), 108 (hexarosette), and 142 (octarosette) cooperative hydrogen bonds, which renders these assemblies stable in CDCl_3 even at concentrations of 10^{-4} M. In this thesis double and tetrarosette assemblies as **receptor molecules** are described.

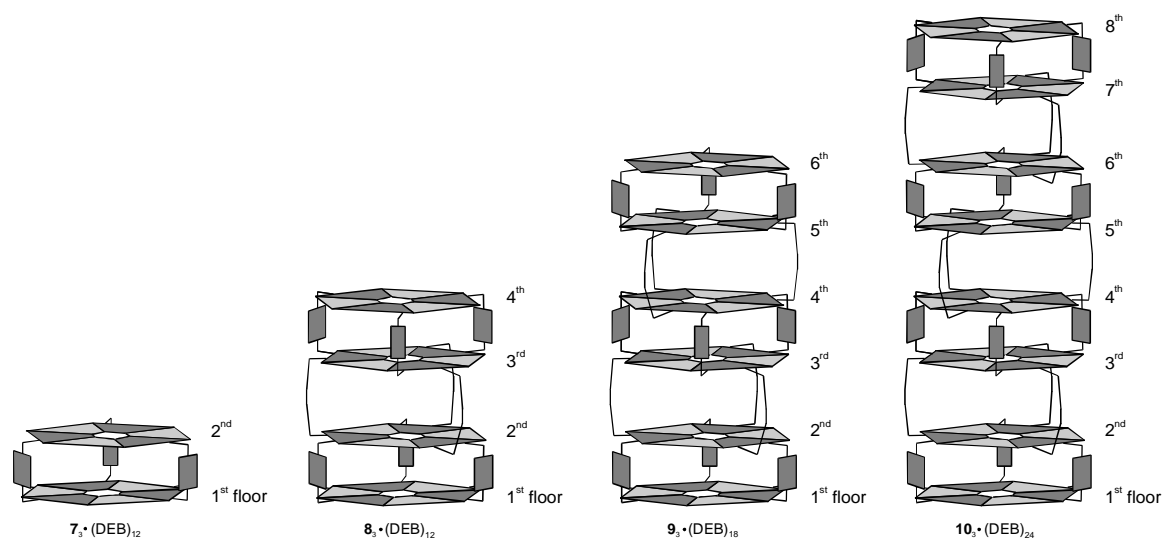


Figure 2.12. Schematic representation of double rosette $7_3 \bullet (\text{DEB})_6$, tetrarosette $8_3 \bullet (\text{DEB})_{12}$, hexarosette $9_3 \bullet (\text{DEB})_{18}$, and octarosette $10_3 \bullet (\text{DEB})_{24}$. (Each floor represents a single rosette motif)

Recently, Fenniri and co-workers⁷⁸ have used the same rosette motif for the self-assembly of receptor functionalities. They generated a self-assembled helical rosette nanotube from heterocyclic base **11**. First **11** underwent a hierarchical self-assembly process in water to produce $\mathbf{11}_6$ (Figure 2.13). The aggregate $\mathbf{11}_6$ then underwent a second level of organization (stacking) to yield a nanotube. Functionalization of **11** with a crown ether gave a self-assembled structure that could complex chiral amino acids in their zwitterionic form.⁷⁹

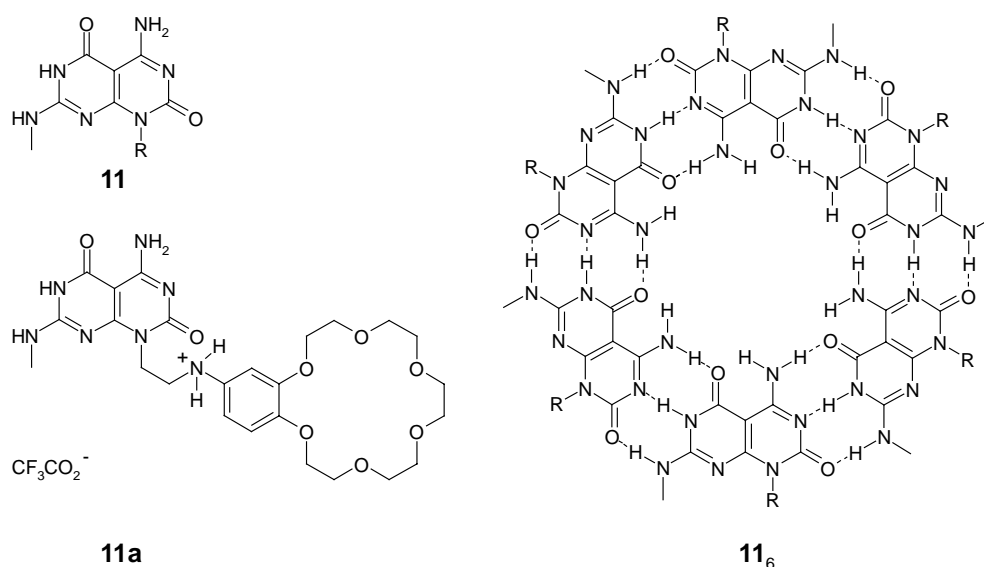


Figure 2.13. Hierarchical self-assembly of rosettes from module 11.

2.4 Combinatorial Chemistry for the Preparation of Artificial Receptors

Despite numerous efforts to mimic the binding properties of natural antibodies in synthetic molecules, chemists have so far not been able to produce adequate artificial substitutes for antibodies. The main reason is that chemists use a rational-based design approach (Section 2.2), which is principally different from the combinatorial (“trial-and-error”) strategy employed by nature. The latter is by far more efficient, because it samples a much larger structural space using random structural variation on the genetic level.¹

Combinatorial chemistry, invented in the early 1980s,⁸⁰ comprises the generation of large collections, or “libraries”, of compounds by synthesizing all possible combinations of a set of smaller chemical structures, or “building blocks”. Instead of a reaction of A with B to form one product AB, different building blocks of type A (A_1 - A_n) are reacted with different building blocks of type B (B_1 - B_m) (Figure 2.14).

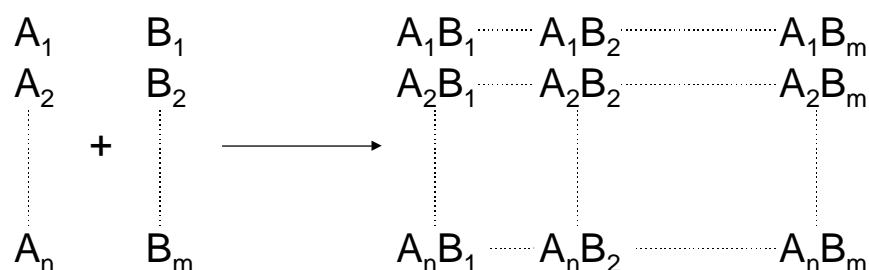


Figure 2.14. Concept of combinatorial chemistry

The ability to determine the activity of new substances (“screening”) extremely fast, has stimulated the development of new synthetic methods. The availability of compounds rather than the screening capacity was the limiting factor in further development. In combinatorial chemistry, many structurally defined substances are created simultaneously instead of synthesizing one substance after another.

2.4.1 “Classical” Combinatorial Chemistry

Two principle steps are involved in combinatorial chemistry (CC) *viz.* the synthesis of the library and the identification of the active compound(s).⁸¹ The generation of the combinatorial libraries (CLs) can be performed either in solution or on solid phase. Both techniques have advantages and disadvantages.⁸² The major advantage of synthesis on a solid support is that isolation of the support-bound reaction products is accomplished by washing away reagents from the support-bound material. The reactions can be driven to completion by the use of excess reagents. Different strategies for the preparation of CLs, both in solution and on solid phase, have been developed; two of which are very important. One is the split synthesis method⁸³ pioneered by Furka⁸⁴ and co-workers for the synthesis of large peptide libraries in 1988. This method is based on splitting-coupling-and-recombine.⁸⁵ The other method is parallel synthesis,⁸⁶ where different compounds are synthesized separately from each other.

Different techniques have been explored to identify the active compound in the library.

(a) In deconvolution,⁸⁷ wells of compounds are prepared such that each separate well has a defined building block at one position, and all building blocks are incorporated at the remaining positions. The second round is then performed with the selected building block in place at the initially defined position, in order to select the optimal building block at the additionally defined position. This method is repeated until all positions are defined.

(b) In positional scanning,⁸⁸ one position in a (peptide) sequence is held constant, while the others are varied. Monitoring the activity of the different mixtures with the same position constant (in every mixture a different amino acid) will yield the most potent amino acid at that position. This is then repeated for all the positions.

(c) In tagging,⁸⁹ readable tags that record the reaction sequence are attached to the resin bead in accordance with the synthesis of the compound on the bead.

(d) In chromatographic affinity,⁹⁰ while passing through a column most of the active compound will remain on the column phase as a complex with the attached target molecule.

Furthermore, direct detection by using labeled target molecules such as fluorescent guests is often used to identify host molecules attached to a solid support.⁹¹

In the remaining part of this section, the preparation of receptor molecules for the recognition of peptides by “classical” static combinatorial synthesis is described. Recent research on peptide receptors has mainly focused on “tweezer” receptors⁹² (Section 2.2), which are highly selective for certain peptide sequences, despite their inherent flexibility. Recently, Kilburn⁹³ and co-workers synthesized a library of “tweezer” receptors, which contained a guanidinium “head group” and two peptide derived side arms (Figure 2.15). Screening the library with various tripeptide derivatives in an aqueous solvent system (15% DMSO/H₂O, pH 8.75) led to the identification of receptor **12** with a K_a of $8.2 \pm 2.5 \times 10^4 \text{ M}^{-1}$ for tripeptide **13**. Liskamp et al. described the combinatorial synthesis of receptor molecules containing a variety of peptide chains, for instance tweezers containing peptidosulfonamide peptidomimetics⁹⁴ or tripodal receptors, i.e. molecules with three different amino acid or peptidic arms.⁹⁵

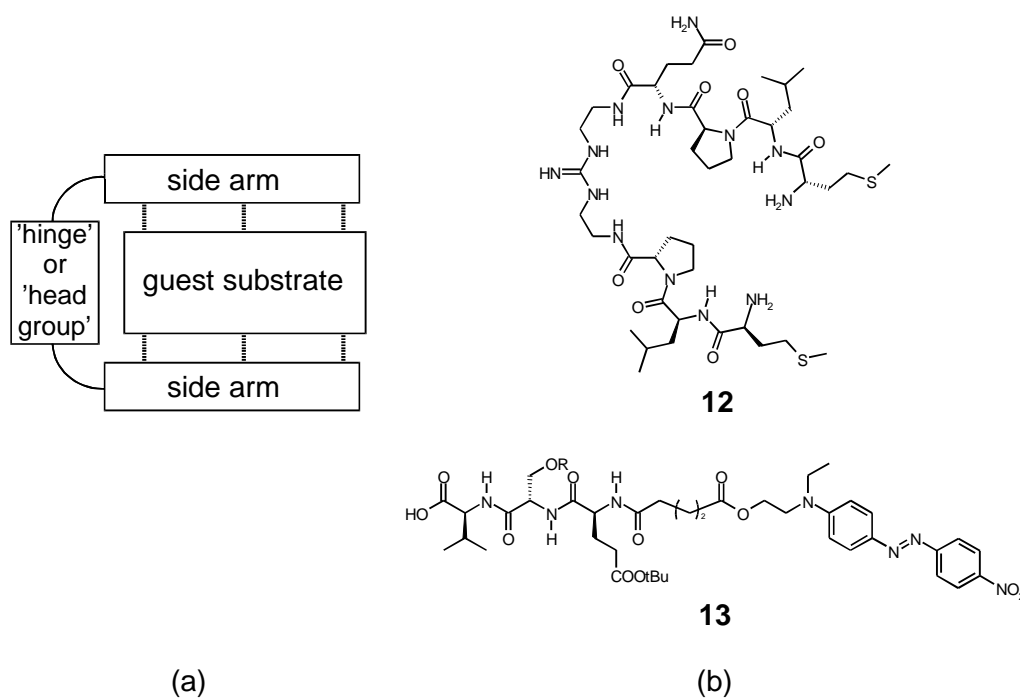


Figure 2.15. (a) Schematic representation of a “tweezer” receptor, and (b) “Tweezer” receptor **12** and tripeptidic guest **13**.

The synthesis of vancomycin mimics (Section 2.2) was also explored by combinatorial approaches. Liskamp et al.⁹⁶ reported the preparation of a 512-member library of receptor molecules using a triazacyclophane scaffold,⁹⁷ which is functionalized with three peptide “binding arms”. So far no selective receptor has been found. However, the article emphasizes the absolute requirement for validation of the hits found during the screening by resynthesizing and testing of the individual compounds. Ellman and co-workers⁹⁸ described an excellent example in which static combinatorial chemistry is used to find a potent receptor. Their receptor design preserved the right-hand carboxylate binding pocket of vancomycin (Figure 2.6a) and replaced the left-hand side of the molecule with variable tripeptide units (Figure 2.16). A library of 39,304 theoretical members was prepared by the split synthesis method and screened on solid support against fluorophore-labeled *L*-Lys-*D*-Ala-*D*-Lac (**14**) and *L*-Lys-*D*-Ala-*D*-Ala (**15**). Active beads were decoded and two of them (AA₁-AA₂-AA₃ = *L*-Tpi-*L*-His-*L*-Dapa and *L*-*N*-Me-Phe-*D,L*-Disc-*L*-Tyr) were resynthesized. The binding constant to **14** and **15** was measured by microcalorimetry. This artificial receptor, as compared to vancomycin, was found to have an enhanced binding affinity for **14**.

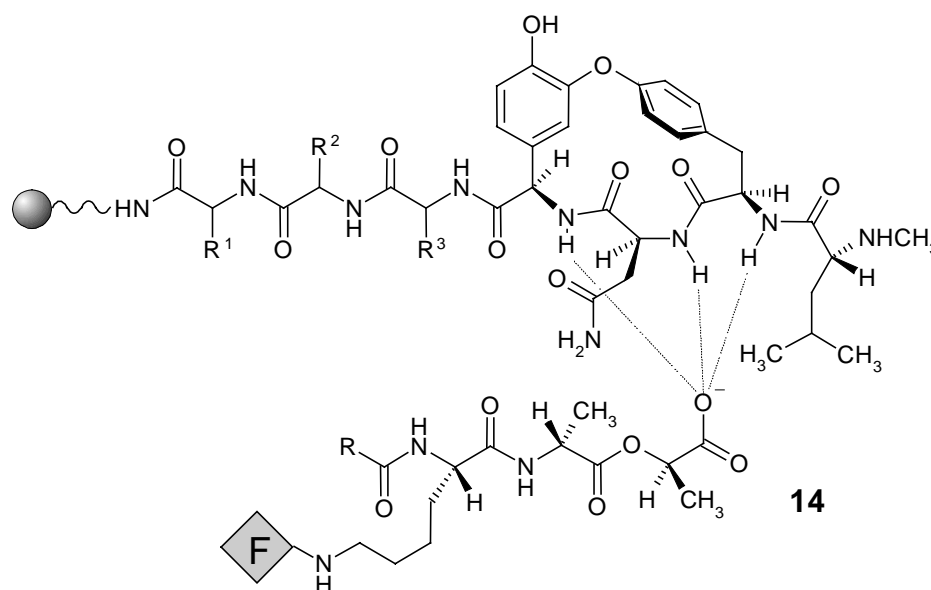


Figure 2.16. Artificial receptor for guests **14** (shown) and **15** designed by Ellman et al.

Hamilton and colleagues used a calix[4]arene core as a template to bring together four peptide loops for the recognition of protein surfaces.⁹⁹ A concave molecular surface of approximately 450-500 Å² for recognition was achieved. The best receptor acted as a

potent inhibitor of α -chymotrysin by specific interaction with the exterior of the protein (initial inhibition constant of $K_i = 0.81 \mu\text{M}$ and final of $K_i^* = 0.11 \mu\text{M}$). They also reported the recognition of cytochrome *c* by a tetraphenylporphyrin scaffold functionalized with different hydrophobic amino acids or peptide amines.¹⁰⁰ A dissociation constant of $K_d = 20 \text{ nM}$ was obtained for the best binder.

Still et al.¹⁰¹ described the discovery of sequence-selective peptide binding to synthetic receptors labeled with a dye by using encoded combinatorial libraries of these peptides on polystyrene or poly(ethylene glycol)/polystyrene beads in both chloroform and water. The library of peptides was mixed with the dye-labeled receptor and the beads that were intensively coloured after 24h were identified. Many structural similarities between the identified peptides were observed. They also created a library of peptidosteroidal receptor molecules, which was screened against a series of labeled pentapeptides.¹⁰² The library consists of 10^4 members which all have a steroidal core functionalized with two different tripeptide arms. The active compounds could be detected by using the same solid phase color assay.

2.4.2 Dynamic Combinatorial Chemistry

Conventional static combinatorial chemistry is hampered by with the analytical problems in identification of the active molecule due to the large number of compounds generated. This problem of sheer numbers in combinatorial chemistry can be reduced by the use of molecular systems that are able to amplify them selves, the so-called dynamic combinatorial systems.¹⁰³ In Table 2.2 the main differences between the “classical” static and the dynamic combinatorial libraries are summarized.¹⁰³

Table 2.2. Main differences between dynamic and static combinatorial libraries.

Dynamic Combinatorial Library	Static Combinatorial Library
Molecular or supramolecular constituents	Molecular constituents
Virtual set	Real set
Collection of components	Collection of molecules
Covalent or noncovalent	Covalent
Reversible	Non-reversible
Adaptive	Neutral, uninformed
Recognition-directed	Systematic
Self-assembled	Performed by synthesis
In presence of the target	In absence of the target

Dynamic combinatorial chemistry (DCC) makes use of reversible connections between the building blocks. These reversible connections can be either covalent,¹⁰⁴ such as imines¹⁰⁵ or disulfides,¹⁰⁶ or noncovalent, such as hydrogen bonds¹⁰⁷ or metal-ligand coordination¹⁰⁸ (Table 2.3). This reversibility allows the library members to interconvert through exchange processes to give a product distribution, which is at thermodynamic equilibrium and can be influenced by template effects. These libraries are sometimes also called “virtual” combinatorial libraries; all the possible combinations can be formed but this is not necessary. Recently, many review articles¹⁰⁹ about DCC have appeared in the literature.

Table 2.3. List of reversible reactions that can be used for the generation of dynamic combinatorial libraries (DCL).

Reversible covalent	Noncovalent
Ester exchange ¹¹⁰	Metal-ligand coordination
Transamination ¹¹¹	Hydrogen bond exchange
Transimination ¹¹²	
Oxime exchange ¹¹³	
Hydrazone exchange	
Olefin metathesis ¹¹⁴	
Disulfide exchange	

In the DCC concept three steps can be distinguished:

1. Selection of the initial building blocks that are capable of interacting reversibly with one another.
2. Establishment of library generation conditions (conditions in which the building blocks are allowed to interchange).
3. Subjection of the library to a selection process, based on binding strength to a receptor.

The building blocks for a dynamic combinatorial library (DCL) should have functional groups that can undergo reversible exchange. They should cover the geometrical and functional space of potential target sites, and their recognition groups need to be organized geometrically for optimal binding. The main difference from classical combinatorial chemistry is the amplification possibility in the DCL. Upon addition of a guest molecule to a library of potential host molecules, the guest selects and binds the best host. This binding event introduces a new equilibrium in the system, which shifts in the direction of the best host at the expense of unfit hosts due to the additional free energy of the binding event.

Huc and Lehn¹⁰⁵ divided the templating of DCLs in two groups, ‘casting’ and ‘molding’. In ‘casting’ the cavity is provided by a macromolecule that traps the good binders and leaves the poor binders in solution, which are re-equilibrated. In ‘molding’ the binder collects the optimum macromolecule around itself and thereby stabilizes the assembly (Figure 2.17).

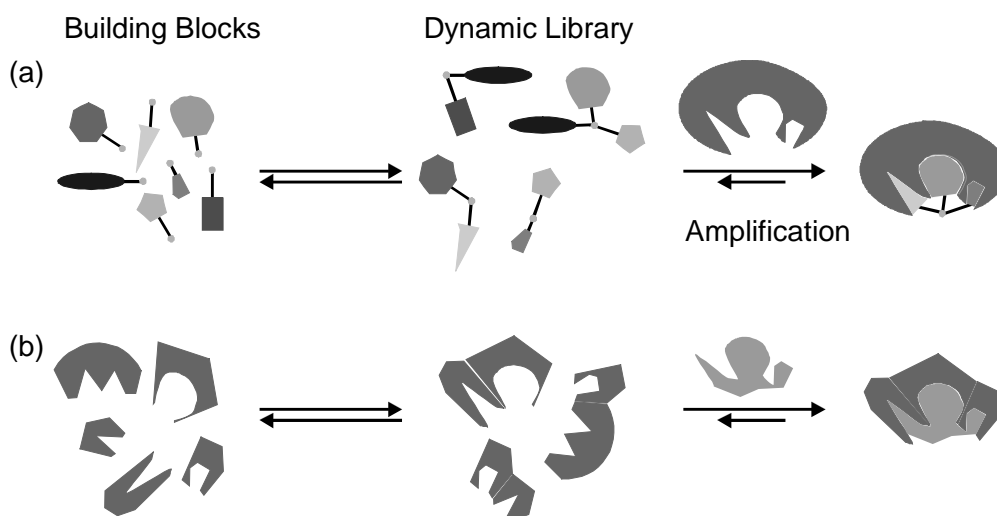


Figure 2.17. Principle of (a) casting and (b) molding.

Examples of DCC generated by reversible covalent and noncovalent interactions and particularly the guest templating in the DCL will be discussed in this section.

2.4.2.1 DCC with Receptors Based on Reversible Covalent Interactions

In 1996, Sanders et al.¹¹⁵ introduced the DCL concept with the thermodynamically-controlled cyclisation and interconversion of oligocholates. Lehn and co-workers¹⁰⁵ synthesized a library of imines by a reversible reaction between 3 aldehydes and 4 amines (Figure 2.18). The preparation of the library was performed in the presence and in the absence of carbonic anhydrase II (CA) in water at pH 6 (20 mM phosphate buffer). HPLC analysis of the resulting mixture of imines showed the amplification of one of the fifteen possible products when the reaction was performed in the presence of CA. Compound **16** binds to CA; presumably, the binding affinity of the intermediate imines for CA determines the abundance of the final product in the mixture.

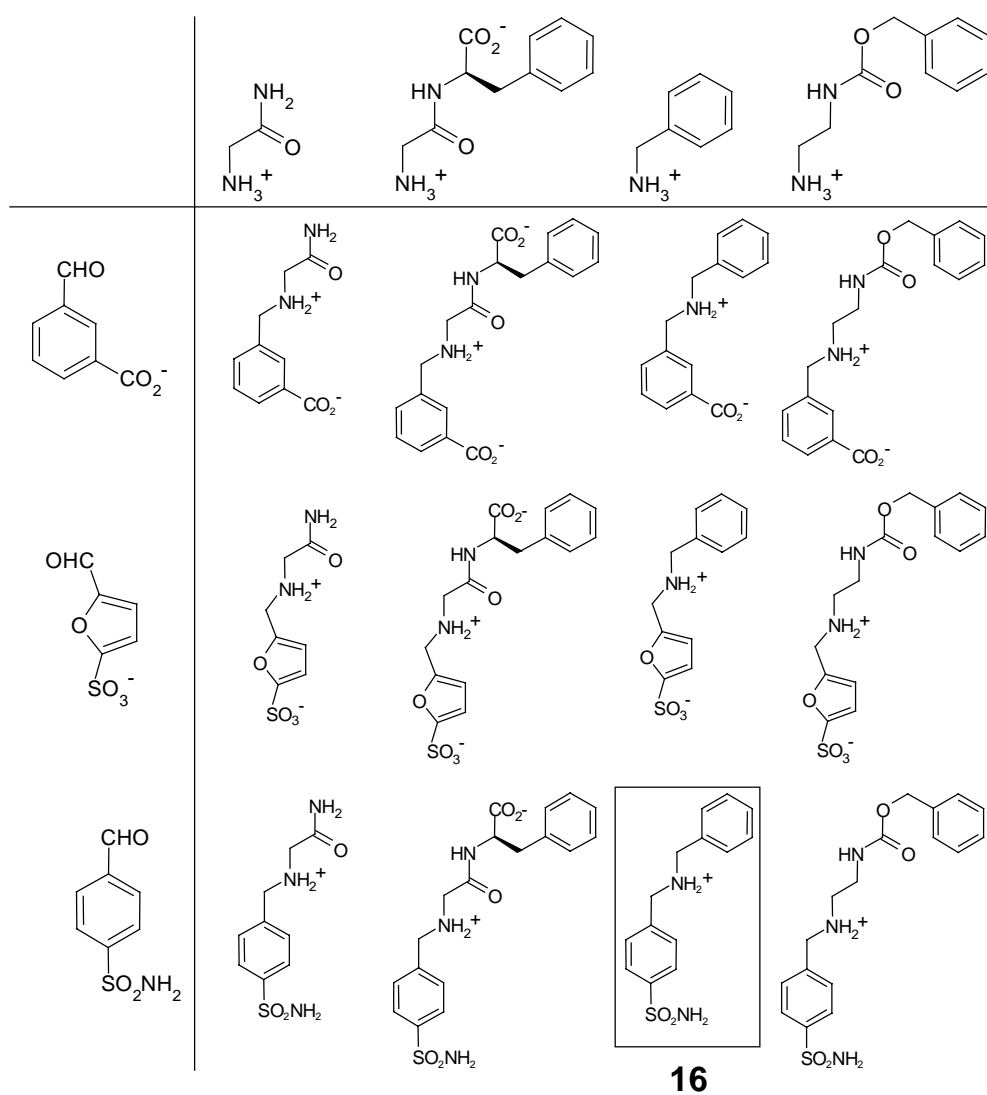


Figure 2.18. Precursor aldehydes and amines and the resulting amines after reaction and hydride reduction. In the square the amplified product **16** in the presence of carbonic anhydrase II is shown.

Still et al.¹¹⁶ showed the template effect in a three-component library synthesized by the reversible formation of disulfides (Figure 2.19). Addition of the tripeptide *L*-Pro-*L*-Val-*L*-Val shifted the equilibrium from 57% A-SS-A and B-SS-B / 43% A-SS-B to 85% A-SS-A and B-SS-B.

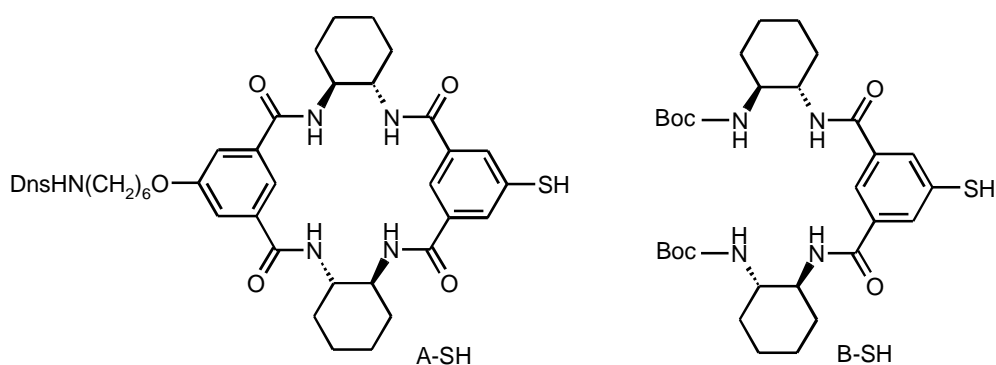


Figure 2.19. Dynamic library based on the reversible formation of disulfides.

Sanders et al.¹¹⁷ prepared a 10-macrocycle library from a single dipeptide building block, which contains both a hydrazide and a protected aldehyde functionality. Hydrazides were mixed under acid conditions with protected aldehydes to yield different hydrazones.¹¹⁸ The resultant mixture was frozen upon neutralization of the solution. The addition of Li⁺ generated the most dramatic response from the library, amplifying the cyclic trimer to account now for 98% of the peptide material in the library. The binding constant of Li⁺ with the trimer is $4 \times 10^4 \text{ M}^{-1}$ in CHCl₃/MeOH (98:2) (Figure 2.20).

The same hydrazone chemistry was also used for molecular amplification from a DCL based on *L*-proline building blocks that selectively binds to acetylcholine and *N*-methyl quinuclidinium salts.¹¹⁹ Using these two salts Sanders et al. were able to thermodynamically bias the product distribution of the dynamic combinatorial library towards the cyclic trimer. They also showed that the large number of compounds generated by the di-functionalized building blocks used could be analyzed by electro-spray ionization Fourier-transform ion cyclotron resonance mass spectrometry (ESI-FTICR-MS).¹²⁰ They suspected that extension of the library size would make it difficult to isolate and/or identify the selected receptors by conventional methods. Therefore, Sanders et al. proposed the use of immobilized templates.^{109e} They showed that an immobilized *N*-methyl ammonium ion template can select and amplify the cyclic trimer from a DCL.¹²¹

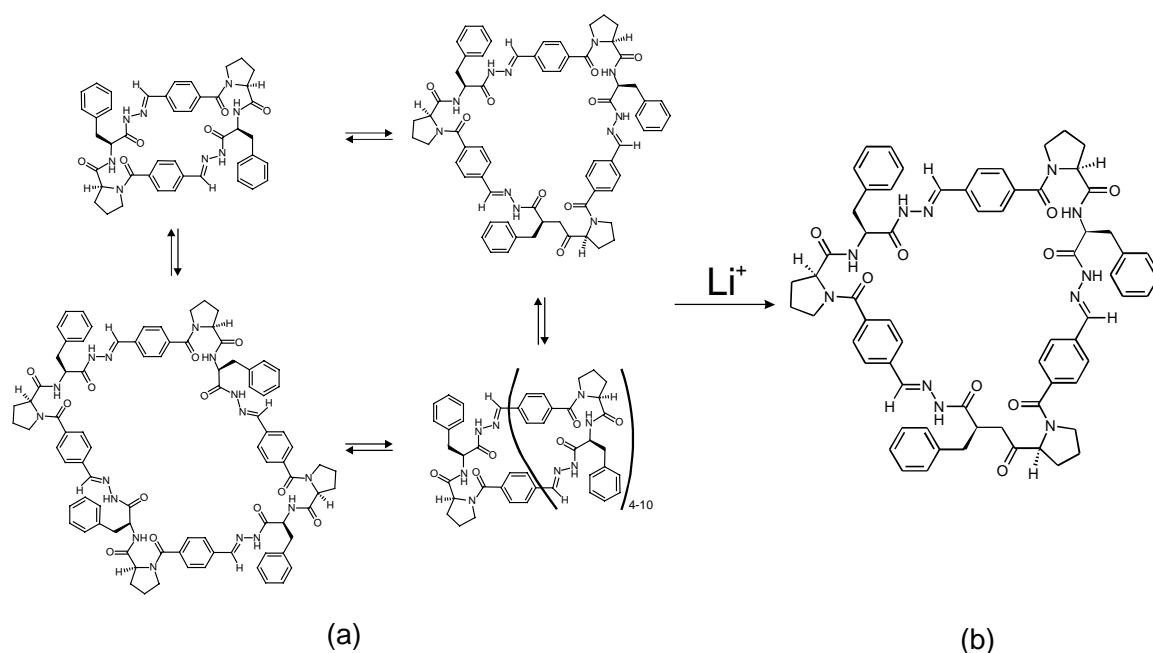


Figure 2.20. Dynamic library of hydrazone-based pseudopeptide macrocycles (a) before and (b) after addition of Li^+ .

In addition to reversible covalent reactions, isomerization processes are also used to generate a thermodynamically driven conformational and/or configurational dynamic library. In 1997 Eliseev and Nelen¹²² showed that a mixture of components can be enriched in the component that possesses the highest affinity for an added ligand. Unsaturated dicarboxylate **17** can exist in three isomeric forms and interconverts by irradiation with UV light (Figure 2.21). The *cis,cis* isomer has the ideal geometry for complexation of the guanidinium moiety of arginine, illustrated by its significant retention on an affinity column loaded with immobilized arginine. By using repetitive isomerization-selection cycles the *cis,cis* receptor could be generated from the mixture in high yield (85%).

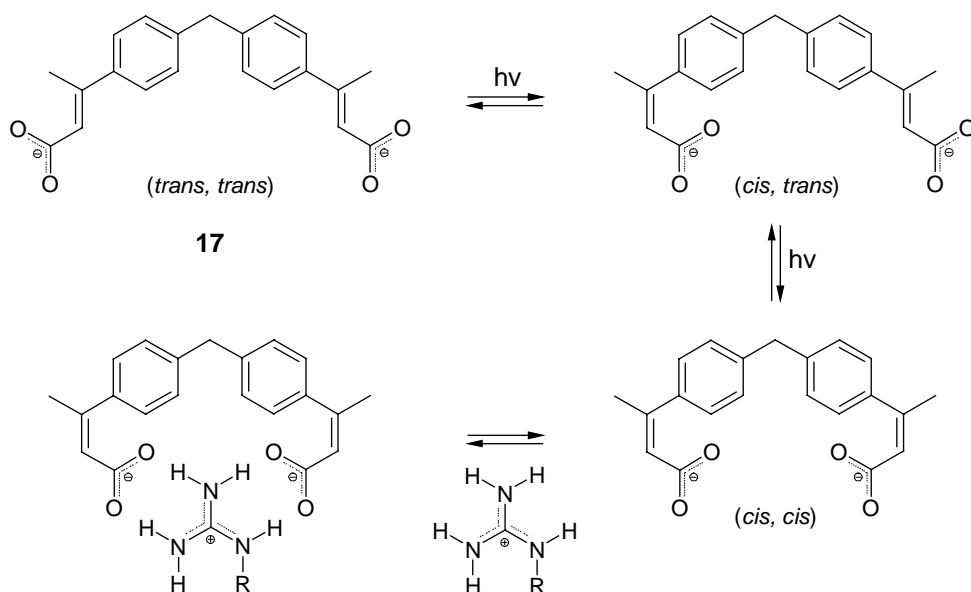


Figure 2.21. Interconversion of unsaturated dicarboxylate **17** by UV light.

Lehn *et al.*¹²³ also used isomerization to prepare a DCL for the induced fit selection from a library of different condensation products of 5,5-dimethyl-1,3-cyclohexanedione and 2-hydrazinopyridine upon addition of dibutylbarbiturate. In addition to configurational isomerization of the dihydrazones leading to the favored (*Z/Z*) isomer, the promotion of the reaction of the monocondensation products with the remaining hydrazino-pyridine is also observed after the addition of the barbiturate.

2.4.2.2 DCC with Receptors Based on Noncovalent Interactions

Thus far only reversible metal coordination¹²⁴ and hydrogen bonding,¹⁰⁷ for the purpose of generating DCLs through noncovalent interactions, has been described in the literature. Hamilton reported a metal-template approach for the formation of libraries of artificial receptor molecules.¹²⁵ Different terpyridine subunits were used to obtain octahedral Ru-bis-terpy complexes **18** in which two recognition sites are held in a fixed relationship (Figure 2.22). A total of $n(n+1)/2$ different receptors are formed when n different substituted terpyridines are combined. This library was screened for the binding of bis(tetrabutylammonium) pimelate in DMSO and for the binding of pentane-1,5-diybis(ammonium)ions in 5% CH₃CN/CH₂Cl₂. The dynamic character of the libraries achieved by metal coordination is not reported, but correlations to natural antibodies are discussed.

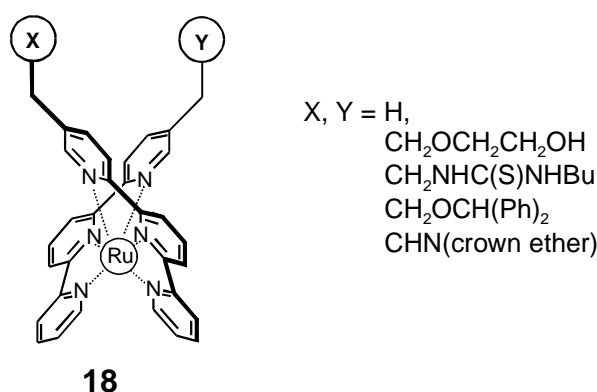


Figure 2.22. Combinatorial library of receptors **18** based on metal-templation.

Helicates are polynuclear metal complexes of helical shape, in which two or three ligand strands wrap around a set of linearly disposed metal ions.¹²⁶ These metal containing circular complexes are capable of binding anions inside their cavity. Lehn et al. reported that depending on the size of the complexed anion a pentamer or hexamer is formed (Figure 2.23).¹²⁷ Furthermore, they showed that addition of Cl⁻ to the hexamer led to the exclusive formation of the pentamer after heating the mixture at 170 °C. In addition to a template effect by an appropriate guest molecule, changes in the concentration and the solvent could also switch the equilibrium between polynuclear metallocylophanes.¹²⁸

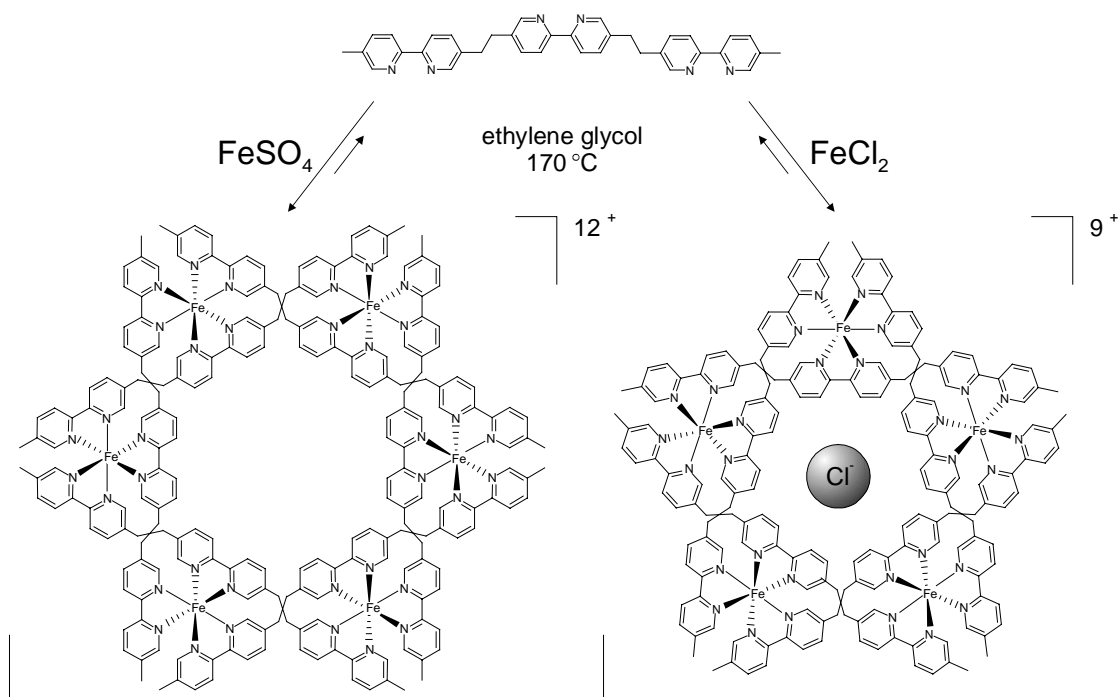


Figure 2.23. Self-assembly of the pentanuclear and hexanuclear circular helicates.

Sasaki and co-workers¹²⁹ described the amplification of a DCL of four diastereomeric isomers (Δ -*fac*, Λ -*fac*, Δ -*mer*, and Λ -*mer*), consisting of three bipyridine-modified 2-acetamido-2-deoxy- α -D-galactopyranose (GalNAc) ligands coordinated to Fe(II), by B₄ lectin (Figure 2.24). The isomer Λ -*mer* provides better complementarity to the multivalent carbohydrate binding site of B₄ lectin, and after addition of B₄ lectin its presence in the mixture is increased from 15% to 85%.

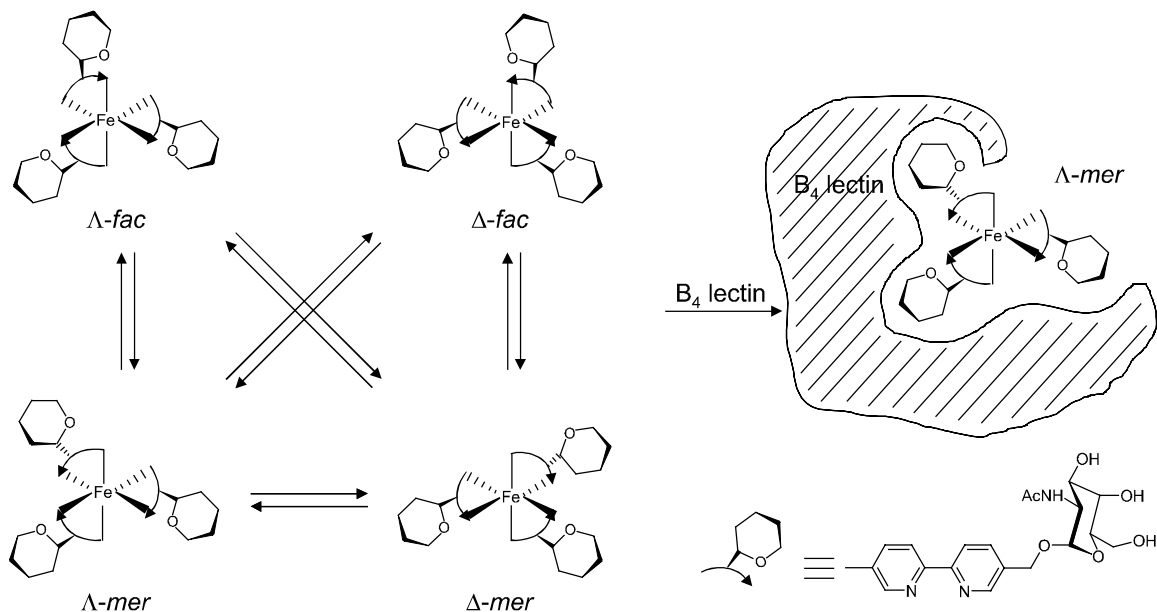


Figure 2.24. Dynamic equilibrium of the diastereomers and spatial arrangement of the three GalNAc residues to fit into the multivalent carbohydrate binding site of B₄ lectin.

Lehn et al. also prepared a DCL of coordination receptors bearing hydrogen bonding units.¹³⁰ Amplification of the coordination receptor bearing the complimentary hydrogen bond donor and acceptor pattern (DAD) was achieved after addition of the guest containing twice the ADA hydrogen bonding pattern. Another example has been shown by Fujita et al.¹³¹ in which a small DCL of Pd(II)-linked cages derived from two different ligands was prepared. Two homoleptic receptors and one heteroleptic were formed. Addition of small or large guest molecules favored the homoleptic receptors, while medium-sized guest molecules preferred the heteroleptic receptor.

DCL are also used for biological systems, such as selecting the best binder for a particular DNA¹³² or RNA sequence. Miller and Karan¹³³ described the selection of a salicylamide-Cu complex from a library of functionalized salicylamide-Cu complexes,

that bind an RNA hairpin with high affinity and extraordinary selectivity relative to the homologous DNA hairpin.

Our group¹⁰⁷ was the first to report the use of hydrogen bonding in the preparation of DCLs. A four compound library was synthesized by mixing two double rosettes (Section 2.3.2.1), one functionalized with three Zn-porphyrin moieties both at the top and bottom and one non-functionalized. Addition of 1,3,5-(4-pyridyl)-benzene to the library shifted the equilibrium towards maximum formation of the strongest receptor (containing six Zn-porphyrin moieties). Rebek and colleagues¹³⁴ also used hydrogen bonding for the preparation of DCLs and showed that addition of an appropriate guest molecule induced a shift in the composition of the DCL. Tetrameric capsules of **19** (Figure 2.25) were prepared by simply mixing the building blocks,¹³⁵ and the composition of the different assemblies was studied by electro-spray mass spectroscopy.¹³⁶ Addition of methylquinuclidinium cation favored the receptor consisting of four molecules of **19a**.

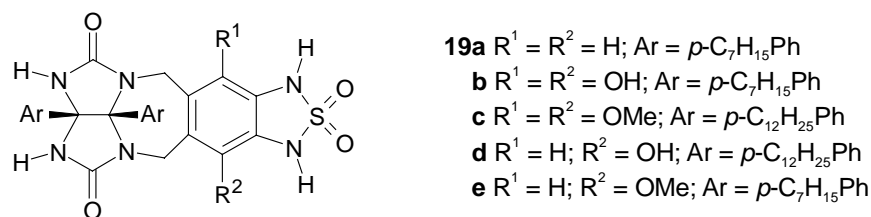


Figure 2.25. Molecular structures of the monomers **19** used for tetrameric capsule formation.

Additional degrees of library diversification can be achieved by using two or more reactions to connect the building blocks. Recently, Lehn¹³⁷ and co-workers prepared a DCL which has two orthogonal levels of diversity, i.e. exchange of terpyridine-based ligands around the cobalt center and hydrazone exchange (Figure 2.26).

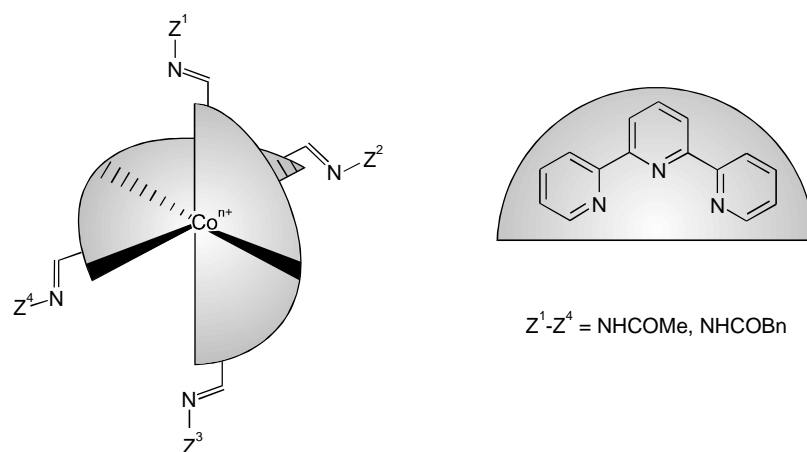


Figure 2.26. Two orthogonal levels of diversity obtained by ligand-cobalt and hydrazone exchange.

As shown by the previous examples, DCLs allow amplification of the best binder in the library, thus performing a self-screening by which the best binders are preferentially expressed and retrieved from the DCL. Sometimes the amplification is not enough to identify the active compound in the DCL, for instance when the number of compounds become large. Therefore, Lehn and co-workers¹³⁸ introduced the dynamic deconvolution procedure, a technique based on the sequential removal of starting building blocks. A pre-equilibrated library prepared from hydrazide and aldehyde building blocks was screened towards the inhibition of acetylcholinesterase. The deconvoluted libraries that showed an increase of enzyme activity, indicated that the removed building blocks are important binders. This technique is ideal to use when the conditions under which the library is dynamic are not compatible with the conditions necessary for the stability of the guest, for instance in the presence of an enzyme.

2.5 Conclusions and Outlook

In this chapter, a short overview of the development of artificial receptor molecules was given. The overview started with rationally designed receptor molecules prepared by *covalent* synthesis. Although this *covalent* approach has led to the synthesis of numerous receptor molecules, for complex receptor molecules the more recent *noncovalent* synthesis seems more promising because the receptors are formed under thermodynamic equilibrium conditions and generally in quantitative yield.

A brief description of combinatorial synthesis and screening as an effective approach for the synthesis of receptor molecules was presented. It has been shown that the

synthesis of a large number of possible receptor molecules by “classical” static and dynamic combinatorial chemistry increases the chance to find a good receptor. Nevertheless, up till now dynamic combinatorial chemistry has mainly been used for the preparation of small model libraries. These small libraries have shown promising results towards the amplification of the best receptor. Future research will show if the identification of the best receptor in large libraries still can be achieved by the amplification of this receptor.

The research described in this thesis comprises the synthesis and complexation abilities of hydrogen-bonded receptor molecules and the generation of dynamic combinatorial libraries of these hydrogen-bonded receptors.

2.6 References

- ¹ Benjamini, E.; Sunshine, G.; Leskowitz, S. *Immunology, A Short Course*, 3rd ed. Wiley, New York, **1996**.
- ² a) Porter, R.R. *Nature*, **1958**, *182*, 670-673; b) Porter, R.R. *Biochem. J.* **1959**, *73*, 119-126.
- ³ Edelman, G.M. *J. Am. Chem. Soc.* **1959**, *81*, 3155-3156.
- ⁴ Picture was taken from Guttman, R.D. *Immunology*, Scope Publication, Michigan, **1985**.
- ⁵ Recent review about synthetic receptors: Hartley, J.H.; James, T.D.; Ward, C.J. *J. Chem. Soc., Perkin Trans. 1* **2000**, 3155-3184.
- ⁶ Schmidtchen, F.P.; Berger, M. *Chem. Rev.* **1997**, *97*, 1609-1646.
- ⁷ Cram, D.J.; *Angew. Chem. Int. Ed. Engl.* **1988**, *27*, 1009-1020.
- ⁸ a) D'Souza, V.T.; Lipkowitz, K.B. *Chem. Rev.* **1998**, *98*, Issue 5; b) Wenz, G. *Angew. Chem. Int. Ed. Engl.* **1994**, *33*, 803-822.
- ⁹ a) Pedersen, C.J. *J. Am. Chem. Soc.* **1967**, *89*, 7017-7036; b) Gokel, G.W. *Crown Ethers and Cryptands* (Ed. Stoddart; J.F.), The Royal Society of Chemistry, Cambridge, **1991**.
- ¹⁰ a) Rüdiger, V.; Schneider, H.-J.; Solov'ev, V.P.; Kazachenko, V.P.; Raevsky, O.A. *Eur. J. Org. Chem.* **1999**, 1847-1856; b) Cantrill, S.J.; Fulton, D.A.; Heiss, A.M.; Pease, A.R.; Stoddart, J.F.; White, A.J.P.; Williams, D.J. *Chem. Eur. J.* **2000**, *6*,

- 2274-2287; c) Tsukube, H.; Wada, M.; Shinoda, S.; Tamiaki, H. *Chem. Commun.* **1999**, 1007-1008.
- ¹¹ Hossain, A.; Schneider, H.-J. *J. Am. Chem. Soc.* **1998**, *120*, 11208-11209.
- ¹² Ikeda, A.; Shinkai, S. *Chem. Rev.* **1997**, *97*, 1713-1734.
- ¹³ Arena, G.; Casnati, A.; Contino, A.; Lombardo, G.G.; Sciotto, D.; Ungaro, R. *Chem. Eur. J.* **1999**, *5*, 738-744.
- ¹⁴ a) Bodenant, B.; Weil, T.; Businelli-Pourel, M.; Fages, F.; Barbe, B.; Pianet, I.; Laguerre, M. *J. Org. Chem.* **1999**, *64*, 7034-7039; b) Ikeda, A.; Shinkai, S. *Chem. Rev.* **1997**, *97*, 1713-1734; c) Arduini, A.; Pochini, A.; Secchi, A. *Eur. J. Org. Chem.* **2000**, *12*, 2325-2334.
- ¹⁵ a) Casnati, A.; Pirondini, L.; Pelizzi, N.; Ungaro, R. *Supramol. Chem.* **2000**, *12*, 53-65; b) Pelizzi, N.; Casnati, A.; Ungaro, R. *Chem. Commun.* **1998**, *23*, 2607-2608; c) Tomapatanaget, B.; Tuntulani, T.; *Tetrahedron Lett.* **2001**, *42*, 8105-8109.
- ¹⁶ a) Arena, G.; Contino, A.; Gulino, F.G.; Magri, A.; Sciotto, D.; Ungaro, R. *Tetrahedron Lett.* **2000**, *41*, 9327-9330; b) Arduini, A.; Nachtigall, F.F.; Pochini, A.; Secchi, A.; Ugozoli, A. *Supramol. Chem.* **2000**, *12*, 273-291.
- ¹⁷ Casnati, A.; Pochini, A.; Ungaro, R.; Bocchi, C.; Ugozoli, F.; Egberink, R.J.M.; Struijk, H.; Lugtenberg, R.; de Jong, F.; Reinhoudt, D.N. *Chem. Eur. J.* **1996**, *2*, 436-445.
- ¹⁸ a) Chen, C.-W.; H. W. Whitlock, Jr, H.W. *J. Am. Chem. Soc.* **1978**, *100*, 4921-4922; b) Zimmerman, S.C.; Wu, W.; Zeng, Z. *J. Am. Chem. Soc.* **1991**, *113*, 196-201.
- ¹⁹ Schrader, T. *Chem. Eur. J.* **1997**, *3*, 1537-1541.
- ²⁰ a) Ruloff, R.; Seelbach, U.P.; Merbach, Klärner, F.-G. *J. Phys. Org. Chem.* **2002**, *15*, 189-196; b) Klärner, F.-G.; Burkert, U.; Kamieth, M.; Boese, R. *J. Phys. Org. Chem.* **2000**, *13*, 604-611; c) Klärner, F.-G.; Burkert, U.; Kamieth, M.; Boese, R.; Benet-Buchholz, J. *Chem. Eur. J.* **1999**, *5*, 1700-1707; d) Kamieth, M.; Burkert, U.; Corbin, P.S.; Dell, S.J.; Zimmerman, S.C.; Klärner, F.-G. *Eur. J. Org. Chem.* **1999**, 2741-2749; e) Kamieth, M.; Klärner, F.-G. *J. Park. Chem.* **1999**, *341*, 245-251.
- ²¹ Takeuchi, M.; Imada, T.; Shinkai, S. *J. Am. Chem. Soc.* **1996**, *118*, 10658-10659.
- ²² Jansen, R.J.; de Gelder, R.; Rowan, A.E.; Scheeren, H.W.; Nolte, R.J.M. *J. Org. Chem.* **2001**, *66*, 2643-2653.

- ²³ a) Cram, D.J.; Cram, J.C. *Container Molecules and Their Guests* (Ed. Stoddart; J.F.), The Royal Society of Chemistry, Cambridge, **1994**; b) Jasat, A.; Sherman, J.C. *Chem. Rev.* **1999**, *99*, 931-967.
- ²⁴ Warmuth, R.; Yoon, J. *Acc. Chem. Res.* **2001**, *34*, 95-105.
- ²⁵ Makeiff, D.A.; Pope, D.J.; Sherman, J.C. *J. Am. Chem. Soc.* **2000**, *122*, 1337-1342.
- ²⁶ a) Bencini, A.; Bionchi, A.; Fusi, V.; Giorgi, C.; Paoletti, P.; Valtancoli, B. *Inorg. Chim. Acta* **1998**, *273*, 326-333; b) Bryant, W.S.; Jones, J.W.; Mason, P.E.; Guzei, I.; Rheingold, A.L.; Fronczek, F.R.; Nagvekar, D.S.; Gibson, H.W. *Org. Lett.* **1999**, *1*, 1001-1004.
- ²⁷ a) Brotin, T.; Lesage, A.; Emsley, L.; Collet, A. *J. Am. Chem. Soc.* **2000**, *122*, 1171-1174; b) Kirchhoff, P.D.; Dutasta, J.-P.; Collet, A.; McCammon, J.A. *J. Am. Chem. Soc.* **1999**, *121*, 381-390; c) Bartik, K.; Luhmer, Dutasta, J.-P.; Collet, A.; Reisse, J. *J. Am. Chem. Soc.* **1998**, *120*, 784-791; d) Collet, A. *Cryptophanes in Comprehensive Supramolecular Chemistry, Vol. 2* (Eds.: Trost, B.M.; Fleming, I.; Heathcock, C.H.), Pergamon, Oxford, **1996**, pp 325-365.
- ²⁸ a) Chopra, N.; Sherman, J.C. *Angew. Chem. Int. Ed.* **1999**, *38*, 1955-1957; b) Cram, D.J.; Karbach, S.; Kim, Y.H.; Baczynskyj, L.; Kallemeyn, G.W. *J. Am. Chem. Soc.* **1985**, *107*, 2575-2576.
- ²⁹ Recent review about peptide and protein recognition by designed molecules: Peczu, M.W.; Hamilton, A.D. *Chem. Rev.* **2000**, *100*, 2479-2494. Examples of synthetic receptors for amino acid and peptide derivatives: a) Pieters, R.J.; Cuntze, J.; Bonnet, M.; Diederich, F. *J. Chem. Soc., Perkin Trans. 2* **1997**, 1891-1900; b) Henley, P.D.; Waymark, C.P.; Gillies, I.; Kilburn, J.D. *J. Chem. Soc., Perkin Trans. 1* **2000**, 1021-1031; d) Pernia, G.J.; Kilburn, J.D.; Essex, J.W.; Mortishire-Smith, R.J.; Rowley, M. *J. Am. Chem. Soc.* **1996**, *118*, 10220-10227; e) Hernández, J.V.; Almaraz, M.; Raposo, C.; Martín, M.; Lithgow, A.; Crego, M.; Caballero, C.; Morán, J.R. *Tetrahedron Lett.* **1998**, *39*, 7401-7404.
- ³⁰ Kyne, G.M.; Light, M.E.; Hursthouse, M.B.; Mendoza, de J.; Kilburn, J.D. *J. Chem. Soc., Perkin. Trans. 1*, **2001**, 1258-1263.
- ³¹ a) Yoon, S.S.; Still, W.C. *J. Am. Chem. Soc.* **1993**, *115*, 823-824; b) Yoon, S.S.; Still, W.C. *Tetrahedron Lett.* **1994**, *35*, 2117-2120.
- ³² Williams, D.H.; Bardsley, B. *Angew. Chem. Int. Ed.* **1999**, *38*, 1172-1193.

- ³³ Walsh, C.T.; Fisher, S.L.; Park, I.S.; Prahaland, M.; Wu, Z. *Chem. Biol.* **1996**, *3*, 21-28.
- ³⁴ Casnati, A.; Fabbi, M.; Pelizzi, N.; Pochini, A.; Sansone, F.; Ungaro, R. *Bioorg. Med. Chem. Lett.* **1996**, *6*, 2699-2704.
- ³⁵ Frish, L.; Sansone, F.; Casnati, A.; Ungaro, R.; Cohen, Y. *J. Org. Chem.* **2000**, *65*, 5026-5030.
- ³⁶ a) Sun, B.; Chen, Z.; Eggert, U.S.; Shaw, S.J.; LaTour, J.V.; Kahne, D. *J. Am. Chem. Soc.* **2001**, *123*, 12722-12723; b) Henley, P.D.; Kilburn, J.D. *Chem. Commun.* **1999**, 1335-1336.
- ³⁷ Philp, D.; Stoddart, J.F. *Angew. Chem. Int. Ed. Engl.* **1996**, *35*, 1154-1196.
- ³⁸ Hobza, P.; Zahradník, R. *Intermolecular Complexes*, Elsevier, Amsterdam, **1988**.
- ³⁹ a) Swiegers, G.F.; Malefetse, T.J. *Chem. Rev.* **2000**, *100*, 3483-3537; b) Leininger, S.; Olenyuk, B.; Stang, P.J. *Chem. Rev.* **2000**, *100*, 853-908; c) Linton, B.; Hamilton, A.D. *Chem. Rev.* **1997**, *97*, 1669-1680.
- ⁴⁰ Drain, C.M.; Nifiatis, F.; Vasenko, A.; Batteas, J.D. *Angew. Chem. Int. Ed.* **1998**, *37*, 2344-2347.
- ⁴¹ Recent review about molecular encapsulation: Hof, F.; Craig, S.L.; Nuckolls, C.; Rebek, Jr., J. *Angew. Chem. Int. Ed.* **2002**, *41*, 1488-1508.
- ⁴² Jacopozi, P.; Dalcanale, E. *Angew. Chem. Int. Ed. Engl.* **1997**, *36*, 613-615.
- ⁴³ Fochi, F.; Jacopozi, P.; Wegelius, E.; Rissanen, K.; Cozzini, P.; Marastoni, E.; Fiscaro, E.; Manini, P.; Fokkens, R.; Dalcanale, E. *J. Am. Chem. Soc.* **2001**, *123*, 7539-7552.
- ⁴⁴ Umemoto, K.; Tsukui, H.; Kusukawa, T.; Biradha, K.; Fujita, M. *Angew. Chem. Int. Ed.* **2001**, *40*, 2620-2622.
- ⁴⁵ a) Takeda, N.; Umemoto, K.; Yamaguchi, K.; Fujita, M. *Nature* **1999**, *398*, 794-799; b) Chand, D.K.; Biradha, K.; Fujita, M. *Chem. Commun.* **2001**, 1652-1653; c) Ikeda, A.; Udzu, H.; Zhong, Z.L.; Shinkai, S.; Sakamoto, S.; Yamaguchi, K. *J. Am. Chem. Soc.* **2001**, *123*, 3872-3877; d) Zhong, Z.L.; Ikeda, A.; Ayabe, M.; Shinkai, S.; Sakamoto, S.; Yamaguchi, K. *J. Org. Chem.* **2001**, *66*, 1002-1008; e) Fox, O.D.; Dalley, N.K.; Harrison, R.G. *J. Am. Chem. Soc.* **1998**, *120*, 7111-7112.

- ⁴⁶ a) Hamelin, B.; Jullien, L.; Derouet, C.; Hervé du Penhoat, C.; Berthault, P. *J. Am. Chem. Soc.* **1998**, *120*, 8438-8447, b) Fiammengo, R.; Timmerman, P.; de Jong, F.; Reinhoudt, D.N. *Chem. Commun.* **2000**, 2313-2314.
- ⁴⁷ Corbellini, F.; Fiammengo, R.; Timmerman, P.; Crego-Calama, M.; Versluis, K. Heck, A.J.R.; Luyten, I.; Reinhoudt, D.N. *J. Am. Chem. Soc.* **2002**, *124*, 6569-6575.
- ⁴⁸ Fiammengo, R.; Wojciechowski, K.; Crego-Calama, M.; Timmerman, P.; Reinhoudt, D.N. submitted.
- ⁴⁹ Recent review on noncovalent synthesis using hydrogen bonding: Prins, L.J.; Reinhoudt, D.N.; Timmerman, P. *Angew. Chem. Int. Ed.* **2001**, *40*, 2382-2426.
- ⁵⁰ a) Sessler, J.L.; Wang, R. *Angew. Chem. Int. Ed.* **1998**, *37*, 1726-1729; b) Voegel, J.J.; Benner, S.A. *J. Am. Chem. Soc.* **1994**, *116*, 6929-6930; c) Faggiani, R.; Lock, C.J.L.; Lippert, B. *J. Am. Chem. Soc.* **1980**, *102*, 5418-5419.
- ⁵¹ Zimmerman, S.C.; Zeng, F.; Reichert, D.E.C.; Kolotuchin, S.V. *Science* **1996**, *271*, 1095-1098.
- ⁵² Geib, S.J.; Vincent, C.; Fan, E.; Hamilton, A.D. *Angew. Chem. Int. Ed. Engl.* **1993**, *32*, 119-121.
- ⁵³ a) Kolotuchin, S.V.; Thiessen, P.A.; Fenlon, E.E.; Wilson, S.R.; Loweth, C.J.; Zimmerman, S.C. *Chem. Eur. J.* **1999**, *5*, 2537-2544; b) Duchamp, D.J.; March, R.E. *Acta Crystallogr., Sect. B: Struct. Sci.* **1969**, *25*, 5-19.
- ⁵⁴ a) Rincon, A.M.; Prados, P, de Mendoza, J. *J. Am. Chem. Soc.* **2001**, *123*, 3493-3498; b) Vysotsky, M.O.; Pop, A.; Broda, F.; Thondorf, I.; Böhmer, V. *Chem. Eur. J.* **2001**, *7*, 4403-4410; c) Vysotsky, M.O.; Thondorf, I.; Böhmer, V. *Angew. Chem. Int. Ed.* **2000**, *39*, 1264-1267; d) Higler, I.; Grave, L.; Breuning, E.; Verboom, W.; de Jong, F.; Fyles, T.M.; Reinhoudt, D.N. *Eur. J. Org. Chem.* **2000**, 1727-1734; e) Rebek Jr., J. *Acc. Chem. Res.* **1999**, *32*, 278-286.
- ⁵⁵ Shivanyuk, A.; Paulus, E.F.; Böhmer, V. *Angew. Chem. Int. Ed.* **1999**, *38*, 2906-2909.
- ⁵⁶ a) Chen, J.; Körner, S.; Craig, S.L.; Rudkevich, D.M.; Rebek Jr., J. *Nature*, **2002**, *415*, 385-386; b) Chen, J.; Körner, S.; Craig, S.L.; Rudkevich, D.M.; Rebek Jr., J. *Proc. Natl. Acad. Sci. U.S.A.* **2002**, *99*, 2593-2596; c) Hayashida, O.; Shivanyuk, A.; Rebek Jr., J. *Angew. Chem. Int. Ed.* **2002**, *41*, 3423-3426; d) Renslo, A.R.; Tucci, F.C.; Rudkevich, D.M.; Rebek Jr., J. *J. Am. Chem. Soc.* **2000**, *122*, 4573-4582; e)

- Rebek Jr., *J. Chem. Commun.* **2000**, 637-643; f) Shivanyuk, A.; Rebek Jr., *J. Chem. Commun.* **2001**, 2374-2375.
- ⁵⁷ a) Smimizu, K.D.; Rebek Jr., *J. J. Proc. Natl. Acad. Sci. USA* **1995**, 92, 12403-12407; b) Cho, Y.L.; Rudkevich, D.M.; Shivanyuk, A.; Risannem K.; Rebek Jr., *J. Chem. Eur. J.* **2000**, 6, 3788-3796.
- ⁵⁸ a) Castellano, R.K.; Nuckolls, C.; Rebek Jr., *J. J. Am. Chem. Soc.* **1999**, 121, 11156-11163; b) Castellano, R.K.; Rebek Jr., *J. J. Am. Chem. Soc.* **1998**, 120, 3657-3663.
- ⁵⁹ Schalley, C.A.; Castellano, R.K.; Brody, M.S.; Rudkevich, D.M.; Rivera, J.M.; Siuzdak, G.; Rebek Jr., *J. J. Am. Chem. Soc.* **1999**, 121, 4568-4579.
- ⁶⁰ Cho, Y.L.; Rudkevich, D.M.; Rebek Jr., *J. J. Am. Chem. Soc.* **2000**, 122, 9868-9869.
- ⁶¹ a) Körner, S.; Tucci, F.; Rudkevich, D.; Heinz, T.; Rebek Jr., *J. Chem. Eur. J.* **2000**, 6, 187-195; b) Heinz, T.; Rudkevich, D.M.; Rebek Jr., *J. Angew. Chem. Int. Ed.* **1999**, 38, 1136-1139; c) Heinz, T.; Rudkevich, D.M.; Rebek Jr., *J. Nature* **1998**, 394, 764-766; d) Ma, S.; Rudkevich, D.M.; Rebek Jr., *J. J. Am. Chem. Soc.* **1998**, 120, 4977-4981.
- ⁶² Smeets, J.W.H.; Sijbesma, R.P.; van Dalen, L.; Spek, A.L.; Smeets, W.J.J.; Nolte, R.J.M. *J. Org. Chem.* **1989**, 54, 3710-3717.
- ⁶³ a) Wyler, R.; de Mendoza, J.; Rebek Jr., *J. Angew. Chem. Int. Ed. Engl.* **1993**, 32, 1699-1701; Articles on "Softballs": b) Rivera, J.M.; Martin, T.; Rebek, Jr. *J. J. Am. Chem. Soc.* **2001**, 123, 5213-5220; c) Rivera, J.M.; Craig, S.L.; Martin, T.; Rebek, Jr. *J. Angew. Chem. Int. Ed.* **2000**, 39, 2130-2132; d) Schalley, C.A.; Rivera, J.M.; Martín, T.; Santamaría, J.; Siuzdak, G.; Rebek Jr., *J. Eur. J. Org. Chem.* **1999**, 1325-1331; e) Meissner, R.; Garcias, X.; Mecozzi, S.; Rebek Jr., *J. J. Am. Chem. Soc.* **1997**, 119, 77-85.
- ⁶⁴ Martín, T.; Obst, U.; Rebek Jr., *J. Science* **1998**, 281, 1842-1845.
- ⁶⁵ a) Kobayashi, K.; Shirasaka, T.; Yamaguchi, K.; Sakamoto, S.; Horn, E.; Furakawa, N. *Chem. Commun.* **2000**, 41-42; b) Drain, C.M.; Fischer, R.; Nolen, E.G.; Lehn, J.-M. *J. Chem. Soc. Chem. Commun.* **1993**, 243-245.
- ⁶⁶ a) Atwood, J.L.; Barbour, L.J.; Jerga, A. *Chem. Commun.* **2001**, 2376-2377; b) Shivanyuk, A.; Rebek Jr., *J. Chem. Commun.* **2001**, 2374-2375; c) Brewster, R.E.; Shuker, S.B. *J. Am. Chem. Soc.* **2002**, 124, 7902-7903.

- ⁶⁷ a) Gellert, M.; Lipsett, M.N.; Davis, D.R. *Proc. Natl. Acad. Sci. USA* **1962**, *48*, 2013-2018; b) Guschlbauer, W.; Chantot, J.F.; Thiele, D.J. *J. Biomol. Struct. Dyn.* **1990**, *8*, 491-511.
- ⁶⁸ a) Davis, J.T.; Tirumala, S.; Jenssen, J.R.; Radler, E.; Fabris, D. *J. Org. Chem.* **1995**, *60*, 4167 - 4176; b) Gottarelli, G.; Masiero, S.; Spada, G.P. *J. Chem. Soc., Chem. Commun.* **1995**, 2555-2557.
- ⁶⁹ a) Shi, X.; Fettinger, J.C.; Davis, J.T. *Angew. Chem. Int. Ed.* **2001**, *40*, 2827-2831; b) Shi, X.; Fettinger, J.C.; Davis, J.T. *J. Am. Chem. Soc.* **2001**, *123*, 6738-6739; c) Forman, S.L.; Fettinger, J.C.; Pieraccini, S.; Gottarelli, G.; Davis, J.T. *J. Am. Chem. Soc.* **2000**, *122*, 4060-4067; d) Kotch, F.W.; Fettinger, J.C.; Davis, J.T. *Org. Lett.* **2000**, *2*, 3277-3280.
- ⁷⁰ Krische, M.J.; Lehn, J.-M.; Kyritsakas, N.; Fischer, J.; Wegelius, E.K.; Rissanen, K. *Tetrahedron* **2000**, *56*, 6701-6706.
- ⁷¹ X-ray structure of the 2D lattice of alternating CA and M molecules: Ranganathan, A.; Pedireddi, V.R.; Rao, C.N.R. *J. Am. Chem. Soc.* **1999**, *121*, 1752-1753.
- ⁷² a) Seto, C.T.; Whitesides, G.M. *J. Am. Chem. Soc.* **1990**, *112*, 6409-6411; b) Zerkowski, J.A.; Seto, C.T.; Wierda, D.A.; Whitesides, G.M. *J. Am. Chem. Soc.* **1990**, *112*, 9025-9026.
- ⁷³ Lehn, J.-M.; Mascal, M.; DeCian, A.; Fischer, J. *J. Chem. Soc., Chem. Commun.* **1990**, 479-480.
- ⁷⁴ Mathias, J.P.; Simanek, E.E.; Zerkowski, J.A.; Seto, C.T.; Whitesides, G.W. *J. Am. Chem. Soc.* **1994**, *116*, 4316-4325.
- ⁷⁵ Bielejewska, A.G.; Marjo, C.E.; Prins, L.J.; Timmerman, P.; de Jong, F.; Reinhoudt, D.N. *J. Am. Chem. Soc.* **2001**, *123*, 7518-7533.
- ⁷⁶ Vreekamp, R.H.; van Duynhoven, J.P.M.; Hubert, M.; Reinhoudt, D.N. *Angew. Chem. Int. Ed. Engl.* **1996**, *35*, 1215-1218.
- ⁷⁷ a) Jolliffe, K.A.; Timmerman, P.; Reinhoudt, D.N. *Angew. Chem. Int. Ed.* **1999**, *38*, 933-937; b) Paraschiv, V.; Crego-Calama, M.; Fokkens, R.H.; Padberg, C.J.; Timmerman, P.; Reinhoudt, D.N. *J. Org. Chem.* **2001**, *66*, 8297-8301; c) Prins, L.J.; Neuteboom, E.E.; Paraschiv, V.; Crego-Calama, M.; Timmerman, P.; Reinhoudt, D.N. *J. Org. Chem.* **2002**, *67*, 4808-4820.

- ⁷⁸ Fenniri, H.; Mathivanan, P.; Vidale, K.L.; Sherman, D.M.; Hallenga, K.; Wood, K.V.; Stowell, J.G. *J. Am. Chem. Soc.* **2001**, *123*, 3854-3855.
- ⁷⁹ Fenniri, H.; Deng, B.-L.; Ribbe, A.E. *J. Am. Chem. Soc.* **2002**, *124*, 11064-11072.
- ⁸⁰ Furka, A. Notarised report No. 36237, Hungary, **1982** on *Studies on Possibilities of Systematic Searching for Pharmaceutically Useful Peptides*.
- ⁸¹ Merrifield, R.B. *J. Am. Chem. Soc.* **1963**, *85*, 2149-2154.
- ⁸² Déprez, B.; Williard, X.; Bourel, L.; Coste, H.; Hyafil, F.; Tartar, A. *J. Am. Chem. Soc.* **1995**, *117*, 5405-5406.
- ⁸³ Lam, K.S.; Salmon, S.E.; Hersh, E.M.; Hruby, V.J.; Kazmiersky, W.M.; Knapp, R.J. *Nature* **1991**, *354*, 82-84.
- ⁸⁴ a) Furka, A. *Proceedings of the 14th International Congress of Biochemistry, Vol. 5*, VSP, Utrecht, **1988**, pp. 47; b) Furka, A.; Sebestyén, F.; Asgedom, M.; Dibo, G. *Int. J. Pept. Prot. Res.* **1991**, *37*, 487-493.
- ⁸⁵ Houghten, R.A.; Pinilla, C.; Blondelle, S.E.; Appel, J.R.; Dooley, C.T.; Cuervo, J.H. *Nature* **1991**, *354*, 84-86.
- ⁸⁶ a) Frank, R.; Heikens, W.; Heisterberg-Moutsis, G.; Blöcker, H. *Nucl. Acid. Res.* **1983**, *11*, 4365-4377; b) Geysen, H.M.; Meloen, R.H.; Barteling, S.J. *Proc. Natl. Acad. Sci. U.S.A.* **1984**, *81*, 3998-4002; c) Houghten, R. A. *Proc. Natl. Acad. Sci. U.S.A.* **1985**, *82*, 5131-5135.
- ⁸⁷ Dooley, C.T.; Chung, N.N.; Wilkes, B.C.; Schiller, P.W.; Bidlack, J.M.; Pasternak, G.W.; Houghten, R.A. *Science* **1994**, *266*, 2019-2022.
- ⁸⁸ Dooley, C.T.; Houghton, R.A. *Life Sci.* **1993**, *52*, 1509-1517.
- ⁸⁹ Brenner, S.; Lerner, R. A. *Proc. Natl. Acad. Sci. U.S.A.* **1992**, *89*, 5381-5383.
- ⁹⁰ Eliseev, A.V.; Nelen, M.N. *J. Am. Chem. Soc.* **1997**, *119*, 1147-1148.
- ⁹¹ Lam, K. S.; Zhao, Z.-G.; Wade, S.; Krchnak, V.; Lebl, M. *Drug. Dev. Res.* **1994**, *33*, 157-160.
- ⁹² Examples of combinatorial libraries of tweezer receptors: a) Braxmeier, T.; Demarcus, M.; Fessmann, T.; McAteer, S; Kilburn, J.D. *Chem. Eur. J.* **2001**, *7*, 1889-1898; b) Fessmann, T.; Kilburn, J.D. *Angew. Chem. Int. Ed.* **1999**, *38*, 1993-1996; c) Krebs, F.C.; Jorgensen, M. *J. Org. Chem.* **2001**, *66*, 6169-6173; d) Klarner, F.-G.; Burkert, U.; Kamieth, M.; Boese, R.; Benet-Buchholtz, J. *Chem. Eur. J.* **1999**,

- 5, 1700-1707; e) Markus, K.; Burkert, U.; Corbin, P.S.; Dell, S.J.; Zimmerman, S.C.; Klarner, F.-G. *Eur. J. Org. Chem.* **1999**, *11*, 2741-2749.
- ⁹³ Jensen, K.B.; Braxmeier, T.M.; Demarcus, M.; Frey, J.G.; Kilburn, J.D. *Chem. Eur. J.* **2002**, *8*, 1300-1309.
- ⁹⁴ Löwik, D.W.P.M.; Weingarten, M.D.; Broekema, M.; Brouwer, A.J.; Still, W.C.; Liskamp, R.M.J. *Angew. Chem. Int. Ed.* **1998**, *37*, 1846-1850.
- ⁹⁵ a) Opatz, T.; Liskamp, R.M.J. *J. Comb. Chem.* **2002**, *4*, 275-284; b) van Wageningen, A.M.A.; Liskamp, R.M.J. *Tetrahedron Lett.* **1999**, *40*, 9347-9351.
- ⁹⁶ Monnee, M.C.F.; Brouwer, A.J.; Verbeek, L.M.; van Wageningen, A.M.A.; Liskamp, R.M.J. *Bioorg. Med. Chem. Lett.* **2001**, *11*, 1521-1525.
- ⁹⁷ Opatz, T.; Liskamp, R.M.J. *Org. Lett.* **2001**, *3*, 3499-3502.
- ⁹⁸ Xu, R.; Greiveldinger, G.; Marenus, L.E.; Cooper, A.; Ellman, J.A. *J. Am. Chem. Soc.* **1999**, *121*, 4898-4899.
- ⁹⁹ a) Park, H.S.; Lin, Q.; Hamilton, A.D. *J. Am. Chem. Soc.* **1999**, *121*, 8-13; b) Hamuro, Y.; Crego-Calama, M.; Park, H.S.; Hamilton, A.D. *Angew. Chem. Int. Ed.* **1997**, *36*, 2680-2683.
- ¹⁰⁰ Jain, R.K.; Hamilton, A.D. *Org. Lett.* **2000**, *2*, 1721-1723.
- ¹⁰¹ a) Borchardt, A.; Still, W.C. *J. Am. Chem. Soc.* **1994**, *115*, 373-374; b) Still, W.C. *Acc. Chem. Res.* **1996**, *29*, 155-163.
- ¹⁰² a) Cheng, Y.A.; Suenaga, T.; Still, W.C. *J. Am. Chem. Soc.* **1996**, *118*, 1813-1814; b) Boyce, R.; Li, G.; Nestler, H.P.; Suenaga, T.; Still, W.C. *J. Am. Chem. Soc.* **1994**, *116*, 7955-7956.
- ¹⁰³ Review about dynamic combinatorial chemistry, partially focused on the difference between “classical” and dynamic combinatorial chemistry: Lehn, J.-M. *Chem. Eur. J.* **1999**, *5*, 2455-2463.
- ¹⁰⁴ Rowan, S.J.; Cantrill, S.J.; Cousins, G.R.L.; Sanders, J.K.M.; Stoddart, J.F. *Angew. Chem. Int. Ed.* **2002**, *41*, 898-952.
- ¹⁰⁵ Huc, I.; Lehn, J.-M. *Proc. Natl. Acad. Sci. U.S.A.* **1997**, *94*, 2106-2110.
- ¹⁰⁶ Otto, S.; Sanders, J.K.M. *J. Am. Chem. Soc.* **2000**, *122*, 12063-12064.
- ¹⁰⁷ a) Crego-Calama, M.; Hulst, R.; Fokkens, R.; Nibbering, N.M.M.; Timmerman, P.; Reinhoudt, D.N. *Chem. Commun.* **1998**, 1021-1022; b) Crego-Calama, M.; Timmerman, P.; Reinhoudt, D.N. *Angew. Chem. Int. Ed.* **2000**, *39*, 755-758.

- ¹⁰⁸ Baxter, P.N.W.; Khoury, R.G.; Lehn, J.-M.; Baum, G.; Fenske, D. *Chem. Eur. J.* **2000**, *6*, 4140-4148.
- ¹⁰⁹ a) Ramström, O.; Lehn, J.-M. *Nature Reviews, Drug Discovery*, **2002**, *1*, 26-36; b) Rowan, S.J.; Cantrill, S.J.; Cousins, G.R.L.; Sanders, J.K.M.; Stoddart, J.F. *Angew. Chem. Int. Ed.* **2002**, *41*, 898-952; c) Otto, S.; Furlan, R.L.E.; Sanders, J.K.M. *Curr. Opin. Chem. Biol.* **2002**, *6*, 321-327; d) Lehn, J.-M.; Eliseev, A.E. *Science* **2001**, *291*, 2331-2332; e) Cousins, G.R.L.; Poulsen, S.-A.; Sanders, J.K.M. *Curr. Opin. Chem. Biol.* **2000**, *4*, 270-279; f) Eliseev, A.V.; Lehn, J.-M. *Combinatorial Chemistry in Biology, Vol. 5*, (Eds.: Famulok, M.; Winnacker, E.-L.; Wong, C.-H.), Springer, Tübingen, **1998**, pp. 159-172; g) Brady, P.A.; Sanders, J.K.M. *Chem. Soc. Rev.* **1997**, *26*, 327-336.
- ¹¹⁰ Brady, P.A.; Sanders, J.K.M. *J. Chem. Soc., Perkin. Trans. 1* **1997**, 3237-3253.
- ¹¹¹ Swann, P.G.; Casanova, R.A.; Desai, A.; Frauenhoff, M.M.; Urbancic, M.; Slomczynska, U.; Hopfinger, A.J.; LeBreton, G.C.; Venton, D.L. *Biopolymers* **1996**, *40*, 617-625.
- ¹¹² Star, A.; Goldberg, I.; Fuchs, B. *Angew. Chem. Int. Ed. Engl.* **2000**, *39*, 2685-2689.
- ¹¹³ Polyakov, V.A.; Nelen, M.I.; Nazarpack-Kandlousy, N.; Ryabov, A.D.; Eliseev, A.V. *J. Phys. Org. Chem.* **1999**, *12*, 357-363.
- ¹¹⁴ Giger, T.; Wigger, M.; Audetat, S.; Benner, S.A. *Synlett.* **1998**, 688-691.
- ¹¹⁵ Brady, P.A.; Bonar Law, R.P.; Rowan, S.J.; Suckling, C.J.; Sanders, J.M.K. *Chem. Commun.* **1996**, 319-320.
- ¹¹⁶ Hioki, H.; Still, W.C. *J. Org. Chem.* **1998**, *63*, 904-905.
- ¹¹⁷ Furlan, R.L.E.; Ng, Y.-F.; Otto, S.; Sanders, J.M.K. *J. Am. Chem. Soc.* **2001**, *123*, 8876-8877.
- ¹¹⁸ Cousins, G.R.L.; Poulsen, S.-A.; Sanders, J.K.M. *Chem. Commun.* **1999**, 1575-1576.
- ¹¹⁹ a) Cousins, G.R.L.; Furlan, R.L.E.; Ng, Y.-F.; Redman, J.E.; Sanders, J.K.M. *Angew. Chem. Int. Ed.* **2001**, *40*, 423-428; b) Furlan, R.L.E., Ng, Y.-F.; Redman, J.E.; Sanders, J.K.M. *Tetrahedron* **2002**, *58*, 771-778.
- ¹²⁰ Poulsen, S.-A.; Gates, P.J.; Cousins, G.R.L.; Sanders, J.K.M. *Rapid Commun. Mass Spectrom.* **2000**, *14*, 44-48.
- ¹²¹ Roberts, S.L.; Furlan, R.L.E.; Cousins, G.R.L.; Sanders, J.K.M. *Chem. Commun.* **2002**, 938-939.

- ¹²² Eliseev, A.V.; Nelen, M.N. *J. Am. Chem. Soc.* **1997**, *119*, 1147-1148.
- ¹²³ Berl, V.; Huc, I.; Lehn, J.-M.; DeCian, A.; Fischer, J. *Eur. J. Org. Chem.* **1999**, 3089-3094.
- ¹²⁴ a) Albrecht, M. *J. Inclusion Phenom. Macrocyclic Chem.* **2000**, *36*, 127-151; b) Johnson, D.W.; Raymond, K.N. *Supramol. Chem.* **2001**, *13*, 639-659.
- ¹²⁵ Goodman, M.S.; Jubian, V.; Linton, B.; Hamilton, A.D. *J. Am. Chem. Soc.* **1995**, *117*, 11610-11611.
- ¹²⁶ Lehn, J.-M. *Supramolecular Chemistry: Concepts and Perspectives*; VCH, Weinheim, **1995**, pp. 139-197.
- ¹²⁷ a) Hasenknopf, B.; Lehn, J.-M.; Kneisel, B.O.; Baum, G.; Fenske, D. *Angew. Chem. Int. Ed. Engl.* **1996**, *35*, 1838-1840; b) Hasenknopf, B.; Lehn, J.-M.; Boumediene, N.; Dupont-Gervais, A.; van Dorsselaer, A.; Kneisel, B.O.; Fenske, D. *J. Am. Chem. Soc.* **1997**, *119*, 10956-10962.
- ¹²⁸ Baxter, P.N.W.; Khoury, R.G.; Lehn, J.-M.; Baum, G.; Fenske, D. *Chem. Eur. J.* **2000**, *6*, 4140-4148.
- ¹²⁹ Sakai, S.; Shigemasa, Y.; Sasaki, T. *Tetrahedron Lett.* **1997**, *38*, 8145-8148.
- ¹³⁰ Huc, I.; Krische, M.J.; Funeriu, D.P.; Lehn, J.-M. *Eur. J. Inorg. Chem.* **1999**, 1415-1420.
- ¹³¹ Hiraoka, S.; Kubota, Y.; Fujita, M. *Chem. Commun.* **2000**, 1509-1510.
- ¹³² a) Klekota, B.; Hammond, M.H.; Miller, B.L. *Tetrahedron Lett.* **1997**, *38*, 8639-8642; b) Klekota, B.; Miller, B.L. *Tetrahedron* **1999**, *55*, 11687-11697.
- ¹³³ Karan, C.; Miller, B.L. *J. Am. Chem. Soc.* **2001**, *123*, 7455-7456.
- ¹³⁴ Hof, F.; Nuckolls, C.; Rebek Jr., J. *J. Am. Chem. Soc.* **2000**, *122*, 4251-4252.
- ¹³⁵ a) Martín, T.; Obst, U.; Rebek Jr., J. *Science* **1998**, *281*, 1842-1845; b) Nuckolls, C.; Hof, F.; Martín, T.; Rebek Jr., J. *J. Am. Chem. Soc.* **1999**, *121*, 10281-10285.
- ¹³⁶ Schalley, C.A.; Martín, T.; Obst, U.; Rebek Jr., J. *J. Am. Chem. Soc.* **1999**, *121*, 2133-2138.
- ¹³⁷ Goral, V.; Nelen, M.N.; Eliseev, A.V.; Lehn, J.-M. *Proc. Natl. Acad. Sci. U.S.A.* **2001**, *98*, 1347-1352.
- ¹³⁸ Bunyapaiboonsri, T.; Ramström, O.; Lohmann, S.; Lehn, J.-M.; Peng, L.; Goeldner, M. *ChemBioChem* **2001**, *2*, 438-444.

Chapter 3

Self-Assembly of Polar Functionalities using Hydrogen-Bonded Rosette Assemblies*

With the objective to generate noncovalent receptor assemblies, the formation and stability of functionalized double rosette assemblies is investigated. In this chapter, the thermodynamic stability of functionalized double rosette assemblies is described as studied by ^1H NMR titrations with $\text{DMSO-}d_6$, and by CD titrations with THF. Assemblies containing six ureido or amido functionalities show a significantly higher stability than the non-functionalized assembly. Structural analysis by ^1H NMR spectroscopy indicates that the higher stability of the ureido and amido derivatives is the result of the formation of an additional hydrogen bond between the urea or amide proton and the nitrogen atom (N-1) of the triazine ring.

* Part of this work has been published: Kerckhoffs, J.M.C.A.; Crego-Calama, M.; Luyten, I.; Timmerman, P.; Reinhoudt, D.N. *Org. Lett.* **2000**, 2, 4121-4124.

3.1 Introduction

The concave 3-D positioning of different amino acid residues around a central cavity via noncovalent interactions provides the basis for natural receptors to bind substrates and catalyze (bio)chemical transformations with exquisite regio- and stereoselectivity.¹ Efforts to mimic such functional group arrays in covalent² or metal-coordinated systems³ have recently led to the synthesis of artificial protein receptors mimicking the binding properties of natural antibodies.⁴ One of the alternatives that has received increasing attention is the synthesis of nanostructures using weak noncovalent interactions, like hydrogen bonding.⁵ Such structures are formed under thermodynamically controlled conditions, generally in quantitative yield. Biological systems construct and modify such functional nanoscale structures with startling efficiency. Natural antibodies provide the perfect example, since they consist of four different peptide chains (two heavy (H) and two light (L) chains, Figure 3.1) that are held together mainly by noncovalent interactions, and are reinforced by covalent disulfide bonds.⁶

For the design of synthetic receptors in our group, a strategy is used that is similar to the natural self-assembly approach. Instead of utilizing the self-assembling properties of high molecular weight polypeptides, synthetic self-assembling platforms are constructed using multiple hydrogen bonds to give a double rosette motif (see Chapter 2). Subsequently, functionalization of the individual building blocks with small oligopeptide fragments (X or Y) would give noncovalent assemblies of oligopeptides that generate a potential guest-binding site. Structural diversity in the guest-binding site can be generated at a covalent (variation in amino acid sequence of the oligopeptides) or at a noncovalent supramolecular level (by a combination of the different functionalized building blocks, see Figure 3.1b).

The self-assembly of polar functionalities using noncovalent interactions has so far received very little attention, presumably due to incompatibility with the noncovalent scaffolds.⁷ It is known that the attachment of hydrogen bond donating or accepting groups to hydrogen-bonded capsules can break the assembly. However, Rebek and co-workers successfully synthesized noncovalent capsules consisting of two calix[4]arenes substituted with ureido functionalities at the upper rim and amide functionalities at the lower rim.⁸

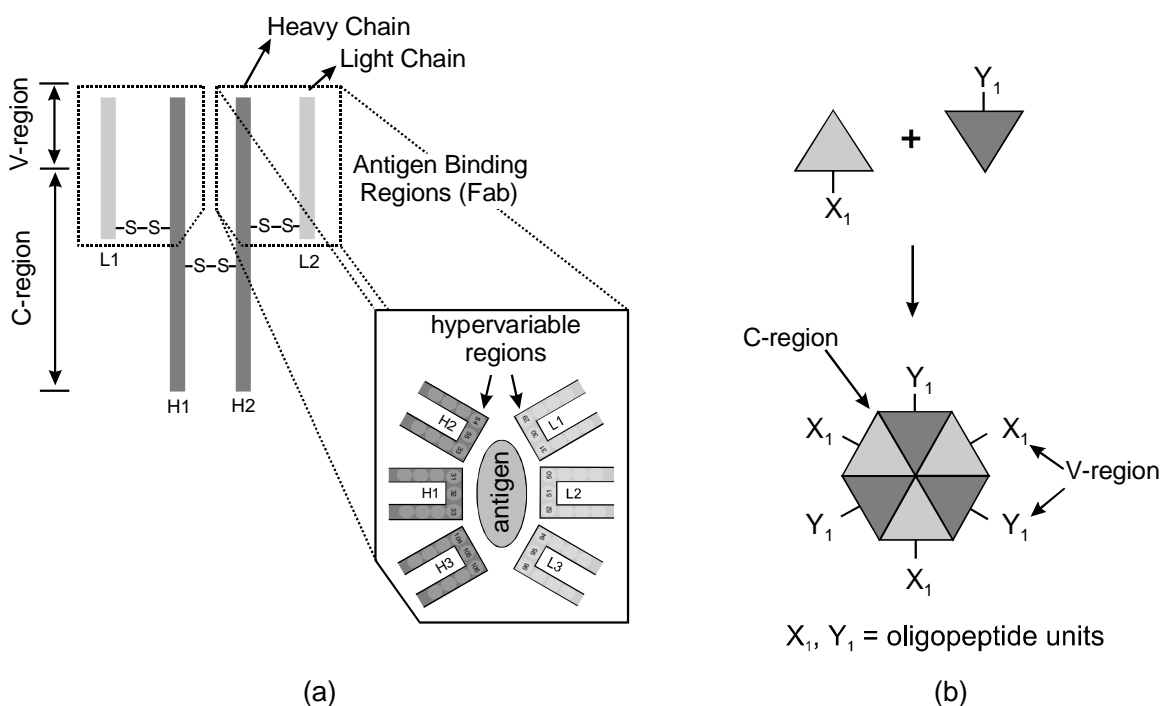


Figure 3.1. (a) Schematic representation of FAB region in natural antibodies, and (b) Self-assembly of oligopeptide units via synthetic self-assembling platforms.

The research started out from the introduction of simple polar functionalities, like amines, amides and ureas as model compounds (described in this chapter) and then moved on to the introduction of amino acids and small peptide fragments (Chapter 4). In this chapter, it is shown that hydrogen bond directed self-assembly (double rosette assemblies, Section 3.2) can indeed be used to assemble simple polar functionalities.

Before discussing the results with polar group functionalized hydrogen-bonded assemblies (Section 3.4), the formation (Section 3.2) and characterization (Section 3.3) of the double rosette assemblies are described.

3.2 Formation of Double Rosette Assemblies

Earlier work in our group has shown the noncovalent synthesis of double rosette assemblies $\mathbf{1}_3 \cdot (\text{DEB/CYA})_6$ via the cooperative formation of 36 hydrogen bonds ($\Delta H^\circ < 0$), using the rosette motif introduced by Whitesides.⁹ The assemblies are formed spontaneously by mixing calix[4]arene dimelamines **1** with either 2 equivalents of barbiturates (BAR) or cyanurates (CYA) in apolar solvents such as chloroform, toluene,

or benzene (Figure 3.2). The assemblies consist of two flat rosette motifs connected via the calix[4]arene moieties (see Section 2.2.3).

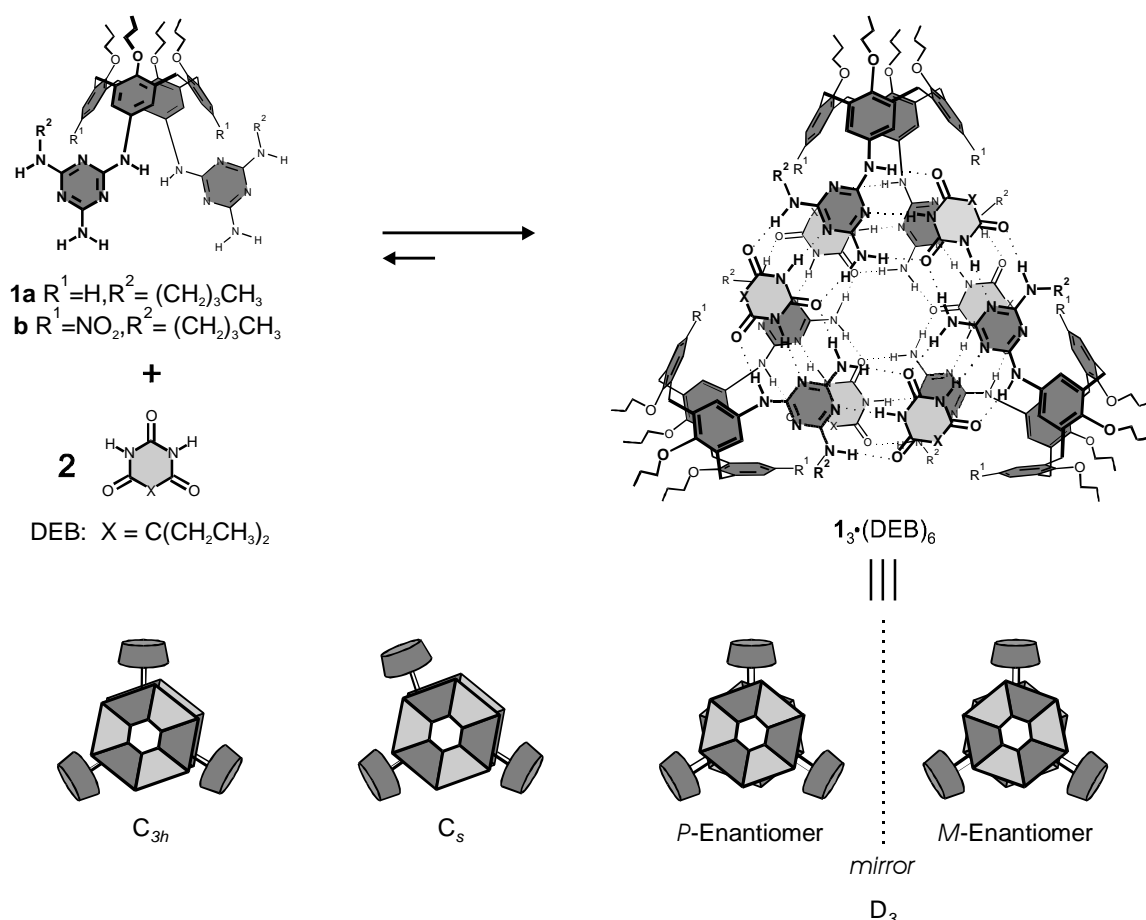


Figure 3.2. Formation of double rosette assembly $1_3 \cdot (DEB)_6$, and the three isomeric forms: staggered (D_3), symmetrical eclipsed (C_{3h}), and unsymmetrical eclipsed (C_s).

The assemblies can exist in three different isomeric forms (Figure 3.2). The D_3 isomer (staggered), has the two melamines in an antiparallel orientation. Consequently, the staggered assembly is chiral (for more details on chirality see Section 3.3). The C_{3h} isomer and the C_s isomer (both eclipsed), have both melamines facing the same side of the calix[4]arene. The difference between C_s and C_{3h} is the 180° rotation of one of the calix[4]arene dimelamines in the case of the C_s . Both assemblies contain a horizontal symmetry plane and are therefore achiral. Earlier studies¹⁰ showed that hydrogen-bonded assemblies formed by the calix[4]arene dimelamines and 5,5-disubstituted barbituric acid derivatives preferentially form the D_3 -isomer. However, the structures of rosette assemblies formed with 5-substituted cyanuric acid derivatives are less predictable. Steric

factors play an important role in the distribution of the possible isomers. The D_3 isomer is the most common one and when not mentioned otherwise in this thesis, this is the isomer that is formed.

3.3 Characterization of Double Rosette Assemblies

Double rosette assemblies can conveniently be characterized by ^1H NMR spectroscopy.^{9a} ^1H NMR titration experiments have clearly proven the 1:2 (calix[4]arene dimelamine versus DEB/CYA) stoichiometry of the assembly. Upon formation of the assembly the diagnostic signals of the imide NH protons of DEB/CYA are observed between $\delta = 13$ and 16 ppm. Depending on the isomeric form of the assembly, 2 (for the D_3 and the C_{3h}) or 6 (for the C_s) different sets of signals for these imide NH protons are observed.

Hydrogen-bonded assemblies are difficult to detect by mass spectrometry due to the ease of destruction of the assemblies upon ionization by strong acids like TFA. Therefore, Ag^+ labeling MALDI-TOF mass spectrometry is used,¹¹ a technique that is extremely mild and provides a nondestructive way to generate charged assemblies. This method is based on the high affinity of Ag^+ for a variety of aromatic π -donors and cyano groups.

Furthermore, the X-ray crystal structure of assembly $\mathbf{1b}_3 \cdot (\text{DEB})_6$ shows that the calix[4]arene molecules are fixed in a *pinched cone* conformation (Figure 3.3). This conformation allows participation of the calix[4]arene units in both the upper and the lower rosette motifs simultaneously. The two rosette motifs are stacked on top of each other with a separation from 3.5 Å at the edges to 3.2 Å in the center of the rosette.^{9a}

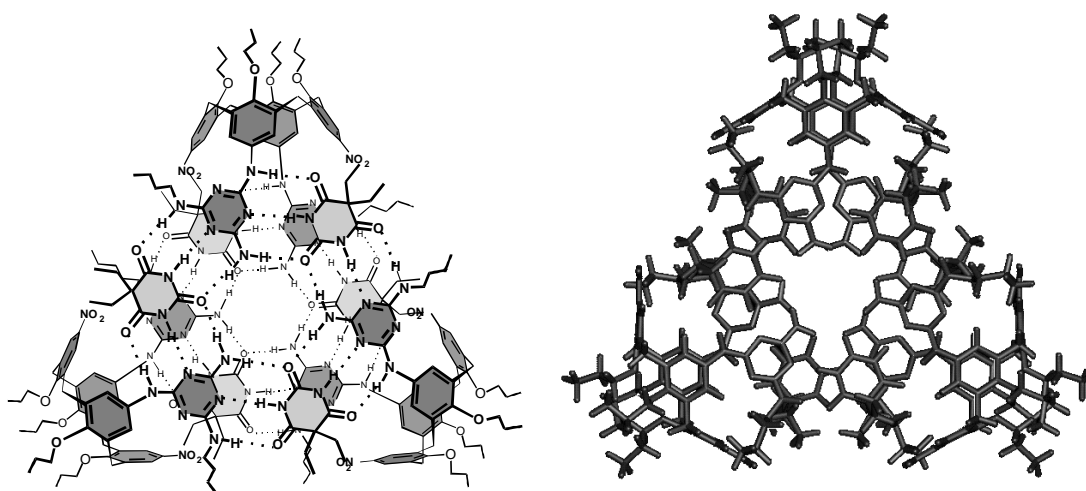


Figure 3.3. X-Ray crystal structure of assembly $\mathbf{1b}_3 \cdot (\text{DEB})_6$.

X-Ray crystallography and NMR experiments showed that assembly $1_3 \cdot (\text{DEB})_6$ exists exclusively as the D_3 isomer, which means that this assembly displays supramolecular chirality.^{9a} The chirality is caused by the antiparallel orientation of the two melamines, which can either be oriented clockwise (*P*) or counterclockwise (*M*). In the absence of any other source of chirality, the assemblies exist as a racemic mixture of the *P*- and *M*-enantiomers. The introduction of chiral substituents on the periphery of the rosette leads to the formation of diastereomers instead of enantiomers. The degree of the chiral induction depends on the difference in free energy at thermodynamic equilibrium. The degree of induction is mainly effected by the proximity of the chiral centers to the core of the assembly and by the solvent.¹² Circular dichroism (CD) spectroscopy, a technique based on the different absorption of left- and right-handed circularly polarized light by chiral molecules ($\epsilon_L \neq \epsilon_R$),¹³ can be used for the characterization of chiral rosette assemblies. The chiral calix[4]arene double rosettes display highly characteristic CD spectra, while the individual components are hardly CD-active.

3.4 Results and Discussion

3.4.1 Functionalization of Double Rosette Assemblies

In view of the objective to generate functional group diversity in or around noncovalently assembled cavities for the synthesis of molecular receptors, the thermodynamic stability of different functionalized assemblies was studied. Previous work in our group showed that functionalization of position R^1 (see Chart 3.2) with hydrogen bond donating or accepting or bulky groups significantly reduces the thermodynamic stability of the assemblies.^{9a} The hydrogen bond donating or accepting groups can form intramolecular hydrogen bonds that interfere with the rosette platform and the bulky groups can cause steric strain in the assembly. In this chapter the thermodynamic stability of assemblies functionalized at the R^2 position is described (Chart 3.1). First, the assembly of calix[4]arene dimelamines **2a-e** carrying amino (**2a**), ureido (**2b**), amido (**2c**), sulfonamido (**2d**), and phosphoramido (**2e**) functionalities that are connected via a 2,2-dimethylpropyl spacer to the melamine units was studied (Chart 3.1). Furthermore, the influence of the spacer on the assembly formation was studied by the use of a propyl spacer (**3a-c**) instead of the more bulky 2,2-dimethylpropyl spacer (**2a-e**).

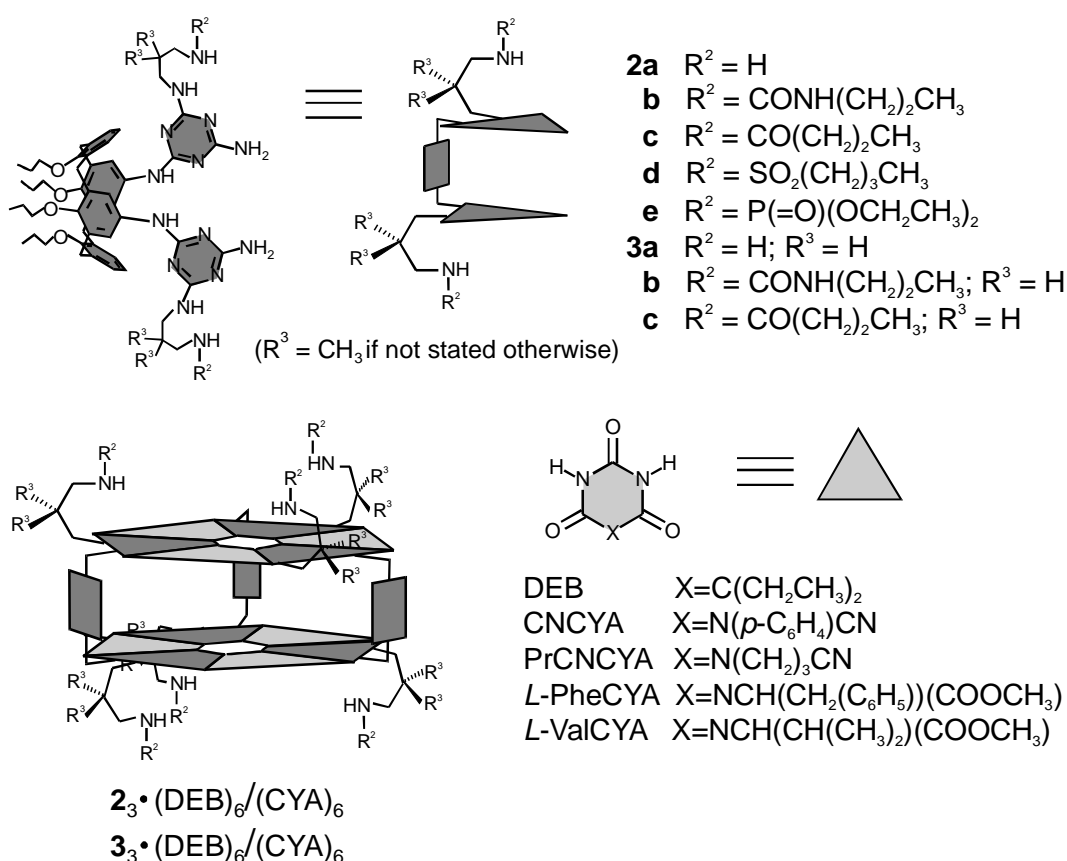


Chart 3.1. Molecular structures and schematic representations of the molecular components 2-3 and the corresponding hydrogen-bonded assemblies $2_3 \cdot (\text{DEB})_6 / (\text{CYA})_6$ and $3_3 \cdot (\text{DEB})_6 / (\text{CYA})_6$.

3.4.2 Synthesis and Characterization of the Assemblies with Polar Functionalities

Dimelamines **1** and bis(chlorotriazine) **4** were synthesized following literature procedures.^{9a} Dimelamines **2** were synthesized starting from bis(chlorotriazine) **4** via reaction with an excess of 2,2-dimethyl-1,3-propane diamine (**2a**, >95%), followed by reaction with propyl isocyanate (**2b**, 78%), butyryl chloride (**2c**, 53%), butanesulfonyl chloride (**2d**, 50%), or diethyl phosphoryl chloride (**2e**, 47%). Similarly, dimelamines **3** were synthesized by a reaction of bis(chlorotriazine) **4** with an excess of 1,3-propane diamine (**3a**, >95%), followed by reaction with propyl isocyanate (**3b**, 89%), or butyryl chloride (**3c**, 70%).

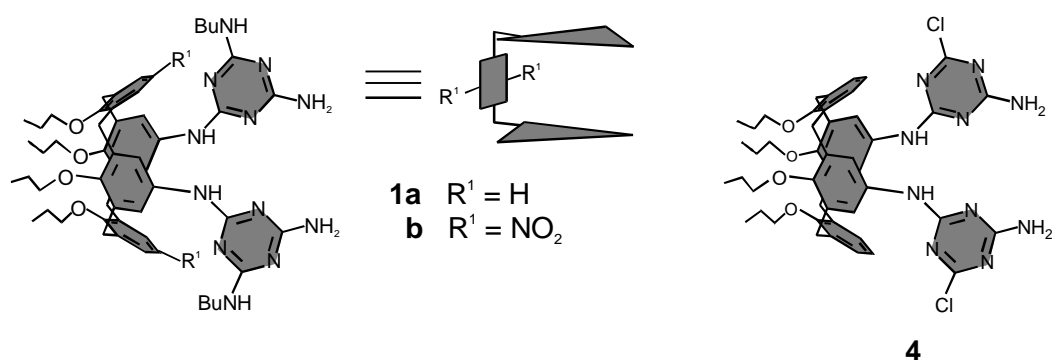


Chart 3.2. Molecular structures and schematic representations of the molecular components **1** and **4**.

Without exception the ^1H NMR spectra of the assemblies $\mathbf{2}_3 \bullet (\text{DEB})_6$ and $\mathbf{3}_3 \bullet (\text{DEB})_6$ exhibit the diagnostic signals at 14.1-14.0 (H_a), 13.3-13.2 (H_b), 8.6-8.4 (H_c), 7.8-7.6 (H_d), 6.7 (H_e), 6.9-7.1 (H_f), 7.1-7.0 (H_g), 6.1-6.0 (H_h) (Figure 3.4). The assemblies are formed in yields varying from 75-99% as determined by integration of the appropriate ^1H NMR signals.¹⁴

Characterization of the corresponding assemblies $\mathbf{2}_3 \bullet (\text{CNCYA})_6$, and $\mathbf{3}_3 \bullet (\text{PrCNCYA})_6$ by MALDI-TOF using Ag^+ -labeling¹¹ also confirmed the successful formation of the hydrogen-bonded assemblies (Table 3.1). The only exceptions are assembly $\mathbf{2a}_3 \bullet (\text{CNCYA})_6$ and $\mathbf{3a}_3 \bullet (\text{PrCNCYA})_6$ which are unstable due to proton transfer between the strongly acidic PrCNCYA ($\text{pK}_a \sim 4.7$) and the basic amino function in the melamine.

Table 3.1. MALDI-TOF mass spectrometry characterization of assemblies $\mathbf{2b}_3 \bullet (\text{CNCYA})_6$ - $\mathbf{2e}_3 \bullet (\text{CNCYA})_6$, $\mathbf{3b}_3 \bullet (\text{PrCNCYA})_6$, and $\mathbf{3c}_3 \bullet (\text{PrCNCYA})_6$ after Ag^+ -labeling.

Assembly	Calc. Mass (Da) of Ag^+ -complex	Observed Mass (Da)
$\mathbf{2b}_3 \bullet (\text{CNCYA})_6$	5029.4	5031.0
$\mathbf{2c}_3 \bullet (\text{CNCYA})_6$	4939.3	4942.4
$\mathbf{2d}_3 \bullet (\text{CNCYA})_6$	5239.2	5240.1
$\mathbf{2e}_3 \bullet (\text{CNCYA})_6$	5271.3	5274.6
$\mathbf{3b}_3 \bullet (\text{PrCNCYA})_6$	4657.3	4661.2
$\mathbf{3c}_3 \bullet (\text{PrCNCYA})_6$	4567.2	4572.2

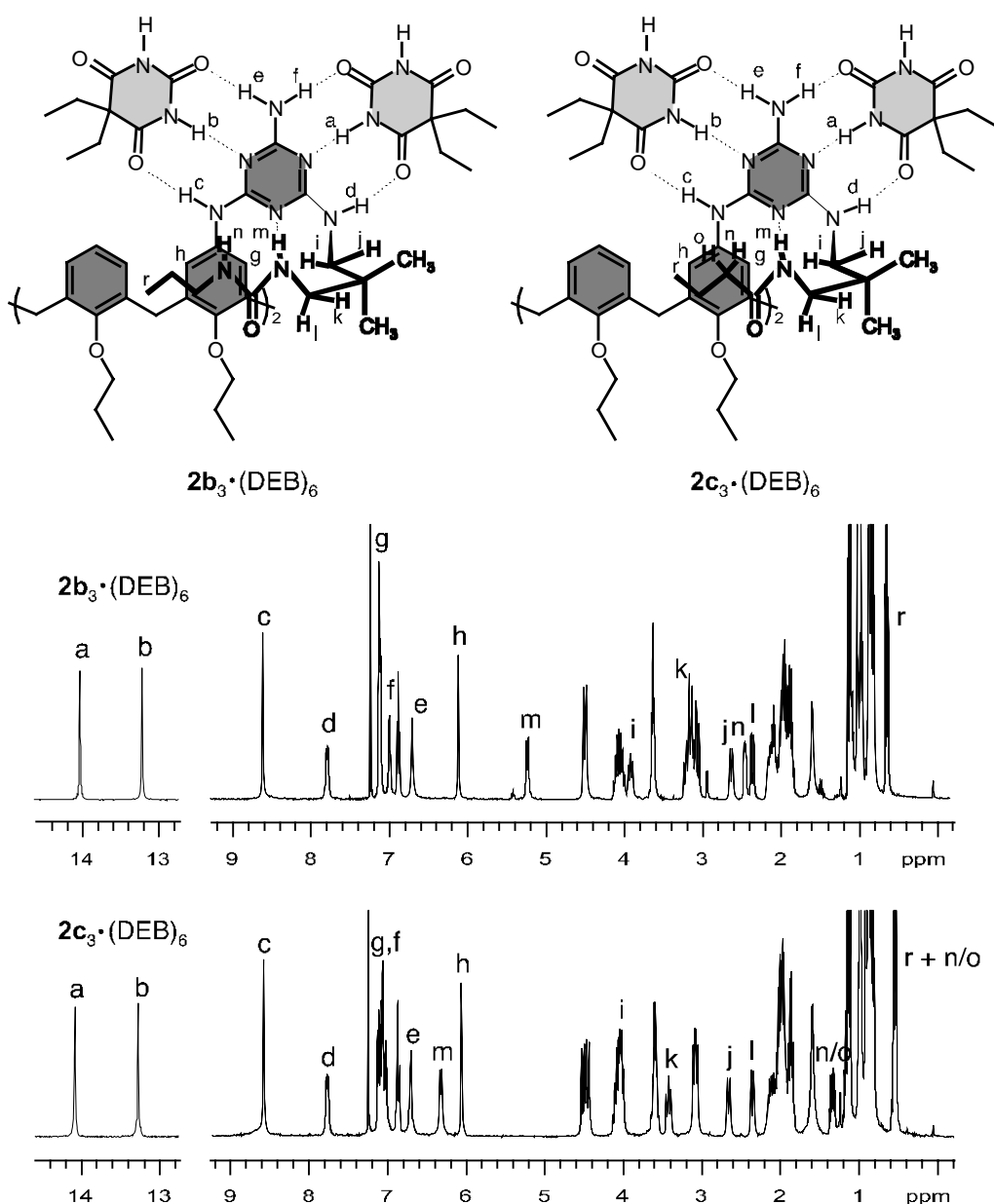


Figure 3.4. Characterization of assemblies $2b_3 \cdot (\text{DEB})_6$ and $2c_3 \cdot (\text{DEB})_6$ by ^1H NMR spectroscopy. Spectra were recorded at 400 MHz in CDCl_3 at 303K.

3.4.3 Thermodynamic Stability

The spontaneous assembly of the calix[4]arene double rosettes in apolar solvents is an enthalpy-driven process that involves the cooperative formation of 36 hydrogen bonds. However, the change in entropy is unfavorable, because upon assembly the translational and rotational degrees of freedom of 9 molecular components are significantly reduced. The overall change in free energy (ΔG°) is negative.

The effect of amino (**2a**), ureido (**2b**) and amido (**2c**) functionalities on the thermodynamic stability of the corresponding hydrogen-bonded assemblies was investigated by ^1H NMR titrations with $\text{DMSO-}d_6$ (see Table 3.2).¹⁵ It was found that the stability of assemblies **2b**₃•(DEB)₆ and **2c**₃•(DEB)₆, carrying six ureido and six amido functionalities, respectively, is significantly higher ($\chi_{\text{DMSO}} = 14$ and 15) than the corresponding assembly **1**₃•(DEB)₆ ($\chi_{\text{DMSO}} = 10$). The stability of assembly **2a**₃•(DEB)₆ is equal to that of **1**₃•(DEB)₆, indicating that there is no effect of the amino substituents.

Table 3.2. Thermodynamic stability measurements of assemblies **2**₃•(DEB)₆ and **2**₃•(CYA)₆.

Assembly	χ_{DMSO} ^[a]	Assembly	χ_{THF} ^[a]
1a ₃ •(DEB) ₆	10	1a ₃ •(L-PheCYA) ₆	34
2a ₃ •(DEB) ₆	10	2b ₃ •(L-PheCYA) ₆	31
2b ₃ •(DEB) ₆	14	2c ₃ •(L-PheCYA) ₆	35
2c ₃ •(DEB) ₆	15	2b ₃ •(L-ValCYA) ₆	34
		2c ₃ •(L-ValCYA) ₆	34 (29) ^[b]

^[a] χ = percentage of polar solvent at which 50% of the assembly is still intact.

^[b] independently determined by THF ^1H NMR titration.

Structural analysis of the assemblies **2b**₃•(DEB)₆ and **2c**₃•(DEB)₆ by ^1H NMR spectroscopy using 2D DQF¹⁶, TOCSY¹⁷ and NOESY¹⁸ experiments clarifies the reasons for the improved stability. In both cases, the 2,2-dimethylpropyl side chain adopts a very rigid conformation as judged from the presence of strong NOE connectivities between H_d and H_j and between H_i and H_m , respectively, and the absence of NOE connectivities between H_d and H_i and between H_k and H_m , respectively (see Figure 3.4 for description of the protons). For assembly **2b**₃•(DEB)₆, the two urea proton signals resonate at very different chemical shifts in the ^1H NMR spectrum, *i.e.* at 5.2 (H_m) and 2.4 ppm (H_n) and H_n shows a distinguished NOE cross peak with one of the propoxy groups of the calix[4]arene unit. Therefore, it was suggested that the side chain is folded back over the calix[4]arene aromatic rings resulting in a highfield chemical shift for H_n because of an anisotropic shielding effect of one of the calix[4]arene aromatic rings. The folding back can be explained by the fact that the other urea proton (H_m) is involved in hydrogen bonding with one of the nitrogen atoms (N-1) of the triazine ring. This view is supported by the fact that the urea proton signals do not shift at all upon the addition of chloride (1-

2 equiv.) or carboxylate (1-2 equiv.) anions, while free urea groups normally interact strongly with these anions, giving rise to 1-2 ppm downfield shifts.¹⁹ Gas-phase molecular modeling calculations (Quanta 97, CHARMM 24.0) in which the observed NOE connectivities were used as distance constraints gave a structure in which the propylureido groups fold back over the calix[4]arene units.

Structural analysis of assembly $2c_3 \cdot DEB_6$ showed similar results. The amide protons (H_m) resonate at 6.33 ppm, while the double triplets observed for the methylene protons ($NH_mC(O)CH_nH_o$) are strongly upfield shifted ($\delta = 1.4$ and 0.6 ppm, respectively) from their normal position between 2 to 3 ppm. These methylene protons also show an NOE cross peak with one of the propoxy groups of the calix[4]arene unit which means that they occupy a well-defined position on top of the electron-rich aromatic ring of the calix[4]arene unit. Moreover, the $NHC(O)CH_2CH_2CH_3$ protons also experience upfield shifts ($\delta = 1.2$ and 0.54 ppm), albeit much smaller. Also in this case, gas-phase molecular modeling studies reproduce the hydrogen bonding interaction between the amide proton and the triazine nitrogen (N-1) (Figure 3.5).

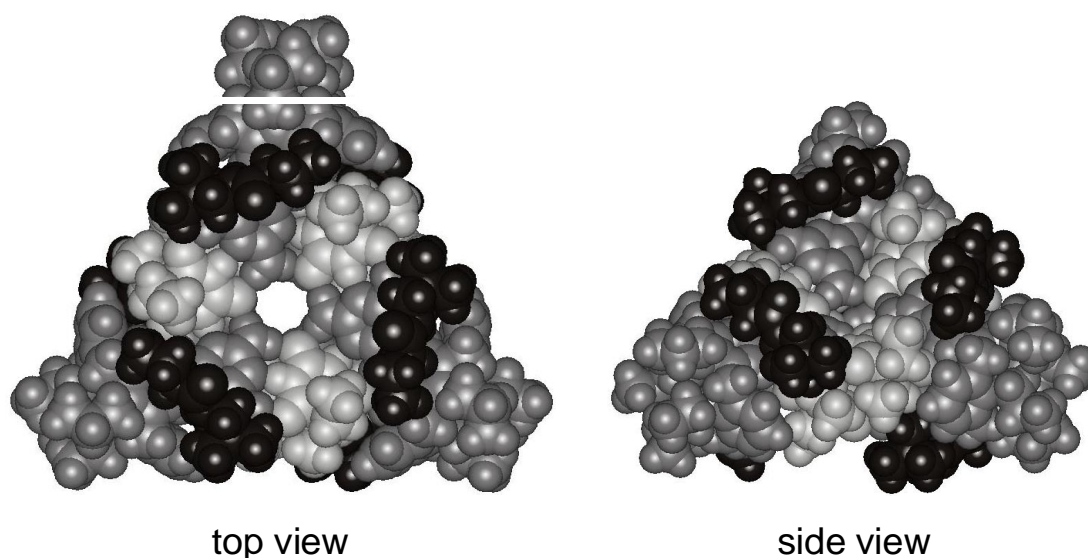


Figure 3.5. Gas-phase-minimized structure of assembly $2c_3 \cdot (DEB)_6$ using the observed NOE connectivities as distance constraints. The dark grey parts represent the calix[4]arene dimelamine components, the light grey parts the barbiturate fragments, and the black parts the amido side chains.

The stability of the functionalized assemblies was also studied by CD spectroscopy via the addition of THF (Table 3.2). These measurements are based on the fact that

double rosette assemblies with chiral cyanurates, like *L*-ValCYA and *L*-PheCYA (see Chart 3.1), display very intense and characteristic CD spectra, which are not observed for the individual components.^{5a,20} For assemblies $2_3 \bullet (L\text{-PheCYA})_6$ and $2_3 \bullet (L\text{-ValCYA})_6$ (Figure 3.6) with ureido (**2b**) and amido (**2c**) functionalities, the thermodynamic stability is essentially equal to that of $1a_3 \bullet (L\text{-PheCYA})_6$. The small difference in relative stability of assemblies $2_3 \bullet (L\text{-PheCYA})_6$ and $2_3 \bullet \text{DEB}_6$ is most likely due to steric interactions between the more bulky side chains of *L*-ValCYA or *L*-PheCYA and the 2,2-dimethylpropyl spacer in **2b** and **2c**, which counterbalances the previously observed stabilizing effect of the formation of the additional hydrogen bond. Assembly $2a_3 \bullet (L\text{-PheCYA})_6$ is unstable, even in neat chloroform, due to proton transfer between the strongly acidic *L*-PheCYA ($\text{p}K_a \sim 4.7$) and the basic amino function.

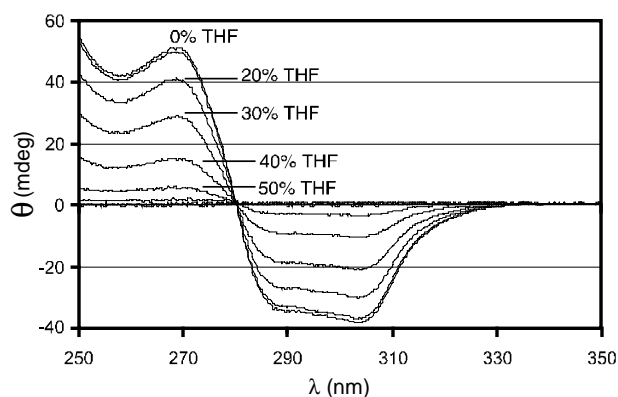


Figure 3.6. Determination of the thermodynamic stability of assembly $2c_3 \bullet (L\text{-ValCYA})_6$ using CD spectroscopy. Spectra were recorded in $\text{CH}_2\text{Cl}_2/\text{THF}$ mixtures (1mM) at 298K.

As pointed out before, the 2,2-dimethylpropyl spacer adopts a very rigid conformation. Therefore, calix[4]arene dimelamines with a propyl spacer were also investigated in order to determine the influence of the spacer flexibility on the assembly process. Structural analysis of both $3b_3 \bullet (\text{DEB})_6$ and $3c_3 \bullet (\text{DEB})_6$ by ^1H NMR spectroscopy using 2D DQF and NOESY indicated that the assemblies are organized in the same way. Both assemblies show NOE connectivities for the methylene ($\text{NH}_m\text{C}(\text{O})\text{CH}_n\text{H}_o$) and the propoxy groups of the calix[4]arene unit. However, the NOE connectivities are weaker, which indicates that the chain adopts a less rigid conformation in comparison to the corresponding assemblies with 2,2-dimethylpropyl spacers.

To determine the thermodynamic stability of the assemblies with the propyl spacer, assemblies $\mathbf{3}_3 \bullet (L\text{-ValCYA})_6$ were prepared. However, ^1H NMR studies showed that the degree of chiral induction is very low for these assemblies in CDCl_3 , which makes thermodynamic stability measurements relatively inaccurate.

The diastereomeric excess (d.e., $([M]-[P])/([M]+[P]) \times 100\%$) of assemblies $\mathbf{3}_3 \bullet (L\text{-ValCYA})_6$ was determined using ^1H NMR spectroscopy, by means of integration of the intensities of the cyanurate NH protons for both diastereomers. The accuracy of these values is limited due to small fluctuations in the NH integral values. As a reference the d.e. of assembly $\mathbf{1a}_3 \bullet (L\text{-ValCYA})_6$ was measured. The assembly showed almost complete chiral induction, d.e. >95%. It was found that chiral induction in assembly $\mathbf{3c}_3 \bullet (L\text{-ValCYA})_6$ is strongly solvent-dependent (Figure 3.7).

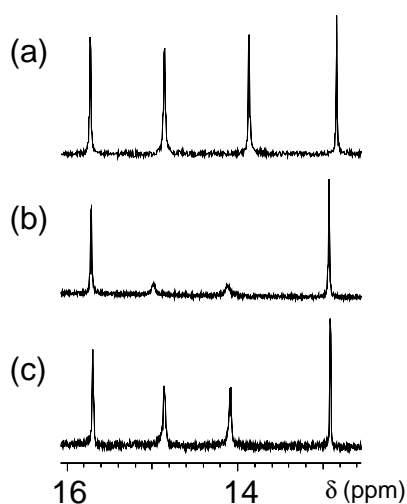


Figure 3.7. Part of the ^1H NMR spectrum of assembly $\mathbf{3c}_3 \bullet (L\text{-ValCYA})_6$ in (a) chloroform- d_1 , (b) toluene- d_8 , and (c) benzene- d_6 . All spectra are recorded at 1.0 mM concentrations at 298K.

For assembly $\mathbf{3c}_3 \bullet (L\text{-ValCYA})_6$, both *P*- and *M*- helices are present in almost equal amounts in CDCl_3 . However, in toluene- d_8 the d.e. is ~80%, while in benzene- d_6 , the assembly exist as a mixture of both diastereomers (d.e. 0%). The polarity of toluene is lower than the polarity of chloroform, however it is higher than the polarity of benzene; therefore it can be concluded that the chiral induction is not only dependent on the polarity of the solvent. The chiral induction can also be dependent on the shape of the molecules. Assembly $\mathbf{3b}_3 \bullet (L\text{-ValCYA})_6$ showed a much higher degree of chiral induction in CDCl_3 (~55%) than assembly $\mathbf{3c}_3 \bullet (L\text{-ValCYA})_6$. In toluene- d_8 the d.e. of assembly $\mathbf{3b}_3 \bullet (L\text{-ValCYA})_6$ is higher, ~90% (Table 3.3).

Table 3.3. Diastereomeric excess in % for assemblies $\mathbf{1a}_3 \cdot (L\text{-ValCYA})_6$, $\mathbf{3b}_3 \cdot (L\text{-ValCYA})_6$, and $\mathbf{3c}_3 \cdot (L\text{-ValCYA})_6$ in different solvents.

Assembly	chloroform- d_1	toluene- d_8	benzene- d_6
$\mathbf{1a}_3 \cdot (L\text{-ValCYA})_6$	>95		
$\mathbf{3b}_3 \cdot (L\text{-ValCYA})_6$	55	90	
$\mathbf{3c}_3 \cdot (L\text{-ValCYA})_6$	0	80	0

An explanation for the difference between the chiral induction of the assemblies $\mathbf{2}_3 \cdot (L\text{-ValCYA})_6$ and $\mathbf{3}_3 \cdot (L\text{-ValCYA})_6$ could be that the chiral cyanurate is not close to the calix[4]arene dimelamine with the propylspacer (**3**) because of the absence of the two methyl groups as in **2**. Therefore no complete chiral induction is obtained. The fact that assembly $\mathbf{1a}_3 \cdot (L\text{-ValCYA})_6$ does show complete chiral induction is most likely due to the freedom of the butyl chains to rotate in such a way that the chain can be close to the chiral cyanurate.

Another explanation can be that the difference in chiral induction may be attributed to a hydrogen bond between the carbonyl of the cyanurate and the proton of the amide/urea functionality in the calix[4]arene dimelamine. Through this hydrogen bond formation, one of the diastereomers which normally is thermodynamically unstable can now probably be stabilized. The formation of this extra hydrogen bond is probably not possible in the assembly with the 2,2-dimethylpropyl spacer because the rigidity of this spacer precludes the $\sim 120^\circ$ rotation of the amide or urea chain needed for this additional hydrogen bond.

3.5 Conclusions

In this chapter it has been shown that the formation of noncovalent hydrogen-bonded assemblies can be used for the self-assembly of polar hydrogen bond donating and accepting functionalities in solution. The results clearly show that the stability of the assemblies is comparable to those of nonfunctionalized assemblies. This opens the way for the synthesis of receptor molecules with polar functionalities (amino acids, small peptide fragments) that more closely mimic antibodies.

The rigid 2,2-dimethylpropyl spacer pre-organizes the side chains such that the side chain is folded back over the calix[4]arene aromatic rings. With the propane spacer the

structural organization is the same, although the side chains have more rotational freedom.

3.6 Experimental Section

^1H NMR spectra were recorded at 400 MHz on a Bruker AMX 400, a Varian Unity 300, or a Varian Unity 400 WB spectrometer with tetramethylsilane (TMS) as internal reference in CDCl_3 solutions or the different solvents as an internal reference. The 2D DQF-COSY consisted of 2048 datapoints in t_2 and 512 increments in t_1 . The data were apodized with a shifted sine-bell square function in both dimensions and processed to a 4K x 1K matrix. For the TOCSY experiment, the total TOCSY mixing time was set to 65 ms. The spectrum was acquired with 1024 data points in t_2 and 512 FIDs in t_1 . The data were apodized with a shifted sine-bell square function in both dimensions and processed to a 2K x 2K matrix. The NOESY experiments were acquired with a mixing time of 150ms, 2K datapoints in t_2 and 512 increments in t_1 . FAB-MS spectra were recorded with a Finnigan MAT 90 spectrometer with *m*-nitrobenzyl alcohol (NBA) as a matrix. MALDI-TOF mass spectra were recorded on a PerSpective Biosystems Voyager-De-RP spectrometer. A 337 nm UV nitrogen laser producing 3 ns pulses was used in the linear and reflectron modes. CD spectra were measured on a JASCO J-715 spectropolarimeter in 0.01 cm width cell.

Formation of assemblies $2_3 \cdot (\text{DEB})_6 / (\text{CYA})_6$ and $3_3 \cdot (\text{DEB})_6 / (\text{CYA})_6$

Hydrogen-bonded assemblies $2_3 \cdot (\text{DEB})_6$ and $3_3 \cdot (\text{DEB})_6$ were prepared by mixing calix[4]arene dimelamines **2** or **3** with 2.1 or 2.5 equivalents of DEB in CDCl_3 for 15 min. Similarly, assemblies $2_3 \cdot (\text{CYA})_6$ and $3_3 \cdot (\text{CYA})_6$ were prepared by mixing the corresponding calix[4]arene dimelamines with 2.1 or 2.5 equivalents of CYA in CDCl_3 , toluene- d_8 , or benzene- d_6 for 15 min.

5,17-Bis({4-amino-6-[(3-amino-2,2-dimethylpropyl)amino]-1,3,5-triazine-2-yl}-amino)-25,26,27,28-tetrapropoxycalix[4]arene (2a). Bis(chlorotriazine) **4** (0.5 g, 0.57 mmol) and 2,2-dimethyl-1,3-propanediamine (10 mL) were heated at 90°C overnight. Addition of H_2O gave **2a** as a white precipitate in 96% yield. FAB-MS Calcd for

$C_{56}H_{78}H_{14}O_4$ $m/z = 1010.6$, Found $m/z = 1011.7$ [M+H]. Anal. Calcd for $C_{56}H_{78}H_{14}O_4 \cdot H_2O$, C=65.34; H=7.83; N=19.05, Found C=65.32; H=7.85; N=19.05.

Assembly 2a₃•(DEB)₆: 1H NMR (400 MHz, $CDCl_3$, 298K) $\delta = 14.12$ (s, 2 H; H_a), 13.33 (s, 2 H; H_b), 8.41 (s, 2 H; H_c) 7.60-7.58 (m, 2 H; H_d), 7.13-7.10 (m, 4 H; ArH), 6.95 (s, 2H; H_f), 6.88 (t, $^3J(H,H)=7.6$ Hz, 2 H; ArH), 6.66 (s, 2 H; H_e), 6.00 (s, 2 H; H_h), 4.53, 4.43, 3.15, 3.12 (2ABq, $^2J(H,H)=13.6$ Hz, 8 H; ArCH₂Ar), 4.11-3.93 (m, 6 H; OCH₂, H_i), 3.62 (t, $^3J(H,H)=6.4$ Hz, 4 H; OCH₂), 2.63 (d, $^2J(H,H)=10.4$ Hz, 2 H; H_j), 2.34 (d, $^2J(H,H)=13.6$ Hz, 2 H; H_k), 2.26-1.80 (m, 18 H; H_l, CH₂(DEB), OCH₂CH₂), 1.36-0.74 (m, 36 H; CH₃).

5,17-Bis({4-amino-6-[(N-propylcarbamoyl-3-amino-2,2-dimethylpropyl)amino]-1,3,5-triazine-2-yl}-amino)-25,26,27,28-tetrapropoxycalix[4]arene (2b). Calix[4]arene dimelamine **2a** (0.22 g, 0.22 mmol) was dissolved in THF (10 mL) and propyl isocyanate (0.2 mL) was added. The mixture was stirred at rt for 2h. The mixture was evaporated to dryness and CH_2Cl_2 was added. The solution was washed with H_2O and brine and dried (Na_2SO_4). Evaporation of the solvent gave the crude product as a white solid, which was purified by column chromatography (CH_2Cl_2 :MeOH: NH_4OH (90:9.5:0.5)) to give the pure product in 78% yield. FAB-MS Calcd for $C_{64}H_{92}N_{16}O_6$ $m/z = 1180.7$, Found $m/z = 1181.7$. Anal. Calcd for $C_{64}H_{92}N_{16}O_6 \cdot 2H_2O$, C=63.13; H=7.95; N=18.41, Found C=63.23; H=7.90; N=18.25.

Assembly 2b₃•(DEB)₆: 1H NMR (400 MHz, $CDCl_3$, 298K) $\delta=14.04$ (s, 2 H; H_a), 13.23 (s, 2 H; H_b) 8.62 (s, 2 H; H_c) 7.81-7.78 (m, 2 H; H_d), 7.14-7.11 (m, 6 H; ArH, H_g), 7.00 (s, 2 H; H_f), 6.89 (t, $^3J(H,H)=7.4$ Hz, 2 H; ArH), 6.71 (s, 2 H; H_e), 6.13 (s, 2 H; H_h), 5.24 (d, $^3J(H,H)=10.4$ Hz, 2 H; H_m), 4.51 (ABq, $^2J(H,H)=13.2$ Hz, 4 H; ArCH₂Ar), 4.14-4.00 (m, 4 H; OCH₂), 3.93 (m, 2 H; H_i), 3.64 (t, $^3J(H,H)=6.6$ Hz, 4 H; OCH₂), 3.24-3.06 (m, 8 H; H_k, H_o, ArCH₂Ar), 2.64 (d, $^2J(H,H)=10.8$ Hz, 2 H; H_j), 2.48-2.45 (m, 2 H; H_n), 2.37 (d, $^2J(H,H)=12.8$ Hz, 2 H; H_l), 2.18-1.84 (m, 18 H; H_p, CH₂), 1.15-0.82 (m, 40 H; NHCH₂CH₂CH₃, CH₃), 0.66 (t, $^3J(H,H)=7.2$ Hz, 6 H; NHCH₂CH₂CH₃).

General Procedure for the Preparation of Calix[4]arene Dimelamines 2c-2e. Calix[4]arene dimelamine **2a** was dissolved in CH_2Cl_2 and the corresponding acid chloride derivative (~50 equivalents) was added. The mixture was stirred at rt for 1h and

then evaporated to dryness. The residue was taken up in Na₂CO₃ (4% w/w) solution and heated for 10 min at 60°C in order to hydrolyze the excess of chloride. The product was extracted with CH₂Cl₂ and washed with water and brine and dried (Na₂SO₄). Evaporation of the solvent gave the crude product as a white solid, which was purified by column chromatography or preparative TLC (CH₂Cl₂:MeOH:NH₄OH (90:9.5:0.5)) to give pure product in 47-53% yield.

5,17-Bis({4-amino-6-[(*N*-propylcarbonyl-3-amino-2,2-dimethylpropyl)amino]-1,3,5-triazine-2-yl)-amino)-25,26,27,28-tetrapropoxycalix[4]arene (2c) was prepared from calix[4]arene dimelamine **2a** (0.10 g, 0.99 mmol) and butyryl chloride (0.2 mL) and obtained as a white solid in 53% yield. FAB-MS Calcd for C₆₄H₉₀N₁₄O₆ m/z = 1150.7, Found m/z = 1150.7 [M+H]. Anal. Calcd for C₆₄H₉₀N₁₄O₆•2.5H₂O, C=64.24;H=8.00; N=16.39, Found C=64.04; H=7.98; N=16.23.

Assembly 2c₃•(DEB)₆: ¹H NMR (400 MHz, CDCl₃, 298K) δ = 14.09 (s, 2 H; H_a), 13.28 (s, 2 H; H_b), 8.58 (s, 2 H; H_c), 7.77 (m, 2 H; H_d), 7.13-7.02 (m, 8 H; H_f, H_g, ArH), 6.87 (t, ³J(H,H)=7.4 Hz, 2 H; ArH), 6.71 (s, 2 H; H_e), 6.33 (d, ³J(H,H)=8.8 Hz, 2 H; H_m), 6.06 (s, 2 H; H_h), 4.52, 4.46 and 3.10, 3.08 (2ABq, ²J(H,H)=13.2 and 13.6 Hz, 8 H; ArCH₂Ar), 4.13-4.00 (m, 6 H; OCH₂, H_i), 3.60 (m, 4 H; OCH₂), 3.42 (t, ²J(H,H)=9.0 Hz, 2 H; H_k), 2.66 (d, ²J(H,H)=8.4 Hz, 2 H; H_j), 2.36 (d, ²J(H,H)=12.4 Hz, 2 H; H_l), 2.17-1.83 (m, 18 H; CH₂), 1.38-1.31 (m, 2 H; H_{n/o}), 1.20-0.81 (m, 40 H; CH₃, N_p), 0.54 (m, 8 H; H_r, H_{n/o}).

5,17-Bis({4-amino-6-[(*N*-butylsulfonyl-3-amino-2,2-dimethylpropyl)amino]-1,3,5-triazine-2-yl)-amino)-25,26,27,28-tetrapropoxycalix[4]arene (2d) was prepared from calix[4]arene dimelamine **2a** (0.10 g, 0.99 mmol) and 1-butanefulfonyl chloride (0.2 mL) and obtained as a white solid in 50% yield. FAB-MS Calcd for C₆₄H₉₄N₁₄O₈S₂ m/z = 1250.7, Found m/z = 1251.7 [M+H]. Anal. Calcd for C₆₄H₉₄N₁₄O₈S₂•2.5H₂O, C= 59.28; H=7.70; N=15.12; S=4.95, Found C=59.66; H=7.28; N=14.62; S=4.43.

Assembly 2d₃•(DEB)₆: ¹H NMR (400 MHz, CDCl₃, 298K) δ=14.01 (s, 2 H; H_a), 13.25 (s, 2 H; H_b) 8.52 (s, 2 H; H_c) 7.80-7.79 (m, 2 H; H_d), 7.13-7.04 (m, 4 H; ArH), 6.95 (s, 2 H; H_f), 6.89-6.83 (m, 4 H, H_g, ArH), 6.67 (s, 2 H; H_e), 6.04 (s, 2 H; H_h), 5.14 (m, 2 H; NH_m), 4.54, 4.48 and 3.28, 3.10 (2ABq, ²J(H,H)=13.6 and 14.0 Hz, 8 H; ArCH₂Ar), 4.15-4.02 (m, 4 H, OCH₂), 3.91-3.82 (m, 4 H; H_i, OCH₂), 3.61 (m, 2 H; OCH₂), 2.76-2.58 (m,

6 H; H_j, H_k, H_l), 2.41-2.34 (m, 2 H; H_n), 2.05-1.83 (m, 18 H; H_o, OCH₂CH₂, CH₂(DEB)), 1.25-0.80 (m, 44 H; H_p, H_q, CH₃), 0.73 (t, ³J(H,H)=7.4 Hz, 6 H; H_r).

5,17-Bis({4-amino-6-[(N-diethylphosphatyl-3-amino-2,2-dimethylpropyl)amino]-1,3,5-triazine-2-yl}-amino)-25,26,27,28-tetrapropoxycalix[4]arene (2e) was prepared from calix[4]arene dimelamine **2a** (0.10 g, 0.99 mmol) and diethyl chlorophosphate (0.2 mL) and obtained as a white solid in 47% yield. FAB-MS Calcd for C₆₄H₉₆N₁₄O₉P₂ *m/z* = 1282.7, Found *m/z* = 1283.7 [M+H]. Anal. Calcd for C₆₄H₉₆N₁₄O₉P₂•2H₂O, C=58.26; H=7.64; N=14.86, Found C=58.67; H=7.48; N=14.77.

Assembly 2e₃•(DEB)₆: ¹H NMR (400 MHz, CDCl₃, 298K) δ=14.13 (s, 2 H; H_a), 13.34 (s, 2 H; H_b), 8.43 (s, 2 H; H_c), 7.67 (m, 2 H; H_d), 7.12 (m, 6 H; ArH + H_e), 6.90 (s, 2 H; H_f), 6.86 (t, 2H, *J* = 7.4 Hz, ArH), 6.67 (s, 2 H; H_e), 6.03 (s, 2 H; H_h), 4.51, 4.47 (2d, ²J(H,H)=13.2 and 13.6 Hz, 4 H; ArCH₂Ar), 4.14-3.64 (m, 18 H; OCH₂, H_i), 3.22-3.08 (m, 6 H; ArCH₂Ar, H_k), 2.74-2.64 (m, 4 H; H_j, H_l), 2.10-1.83 (m, 16 H; OCH₂CH₂, CH₂(DEB)), 1.31-0.86 (m, 42 H; CH₃), 0.81 (t, ²J(H,H)= 7.4 Hz, 6 H; CH₃(ethyl)).

5,17-Bis({4-amino-6-[(3-aminopropyl)amino]-1,3,5-triazine-2-yl}-amino)-25,26,27,28-tetrapropoxycalix[4]arene (3a). Bis(chlorotriazine) **4** (0.5 g, 0.57 mmol) and 1,3-propanediamine (10 mL) were heated at 90°C overnight. Addition of H₂O gave **3a** as a white precipitate in quantitative yield. FAB-MS Calcd for C₅₂H₇₀H₁₄O₄ *m/z* = 954.6, Found *m/z* = 955.5 [M+H]. Anal. Calcd for C₅₂H₇₀H₁₄O₄•10.3H₂O, C=54.75; H=8.00; N=17.19, Found C=54.64; H=7.90; N=17.50.

Assembly 3a₃•(DEB)₆: ¹H NMR (300 MHz, CDCl₃, 298K) δ = 14.08 (s, 2 H; H_a), 13.29 (s, 2 H; H_b), 8.34 (s, 2 H; H_c), 7.44-7.53 (m, 2 H; H_d), 7.08-6.79 (m, 6 H; ArH), 6.89-6.79 (m, 4H; ArH, H_f), 6.61 (s, 2 H; H_e), 5.96 (d, 2 H; ³J(H,H)=2.0 Hz 2 H; H_h), 4.42 (t, ²J(H,H)=15.0 Hz, 4 H; ArCH₂Ar), 4.00 (q, 4H; OCH₂), 3.78 (m, 2H; H_i), 3.56 (t, ³J(H,H)=6.3 Hz, 4 H; OCH₂), 3.13-3.05 (m, 4H; ArCH₂Ar); 2,70 (t, ³J(H,H)=6.8 Hz, 4 H; H_j, H_k), 2.03-1.62 (m, 22 H; H_l, H_t, H_u, CH₂(DEB), OCH₂CH₂), 1.05 (t, ³J(H,H)=7.2 Hz, 6 H; OCH₂CH₂CH₃) 1.08-0.70 (m, 18 H; CH₃(DEB, OCH₂CH₂CH₃)).

5,17-Bis({4-amino-6-[(N-propylcarbamoyl-3-aminopropyl)amino]-1,3,5-triazine-2-yl}-amino)-25,26,27,28-tetrapropoxycalix[4]arene (3b). Calix[4]arene dimelamine **3a** (0.20 g, 0.21 mmol) was dissolved in a mixture of THF/DMF (110 mL (8:3)) and propyl

isocyanate (51.4 μL , 0.59 mmol) was added. The mixture was stirred at rt for 1h. H_2O was added to the solution. The mixture was evaporated to dryness and CH_2Cl_2 was added. The solution was washed with H_2O and brine and dried (Na_2SO_4). Evaporation of the solvent gave the crude product as a white solid, which was purified by column chromatography ($\text{CH}_2\text{Cl}_2:\text{MeOH}:\text{NH}_4\text{OH}$ (90:9.5:0.5)) to give the pure product in 89% yield. FAB-MS Calcd for $\text{C}_{60}\text{H}_{84}\text{N}_{16}\text{O}_6$ m/z = 1124.7, Found m/z = 1125.56 [M+H]. Anal. Calcd for $\text{C}_{60}\text{H}_{84}\text{N}_{16}\text{O}_6 \cdot 11.8\text{H}_2\text{O}$ C=53.86 ;H=8.11 ;N=16.75, Found C=53.68; H=8.17; N=17.39.

Assembly 3b₃•(DEB)₆: ^1H NMR (300 MHz, CDCl_3 , 298K) δ =13.97 (s, 2 H; H_a), 13.20 (s, 2 H; H_b) 8.48 (s, 2 H; H_c) 7.51 (d, $^3J(\text{H,H})=5.1$ Hz 2 H; H_d), 7.09-7.02 (m, 6 H; ArH, H_e), 6.90 (s, 2 H; H_f), 6.83 (t, $^3J(\text{H,H})=7.2$ Hz, 2 H; ArH), 6.66 (s, 2 H; H_e), 6.04 (d, $^3J(\text{H,H})=2.4$ Hz 2 H; H_h), 4.94 (d, $^3J(\text{H,H})=6.3$ Hz, 2 H; H_m), 4.46 (ABq, $^2J(\text{H,H})=13.2$ Hz, 4 H; ArCH₂Ar), 4.10-3.86 (m, 6 H; OCH₂, H_i), 3.58 (t, $^3J(\text{H,H})=6.5$ Hz, 4 H; OCH₂), 3.51-3.40 (m, 2 H; H_k), 3.20-2.90 (m, 10 H; H_j, H_n, H_o, ArCH₂Ar), 2.72-2.61 (m, 2 H; H_l), 2.45-2.32 (m, 2 H; H_p), 2.10-1.74 (m, 16 H; CH₂(DEB), OCH₂CH₂), 1.74-1.56 (m, 4 H; H_r, H_u), 1.21-1.10 (m, 4 H; H_r, H_s), 1.06 (t, $^3J(\text{H,H})=7.5$ Hz, 6 H; OCH₂CH₂CH₃), 0.93 (t, $^3J(\text{H,H})=7.2$ Hz, 6 H; CH₃(DEB)), 0.84-0.74 (m, 12 H; OCH₂CH₂CH₃, CH₃(DEB)), 0.67 (t, $^3J(\text{H,H})=7.4$ Hz, 6 H; H_s).

5,17-Bis({4-amino-6-[(N-propylcarbonyl-3-aminopropyl)amino]-1,3,5-triazine-2-yl}-amino)-25,26,27,28-tetrapropoxycalix[4]arene (3c). Calix[4]arene dimelamine **3a** (0.20 g, 0.21 mmol) was dissolved in CH_2Cl_2 (50 mL) and butyrylchloride (62.5 μL , 0.60 mmol) was added. The mixture was stirred at rt for 1h then H_2O was added. The mixture was evaporated to dryness and CH_2Cl_2 was added. The solution was washed with H_2O and brine and dried (Na_2SO_4). Evaporation of the solvent gave the crude product as a white solid, which was purified by column chromatography ($\text{CH}_2\text{Cl}_2:\text{MeOH}:\text{NH}_4\text{OH}$ (90:9.5:0.5)) to give pure product in 70% yield. FAB-MS Calcd for $\text{C}_{60}\text{H}_{82}\text{H}_{14}\text{O}_6$ m/z = 1094.7, Found m/z = 1095.6 [M+H]. Anal. Calcd for $\text{C}_{60}\text{H}_{82}\text{N}_{14}\text{O}_6 \cdot 11.5\text{H}_2\text{O}$ C=55.33; H=8.12; N=15.05, Found C=55.23; H=8.03; N=15.29.

Assembly 3c₃•(DEB)₆: ^1H NMR (300 MHz, CDCl_3 , 298K) δ = 14.04 (s, 2 H; H_a), 13.25 (s, 2 H; H_b), 8.41 (s, 2 H; H_c), 7.55-7.46 (m, 2 H; H_d), 7.08-7.00 (m, 6 H; H_e, ArH), 6.89

(s, 2 H; H_f), 6.81 (t, ³J(H,H)=7.4 Hz, 2 H; ArH), 6.65 (s, 2 H; H_e), 5.99-5.96 (m, 2 H; H_h), 5.93(t, ³J(H,H)=6.0 Hz, 2 H; H_m), 4.43 (t, ²J(H,H)=14.4 Hz, 4 H; ArCH₂Ar), 4.10-3.82 (m, 6 H; OCH₂, H_i), 3.56 (t, ³J(H,H)=6.6 Hz, 4 H; OCH₂), 3.50-3.36 (m, 2 H; H_k), 3.17-3.01 (m, 6 H; ArCH₂Ar, H_j), 3.00-2.86 (m, 2 H; H_l), 2.04-1.62 (m, 20 H; H_s, H_t, OCH₂CH₂, CH₂ (DEB)), 1.40-1.29 (m, 6 H; H_{n/o}, H_p, H_q), 1.06 (t, ³J(H,H)=7.5 Hz, 6 H, OCH₂CH₂CH₃), 0.98-0.72 (m, 18 H; CH₃(DEB), OCH₂CH₂CH₃), 0.69 (t, ³J(H,H)=7.2 Hz, 6 H; H_r).

3.7 References

- ¹ a) Ma, L.; Sweet, E.H.; Schultz, P.G. *J. Am. Chem. Soc.* **1999**, *121*, 10227-10228; b) Mundorff, E.C.; Hanson, M.A.; Varvak, A.; Ulrich, H.; Schultz, P.G.; Stevens, R.C. *Biochemistry*, **2000**, *39*, 627-632.
- ² a) Mutter, M.; Vuilleumier, S. *Angew. Chem., Int. Ed. Engl.* **1989**, *28*, 535-554; b) Akerfeld, K.S.; DeGrado, W. F. *Tetrahedron Lett.* **1994**, *35*, 4489-4492; c) Mezo, A.R.; Sherman, J.C. *J. Am. Chem. Soc.* **1999**, *121*, 8983-8994.
- ³ a) Ghadiri, M.R.; Soares, C.; Choi, C. *J. Am. Chem. Soc.* **1992**, *114*, 825-831; b) Rowan, S.J.; Hamilton, D.G.; Brady, P. A.; Sanders, J.K.M. *J. Am. Chem. Soc.* **1997**, *119*, 2578-2579; c) Suzuki, K.; Hiroaki, H.; Nakamura, H.; Tanaka, T. *J. Am. Chem. Soc.* **1998**, *120*, 13008-13015; d) Case, M.A.; Ghadiri, M.R.; Mutz, M.W.; McLendon, G.L. *Chirality*, **1998**, *10*, 35-40.
- ⁴ a) Still, W.C. *Acc. Chem. Res.* **1996**, *29*, 155-163; b) Fessmann, T.; Kilburn, J.D. *Angew. Chem., Int. Ed. Engl.* **1999**, *38*, 1993-1996; c) Goodman, M.S.; Jubian, V.; Linton, B.; Hamilton, A.D. *J. Am. Chem. Soc.* **1995**, *117*, 11610-11611; d) Löwik, D.W.P.M.; Weingarten, M.D.; Broekema, M.; Brouwer, A.J.; Still, W.C.; Liskamp, R.M.J. *Angew. Chem., Int. Ed. Engl.* **1998**, *37*, 1846-1850; e) Xu, R.; Greiveldinger, G.; Marenus, L.E.; Cooper, A.; Ellman, J.A. *J. Am. Chem. Soc.* **1999**, *121*, 4898-4899; f) Hamuro, Y.; Crego-Calama, M.; Park, H.S.; Hamilton, A.D. *Angew. Chem. Int. Ed.* **1997**, *36*, 2680-2683. Recent review about protein and peptide recognition: Peczu, M.W.; Hamilton, A.D. *Chem. Rev.* **2000**, *100*, 2479-2494.
- ⁵ a) Whitesides, G.M. *Acc. Chem. Res.* **1995**, *28*, 37-44; b) Heinz, T.; Rudkevich, D.M.; Rebek Jr., J. *Nature*, **1998**, *394*, 764-766; c) Rincon, A.M.; Prados, P.; de Mendoza, J. *J. Am. Chem. Soc.* **2001**, *123*, 3493-3498.

- ⁶ Benjamini, E.; Sunshine, G.; Leskowitz, S. *Immunology, A Short Course*, 3rd e.d. Wiley, New York, **1996**.
- ⁷ a) Simanek, E.E.; Isaacs, I.; Li, X.; Wang, C.C.C.; Whitesides, G.M. *J. Org. Chem.* **1997**, *62*, 8994-9000; b) Huck, W.T.S.; Hulst, R.; Timmerman, P.; van Veggel, F.C.J.M.; Reinhoudt, D.N. *Angew. Chem., Int. Ed. Engl.* **1997**, *36*, 1006-1008.
- ⁸ Cho, Y.L.; Rudkevich, D.M.; Shivanyuk, A.; Rissanen, K.; Rebek Jr., J. *J. Chem. Eur. J.* **2000**, *6*, 3788-3796.
- ⁹ a) Timmerman, P.; Vreekamp, R.H.; Hulst, R.; Verboom, W.; Reinhoudt, D.N.; Rissanen, K.; Udachin, K.A.; Ripmeester, J. *Chem. Eur. J.* **1997**, *3*, 1823-1832; b) Vreekamp, R.H.; Van Duynhoven, J.P.M.; Hubert, M.; Verboom, W.; Reinhoudt, D.N. *Angew. Chem., Int. Ed. Engl.* **1996**, *35*, 1215-1218.
- ¹⁰ Prins, L.J.; Jolliffe, K.A.; Hulst, R.; Timmerman, P.; Reinhoudt, D.N. *J. Am. Chem. Soc.* **2000**, *122*, 3617-3627.
- ¹¹ a) Timmerman, P.; Jolliffe, K.A.; Crego-Calama, M.; Weidmann, J.-L.; Prins, L.J.; Cardullo, F.; Snellink-Ruël, B.H.M.; Fokkens, R.; Nibbering, N.M.M.; Shinkai, S.; Reinhoudt, D.N. *Chem. Eur. J.* **2000**, *6*, 4104-4115; b) Jolliffe, K.A.; Crego-Calama, M.; Fokkens, R.; Nibbering, N.M.M.; Timmerman, P.; Reinhoudt, D.N. *Angew. Chem. Int. Ed.* **1998**, *37*, 1247-1251.
- ¹² Prins, L.J.; Huskens, J.; de Jong, F.; Timmerman, P.; Reinhoudt, D.N. *Nature*, **1999**, *398*, 498-502.
- ¹³ For an explanation of CD see: Eliel, E.L.; Wilen, S.H. *Stereochemistry of Organic Compounds*; John Wiley & Sons, Inc.: New York, **1994**.
- ¹⁴ The percentage of assembly formed was determined by comparison of the H_a+H_b integral with the $ArCH_2Ar$ integral of the calix[4]arene part. As a standard we use assembly **1**₃•(DEB)₆, for which the integral ratio was arbitrarily set to 100%.
- ¹⁵ a) Mammen, M.; Simanek, E.E.; Whitesides, G.M. *J. Am. Chem. Soc.* **1996**, *118*, 12614-12623; b) The stability of the hydrogen-bonded assemblies was measured by titration of a chloroform-*d*₁ solution of the assembly with DMSO-*d*₆ using 1,4-dinitrobenzene (δ = 8.3-8.4 ppm) as an internal standard. The χ_{DMSO} value represents the % of DMSO corresponding to formation of only 50% of the assembly.
- ¹⁶ Rance, M.; Sørensen, O.W.; Bodenhausen, G.; Wagner, G.; Ernst, R.R.; Wütrich, K. *Biochem. Biophys. Res. Commun.* **1983**, *117*, 479-485.

- ¹⁷ Bax, A.; Davis, D.G. *J. Magn. Reson.* **1985**, *65*, 355-360.
- ¹⁸ Jeener, J.; Meier, B.H.; Bachman, P.; Ernst, R.R. *J. Chem. Phys.* **1979**, *71*, 4546-4569.
- ¹⁹ Scheerder, J.; van Duynhoven, J.P.M.; Engbersen, J.F.J.; Reinhoudt, D.N. *Angew. Chem., Int. Ed. Engl.* **1996**, *35*, 1090-1093.
- ²⁰ In the absence of any other source of chirality, the double rosette assembly exists as a racemic mixture of the *M*- and *P*-enantiomers. An assembly of 3 equivalents calix[4]arene dimelamine with 6 equivalents *L*- or *D*-PheCYA, respectively, gives quantitatively either the *M*- or the *P*-enantiomer, both with a highly characteristic CD. The maximum of the CD signals is measured as a function of the volume fraction of THF in CH₂Cl₂. In analogy to the DMSO titrations, the χ_{THF} value represents the % of THF corresponding to the formation of only 50% of the assembly.

Chapter 4

Self-Assembly of Amino Acid and Peptide Functions on a Noncovalent Platform

In Chapter 3 it was demonstrated that small polar functionalities can be introduced onto the rosette platform. This chapter describes the introduction of amino acids at the periphery of the hydrogen-bonded assemblies. The amino acids can be coupled to the calix[4]arene dimelamines via an ureido or amide bond. The introduction of peptides or bulky amino acids inhibits partially or completely the formation of the double rosette assemblies. Thermodynamic stabilities of several amino acid functionalized hydrogen-bonded assemblies were determined by CD titrations in CH_2Cl_2 with THF. The stability of the assemblies depends on the size of the side chain of the amino acids, the spacer that connects the amino acids to the melamines, and the type of linker that connects the amino acid and the spacer (ureido or amide).

4.1 Introduction

Natural antibodies (Chapters 2 and 3) contain peptidic arms that recognize an antigen. The simple combination of 20 natural amino acids allows the immune system to create an astonishing variety of antibodies for the specific recognition of antigens. So far the research towards the development of molecular receptors bearing peptides has been mainly focused on the preorganization of the functionalities (amino acids/ peptides) using covalent platforms.¹ An excellent example wherein four peptidic loops are arrayed around a central calix[4]arene core is reported by Hamilton et al. (Figure 4.1).² This synthetic receptor binds to the surface of cytochrome c in a manner similar to the natural protein partners.

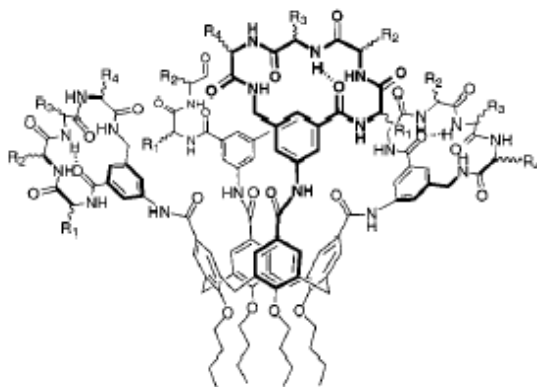


Figure 4.1. Calix[4]arenes functionalized with four peptide loops designed by Hamilton et al.

In this chapter, the focus is on the noncovalent synthesis of molecular receptors bearing amino acids and peptides using the double rosette assembly as a platform. As described in Chapter 3, structural diversity at the supramolecular level in the rosettes can be generated in an extremely simple way by mixing the individual components under thermodynamically controlled conditions.³ Different polar functionalities (ureas, amides, and amines) were attached to the double rosette without interfering with the formation of the hydrogen-bonded network.

In this chapter, the synthesis of different amino acid or peptide functionalized calix[4]arene dimelamines and their assembly formation with either DEB or CYA is described. Furthermore, it is shown that the thermodynamic stability of these double rosette assemblies $Y_3 \cdot (DEB)_6$ ($Y=1-5$; Chart 4.1, 4.2; Figure 4.4, 4.5) is highly dependent

on the bulkiness of the side chains and the linkage used for connecting the amino acids to the double rosette platform.

4.2 Results and Discussion

4.2.1 Single Amino Acid Functionalized Calix[4]arene Dimelamines **2**

The amido functionalities in **1c** (Chart 4.1) significantly stabilize the corresponding double rosette assembly due to the formation of an additional hydrogen bond between the amide proton and one of the nitrogen atoms (N-1) of the triazine ring (see Section 3.4.3). Thus, calix[4]arene dimelamines **2a-f** that are functionalized with the N-t-Boc-protected amino acids via an amide bond (Chart 4.1) were investigated as building blocks for the formation of the corresponding assemblies $2_3 \cdot (\text{DEB})_6$.

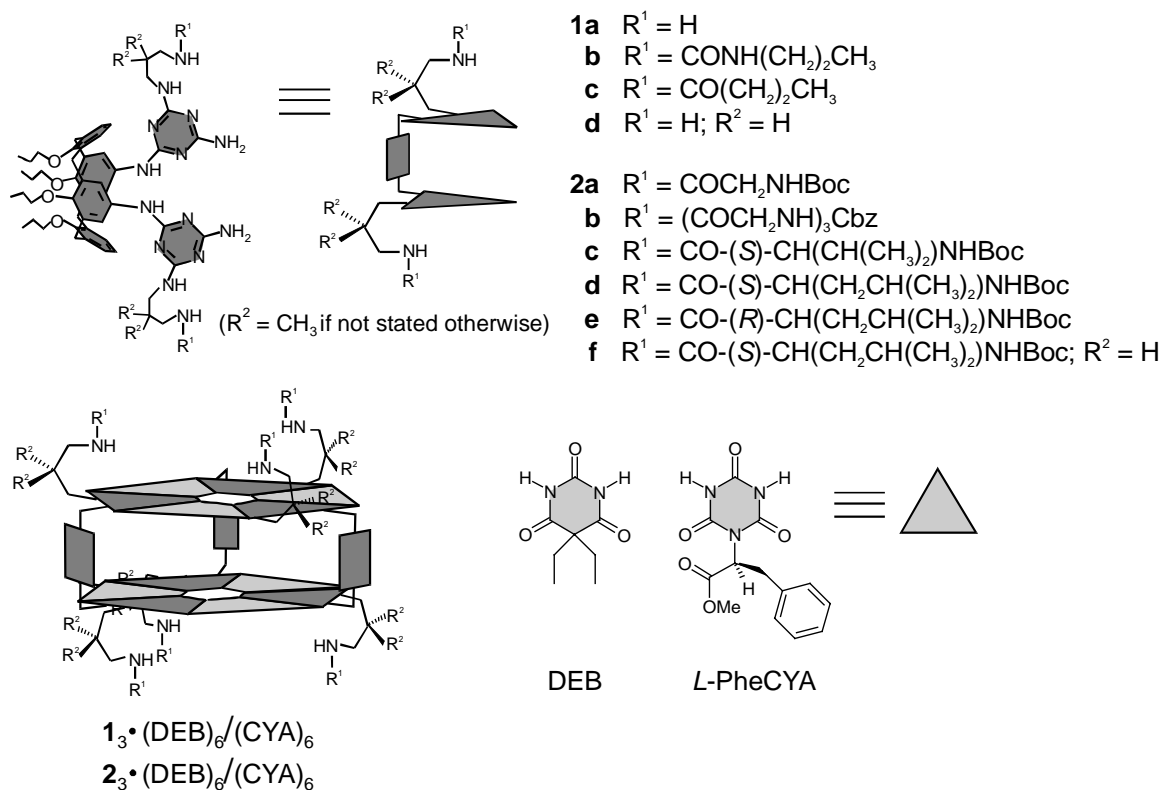


Chart 4.1. Molecular structures and schematic representations of the molecular components **1-2**, **DEB**, and **L-PheCYA**, and the corresponding hydrogen-bonded assemblies $1_3 \cdot (\text{DEB})_6 / (\text{CYA})_6$ and $2_3 \cdot (\text{DEB})_6 / (\text{CYA})_6$.

Dimelamines **2a-e** were synthesized from amino substituted dimelamine **1a** and the corresponding N-t-Boc-protected amino acid (except for **2b** that is Cbz protected; see

Appendix for abbreviations), using standard peptide coupling conditions (EDC/HATU, DIPEA, see experimental section). The hydrogen-bonded assemblies are formed spontaneously by mixing calix[4]arene dimelamines **2a-e** with either 2 equivalents of 5,5-diethylbarbiturate (DEB) or cyanurates (CYA) in apolar solvents such as chloroform, dichloromethane, and toluene.

The ^1H NMR spectrum of **2a₃•(DEB)₆** (N-t-Boc-protected glycine side chains) showed that the assembly is formed quantitatively in chloroform (Figure 4.2).

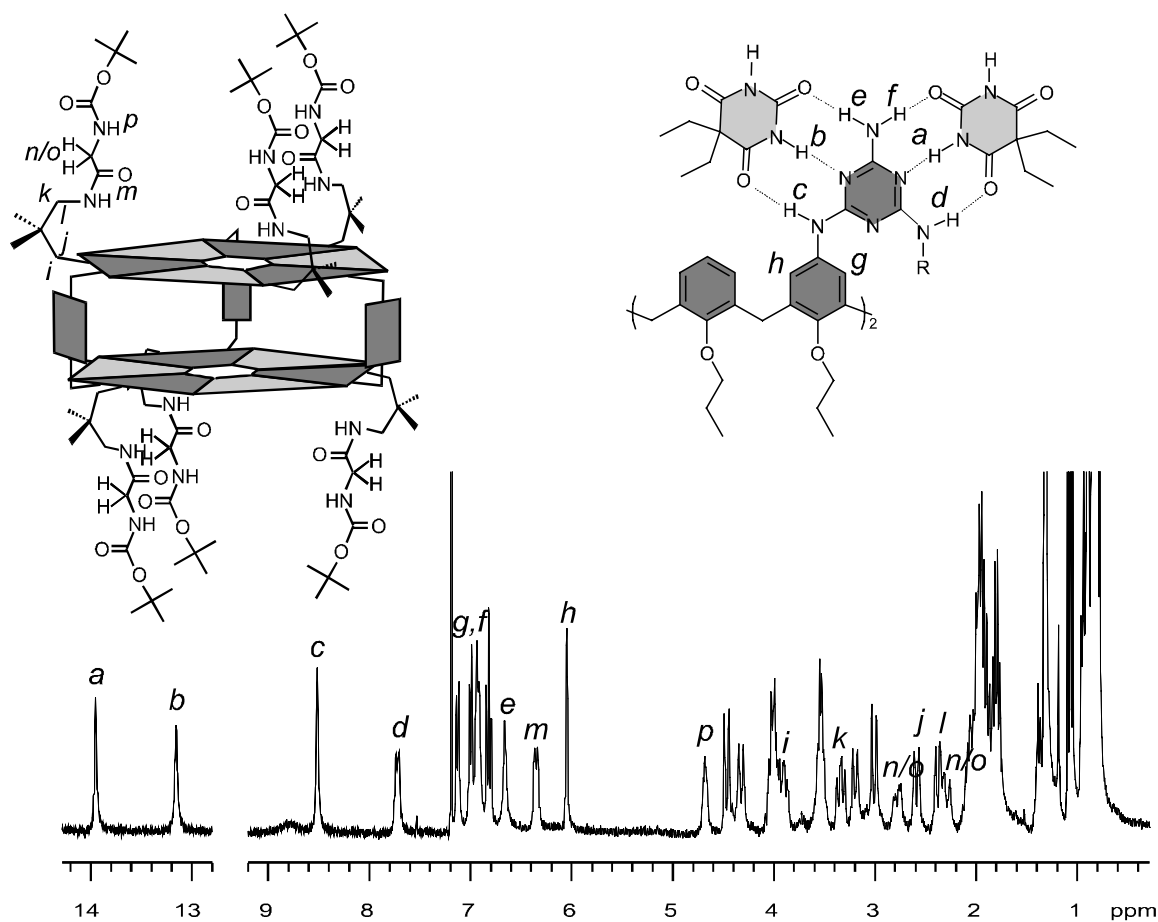


Figure 4.2. ^1H NMR spectrum of assembly **2a₃•(DEB)₆** (1 mM) recorded in CDCl_3 at 300 MHz at 298 K.

The very close similarity between the ^1H NMR spectra of **2a₃•(DEB)₆** and **1c₃•(DEB)₆** (described in detail in Chapter 3) suggested that both assemblies have very similar structures. Moreover, the corresponding chiral assembly **2a₃•(L-PheCYA)₆** displayed a CD spectrum (Figure 4.3a) virtually identical to that of assembly **1c₃•(L-PheCYA)₆** (see Sections 3.2 and 4.2.2.2 for a discussion about chirality in double rosettes).

After confirming the successful assembly formation of $2\mathbf{a}_3\bullet(\text{DEB})_6$, the assembly formations of $2\mathbf{b}_3\bullet(\text{DEB})_6$ and $2\mathbf{b}_3\bullet(\text{L-PheCYA})_6$ (Chart 4.1) were studied by ^1H NMR and CD spectroscopy. The ^1H NMR spectrum of $2\mathbf{b}_3\bullet(\text{DEB})_6$, containing six triglycine peptides for a total of 18 amide and 6 carbamate functionalities, clearly shows that the assembly is formed in 80 % yield in chloroform (comparison of the intensities of the H_a and H_b protons with the intensity of the signal from ArCH_2Ar). The spectrum was slightly broadened, most likely as a result of non-specific aggregation. Assembly $2\mathbf{b}_3\bullet(\text{L-PheCYA})_6$ displays a CD spectrum characteristic of its formation (Figure 4.3a). The CD intensity is 25 % lower than that of $2\mathbf{a}_3\bullet(\text{L-PheCYA})_6$, which corresponds well with the yield determined by NMR, assuming that the molar CD-absorptivities of both assemblies are comparable.

Subsequently, calix[4]arene dimelamines $2\mathbf{c-2e}$ were studied to probe the effect of the chain length and geometry of the amino acids on the assembly formation. For dimelamine $2\mathbf{c}$, bearing the bulky isopropyl side chain of *L*-valine, the ^1H NMR spectrum revealed that the formation of the assembly $2\mathbf{c}_3\bullet(\text{DEB})_6$ in CDCl_3 occurred only partially (~ 40%), likely due to steric hindrance from the isopropyl group. In the ^1H NMR spectrum in CDCl_3 of assembly $2\mathbf{d}_3\bullet(\text{DEB})_6$, which bear an even bulkier side chain (*L*-leucine), signals for the hydrogen-bonded NH_{DEB} -protons H_a and H_b were not observed, indicating little or no formation of the double rosette. However, in a less polar solvent such as toluene, the assembly is formed quantitatively (>95%). These results clearly show that the formation and stability of assemblies $2\mathbf{3}\bullet(\text{DEB})_6$ is extremely sensitive to steric effects and solvent polarity. However, it seems only marginally affected by the presence of the amide or carbamate functionalities.

The assemblies $2\mathbf{c}_3\bullet(\text{DEB})_6$ and $2\mathbf{d}_3\bullet(\text{DEB})_6$ display the highly characteristic CD signal for calix[4]arene double rosette assemblies, which originates from the diastereoselective formation of the *P*-isomer (Figure 4.3b).⁴ Despite the fact that the chiral centers in the side chains are six atoms away from the core of the assembly, the induction of the *P*-helicity is virtually complete (>95%) as judged from the single set of signals for the hydrogen-bonded H_a and H_b protons in the ^1H NMR spectrum. This fact further emphasizes the close proximity of the chiral side chains to the assembly as suggested in Chapter 3. As expected assembly $2\mathbf{e}_3\bullet(\text{DEB})_6$, also bearing leucine but with

reversed stereochemistry (*D*-leucine) from **2d₃**•(DEB)₆, showed the opposite CD spectrum (Figure 4.3b).

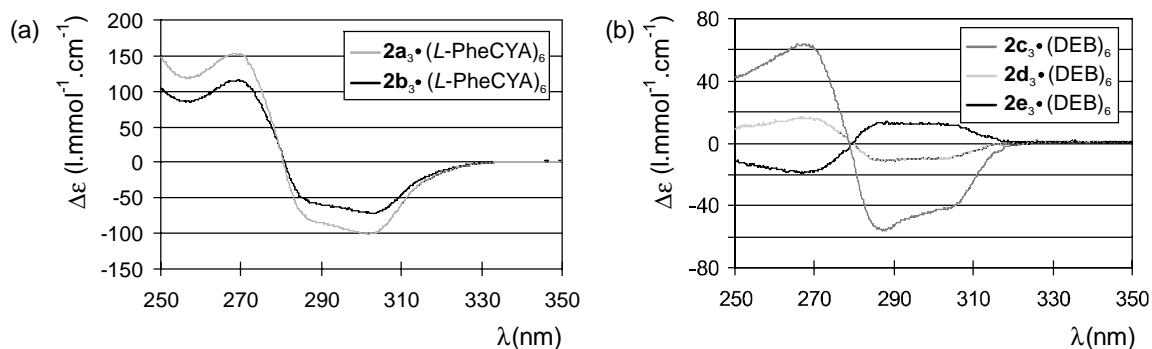


Figure 4.3. CD spectra of assemblies (a) **2a₃**•(L-PheCYA)₆ and **2b₃**•(L-PheCYA)₆, and (b) **2c₃**•(DEB)₆, **2d₃**•(DEB)₆, and **2e₃**•(DEB)₆. Spectra were recorded in CH₂Cl₂ (1.0 mM) at 298 K.

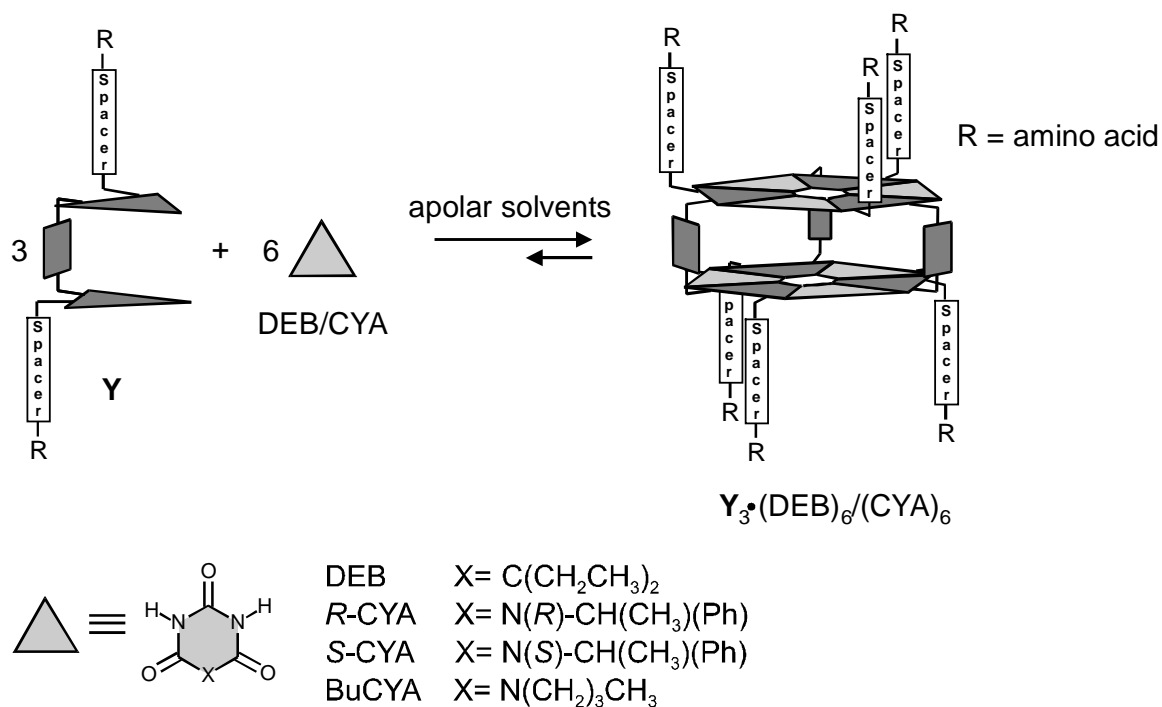
Assembly **2f₃**•(DEB)₆ (Chart 4.1), which bears a *N*-*t*-Boc-protected *L*-Leu as in assembly **2d₃**•(DEB)₆ but with a propyl instead of a 2,2-dimethylpropyl spacer, was investigated by ¹H NMR spectroscopy. Surprisingly, the assembly **2f₃**•(DEB)₆ is formed quantitatively (>95 %) in CDCl₃ according to the relative intensities of the hydrogen-bonded NH_{DEB} protons H_a and H_b. Thus, the absence of the geminal methyl groups in assembly **2f₃**•(DEB)₆ makes it possible to introduce amino acids with bulkier substituents without destroying the rosette. The absence of the geminal methyl group increases the conformational flexibility of the spacer allowing the bulky side chain of *N*-*t*-Boc-protected *L*-Leu not to interfere with the rosette platform.

The results described in this section indicate clearly that the formation of the double rosette assembly depends very much on the size of the side chain of the amino acid. Furthermore, the difference between **2d₃**•(DEB)₆ and **2f₃**•(DEB)₆ indicates that the introduction of amino acids with bulky side chains is feasible when the spacer is more flexible (see Scheme 4.1).

4.2.2 Formation and Stability of Assemblies of Amino Acid Functionalized Calix[4]arene Dimelamines **3** and **4**

As described in Section 4.2.1, amino acids bearing bulky side chains strongly decrease the thermodynamic stability of the double rosette assemblies in CDCl₃. Therefore, to probe the scope of the side chain influence, an extensive systematic study

concerning the formation and stability of a series of amino acid functionalized double rosettes was carried out (Scheme 4.1).



Scheme 4.1. Formation of the double rosette assemblies $Y_3 \cdot (DEB)_6$ and $Y_3 \cdot (CYA)_6$ ($Y=1-5$).

4.2.2.1 Synthesis and Characterization of Double Rosette Assemblies

Amino acid functionalized dimelamines **3** and **4** (Figure 4.4 and 4.5) were synthesized starting from amino substituted calix[4]arene dimelamines **1a** (2,2-dimethyl propyl spacer) or **1d** (propyl spacer).⁵ Coupling of the corresponding amino acids to the dimelamines **1a** or **1d** was performed either via a urea (**3**) or an amide (**4**) bond. Amino acid functionalized dimelamines **3a-1** (urea linkage)⁶ were obtained in 36-90 % yield (Figure 4.4) by reaction of **1a** or **1d** with the appropriate amino acid isocyanate derivative OCN-X-OMe (X = Gly (**3a,b**), L-Ala (**3c,d**), L-Phe (**3e,f**), L-Ser(tBu) (**3g,i**), L-Gln(Trt) (**3j, 3k**), L-Lys(Boc) (**3l**)) (only Gly is protected as an ethyl ester).⁷ The reaction was initiated with the synthesis of *N*-(4-nitrophenoxycarbonyl)amino acid esters by reaction of the corresponding amino acid hydrochloride with 1 equiv. 4-nitrophenyl chloroformate in the presence of 1 equiv. NaHCO₃.⁸ The isocyanates were generated *in situ* from the corresponding *N*-(4-nitrophenoxycarbonyl)amino acid ester by reaction with 1 equiv. DIPEA.

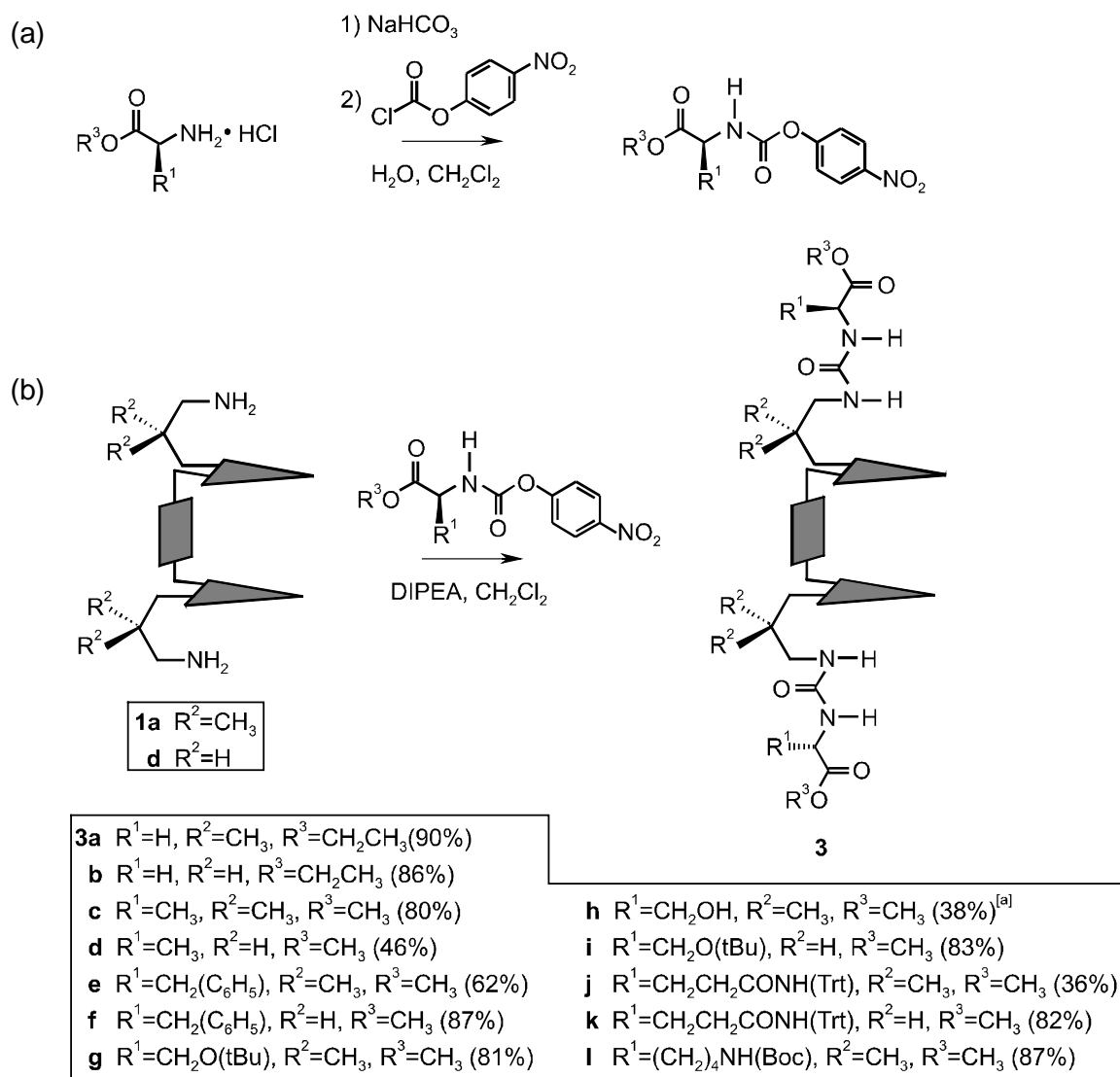


Figure 4.4. Synthesis of (a) the *N*-(4-nitrophenoxycarbonyl)amino acid esters and (b) amino acid functionalized calix[4]arene dimelamines **3** via an ureido linkage.

^[a] **3h** is synthesized from **3g** by reaction with TFA.

Amino acid functionalized dimelamines **4** (amide linkage) were synthesized in 27-75 % yield (Figure 4.5) from amino substituted dimelamines **1a** or **1d** and the corresponding *N*-t-Fmoc-protected amino acid Fmoc-X-OH (X =Gly (**4a,b**), *L*-Phe (**4c,d**), *L*-Gln(Trt) (**4e,f**), *L*-Lys(Boc) (**4g,h**), *L*-Cys(Trt) (**4i,j**), *L*-Ser(tBu) (**4k**), *L*-Met-OH (**4m**), *L*-His(Trt) (**4n**), *L*-Arg(Pbf) (**4o,p**)) using standard peptide coupling conditions (HBTU, DIPEA).

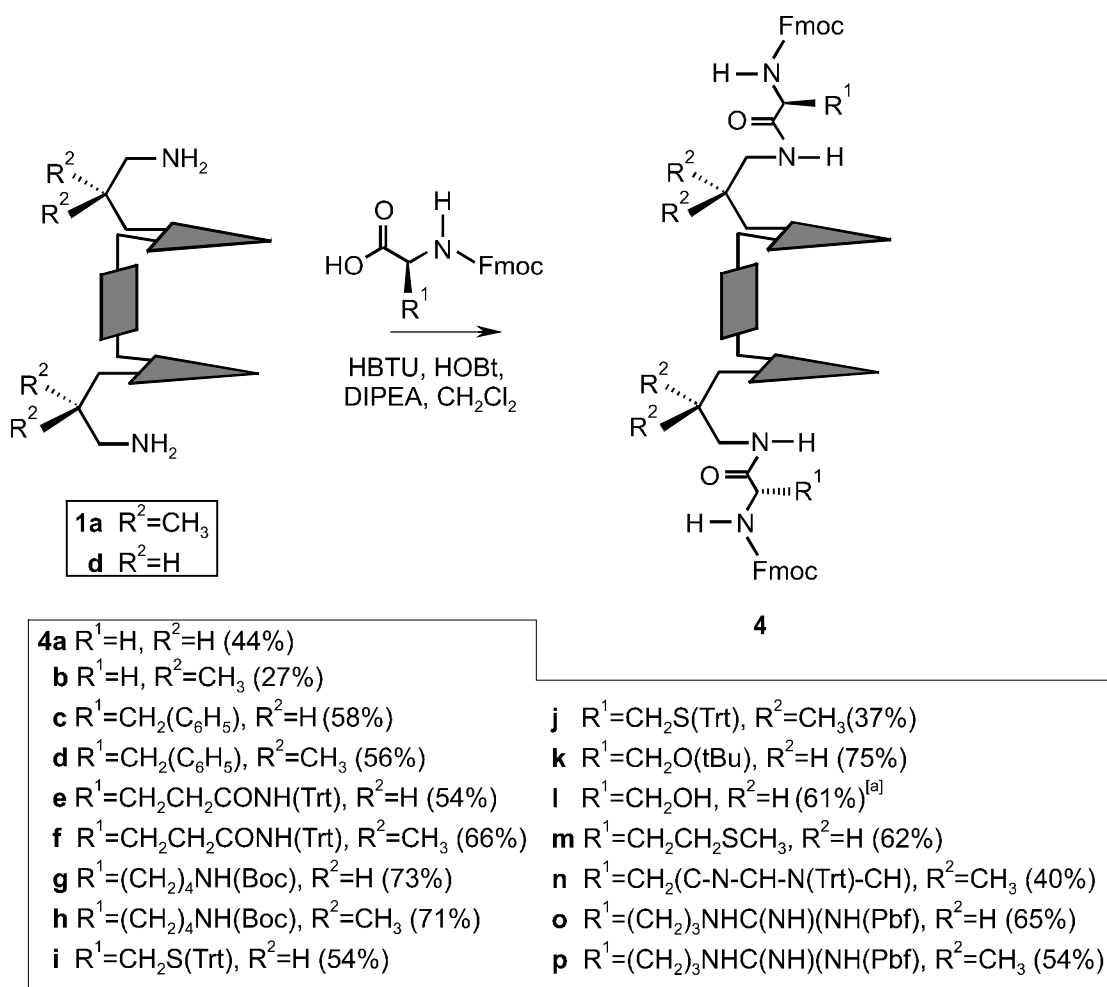


Figure 4.5. Synthesis of amino acid functionalized calix[4]arene dimelamines **4** via an amido linkage.

^[a] **4l** is synthesized from **4k** by reaction with TFA.

The formation of the corresponding hydrogen-bonded assemblies was studied by ¹H NMR spectroscopy. For assemblies **4₃•(DEB)₆** the percentage of assembly formed was determined by comparing the intensities of the signals of the hydrogen-bonded NH_{DEB}-protons H_a and H_b with those of the Fmoc signal at 7.62 ppm.⁹ For the assemblies **3₃•(DEB)₆** the percentage of assembly was determined by comparison of the intensities of the H_a and H_b protons with the intensity of the signal from ArCH₂Ar. The assemblies **3₃•(DEB)₆** are formed in quantitative yield (>95 %) in contrast to the assemblies **4₃•(DEB)₆** (Table 4.1). From the values in Table 4.1 it can be seen that the rosette formation for **4₃•(DEB)₆** is dependent on the size of the amino acid. The assemblies functionalized with Gly (**4a,b**) are formed quantitatively (> 95%), while assemblies bearing amino acids with a bulky side chain, e.g. **4d₃•(DEB)₆** (*L*-Phe), **4g₃•(DEB)₆** (*L*-

Lys(Boc)), or **4j**₃•(DEB)₆ (*L*-Cys(Trt)) are formed only partially. Furthermore, it seems that the spacer also has some influence on the yield of the assembly. In general, the hydrogen-bonded assemblies deriving from calix[4]arene melamines containing a propyl spacer as in **4c** (*L*-Phe) and **4i** (*L*-Cys(Trt)) are formed in a higher yield than the assemblies containing a 2,2-dimethylpropyl spacer (**4d** (*L*-Phe) and **4j** (*L*-Cys(Trt))). This is likewise observed for the assemblies **2d**₃•(DEB)₆ and **2f**₃•(DEB)₆ (Section 4.2.1).

Table 4.1. Percentage of amino acid functionalized double rosette assemblies formed in CDCl₃ (1 mM, 298 K)

Assembly		% Rosette Formation	Assembly		% Rosette Formation
3a ₃ •(DEB) ₆ ^[b]	Gly	> 95 %	4a ₃ •(DEB) ₆	Gly	> 95 %
3b ₃ •(DEB) ₆ ^[c]	Gly	> 95 %	4b ₃ •(DEB) ₆	Gly	> 95 %
3c ₃ •(DEB) ₆ ^[b]	<i>L</i> -Ala	> 95 %	4c ₃ •(DEB) ₆ ^[b]	<i>L</i> -Phe	> 95 %
3d ₃ •(DEB) ₆ ^[c]	<i>L</i> -Ala	> 95 %	4d ₃ •(DEB) ₆	<i>L</i> -Phe	~ 55 % ^[a]
3e ₃ •(DEB) ₆ ^[c]	<i>L</i> -Phe	> 95 %	4e ₃ •(DEB) ₆	<i>L</i> -Gln(Trt)	not determined
3f ₃ •(DEB) ₆ ^[c]	<i>L</i> -Phe	> 95 %	4f ₃ •(DEB) ₆	<i>L</i> -Gln(Trt)	not determined
3g ₃ •(DEB) ₆ ^[c]	<i>L</i> -Ser(tBu)	> 95 %	4g ₃ •(DEB) ₆	<i>L</i> -Lys(Boc)	~ 52 % ^[a]
3h ₃ •(DEB) ₆ ^[c]	<i>L</i> -Ser(OH)	> 95 %	4h ₃ •(DEB) ₆	<i>L</i> -Lys(Boc)	not determined
3i ₃ •(DEB) ₆ ^[c]	<i>L</i> -Ser(tBu)	> 95 %	4i ₃ •(DEB) ₆ ^[b]	<i>L</i> -Cys(Trt)	~ 90 % ^[a]
3j ₃ •(DEB) ₆ ^[c]	<i>L</i> -Gln(Trt)	> 95 %	4j ₃ •(DEB) ₆ ^[b]	<i>L</i> -Cys(Trt)	~ 35 % ^[a]
3k ₃ •(DEB) ₆ ^[b]	<i>L</i> -Gln(Trt)	> 95 %	4k ₃ •(DEB) ₆	<i>L</i> -Ser(tBu)	> 95 %
3l ₃ •(DEB) ₆ ^[c]	<i>L</i> -Lys(Boc)	> 95 %	4l ₃ •(DEB) ₆	<i>L</i> -Ser(OH)	> 90 %
			4m ₃ •(DEB) ₆	<i>L</i> -Met	> 95 %
			4n ₃ •(DEB) ₆	<i>L</i> -His(Trt)	not determined
			4o ₃ •(DEB) ₆	<i>L</i> -Arg(Pbf)	not determined
			4p ₃ •(DEB) ₆	<i>L</i> -Arg(Pbf)	~ 29 % ^[a]

^[a] Due to complicated ¹H NMR spectra, the determination of the yields is not precise.

^[b] 3.0 mM rosette.

^[c] 1.0 mM rosette in CD₂Cl₂.

The effect of the deprotection of side group of **3h** and **4l** on the rosette formation was found to be negligible. The ¹H NMR spectrum of the corresponding assemblies

$3\mathbf{h}_3\bullet(\text{DEB})_6$ and $4\mathbf{l}_3\bullet(\text{DEB})_6$ showed that both assemblies were formed in > 95 % and > 90 % yield, respectively, and comparable to the fully protected assemblies $3\mathbf{g}_3\bullet(\text{DEB})_6$ or $4\mathbf{k}_3\bullet(\text{DEB})_6$.

A possible explanation for the difference between the assemblies $3_3\bullet(\text{DEB})_6$ and $4_3\bullet(\text{DEB})_6$ can be extracted after reexamination of the minimized structures obtained from the gas-phase molecular modeling calculations (Quanta 97, CHARMM 24.0) of assembly $1\mathbf{b}_3\bullet(\text{DEB})_6$ (bearing propyl urea) and $1\mathbf{c}_3\bullet(\text{DEB})_6$ (bearing propyl amide) (see also Chapter 3, Figure 4.6). Due to the presence of the urea linkage, the side chains of the amino acids in assemblies $3_3\bullet(\text{DEB})_6$ are positioned one atom further from the core of the rosette (Figure 4.6a) than in assemblies $4_3\bullet(\text{DEB})_6$, bearing an amide linkage (Figure 4.6b). Therefore, the side chains in assemblies $3_3\bullet(\text{DEB})_6$ are directed away from the rosette plane while in assemblies $4_3\bullet(\text{DEB})_6$ the side chains are directed towards the rosette plane. Steric strain due to the side chains pointing towards the double rosette plane in assemblies $4_3\bullet(\text{DEB})_6$ shifts the equilibrium towards the building blocks.

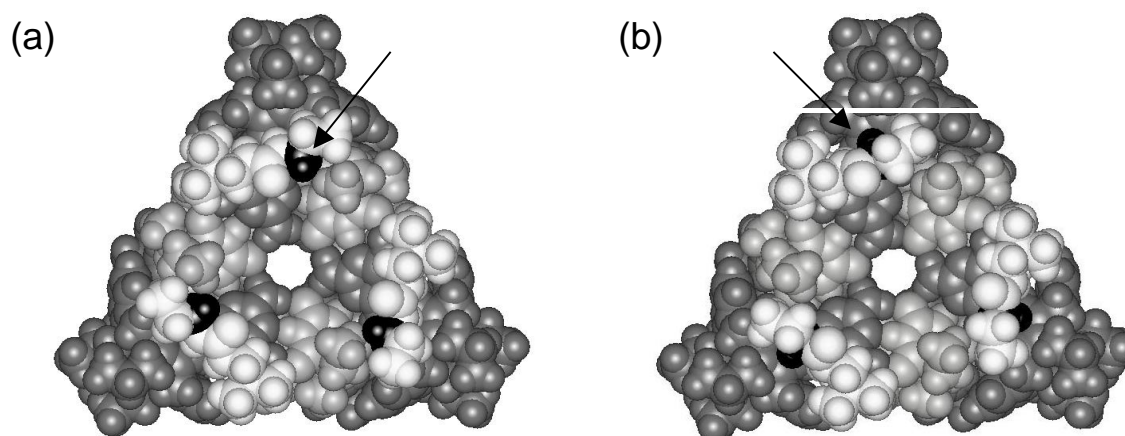


Figure 4.6. Gas-phase-minimized structure of assembly (a) $1\mathbf{b}_3\bullet(\text{DEB})_6$ and (b) $1\mathbf{c}_3\bullet(\text{DEB})_6$, in which the position of the side chains are colored in black. In (a) the functional groups will point away from the rosette plane, while in (b) the functional groups will point towards the rosette plane.

These results indicate that the linkage type (ureido *versus* amido) has influence on the formation of the double rosette assemblies. Ureido seems to be a better linker, due to less steric strain between the amino acids side chain and the rosette platform. In assemblies $4_3\bullet(\text{DEB})_6$ the length and bulkiness of the side chain and the spacer between the amino acid and the rosette platform seems to have an effect on the rosette formation.

In comparison to the 2,2-dimethylpropyl spacer, the more flexible propyl spacer allows better introduction of amino acids with bulky side chains.

4.2.2.2 Chiral Induction and Thermodynamic Stability

The double rosette structure is chiral as a result of the nonsymmetrical arrangement of the building blocks. In the absence of any source of chirality, the assembly exists as a racemic mixture of the *M*- and *P*-enantiomers (see Section 3.2). Chiral substituents at the periphery of the rosette assembly can strongly induce the formation of only one diastereomer. In this case, the double rosette displays a highly characteristic CD spectrum, while the individual compounds are hardly CD active. The extent of chiral induction can be quantified by ^1H NMR spectroscopy. If the assembly is present as a diastereomeric mixture (*M*- and *P*-), four signals for the NH_{DEB} -protons H_a and H_b are expected, while if only one diastereomer (*M*- or *P*-) is present, only two signals for the NH_{DEB} -protons H_a and H_b are expected. The integration of the signals of protons H_a and H_b allows the facile determination of the diastereomeric excess (d.e.).

Assembly $\mathbf{3g}_3\cdot(\text{DEB})_6$ (*L*-Ser(*t*Bu) and 2,2-dimethylpropyl spacer) and $\mathbf{3j}_3\cdot(\text{DEB})_6$ (*L*-Gln(*Trt*) and 2,2-dimethylpropyl spacer) do not show complete chiral induction, while assembly $\mathbf{3i}_3\cdot(\text{DEB})_6$ (*L*-Ser(*t*Bu) and propyl spacer) and $\mathbf{3k}_3\cdot(\text{DEB})_6$ (*L*-Gln(*Trt*) and propyl spacer) do. These results indicate that the degree of chiral induction is small for the less flexible spacer. A possible reason for this observation is that the 2,2-dimethylpropyl spacer, due to the steric bulk of the two geminal CH_3 groups, adopts a conformation in which the *t*Bu-protected *L*-Ser and *Trt*-protected *L*-Gln units experience steric hindrance regardless of the helicity of the rosette. Hence, the free energy difference between the two diastereomers is smaller.

However, with *R*-CYA or *S*-CYA (Scheme 4.1) instead of DEB the assembly formation with calix[4]arene dimelamines $\mathbf{3g}$ and $\mathbf{3i}$ gave a quantitative chiral induction and, as expected for enantiomers, the CD spectra of the assemblies $\mathbf{3g}_3\cdot(\text{R-CYA})_6$ and $\mathbf{3g}_3\cdot(\text{S-CYA})_6$ display opposite signals. Thus, ^1H NMR spectroscopy combined with CD spectroscopy showed that the *R*- or *S*-CYA determines the helicity completely, without interference of the chirality of the calix[4]arene dimelamine.

The chiral induction of the assemblies $\mathbf{4}_3\bullet(\text{DEB})_6$ was not studied in detail. In general, the signals for protons H_a and H_b are broad in the ^1H NMR spectra, which makes it difficult to determine how many signals are present in the spectra.

Thermodynamic Stability

The thermodynamic stability of an assembly is given by the difference in free energy, ΔG° , between the assembly and the free components. ΔH° is mainly determined by the enthalpy of hydrogen bond formation and is therefore proportional to the number of hydrogen bonds formed ($a_1 \times \text{HB}$). ΔS° is determined by the changes in translation and rotation entropy, and the entropy (de)solvation. These are related to $N-1$, in which N is the number of components involved ($a_2 \times (N-1)T$). The difference in free energy is given by $\Delta G^\circ = a_1 \times \text{HB} - a_2 \times (N-1)T$. The melting point index, I_{Tm} , corresponds to the temperature at which the assembly would dissociate into its separate components. At this temperature $\Delta G=0$, thus $\Delta H = T\Delta S$. Therefore Whitesides and co-workers¹⁰ defined $I_{\text{Tm}} = \text{HB} / (N-1)$ as a measure for the stability of hydrogen-bonded assemblies. In order to reach $\Delta G=0$ experimentally, the temperature can be increased ($T\Delta S$), or ΔH can be decreased by addition of a competing solvent.

^1H NMR titrations with $\text{DMSO-}d_6$ have been used to measure the stability of the assemblies¹⁰ (see also Chapter 3). The thermodynamic stability of the assemblies is given by χ , in which the χ -value represents the % of polar solvent present corresponding to the formation of only 50% of the assembly. These measured values were in good agreement with the calculated I_{Tm} values. Nevertheless, I_{Tm} values can only be used to compare the thermodynamic stability of comparable structures. If the entropy of the individual components is different, e.g. due to different flexibility, the calculated I_{Tm} values are not comparable. The net enthalpy strongly depends on the hydrogen bond formed, i.e. cyanurates form much stronger hydrogen bonds than barbiturates.¹¹

The effect of the different functional groups of **3** and **4** on the thermodynamic stability in CD_2Cl_2 of the corresponding hydrogen-bonded assemblies was investigated by addition of THF and monitoring of the CD spectra (see Table 4.3). The results indicate that the stability of assemblies depends on the side chain bulkiness of the amino acids.

Assemblies formed with 5,5-diethylbarbiturate ($\mathbf{3}_3\bullet(\text{DEB})_6$, 2,2-dimethylpropyl spacer), decrease in stability: $\mathbf{3c}_3\bullet(\text{DEB})_6$ ($\chi_{\text{THF}} = 26$; *L*-Ala) > $\mathbf{3e}_3\bullet(\text{DEB})_6$ ($\chi_{\text{THF}} = 20$; *L*-

Phe) and $\mathbf{3l}_3\bullet(\text{DEB})_6$ ($\chi_{\text{THF}} = 17$; *L*-Lys(Boc)). A similar trend is observed for assemblies formed with cyanurate ($\mathbf{3}_3\bullet(\text{R-CYA})_6$, 2,2-dimethylpropyl spacer). The highest thermodynamic stability is observed for assembly $\mathbf{3a}_3\bullet(\text{R-CYA})_6$ ($\chi_{\text{THF}} = 89$; Gly), while the thermodynamic stability of assemblies bearing a bulkier amino acid is significantly lower ($\mathbf{3g}_3\bullet(\text{RCYA})_6$ ($\chi_{\text{THF}} = 54$; *L*-Ser(*t*Bu)), and $\mathbf{3j}_3\bullet(\text{RCYA})_6$ ($\chi_{\text{THF}} = 59$; *L*-Gln(Trt)). Table 4.3 further indicates that assemblies of $\mathbf{3}$ with ureido linkages have a higher thermodynamic stability than assemblies of $\mathbf{4}$ with an amido linkage ($\mathbf{3a}_3\bullet(\text{R-CYA})_6$ ($\chi_{\text{THF}} = 89$) versus $\mathbf{4b}_3\bullet(\text{R-CYA})_6$ ($\chi_{\text{THF}} = 79$) and $\mathbf{3i}_3\bullet(\text{DEB})_6$ ($\chi_{\text{THF}} = 20$) versus $\mathbf{4k}_3\bullet(\text{DEB})_6$ ($\chi_{\text{THF}} = 10$), respectively). The results show once more that assemblies with cyanurates (CYA) are more stable than with barbiturates (DEB) due to the formation of stronger hydrogen bonds.¹¹

Table 4.3. Thermodynamic stability measurements of assemblies $\mathbf{3}_3\bullet(\text{DEB})_6$, $\mathbf{3}_3\bullet(\text{RCYA})_6$, $\mathbf{4}_3\bullet(\text{DEB})_6$, and $\mathbf{4}_3\bullet(\text{RCYA})_6$.

Assembly (ureido linkage)			Assembly (amido linkage)		
		$\chi_{\text{THF}}^{[a]}$			$\chi_{\text{THF}}^{[a]}$
$\mathbf{3a}_3\bullet(\text{R-CYA})_6$	Gly	89	$\mathbf{4b}_3\bullet(\text{R-CYA})_6$	Gly	79
$\mathbf{3b}_3\bullet(\text{R-CYA})_6$	Gly	88	$\mathbf{4c}_3\bullet(\text{DEB})_6$	<i>L</i> -Phe	17
$\mathbf{3c}_3\bullet(\text{DEB})_6$	<i>L</i> -Ala	26	$\mathbf{4d}_3\bullet(\text{DEB})_6$	<i>L</i> -Phe	7 ^[b]
$\mathbf{3e}_3\bullet(\text{DEB})_6$	<i>L</i> -Phe	20	$\mathbf{4g}_3\bullet(\text{DEB})_6$	<i>L</i> -Lys(Boc)	7 ^[b]
$\mathbf{3g}_3\bullet(\text{R-CYA})_6$	<i>L</i> -Ser(<i>t</i> Bu)	54	$\mathbf{4k}_3\bullet(\text{DEB})_6$	<i>L</i> -Ser(<i>t</i> Bu)	10
$\mathbf{3h}_3\bullet(\text{R-CYA})_6$	<i>L</i> -Ser(OH)	62	$\mathbf{4l}_3\bullet(\text{DEB})_6$	<i>L</i> -Ser(OH)	5 ^[c]
$\mathbf{3i}_3\bullet(\text{DEB})_6$	<i>L</i> -Ser(<i>t</i> Bu)	20			
$\mathbf{3j}_3\bullet(\text{R-CYA})_6$	<i>L</i> -Gln(Trt)	59			
$\mathbf{3l}_3\bullet(\text{DEB})_6$	<i>L</i> -Lys(Boc)	17			

^[a] χ = percentage of polar solvent at which 50% of the assembly is intact.

^[b] In 100% CH_2Cl_2 , the assemblies are only partially formed, therefore χ = percentage of polar solvent at which 50% of the assembly that was present at 100% CH_2Cl_2 is still intact.

^[c] No S-shape curve was observed.

The trend in the thermodynamic stability of the different assemblies $\mathbf{3}_3\bullet(\text{DEB})_6$ and $\mathbf{4}_3\bullet(\text{DEB})_6$ measured by CD is in agreement with the earlier ^1H NMR measurements, i.e.

- (i) the bulkiness of the amino acid side chain decreases the stability of the assemblies, and
 (ii) assemblies with ureido linkages are more stable than with amido linkages.

4.2.3 Peptide Functionalized Calix[4]arene Dimelamines **5**

Double rosette assemblies formed of dimelamines containing peptidic arms **5a-5e** (Chart 4.2) were investigated, because these would allow for a rapid increase in the chemical diversity of rosette libraries (Chapter 7). Assembly **2b₃•(DEB)₆** with triamino acid (Gly₃Cbz) side chains is formed in high yield (80 %) in CDCl₃ (see Section 4.2.1). Therefore, the first approach to introduce different amino acids onto the rosette platform concerned the assembly of calix[4]arene dimelamines containing linear peptides (**5a-e**, Chart 4.2). To avoid steric strain close to the rosette platform, Gly was always chosen as the first amino acid.

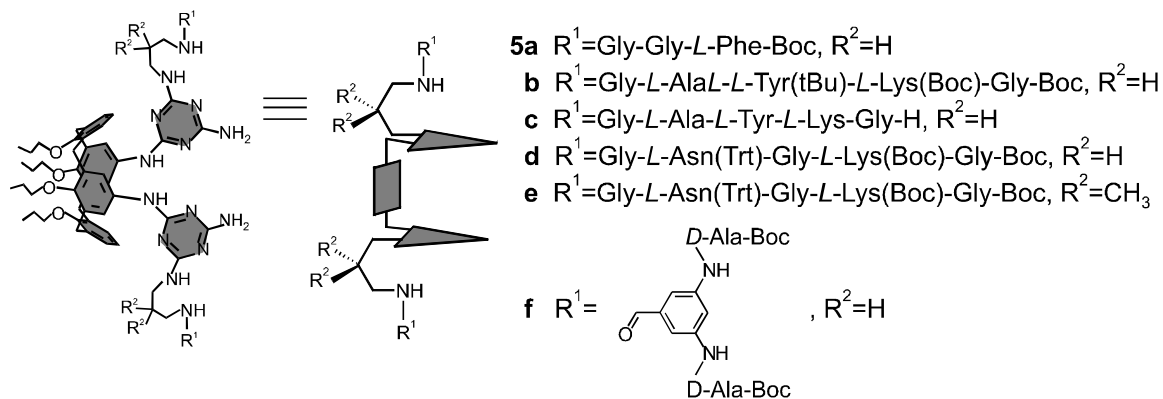


Chart 4.2. Molecular structure and schematic representation of peptide calix[4]arene dimelamine derivatives **5**.

The linear peptides were synthesized using solid-phase synthesis. The first amino acid, Fmoc-Gly-OH (4 equiv), was coupled to the ArgoGel-OH resin by using 2,6-dichlorobenzoylchloride (4 equiv) and pyridine (6.6 equiv). The following Fmoc-protected amino acids (4 equiv) were coupled to the resin using HBTU (4 equiv), and DIPEA (8 equiv) in an automated procedure.¹² Upon completion of the synthesis of the desired peptide, cleavage from the solid support was accomplished with 10% Et₃N in MeOH, yielding the methyl ester protected peptide (Figure 4.7). Deprotection of the methyl ester of the obtained peptide was achieved using LiOH (5 equiv) in a mixture of THF/MeOH (1:1). Subsequently, the peptide was coupled to the calix[4]arene

dimelamine **1a** or **1d** using standard peptide coupling conditions (HATU, HOBt, DIPEA, see experimental section).

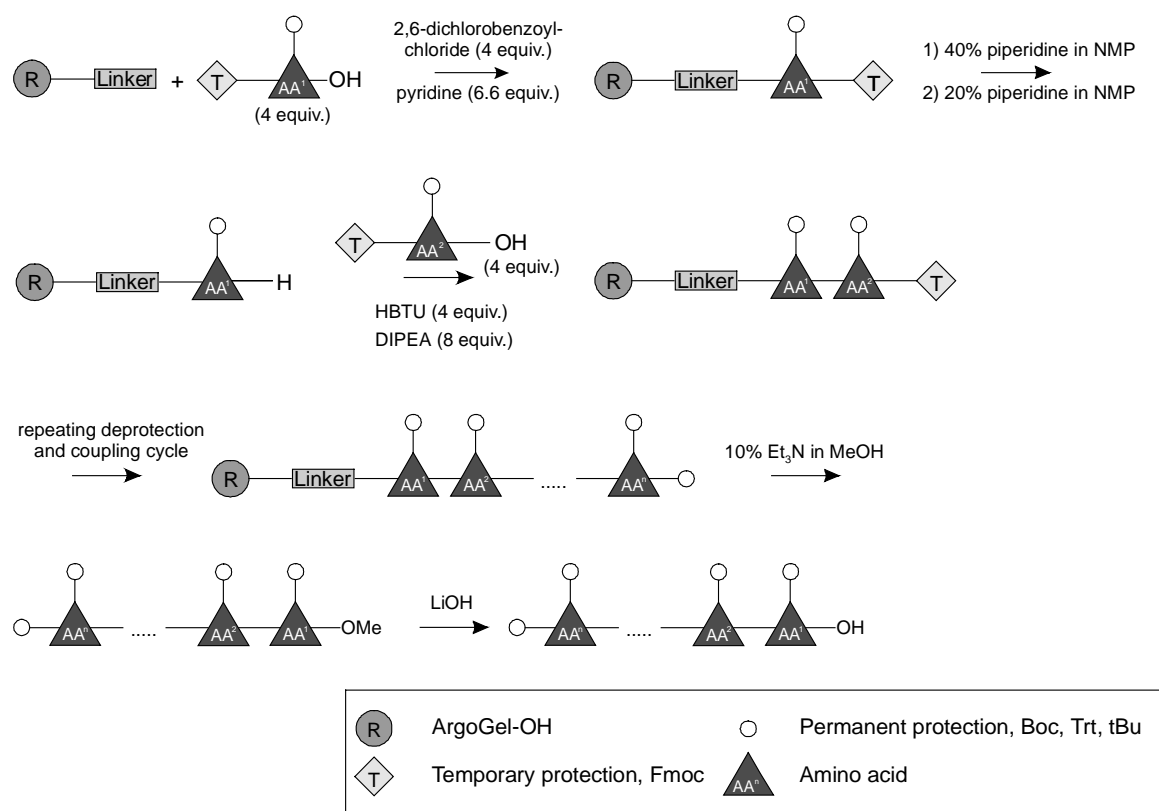


Figure 4.7. Solid-phase synthesis of the peptidic chains.

Assembly **5a₃•(DEB)₆** containing triamino acid Gly₂PheBoc is formed in ~ 80 % yield according to the intensities of the signals in the ¹H NMR spectrum of this assembly. This result is comparable to Gly₃Cbz (**2b₃•(DEB)₆**, Section 4.2.1).

In assembly **5a₃•(DEB)₆** the chain attached to the rosette platform is chiral (bearing *L*-Phe) and therefore, the assembly could exist as a mixture of the *P*- and *M*-diastereomers (see Chapter 3 and Section 4.2.2.2 for a more detailed discussion about chirality), giving two signals for a single proton in the ¹H NMR spectrum. The spectrum clearly shows two signals for both NH_{DEB}-proton H_a and the H_c proton, indicating that indeed both diastereomers are formed (Figure 4.8). This result is expected because the chiral centers in the assembly are twelve atoms away from the core of the double rosette. Integration of the signals of the NH_{DEB}-protons H_a and H_b should give the relative concentration of the *M*- and the *P*-diastereomers formed. Unfortunately the ¹H NMR

signals for the diastereomeric protons overlap with each other, making the accurate determination of the diastereomeric excess impossible. Nevertheless, CD spectroscopy of assembly **5a₃**•(DEB)₆ (1 mM in CDCl₃) showed a maximum intensity of $\Delta\epsilon = 7 \text{ l}\cdot\text{mol}^{-1}\cdot\text{cm}^{-1}$ at 290 nm. This small intensity indicates that both diastereomers must be present in an almost equimolar amounts in CDCl₃.

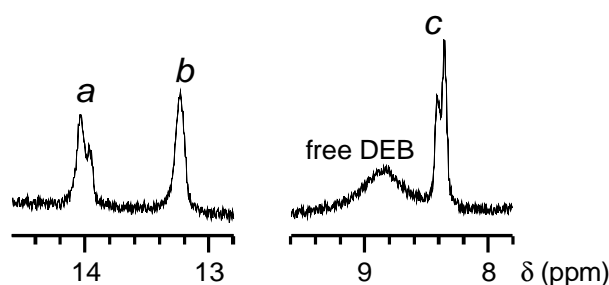


Figure 4.8. Part of the ¹H NMR spectrum of assembly **5a₃**•(DEB)₆, showing the formation of the *M*- and *P*-diastereomers (2 signals for NH_{DEB}-proton H_a and proton H_c)

Calix[4]arene dimelamines **5c** and **5d** (Chart 4.2) bearing pentapeptidic chains hardly showed rosette formation (< 20 %) with either DEB or BuCYA in the ¹H NMR spectrum. Contrary to what is observed for the single amino acid functionalized calix[4]arene dimelamines **4**, assembly **5e₃**•(DEB)₆, containing the 2,2-dimethylpropyl spacer, is formed in a high yield (> 80 %),¹³ while **5d**, bearing the less sterically demanding propyl spacer, does not form the rosette assembly.

A second approach for the introduction of multiple amino acids onto the rosette platform was also investigated. Instead of a linear peptide, a phenyl ring meta-substituted with amino acids was coupled to calix[4]arene dimelamines. In this way, additional preorganized binding cavities on both the top and bottom of the double rosette are introduced, thus reducing the loss in entropy upon complexation. The synthesis started with the protection of the carboxylic acid of 3,5-diaminobenzoic acid as the methyl ester, followed by the coupling of *N*-t-Boc-*D*-Ala-OH using standard peptide coupling conditions (HBTU, HOBt, DIPEA) to yield **6**. Deprotection of **6** by LiOH yielded carboxylic acid **7** (Figure 4.9), that is then coupled to the calix[4]arene dimelamine **1d** yielding **5f** (Chart 4.2).

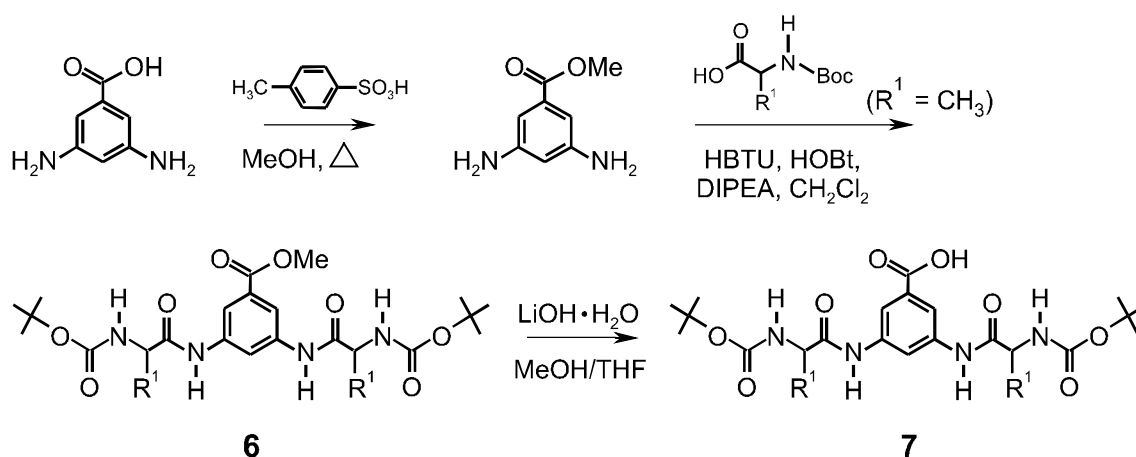


Figure 4.9. Synthesis of the di-amino acid functionalized building block **7**.

Calix[4]arene dimelamine **5f** does not form the rosette assembly with DEB in CDCl_3 , according to ^1H NMR spectroscopy (no signals were observed at 13-15 ppm). Fortunately, by changing to BuCYA (which forms stronger hydrogen bonds than DEB)¹¹ and using a less polar solvent (benzene- d_6), the assembly $\mathbf{5f}_3 \cdot (\text{BuCYA})_6$ was formed in > 80 % yield.¹³

4.3 Conclusions

The results shown in this chapter demonstrate that steric strain (i.e. the flexibility of the spacer connecting the amino acid to the double rosette, and the nature of the linkage connecting the amino acid to the spacer) in the assembly is an important factor that determines to what extent an assembly is formed. The double rosette assemblies $\mathbf{3}_3 \cdot (\text{DEB})_6$ (amino acids connected via an ureido linkage) are, in contrast to the assemblies $\mathbf{4}_3 \cdot (\text{DEB})_6$ (amino acids connected via an amido linkage), all formed in quantitative yield. The reason is that in assemblies $\mathbf{3}_3 \cdot (\text{DEB})_6$ the side chain is pointing away from the rosette platform, while for assemblies $\mathbf{4}_3 \cdot (\text{DEB})_6$, this side chain is pointing towards the rosette. The chiral induction is also strongly affected by the steric strain in the assemblies. Assemblies $\mathbf{3}_3 \cdot (\text{DEB})_6$ with propyl spacers show complete chiral induction, while in assemblies with the 2,2-dimethylpropyl spacer the induction of chirality is not always complete, i.e. more than one diastereomer is formed. Moreover, it is also shown that for the assemblies $\mathbf{3}_3 \cdot (\text{CYA})_6$ only the chiral center in the cyanurates (*R*- or *S*-CYA) determines the helicity and the degree of chiral induction of the assembly, irrespective of the chirality of the calix[4]arene dimelamines.

Furthermore, stability of the rosettes upon the introduction of longer peptidic chains onto the hydrogen-bonded platform seems to depend on the same factors. Therefore, a combinatorial approach towards the synthesis of hydrogen-bonded assemblies bearing peptidic chains is feasible.

4.4 Experimental Section

¹H NMR spectra were recorded on a Varian Unity 300 spectrometer using tetramethylsilane (TMS) or the corresponding solvent as internal reference. The 2D DQF-COSY consisted of 1024 datapoints in t_2 and 256 increments in t_1 . FAB-MS spectra were recorded with a Finnigan MAT 90 spectrometer with *m*-nitrobenzyl alcohol (NBA) as a matrix. MALDI-TOF mass spectra were recorded on a PerSpective Biosystems Voyager-De-RP spectrometer. A 337 nm UV nitrogen laser producing 3 ns pulses was used in the linear and reflectron modes. CD spectra were measured on a JASCO J-715 spectropolarimeter in a 0.01 cm width cell at 298 K. The synthesis of compounds **1a-d** is described in Chapter 3.

Formation of assemblies $Y_3 \cdot (DEB)_6 / (CYA)_6$ ($Y = 1-5$)

Hydrogen-bonded assemblies $Y_3 \cdot (DEB)_6$ were prepared by mixing calix[4]arene dimelamines **Y** with 2.5 or 4 equivalents of DEB in CDCl₃, CD₂Cl₂ or THF for 15 min. Similarly, assemblies $Y_3 \cdot (CYA)_6$ were prepared by mixing the corresponding calix[4]arene dimelamines **Y** with 2.5 equivalents of CYA in CDCl₃, CH₂Cl₂, C₆D₆ or THF for 15 min.

Calix[4]arene dimelamine 2a. Calix[4]arene dimelamine **1a** (0.050 g, 0.049 mmol), N-*t*-Boc-Gly-OH (0.019 g, 0.11 mmol), and DMAP (0.036 g, 0.30 mmol) were dissolved in CH₂Cl₂ (15 mL) and the mixture was stirred at 0 °C. EDC.HCl (0.038 mg, 0.11 mmol) was added and the mixture was stirred 1 hour at 0 °C, followed by 1 week at room temperature (after 3 days, extra DMAP (0.010 g, 0.082 mmol) and EDC.HCl (0.010 mg, 0.52 mmol) were added). The organic layer was washed with HCl (1N), H₂O, sat. Na₂CO₃ solution, and brine and dried (MgSO₄). Evaporation of the solvent gave the crude product as a white solid, which was purified by preparative TLC (CH₂Cl₂:MeOH:NH₄OH (90:9.5:0.5)) to give pure product in 34% (0.022 g, 0.017 mmol). ¹H NMR (300 MHz,

CDCl₃, 298K) δ = 7.6 (br s, 1 H; NH), 7.1-6.7, 6.5-5.9 (br m, 21 H; NH, ArH), 4.37 (ABq, $^2J(\text{H,H})=13.2$ Hz, 4 H; ArCH₂Ar), 3.94 (t, $^3J(\text{H,H})=6.9$ Hz, 4 H; OCH₂), 3.7 (br s, 2 H; CHH (Gly)), 3.59 (t, $^3J(\text{H,H})=6.3$ Hz, 4 H; OCH₂), 3.1-3.0 (m, 8 H; ArCH₂Ar, NCH₂C), 2.9 (br s, 4 H; NCH₂C), 2.4-2.0 (br s, 2 H; CHH (Gly)), 2.0- 1.7 (m, 8 H; OCH₂CH₂), 1.40 (s, 18 H; Boc), 1.02 (t, $^3J(\text{H,H})=7.4$ Hz, 6 H; OCH₂CH₂CH₃), 0.85-0.80 (m, 18 H; CCH₃, OCH₂CH₂CH₃). FAB-MS Calcd for C₇₀H₁₀₀N₁₆O₁₀ m/z = 1324.8, Found m/z = 1325.9 [M+H].

Calix[4]arene dimelamine 2b. Calix[4]arene dimelamine **1a** (0.050 g, 0.049 mmol), N-Cbz-Gly-Gly-Gly-OH (0.035 g, 0.11 mmol), and Et₃N (0.028 mL, 0.20 mmol) were dissolved in DMF (15 mL). HATU (0.041 mg, 0.11 mmol) was added and the mixture was stirred 1 day at room temperature. The solvent was evaporated and the solid was dissolved in CH₂Cl₂. The organic layer was washed with HCl (1N), H₂O, sat. Na₂CO₃ solution, and brine. Evaporation of the solvent gave the crude product as a white solid, which was purified by preparative TLC (CH₂Cl₂:MeOH:NH₄OH (90:9.5:0.5)) to give pure product in 44% (0.035 g, 0.022 mmol). FAB-MS Calcd for C₈₄H₁₀₈N₂₀O₁₄ m/z = 1620.8, Found m/z = 1622.3 [M+H].

Assembly 2b₃•(DEB)₆: ¹H NMR (400 MHz, CDCl₃, 298K) δ = 13.98 (s, 2 H; H_a), 13.19 (s, 2 H; H_b), 8.56 (s, 2 H; H_c), 7.77 (s, 2 H; H_d), 7.27-7.20 (m, 12 H; Cbz, ArH), 7.15-6.82 (m, 10 H; ArH, H_f, NH), 6.71 (s, 2 H; H_e), 6.53 (s, 2 H; NH), 6.38 (s, 2 H; NH), 6.12 (s, 2 H; H_h), 5.69 (s, 2 H; NH), 4.49 (ABq, $^2J(\text{H,H})=13.4$ Hz, 4 H; ArCH₂Ar), 4.16-3.78 (m, 16 H; OCH₂, NCH, CH₂(Cbz), CH(Gly)), 3.77-3.42 (m, 6 H; OCH₂, CH(Gly)), 3.40-2.94 (m, 8 H; NCH, CH(Gly), ArCH₂Ar), 2.76-2.60 (m, 4 H; NCH, CH(Gly)), 2.47 (d, $^2J(\text{H,H})=11.4$ Hz, 2 H; NCH), 2.25-1.80 (m, 16 H; OCH₂CH₂, CH₂(DEB)), 1.11 (t, $^3J(\text{H,H})=7.3$ Hz, 6 H; OCH₂CH₂CH₃), 1.05-0.68 (m, 30 H; OCH₂CH₂CH₃, CH₃(DEB), CH₃). Integrals are not exactly due to only 80% formation of the assembly.

Calix[4]arene dimelamine 2c. Calix[4]arene dimelamine **1a** (0.050 g, 0.049 mmol), N-t-Boc-L-Val-OH (0.024 g, 0.11 mmol), and DMAP (0.036 g, 0.30 mmol) were dissolved in CH₂Cl₂ (15 mL) and the mixture was stirred at 0 °C. EDC.HCl (0.038 mg, 0.11 mmol) was added and the mixture was stirred 1 hour at 0 °C, followed by 2 days at room temperature. The organic layer was washed with HCl (1N), H₂O, sat. Na₂CO₃ solution,

and brine and dried (MgSO₄). Evaporation of the solvent gave the crude product as a white solid, which was purified by preparative TLC (CH₂Cl₂:MeOH:NH₄OH (90:9.5:0.5)) to give pure product in 37% (0.026 g, 0.018 mmol). ¹H NMR (300 MHz, CDCl₃, 298K) δ = 7.9 (br s, 1 H; NH), 7.1-6.0, 5.6-4.8 (br m, 21 H; ArH, NH), 4.37, 3.06 (ABq, ²J(H,H)= 13.2 Hz, 8 H; ArCH₂Ar), 4.0-3.6 (m, 12 H; OCH₂, CH (Val)), 3.1-2.8 (m, 8 H; NCH₂), 2.15-1.96 (m, 2 H; CH (Val)), 1.95-1.73 (m, 8 H; OCH₂CH₂), 1.37 (s, 18 H; Boc), 1.00 (br t, 6 H; OCH₂CH₂CH₃), 0.95-0.70 (m, 30 H; CCH₃, CH₃(Val), OCH₂CH₂CH₃). FAB-MS Calcd for C₇₆H₁₁₂N₁₆O₁₀ *m/z* = 1408.9, Found *m/z* = 1409.8 [M+H].

Calix[4]arene dimelamine 2d. Calix[4]arene dimelamine **1a** (0.050 g, 0.049 mmol), N-t-Boc-L-Leu-OH (0.025 g, 0.11 mmol), and DMAP (0.036 g, 0.30 mmol) were dissolved in CH₂Cl₂ (15 mL) and the mixture was stirred at 0 °C. EDC.HCl (0.038 mg, 0.11 mmol) was added and the mixture was stirred 1 hour at 0 °C, followed by 2 days at room temperature. The organic layer was washed with HCl (1N), H₂O, sat. Na₂CO₃ solution, and brine and dried (MgSO₄). Evaporation of the solvent gave the crude product as a white solid, which was purified by preparative TLC (CH₂Cl₂:MeOH:NH₄OH (90:9.5:0.5)) to give pure product in 31% (0.022 g, 0.015 mmol). ¹H NMR (300 MHz, CDCl₃, 298K) δ = 7.8 (br s, 1 H; NH), 7.0-6.0, 6.1-4.8 (br m, 21 H; ArH, NH), 4.37, 3.06 (ABq, ²J(H,H)= 13.2 Hz, 8 H; ArCH₂Ar), 4.1-3.8 (m, 6 H; OCH₂, CHCH₂(Leu)), 3.6 (br s, 4 H; OCH₂), 3.1-2.8 (br m, 8 H; NCH₂C), 2.0-1.7 (m, 10 H; OCH₂CH₂, CH(Leu)), 1.7-1.5 (m, 4 H; CH₂(Leu)), 1.44-1.32 (m, 24 H; Boc, CH₃ (Leu)), 1.01 (br t, 6 H; OCH₂CH₂CH₃), 0.90-0.76 (m, 30 H; CCH₃, CH₃ (Leu), OCH₂CH₂CH₃). FAB-MS Calcd for C₇₈H₁₁₆N₁₆O₁₀ *m/z* = 1436.9, Found *m/z* = 1437.7 [M+H].

Calix[4]arene dimelamine 2e. Calix[4]arene dimelamine **1a** (0.050 g, 0.049 mmol), N-t-Boc-D-Leu-OH (0.025 g, 0.11 mmol), and DMAP (0.036 g, 0.30 mmol) were dissolved in CH₂Cl₂ (15 mL) and the mixture was stirred at 0 °C. EDC.HCl (0.038 mg, 0.11 mmol) was added and the mixture was stirred 1 hour at 0 °C, followed by 2 days at room temperature. The organic layer was washed with HCl (1N), H₂O, sat. Na₂CO₃ solution, and brine and dried (MgSO₄). Evaporation of the solvent gave the crude product as a white solid, which was purified by preparative TLC (CH₂Cl₂:MeOH:NH₄OH

(90:9.5:0.5)) to give pure product in 34% (0.024 g, 0.017 mmol). FAB-MS Calcd for $C_{78}H_{116}N_{16}O_{10}$ $m/z = 1436.9$, Found $m/z = 1437.8$ [M+H]. 1H NMR is identical to calix[4]arene dimelamine **2d**.

Calix[4]arene dimelamine 2f. Calix[4]arene dimelamine **1d** (0.10 g, 0.11 mmol), N-t-Boc-*L*-Leu-OH (0.055 g, 0.24 mmol), HBTU (0.18 g, 0.44 mmol) and DIPEA (0.08 mL, 0.44 mmol) were dissolved in CH_2Cl_2 (20 mL) and the mixture was stirred for 2 days at room temperature. The organic layer was washed with HCl (1N), H_2O , sat. Na_2CO_3 solution, and brine and dried ($MgSO_4$). Evaporation of the solvent gave the crude product as a white solid, which was purified by column chromatography (CH_2Cl_2 :MeOH: NH_4OH (90:9.5:0.5)) to give pure product in 62% (0.102 g, 0.068 mmol). 1H NMR (300 MHz, $DMSO-d_6$, 298 K) $\delta = 8.6, 8.4, 7.8, 7.5, 7.4, 6.9-6.6, 6.3-6.0$ (br s and m, 22 H; NH, ArH), 4.31 (ABq, $^2J(H,H) = 12.6$ Hz, 4 H; Ar CH_2 Ar), 3.88 (t, $^3J(H,H) = 7.8$ Hz, 4 H; OCH₂), 3.60 (t, $^3J(H,H) = 6.6$ Hz, 4 H; OCH₂), 3.3-2.97 (m, 12 H; Ar CH_2 Ar, NCH₂), 1.96-1.75 (m, 8 H; OCH₂CH₂), 1.6 (br s, 4 H; CH₂), 1.34 (s, 18 H; Boc), 1.06 (t, $^3J(H,H) = 7.2$ Hz, 6 H; OCH₂CH₂CH₃), 0.87 (t, $^3J(H,H) = 7.2$ Hz, 6 H; OCH₂CH₂CH₃). FAB-MS Calcd for $C_{74}H_{108}N_{16}O_{10}$ $m/z = 1380.8$, Found $m/z = 1381.8$ [M+H].

***N*-(*p*-Nitrophenoxycarbonyl)glycine ethyl ester.** Glycine ethyl ester hydrochloride (0.70 g, 5 mmol) was suspended in CH_2Cl_2 (10 mL). A solution of $NaHCO_3$ (0.42 g, 5 mmol) in H_2O (10 mL) was added. After 5 min of vigorous stirring $NaCl$ (0.5g) was added. Then, a solution of 4-nitrophenyl chloroformate (1.02 g, 5.05 mmol) in CH_2Cl_2 (2 mL) was added and the mixture was stirred overnight at room temperature. The aqueous layer was extracted with CH_2Cl_2 and the organic layers were combined and dried over $MgSO_4$. The solvents were evaporated and the solid was recrystallized from CH_2Cl_2 with hexane. The product was obtained as a crystalline solid in 34% yield (0.45 g, 1.7 mmol). 1H NMR (300 MHz, $CDCl_3$, 298K) $\delta = 8.29$ (d, $^3J(H,H) = 8$ Hz, 2 H; ArH), 7.37 (d, $^3J(H,H) = 8$ Hz, 2 H; ArH), 5.68 (s, 1 H; NH), 4.29 (q, $^3J(H,H) = 8$ Hz, 2 H; OCH₂), 4.11 (d, $^3J(H,H) = 8$ Hz, 2 H; α -CH₂), 1.37 (t, $^3J(H,H) = 8$ Hz, 3 H; OCH₂CH₃). FAB-MS Calcd for $C_{11}H_{12}N_2O_6$ $m/z = 268.1$, Found $m/z = 269.07$ [M+H].

***N*-(*p*-Nitrophenoxycarbonyl) phenylalanine methyl ester.** A solution of *L*-phenylalanine methyl ester hydrochloride (0.200 g, 0.93 mmol) and DIPEA (0.323 ml, 1.83 mmol) in CH₂Cl₂ (50 ml) was added drop by drop to a solution of *p*-nitrophenylchloroformate (0.374 g, 1.83 mmol) in CH₂Cl₂ (50 ml). After stirring for 2 h at room temperature, a few drops of acetic acid were added and the solvents were evaporated. The crude product was purified by column chromatography (CH₂Cl₂ : MeOH : AcOH = 99.25:0.50:0.25 (v/v)). The product was obtained as a white solid in 60% (0.192 g, 0.56 mmol) yield. ¹H NMR (300 MHz, CDCl₃, 298K) δ = 8.25 (d, ³*J*(H,H)= 8 Hz, 2 H; ArH), 7.45-7.25 (m, 5 H; ArH), 7.20 (d, ³*J*(H,H)= 8 Hz, 2 H; ArH), 5.63 (m, 1 H; NH), 4.74 (m, 1 H; α-CH), 3.83 (s, 3 H; OCH₃), 3.40-3.00 (m, 2 H; ArCH₂). FAB-MS Calcd for C₁₇H₁₆N₂O₆ *m/z* = 344.34, Found *m/z* = 345.05 ([M+H]).

General Procedure for the Preparation of *N*-(*p*-Nitrophenoxycarbonyl)amino Acid Esters. The HCl salt of the corresponding amino acid (1.0 mmol) was suspended in CH₂Cl₂ and a solution of NaHCO₃ (0.084 g, 1.0 mmol) in H₂O was added. The mixture was stirred vigorously for 5 min. and NaCl (0.5 g) was added, followed by the addition of 4-nitrophenyl chloroformate (0.20 g, 1.01 mmol) in CH₂Cl₂. The mixture was stirred overnight and the aqueous layer was extracted with CH₂Cl₂, the organic layers were combined and dried (MgSO₄). Evaporation of the solvent gave the crude product, which was recrystallized from CH₂Cl₂ and hexane to give the pure product in yields varying from 18-65 %.

***N*-(*p*-Nitrophenoxycarbonyl)alanine methyl ester.** The product was obtained in 18 % (0.049 g, 0.18 mmol) yield. ¹H NMR (300 MHz, CDCl₃, 298K) δ = 8.28 (d, ³*J*(H,H)=9 Hz, 2 H; ArH), 7.36 (d, ³*J*(H,H)= 9 Hz, 2 H; ArH), 5.76 (m, 1 H; NH), 4.48 (m, 1 H; NCH), 3.83 (s, 3 H; OCH₃), 1.70-1.50 (d, ³*J*(H,H)= 6 Hz, 3 H; CCH₃). FAB-MS Calcd for C₁₁H₁₂N₂O₆ *m/z* = 268.1, Found *m/z* = 269.0 ([M+H]).

***N*-(*p*-Nitrophenoxycarbonyl)-*O*-(*tert*-butyl)serine methyl ester.** The product was obtained in 65% (0.220 g, 0.65 mmol) yield. ¹H NMR (300, CDCl₃, 298K) δ = 8.28 (d, ³*J*(H,H)= 9 Hz, 2 H; ArH), 7.37 (d, ³*J*(H,H)= 9 Hz, 2 H; ArH), 6.02 (m, 1 H; NH), 4.52

(m, 1 H; NCH), 3.92 (m, 2 H; CH₂), 3.83 (s, 3 H; OCH₃), 3.70 (m, 2 H; CH₂), 1.27 (s, 9 H; CH₃); FAB-MS Calcd for C₁₅H₂₀N₂O₇ m/z = 340.1, Found m/z = 341.1 ([M+H]).

***N*^α-(*p*-Nitrophenoxycarbonyl)-*N*^γ-(triphenylmethyl)glutamine methyl ester.** The crude product was obtained in 94% (0.532 g, 0.94 mmol) yield. The crude product was used without further purification. ¹H NMR (300 MHz, CDCl₃, 298K) δ = 8.26 (d, ³*J*(H,H)= 9 Hz, 2 H; ArH), 7.40-7.15 (m, 17 H; ArH), 6.81 (s, 1 H; N^γH), 6.33 (m, 1 H; N^αH), 4.40 (m, 1 H; N^αCH), 3.79 (s, 3 H; OCH₃), 2.52 (m, 2 H; CH₂), 2.28 (m, 1 H; CH₂), 2.13 (m, 1 H; CH₂); FAB-MS Calcd for C₃₂H₂₈N₃O₇ m/z = 566.2, Found m/z = 567.2 [M+H].

***N*^α-(*p*-Nitrophenoxycarbonyl)-*N*^ε-(*tert*-butyloxycarbonyl)lysine methyl ester.** The product was obtained in 54 % (0.23 g, 0.54 mmol) yield. ¹H NMR (300 MHz, CDCl₃, 298K) δ = 8.27 (d, ³*J*(H,H)= 9 Hz, 2 H; ArH), 7.36 (d, ³*J*(H,H)= 9 Hz, 2 H; ArH), 5.98 (m, 1 H; N^αH), 4.62 (s, 1 H; N^εH), 4.41 (m, 1 H; N^αCH), 3.83 (s, 3 H; OCH₃), 3.18 (m, 2 H; CH₂), 2.05-1.75 (br m, 2 H; CH₂), 1.70-1.35 (br m, 13 H; CH₂, CH₃). FAB-MS Calcd for C₁₉H₂₇N₃O₈ m/z = 425.2, Found m/z = 426.3 [M+H].

General Procedure for the Preparation of Amino Acid Functionalized Calix[4]arene Dimelamines 3. Calix[4]arene dimelamine **1a** or **1d** (0.10 mmol) and DIPEA (0.21 mmol) were dissolved in CH₂Cl₂ and cooled to -70 °C and a solution of the corresponding N-(*p*-nitrophenoxycarbonyl)amino acid ester (0.21 mmol) in CH₂Cl₂ was added dropwise. The mixture was stirred 1 hour at -70 °C, followed by 1-2 days at room temperature. A 25% NH₄OH (aq) solution was added and the mixture was stirred for an additional 10 minutes. The organic layer was washed several times with sat. NaHCO₃ and brine and dried (MgSO₄). Evaporation of the solvent and purification by column chromatography (if necessary) gave the product in yields varying from 36-90 %.

Calix[4]arene dimelamine 3a was prepared from calix[4]arene dimelamine **1a** (0.10 g, 0.10 mmol) *N*-(*p*-nitrophenoxycarbonyl)glycine ethyl ester (0.56 g, 0.20 mmol) and the crude product was obtained as a yellow solid in 90% yield. FAB-MS Calcd for C₆₆H₉₂N₁₆O₁₀ m/z = 1269.5, Found m/z = 1269.80 [M+H].

Assembly 3a₃•(DEB)₆: ¹H NMR (300 MHz, CDCl₃, 298K) δ = 13.98 (s, 2 H; H_a), 13.21 (s, 2 H; H_b), 8.67 (s, 2 H; H_c), 7.71 (m, 2 H; H_d), 7.13 (m, 6 H; ArH, H_g), 6.98 (s, 2 H; H_f), 6.93-6.83 (t, 2 H; ArH), 6.75 (s, 2 H; H_e), 6.12 (s, 2 H; H_h), 5.58 (d, 2 H; H_m), 4.46 (ABq, ²J(H,H)= 12 Hz, 4 H; ArCH₂Ar), 4.06 (m, 8 H; OCH₂), 3.92 (m, 2 H; CH(Gly)), 3.72 (m, 2 H; H_i), 3.70-3.50 (br m, 4 H; OCH₂), 3.30-3.12 (br m, 6 H; ArCH₂Ar, CH(Gly)), 3.04 (d, ³J(H,H)= 12 Hz, 2 H; H_n), 2.82 (m, 2 H; H_k), 2.63 (d, ²J(H,H)= 12 Hz, 2 H; H_j), 2.40 (d, ²J(H,H)= 12 Hz, 2 H; H_l), 2.20-1.80 (br m, 16 H; OCH₂CH₂, CH₂(DEB)), 1.30-1.17 (br m, 6 H; CH₃), 1.17-1.06 (br m, 6 H; CH₃), 1.06-0.96 (br m, 12 H; CH₃), 0.96-0.75 (br m, 18 H; CH₃).

Calix[4]arene dimelamine 3b was prepared from calix[4]arene dimelamine **1d** (0.10 g, 0.10 mmol) and *N*-(*p*-nitrophenoxycarbonyl)glycine ethyl ester (0.056 g, 0.20 mmol) and obtained as a white solid in 86% yield. FAB-MS Calcd for C₆₂H₈₄N₁₆O₁₀ *m/z* = 1212.7, Found *m/z* = 1213.74 [M+H].

Assembly 3b₃•(DEB)₆: ¹H NMR (300 MHz, CDCl₃, 298K) δ = 13.94 (s, 2 H; H_a), 13.19 (s, 2 H; H_b), 8.45 (s, 2 H; H_c), 7.50 (m, 2 H; H_d), 7.10-6.98 (m, 6 H; ArH, H_g), 6.88 (s, 2 H; H_f), 6.93-6.83 (t, 2 H; ArH), 6.66 (s, 2 H; H_e), 6.02 (s, 2 H; H_h), 5.18 (m, 2 H; H_m), 4.46 (ABq, ²J(H,H)= 15 Hz, 4 H; ArCH₂Ar), 4.32-3.35 (m, 20 H; OCH₂, CH₂), 3.18-2.97 (m, 6 H; ArCH₂Ar, CHH), 2.75 (m, 2 H; CHH), 2.10-1.50 (m, 16 H; OCH₂CH₂, CH₂(DEB)), 1.16 (t, ³J(H,H)= 7 Hz, 6 H; CH₃), 1.05 (t, ³J(H,H)= 7 Hz, 6 H; CH₃), 0.94 (br t, 6 H; CH₃), 0.88-0.75 (m, 12 H; CH₃).

Calix[4]arene dimelamine 3c was prepared from calix[4]arene dimelamine **1a** (0.10 g, 0.10 mmol) and *N*-(*p*-nitrophenoxycarbonyl)alanine methyl ester (0.054 g, 0.20 mmol) and obtained as a white solid in 80% yield. FAB-MS Calcd for C₆₆H₉₂N₁₆O₁₀ *m/z* = 1269.5, Found *m/z* = 1268.71 [M+H]. Anal. Calcd for C₆₆H₉₂N₁₆O₁₀ •0.17(CH₂Cl₂)=C=61.90; H=7.25; N=17.45, Found C=62.31; H=7.05; N=16.79.

Assembly 3c₃•(RCYA)₆: ¹H NMR (300 MHz, CD₂Cl₂, 298K) δ = 14.38 (s, 2 H; H_a), 14.00 (s, 2 H; H_b), 8.83 (s, 2 H; H_c), 7.70 (m, 2 H; H_d), 7.48 (m, 4 H; ArH), 7.37 (m, 4 H; ArH), 7.30-7.10 (m, 10 H; ArH, H_e, H_f), 6.92 (d, ³J(H,H)= 6 Hz, 2 H; ArH), 6.70 (t, ³J(H,H)= 6 Hz, 2 H; ArH), 6.11 (q, ³J(H,H)= 8 Hz, 2 H; CH cyanurate), 6.04 (s, 2 H; H_h), 5.40 (m, 2 H; H_m), 4.48 (ABq, ²J(H,H)= 15 Hz, 4 H; ArCH₂Ar), 4.20-3.85 (m, 8 H; H_o,

OCH₂, H_i), 3.60 (m, 4 H; OCH₂), 3.53 (m, 6 H; OCH₃), 3.27 (d, ²*J*(H,H)= 15 Hz, 2 H; ArCH₂Ar), 3.20-2.90 (m, 6 H; H_k, ArCH₂Ar, H_n), 2.73 (d, ²*J*(H,H)= 13 Hz, 2 H; H_j), 2.26 (d, ²*J*(H,H)= 14 Hz, 2 H; H_l), 2.11 (d, ³*J*(H,H)= 6 Hz, 6 H; CH₃ cyanurate), 2.00-1.70 (m, 8 H; OCH₂CH₂), 1.03 (m, 12 H; OCH₂CH₂CH₃, CCH₃), 0.91 (d, ³*J*(H,H)= 7 Hz, 6 H; H_q), 0.78 (t, ³*J*(H,H)= 7 Hz, 6 H; OCH₂CH₂CH₃), 0.70 (s, 6 H; CCH₃).

Calix[4]arene dimelamine 3d was prepared from calix[4]arene dimelamine **1d** (0.052 g, 0.055 mmol) and *N*-(*p*-nitrophenoxycarbonyl)alanine methyl ester (0.031 g, 0.11 mmol) and obtained as a white solid in 46% yield. ¹H NMR (300 MHz, DMSO-*d*₆, 298 K) δ = 8.6, 8.4, 7.5, 7.4, 6.5-5.9 (br s and m, 22 H; ArH, NH), 4.13 (ABq, ²*J*(H,H)= 13.3 Hz, 4 H; ArCH₂Ar), 4.13 (m, 2 H; CH(Ala)), 3.89 (t, ³*J*(H,H)= 8.6 Hz, 4 H; OCH₂), 4.07-3.53 (m, 10 H; OCH₂, OCH₃), 3.2-2.93 (m, 12 H; ArCH₂Ar, NCH₂), 2.02-0.75 (m, 8 H; OCH₂CH₂), 1.57 (br s, 4 H; CH₂), 1.12 (br s, 6 H; CH₃(Ala)), 1.06 (t, ³*J*(H,H)= 7.5 Hz, 6 H; OCH₂CH₂CH₃), 0.88 (t, ³*J*(H,H)= 7.5 Hz, 6 H; OCH₂CH₂CH₃). FAB-MS Calcd for C₆₂H₈₄N₁₆O₁₀ *m/z* = 1212.7, Found *m/z* = 1213.9 [M+H].

Calix[4]arene dimelamine 3e was prepared from calix[4]arene dimelamine **1a** (0.10 g, 0.10 mmol) and *N*-(*p*-nitrophenoxycarbonyl) phenylalanine methyl ester (0.68 g, 0.19 mmol) and obtained as a white solid in 80% yield. ¹H NMR (300 MHz, CDCl₃, 298K) δ = 7.60-7.06 (m, 18 H; ArH), 6.94 (m, 2 H; ArH), 6.40-6.00 (m, 4 H; NH), 4.80-4.60 (m, 2 H; α-CH), 4.50 (d, ²*J*(H,H)= 12 Hz, 4 H; ArCH₂Ar), 4.08 (t, ³*J*(H,H)= 8 Hz, 4 H; OCH₂), 3.80-3.50 (m, 10 H; OCH₂, OCH₃), 3.30-2.60 (m, 16 H; ArCH₂Ar, ArCH₂, NCH₂), 2.20-1.40 (m, 8 H; OCH₂CH₂), 1.13 (t, ³*J*(H,H)= 8 Hz, 6 H; OCH₂CH₂CH₃), 1.00-0.60 (m, 16 H; OCH₂CH₂CH₃, CCH₃). FAB-MS Calcd for C₇₈H₁₀₀N₁₆O₁₀ *m/z* = 1420.76, Found *m/z* = 1421.85 [M+H]. Anal. Calcd for C₇₈H₁₀₀N₁₆O₁₀ C=65.89; H=7.09; N=15.76, Found C=65.42; H=6.76; N=15.54.

Assembly 3e₃•(DEB)₆: ¹H NMR (300 MHz, CDCl₃, 298K) δ = 13.96 (s, 2 H; H_a), 13.25 (s, 2 H; H_b), 8.61 (s, 2 H; H_c), 7.80 (s, 2 H; H_d), 7.33 (s, 2 H; H_e), 7.20-7.10 (m, 10 H; ArH), 7.03 (m, 4 H; ArH), 6.99 (s, 2 H; H_f), 6.86 (t, ³*J*(H,H)= 7 Hz, 2 H; ArH), 6.74 (s, 2 H; H_e), 6.22 (s, 2 H; H_h), 5.32 (d, ³*J*(H,H)= 9 Hz, 2 H; H_m), 4.56 (ABq, ²*J*(H,H)= 13 Hz, 4 H; ArCH₂Ar), 4.35 (q, ³*J*(H,H)= 8 Hz, 2 H; H_o), 4.20-3.90 (m, 6 H; OCH₂, H_i), 3.71 (m, 4 H; OCH₂), 3.55 (s, 6 H; OCH₃), 3.41 (d, ³*J*(H,H)= 9 Hz, 2 H; H_n), 3.29 (d, ²*J*(H,H)= 13

Hz, 2 H; ArCH₂Ar), 3.20 (d, 2 H; ²J(H,H)= 13 Hz, ArCH₂Ar), 3.08 (m, 2 H; H_k), 2.79 (m, 2 H; H_q), 2.70 (d, ²J(H,H)= 11 Hz, 2 H; H_j), 2.50 (d, ²J(H,H)= 11 Hz, 2 H; H_i), 2.36 (m, 2 H; H_r), 2.02 (m, 8 H; OCH₂CH₂, CH₂(DEB)), 1.93 (m, 4 H; OCH₂CH₂), 1.81 (m, 4 H; CH₂(DEB)), 1.15 (t, ³J(H,H)= 6 Hz, 6 H; OCH₂CH₂CH₃), 1.01 (m, 12 H; CH₃, CH₃(DEB)), 0.86 (m, 12 H; CH₃, OCH₂CH₂CH₃), 0.68 (t, ³J(H,H)= 6 Hz, 6 H; CH₃(DEB)).

Calix[4]arene dimelamine 3f was prepared from calix[4]arene dimelamine **1d** (0.050 g, 0.050 mmol) and *N*-(*p*-nitrophenoxycarbonyl) phenylalanine methyl ester (0.036g, 0.10 mmol) and obtained as a white solid in 80% yield. ¹H NMR (300 MHz, DMSO-*d*₆, 298 K) δ = 8.6, 8.4, 7.5-7.0, 6.9-6.0 (br s and m, 32 H; ArH, NH), 4.2-4.1 (m, 6 H; ArCH₂Ar, CH(Ph)), 3.90 (t, ³J(H,H)= 7.2 Hz, 4 H; OCH₂), 3.78-3.49 (m, 10 H; OCH₂, OCH₃), 3.4-2.9 (m, 16 H; ArCH₂Ar, CH₂(Ph), NCH₂), 2.0-1.7 (m, 8 H; OCH₂CH₂), 1.55 (br s, 4 H; CH₂), 1.13 (t, ³J(H,H)=7.5 Hz, 6 H; OCH₂CH₂CH₃), 1.00-0.60 (t, ³J(H,H)=7.5 Hz, 6 H; OCH₂CH₂CH₃). FAB-MS Calcd for C₇₄H₉₂N₁₆O₁₀ *m/z* = 1364.7, Found *m/z* = 1399.20 [M+Cl].

Calix[4]arene dimelamine 3g was prepared from calix[4]arene dimelamine **1a** (0.050 g, 0.050 mmol) and *N*-(*p*-nitrophenoxycarbonyl)-*O*-(*tert*-butyl)serine methyl ester (0.036 g, 0.11 mmol) and obtained as a white solid in 81% yield. FAB-MS Calcd for C₇₄H₁₀₈N₁₆O₁₂ *m/z* = 1412.8, Found *m/z* = 1413.7 [M+H].

Assembly 3g₃•(R-CYA)₆: ¹H NMR (300 MHz, CD₂Cl₂, 298K) δ = 14.55 (s, 2 H; H_a), 14.12 (s, 2 H; H_b), 8.87 (s, 2 H; H_c), 7.72 (d, ³J(H,H)= 7 Hz, 2 H; H_d), 7.46 (d, ³J(H,H)= 7 Hz, 2 H; ArH), 7.39 (s, 2 H; ArH), 7.35-7.12 (br m, 6 H; ArH), 7.15 (d, ³J(H,H)= 6 Hz, 2 H; ArH), 6.86 (d, ³J(H,H)= 6 Hz, 2 H; ArH), 6.65 (t, ³J(H,H)= 6 Hz, 2 H; ArH), 6.15 (q, ³J(H,H)= 6 Hz, 2 H; CH cyanurate), 6.02 (s, 2 H; H_h), 4.84 (m, 2 H; H_m), 4.43 (ABq, ²J(H,H)= 14 Hz, 4 H; ArCH₂Ar), 4.15-3.90 (br m, 8 H; H_o, OCH₂, H_i), 3.67-3.42 (br m, 10 H; OCH₂, OCH₃), 3.35 (m, 2 H; H_q), 3.20 (m, 4 H; ArCH₂Ar, H_n), 3.10-2.85 (br m, 4 H; ArCH₂Ar, H_k), 2.79 (d, ²J(H,H)= 14 Hz, 2 H; H_j), 2.46 (d, ²J(H,H)= 14 Hz, 2 H; H_i), 2.08 (d, ³J(H,H)= 8 Hz, 6 H; CH₃ cyanurate), 1.77 (m, 10 H; OCH₂CH₂, H_r) 1.05 (t, ³J(H,H)= 7 Hz, 6 H; OCH₂CH₂CH₃), 1.00 (s, 18 H; tBu), 0.88 (s, 6 H; CCH₃), 0.78 (t, ³J(H,H)= 7 Hz, 6 H; OCH₂CH₂CH₃), 0.73 (s, 6 H; CCH₃).

Calix[4]arene dimelamine 3h. Calix[4]arene dimelamine **3g** (70 mg, 50 μmol) was dissolved in TFA (2 ml) and stirred overnight. The mixture was evaporated to dryness and the residue was dissolved in CH_2Cl_2 (10 ml). It was washed with NaOH (1N). After column chromatography (CH_2Cl_2 : MeOH : NH_4OH (aq) = 90:9:1 (v/v)) the product was obtained in 38 % yield (25 mg, 1.9 μmol). FAB-MS Calcd for $\text{C}_{66}\text{H}_{92}\text{N}_{16}\text{O}_{12}$ m/z = 1300.7, Found m/z = 1302.2 [M+H].

Assembly 3h \cdot (R-CYA) $_6$ ^1H NMR (300 MHz, CDCl_3 , 298K) δ = 14.43 (s, 2 H; H_a), 13.98 (s, 2 H; H_b), 8.80 (s, 2 H; H_c), 7.72 (d, $^3J(\text{H,H})$ = 10 Hz, 2 H; H_d), 7.42 (m, 4 H; ArH), 7.40-7.15 (br m; 8 H, ArH), 7.11 (d, $^3J(\text{H,H})$ = 8 Hz, 2 H; ArH), 6.91 (d, $^3J(\text{H,H})$ = 6 Hz, 2 H; ArH), 6.67 (t, $^3J(\text{H,H})$ = 7 Hz, 2 H; ArH), 6.13 (q, $^3J(\text{H,H})$ = 8 Hz, 2 H; CH cyanurate), 5.98 (s, 2 H; H_h), 5.38 (d, $^3J(\text{H,H})$ = 10 Hz, 2 H; H_m), 4.44 (ABq, $^2J(\text{H,H})$ = 14 Hz, 4 H; ArCH_2Ar), 3.99 (m; 6 H, OCH_2 , H_o), 3.80-3.45 (br m, 12 H; OCH_2 , OCH_3), 3.41 (m, 2 H; H_q), 3.20 (m, 4 H; ArCH_2Ar , H_n), 3.02 (m, 4 H; ArCH_2Ar , H_k), 2.74 (d, $^2J(\text{H,H})$ = 14 Hz, 2 H; H_j), 2.31 (d, $^2J(\text{H,H})$ = 14 Hz, 2 H; H_i), 2.10 (d, $^3J(\text{H,H})$ = 8 Hz, 6 H; CH_3 cyanurate), 1.91 (m, 10 H; OCH_2CH_2 , H_r), 2.03 (m, 12 H; $\text{OCH}_2\text{CH}_2\text{CH}_3$, CCH_3), 0.79 (t, $^3J(\text{H,H})$ = 8 Hz, 6 H; $\text{OCH}_2\text{CH}_2\text{CH}_3$), 0.68 (s, 6 H; CCH_3).

Calix[4]arene dimelamine 3i was prepared from calix[4]arene dimelamine **1d** (0.070 g, 0.073 mmol) and *N*-(*p*-nitrophenoxycarbonyl)-*O*-(*tert*-butyl)serine methyl ester (0.053 g, 0.15 mmol) and obtained as a white solid in 83% yield. ^1H NMR (300 MHz, $\text{DMSO}-d_6$, 298 K) δ = 8.6, 8.4, 7.5-7.4, 6.6-6.7, 6.4-6.0 (br s and m, 22 H; NH, ArH), 4.32 (ABq, $^2J(\text{H,H})$ =12.8 Hz, 6 H; ArCH_2Ar ; $\text{CH}(\text{Ser})$), 3.89 (t, $^3J(\text{H,H})$ =8.6 Hz, 4 H; OCH_2), 3.68-3.52 (m, 12 H; OCH_2 , OCH_3 , CH), 3.3-3.0 (m, 16 H; NCH, ArCH_2Ar , CH), 2.00-1.76 (m, 8 H; OCH_2CH_2), 1.58 (br s, 4 H; CH_2), 1.14-1.00 (m, 24 H; tBu, $\text{OCH}_2\text{CH}_2\text{CH}_3$), 0.88 (t, $^3J(\text{H,H})$ =8.5 Hz, 6 H; $\text{OCH}_2\text{CH}_2\text{CH}_3$). FAB-MS Calcd for $\text{C}_{70}\text{H}_{100}\text{N}_{16}\text{O}_{12}$ m/z = 1356.8, Found m/z = 1357.9 [M+H].

Calix[4]arene dimelamine 3j was prepared from calix[4]arene dimelamine **1a** (0.065 g, 0.065 mmol) and *N* $^\alpha$ -(*p*-nitrophenoxycarbonyl)-*N* $^\gamma$ -(triphenylmethyl)glutamine methyl ester (0.079 g, 0.14 mmol) and obtained as a white solid in 36% yield (Column chromatography EtOAc:EtOH:H $_2$ O (50:7:4)). FAB-MS Calcd for $\text{C}_{108}\text{H}_{126}\text{N}_{18}\text{O}_{12}$ m/z = 1867.0, Found m/z = 1869.2 [M+H].

Assembly 3j₃•(RCYA)₆. ¹H NMR (300 MHz, CD₂Cl₂, 298K) δ = 14.38 (s, 2 H; H_a), 14.01 (s, 2 H; H_b), 8.85 (s, 2 H; H_c), 7.77 (d, ³J(H,H)= 10 Hz, 2 H; H_d), 7.49 (m, 4 H; ArH), 7.40-6.95 (br m, 38 H; ArH), 6.90 (d, ³J(H,H)= 8 Hz, 2 H; ArH), 6.81 (s, 2 H; ArH), 6.73 (t, ³J(H,H)= 7 Hz, 2 H; ArH), 6.14 (q, ³J(H,H)= 8 Hz, 2 H; CH cyanurate), 6.02 (s, 2 H; H_h), 5.46 (d, ³J(H,H)= 8 Hz, 2 H; H_m), 4.65-4.15 (m, 6 H; ArCH₂Ar, H_o), 4.04 (m, 6 H; OCH₂, H_i), 3.70-3.40 (br m, 10 H; OCH₂; OCH₃), 3.24 (d, ³J(H,H)= 13 Hz, 2 H; H_n), 3.10-2.70 (br m, 6 H; ArCH₂Ar, H_j), 2.30 (m, 4 H; H_l, H_q), 2.12 (m, 6 H; CH₃ cyanurate), 2.10-1.70 (br. m, 10 H; H_r, OCH₂CH₂), 1.20 (m, 4 H; CH₂), 1.04 (m, 12 H; OCH₂CH₂CH₃, CCH₃), 0.79 (m, 12 H, OCH₂CH₂CH₃, CCH₃).

Calix[4]arene dimelamine 3k was prepared from calix[4]arene dimelamine **1d** (0.075 g, 0.079 mmol) and *N*^α-(*p*-nitrophenoxycarbonyl)-*N*^γ-(triphenylmethyl)glutamine methyl ester (0.13 g, 0.20 mmol) and obtained as a white solid in 82% yield. ¹H NMR (300 MHz, DMSO-*d*₆, 298 K) δ = 8.7-9.6, 8.4, 7.4, 7.3-7.1, 6.7, 6.4-6.0, 5.6 (br s and m, 54 H; NH, ArH), 4.33 (ABq, ²J(H,H)= 12.8 Hz, 4 H; ArCH₂Ar), 4.10 (m, 2 H; CH(Gln)), 3.87 (t, ³J(H,H)= 8.6 Hz, 4 H; OCH₂), 3.69-3.53 (m, 12 H; OCH₂, OCH₃, CH), 3.47-2.97 (m, 16 H; NCH, ArCH₂Ar, CH), 2.3 (m, 4 H; CH), 2.00-1.73 (m, 8 H; OCH₂CH₂), 1.59 (br s, 4 H; CH₂), 1.06 (t, ³J(H,H)= 7.7 Hz, 6 H; OCH₂CH₂CH₃), 0.88 (t, ³J(H,H)= 7.7 Hz, 6 H; OCH₂CH₂CH₃). FAB-MS Calcd for C₁₀₄H₁₁₈N₁₈O₁₂ *m/z* = 1810.9, Found *m/z* = 1812.1 [M+H].

Calix[4]arene dimelamine 3l was prepared from calix[4]arene dimelamine **1a** (0.15 g, 0.15 mmol) and *N*^α-(*p*-nitrophenoxycarbonyl)-*N*^ε-(*tert*-butyloxycarbonyl)lysine methyl ester (0.136 g, 0.32 mmol) and obtained as a white solid in 87%. FAB-MS Calcd for C₈₂H₁₂₂N₁₈O₁₄ *m/z* = 1582.9, Found *m/z* = 1583.2 [M+H]. Anal. Calcd for C₈₂H₁₂₂N₁₈O₁₄ C=62.18; H=7.76; N=15.92, Found C=62.42; H=7.75; N=15.34.

Assembly 3l₃•(DEB)₆. ¹H NMR (300 MHz, CDCl₃, 298K) δ = 13.84 (s, 2 H; H_a), 13.16 (s, 2 H; H_b), 8.62 (s, 2 H; H_c), 7.87 (d, ³J(H,H)= 8 Hz, 2 H; H_d), 7.41 (s, 2 H; H_g), 7.19 (t, ³J(H,H)= 8 Hz, 4 H; ArH), 6.89 (t, ³J(H,H)= 6 Hz, 4 H; ArH), 6.72 (s, 2 H; NHBoc), 6.15 (s, 2 H; H_h), 5.56 (d, ³J(H,H)= 7 Hz, 2 H; H_m), 4.53 (m, 6 H; ArCH₂Ar, H_o), 4.25-3.90 (br m, 6 H; OCH₂, H_i), 3.85-3.50 (br m, 10 H; OCH₂, OCH₃), 3.40-3.20 (br m, 4 H; ArCH₂Ar, H_k), 3.20-2.95 (br m, 4 H; ArCH₂Ar, H_n), 2.77 (d, ²J(H,H)= 13 Hz, 2 H; H_j),

2.53 (d, $^3J(\text{H,H})=13$ Hz, 2 H; H_i), 2.25-1.85 (br m, 20 H; OCH₂CH₂, CH₂(DEB), CH₂), 1.44 (m, 26 H; C(CH₃)₃, CH₂), 1.15-1.00 (br m, 12 H; OCH₂CH₂CH₃, CH₃(DEB)), 0.95-0.80 (br m, 24 H; OCH₂CH₂CH₃, CCH₃, CH₃(DEB)).

General Procedure for the Preparation of Amino Acid Functionalized Calix[4]arene Dimelamines 4. Calix[4]arene dimelamine **1a** or **1d** (0.15 mmol), the corresponding Fmoc-Amino Acid-OH (0.60 mmol), HBTU (0.23 g, 0.60 mmol), HOBT (0.080 mg, 0.60 mmol) and DIPEA (0.22 mL, 1.2 mmol) were dissolved in CH₂Cl₂ and the mixture was stirred at room temperature for 1-2 days. The organic layer was washed with HCl (1N), H₂O, NaHCO₃ and brine and dried (MgSO₄). Evaporation of the solvent and purification by column chromatography (CH₂Cl₂ : MeOH : NH₄OH (aq)) gave the product in yields varying from 27-75 %.

Calix[4]arene dimelamine 4a was prepared from calix[4]arene dimelamine **1d** (0.15 g, 0.16 mmol) and Fmoc-Gly-OH (0.19 g, 0.63 mmol) and was obtained as a white solid in 44% yield. MALDI-TOF-MS Calcd for C₈₆H₉₆N₁₆O₁₀ $m/z = 1512.7$, Found $m/z = 1514.1$ [M+H].

Assembly 4a₃•(DEB)₆: ¹H NMR (300 MHz, CDCl₃, 298K) $\delta = 14.00$ (s, 2 H; H_a), 13.23 (s, 2 H; H_b), 8.39 (s, 2 H; H_c), 7.66 (d, $^3J(\text{H,H})=7.8$ Hz, 4 H; Fmoc), 7.54-7.40 (m, 6 H; Fmoc, H_d), 7.30 (t, $^3J(\text{H,H})=7.2$ Hz, 4 H; Fmoc), 7.21 (t, $^3J(\text{H,H})=7.2$ Hz, 4 H; Fmoc), 7.13 (m, 6 H; ArH), 6.87 (s, 2H; H_f), 6.80 (t, $^3J(\text{H,H})=7.2$ Hz, 2 H; ArH), 6.66 (s, 2H; H_e), 6.12 (br t, 2 H; NH), 6.01 (s, 2 H; H_h), 5.15 (m, 2 H; NH), 4.42 (ABq, $^2J(\text{H,H})=13.2$ Hz, 4 H; ArCH₂Ar), 4.32-4.21 (m, 4 H; Fmoc), 4.18-3.90 (br m, 6 H; OCH₂, Fmoc), 3.90-3.72 (br m, 2 H; CH), 3.56 (t, $^3J(\text{H,H})=6.6$ Hz, 4 H; OCH₂), 3.50-2.95 (br m, 14 H; ArCH₂Ar, CH), 2.1-1.6 (m, 20 H; OCH₂CH₂, CH₂(DEB), CH₂), 1.02 (t, $^3J(\text{H,H})=7.2$ Hz, 6 H; OCH₂CH₂CH₃), 0.98-0.65 (m, 18 H; OCH₂CH₂CH₃, CH₃(DEB)).

Calix[4]arene dimelamine 4b was prepared from calix[4]arene dimelamine **1a** (0.15 g, 0.15 mmol) and Fmoc-Gly-OH (0.18 g, 0.60 mmol) and was obtained as a white solid in 27% yield. M.p. 153-155 °C. ¹H NMR (300 MHz, DMSO-*d*₆, 298 K) $\delta = 8.6, 8.5, 7.9$ (br s, 4 H; NH), 7.87 (d, $^3J(\text{H,H})=7.2$ Hz, 4 H; Fmoc), 7.69 (d, $^3J(\text{H,H})=7.2$ Hz, 4 H; Fmoc), 7.6-7.4 (m, 6 H; ArH, NH), 7.40 (t, $^3J(\text{H,H})=7.2$ Hz, 4 H; Fmoc), 7.30 (t, $^3J(\text{H,H})=7.8$

Hz, 4 H; Fmoc), 6.8-6.6 (br m, 2 H; NH), 6.4-6.0 (m, 10 H; ArH, NH), 4.38-4.14 (m, 10 H; ArCH₂Ar, CH(Fmoc), CH₂(Fmoc)), 3.89 (br t, 4 H; OCH₂), 3.72-3.52 (m, 8 H; OCH₂, CH₂(Gly)), 3.20-2.86 (m, 12 H; ArCH₂Ar, NCH₂), 1.94-1.74 (m, 8 H; OCH₂CH₂), 1.05 (t, ³J(H,H)=7.5 Hz, 6 H; OCH₂CH₂CH₃), 0.87 (br t, ³J(H,H)=7.5 Hz, 6 H; OCH₂CH₂CH₃), 0.80 (s, 12 H; CCH₃). FAB-MS Calcd for C₉₀H₁₀₄N₁₆O₁₀ *m/z* = 1568.8, Found *m/z* = 1569.3 [M+H].

Calix[4]arene dimelamine 4c was prepared from calix[4]arene dimelamine **1d** (0.15 g, 0.15 mmol) and Fmoc-*L*-Phe-OH (0.23 g, 0.60 mmol) and was obtained as a white solid in 58% yield. M.p. 135-138 °C. ¹H NMR (300 MHz, DMSO-*d*₆, 298 K) δ = 8.6, 8.4, 8.0 (br s, 4 H; NH), 7.85 (d, ³J(H,H)= 7.8 Hz, 4 H, Fmoc), 7.67-7.06 (m, 28 H; ArH, NH), 6.5-6.7 (br m, 2 H; NH), 6.3-6.0 (m, 10 H; ArH, NH), 4.30 (ABq, ²J(H,H)= 13.2 Hz, 4 H; ArCH₂Ar), 4.2-4.0 (m, 8 H; CH(Phe), CH(Fmoc), CH₂(Fmoc)), 3.87 (t, ³J(H,H)= 8.1 Hz, 4 H; OCH₂), 3.59 (br t, 4 H; OCH₂), 3.3-2.7 (m, 16 H; ArCH₂Ar, NCH₂, CH₂(Phe)), 1.96-1.75 (m, 8 H; OCH₂CH₂), 1.6 (br s, 4 H; CH₂), 1.04 (t, ³J(H,H)=7.5 Hz, 6 H; OCH₂CH₂CH₃), 0.86 (t, ³J(H,H)=7.5 Hz, 6 H; OCH₂CH₂CH₃). MALDI-TOF-MS Calcd for C₁₀₀H₁₀₈N₁₆O₁₀ *m/z* = 1692.8, Found *m/z* = 1695.7 [M+H].

Calix[4]arene dimelamine 4d was prepared from calix[4]arene dimelamine **1a** (0.15 g, 0.15 mmol) and Fmoc-*L*-Phe-OH (0.23 g, 0.60 mmol) and obtained as a white solid in 56% yield. M.p. 151-154 °C. ¹H NMR (300 MHz, DMSO-*d*₆, 298 K) δ = 8.6, 8.5, 8.0 (br s, 4 H; NH), 7.85 (d, ³J(H,H)= 7.2 Hz, 4 H; Fmoc), 7.81-7.11 (m, 28 H; ArH, NH), 6.5-6.7 (br m, 2 H; NH), 6.3-6.1 (m, 10 H; ArH, NH), 4.40-4.24 (m, 6 H; ArCH₂Ar, CH(Phe)), 4.21-4.08 (m, 6 H; CH(Fmoc), CH₂(Fmoc)), 3.88 (t, ³J(H,H)= 7.2 Hz, 4 H; OCH₂), 3.58 (m, 4 H; OCH₂), 3.14-2.74 (m, 16 H; ArCH₂Ar, NCH₂, CH₂(Phe)), 1.95-1.75 (m, 8 H; OCH₂CH₂), 1.05 (t, ³J(H,H)= 7.5 Hz, 6 H; OCH₂CH₂CH₃), 0.86 (br t, ³J(H,H)= 7.5 Hz, 6 H; OCH₂CH₂CH₃), 0.82-0.71 (m, 12 H; CCH₃). MALDI-TOF-MS Calcd for C₁₀₄H₁₁₆N₁₆O₁₀ *m/z* = 1748.9, Found *m/z* = 1752.2 [M+H].

Calix[4]arene dimelamine 4e was prepared from calix[4]arene dimelamine **1d** (0.050 g, 0.052 mmol) and Fmoc-*L*-Gln(Trt)-OH (0.067 g, 0.11 mmol) and obtained as a white solid in 54% yield. ¹H NMR (300 MHz, CDCl₃, 298 K) δ = 7.65 (d, ³J(H,H)= 7.8 Hz, 4

H; Fmoc), 7.48 (d, $^3J(\text{H,H})= 6.6$ Hz, 4 H; Fmoc), 7.3-6.5, 6.3-5.8, 5.2-4.6 (br m, 62 H; NH, ArH), 4.42-4.22 (m, 8 H; ArCH₂Ar, CH₂(Fmoc)), 4.09 (t, $^3J(\text{H,H})= 6.3$ Hz, 4 H; CH(Fmoc), CH(Gln), 3.93 (t, $^3J(\text{H,H})= 8.1$ Hz, 4 H; OCH₂), 3.58 (t, $^3J(\text{H,H})= 6.9$ Hz, 4 H; OCH₂), 3.26-2.98 (m, 12 H; ArCH₂Ar, NCH), 2.28-1.70 (m, 16 H; CH₂, OCH₂CH₂), 1.43 (br s, 4 H; CH₂), 1.01 (t, $^3J(\text{H,H})= 7.5$ Hz, 6 H; OCH₂CH₂CH₃), 0.81 (br t, $^3J(\text{H,H})= 7.5$ Hz, 6 H; OCH₂CH₂CH₃). FAB-MS Calcd for C₁₃₀H₁₃₄N₁₈O₁₂ $m/z = 2139.0$, Found $m/z = 2141.12$ [M+H].

Calix[4]arene dimelamine 4f was prepared from calix[4]arene dimelamine **1a** (0.050 g, 0.049 mmol) and Fmoc-*L*-Gln(Trt)-OH (0.064 g, 0.10 mmol) and obtained as a white solid in 66% yield. ¹H NMR (300 MHz, DMSO-*d*₆, 298 K) $\delta = 8.6$ -8.0 (br m, 4 H; NH), 8.0-7.1 (m, 56 H; ArH, NH), 6.8-6.5 (br m, 2 H; NH), 6.4-6.0 (m, 10 H; ArH, NH), 4.4-4.1 (m, 10 H; ArCH₂Ar, CH), 4.1-4.0 (m, 6 H; OCH₂, CH), 3.7-3.5 (m, 8 H; OCH₂, CH), 3.2-2.9 (m, 12 H; ArCH₂Ar, CH), 2.3 (br s, 4 H; CH), 2.0-1.6 (m, 10 H; OCH₂CH₂, CH), 1.05 (t, $^3J(\text{H,H})= 7.5$ Hz, 6 H; OCH₂CH₂CH₃), 0.86 (br t, $^3J(\text{H,H})= 7.5$ Hz, 6 H; OCH₂CH₂CH₃), 0.82-0.71 (m, 12 H; CH₃), 0.78 (s, 12 H; CCH₃). FAB-MS Calcd for C₁₃₄H₁₄₂N₁₈O₁₂ $m/z = 2196.7$, Found $m/z = 2198.9$ [M+H].

Calix[4]arene dimelamine 4g was prepared from calix[4]arene dimelamine **1d** (0.15 g, 0.16 mmol) and Fmoc-*L*-Lys(Boc)-OH (0.29 g, 0.63 mmol) and obtained as a white solid in 73% yield. M.p. 126-129 °C. MALDI-TOF-MS Calcd for C₁₀₄H₁₃₀N₁₈O₁₄ $m/z = 1855.0$, Found $m/z = 1857.4$ [M+H].

Assembly 4g₃•(DEB)₆. ¹H NMR (300 MHz, CDCl₃, 298K) $\delta = 14.06$ (s, 2 H, H_a), 13.28 (s, 2 H, H_b), 8.33 (s, 2 H, H_c), 7.66 (d, 4 H, $^3J(\text{H,H})= 7.2$ Hz, Fmoc), 7.60-7.42 (m, 6 H, Fmoc, H_d), 7.30 (t, 4 H, $^3J(\text{H,H})= 7.2$ Hz, Fmoc), 7.21 (m, 4 H, $^3J(\text{H,H})= 7.2$ Hz, Fmoc), 7.11-6.90 (m, 6 H, ArH; H_g), 6.84 (s, 2H, H_f), 6.78 (t, 2 H, $^3J(\text{H,H})= 7.5$ Hz, ArH), 6.62 (s, 2H, H_e), 6.18 (br s, 2 H, NH), 5.97 (s, 2 H, H_h), 5.38 (m, 2 H, NH), 4.60-4.22 (m, 10 H, ArCH₂Ar; CH₂(Fmoc), CH(Lys)), 4.18-3.50 (m, 16 H, OCH₂; CH), 3.40-2.88 (m, 16 H, ArCH₂Ar; CH), 2.10-1.5 (m, 20 H, OCH₂CH₂; CH₂(DEB); CH₂), 1.33 (s, 18 H, Boc), 1.4-1.12 (m, 4 H, CH₂), 1.02 (t, 6 H, $^3J(\text{H,H})= 7.2$ Hz, OCH₂CH₂CH₃), 0.96-0.64 (m, 18 H, OCH₂CH₂CH₃; CH₃(DEB)).

Calix[4]arene dimelamine 4h was prepared from calix[4]arene dimelamine **1a** (0.050 g, 0.052 mmol) and Fmoc-*L*-Lys(Boc)-OH (0.049 g, 0.10 mmol) and obtained as a white solid in 71% yield. ^1H NMR (300 MHz, DMSO- d_6 , 298 K) δ = 8.6, 8.4, 7.8 (br s, 4 H; NH), 7.85 (d, $^3J(\text{H,H})=7.8$ Hz, 4 H; Fmoc), 7.74-7.64 (m, 2 H; Fmoc), 7.50-7.33 (m, 10 H; ArH, NH), 7.29 (t, $^3J(\text{H,H})=7.5$ Hz, 4 H; Fmoc), 6.8-6.5 (br m, 4 H; NH), 6.4-6.0 (m, 10 H; ArH, NH), 4.34-4.13 (m, 10 H; ArCH₂Ar, CH(Fmoc), CH₂(Fmoc)), 3.86 (t, $^3J(\text{H,H})=7.8$ Hz, 6 H; OCH₂, CH(Lys)), 3.58 (br t, 4 H; OCH₂), 3.15-2.96 (m, 8 H; ArCH₂Ar, NCH₂), 2.90-2.79 (m, 4 H; NCH₂(Lys)), 1.94-1.76 (m, 8 H; OCH₂CH₂), 1.67-1.42 (m, 4 H; CH₂(Lys)), 1.38-1.15 (m, 26 H; Boc, CH₂(Lys)), 1.04 (t, $^3J(\text{H,H})=7.5$ Hz, 6 H; OCH₂CH₂CH₃), 0.85 (t, $^3J(\text{H,H})=7.8$ Hz, 6 H; OCH₂CH₂CH₃), 0.81-0.70 (m, 12 H; CCH₃). FAB-MS Calcd for C₁₀₈H₁₃₈N₁₈O₁₄ m/z = 1911.1, Found m/z = 1912.94 [M+H].

Calix[4]arene dimelamine 4i was prepared from calix[4]arene dimelamine **1d** (0.14 g, 0.15 mmol) and Fmoc-*L*-Cys(Trt)-OH (0.35 g, 0.59 mmol) and obtained as a white solid in 54% yield. M.p. 137-138 °C. ^1H NMR (300 MHz, DMSO- d_6 , 298 K) δ = 8.6, 8.4, 7.8 (br s, 4 H; NH), 7.84 (d, $^3J(\text{H,H})=7.5$ Hz, 4 H; Fmoc), 7.69 (d, $^3J(\text{H,H})=7.8$ Hz, 4 H; Fmoc), 7.66-7.13 (m, 44 H; ArH, NH), 6.7-6.5 (br m, 2 H; NH), 6.34-6.04 (m, 10 H; ArH, NH), 4.31-4.13 (m, 10 H; ArCH₂Ar, CH(Fmoc), CH₂(Fmoc)), 4.02-3.90 (m, 2 H; CH(Cys)), 3.86 (t, $^3J(\text{H,H})=8.1$ Hz, 4 H; OCH₂), 3.57 (br s, 4 H; OCH₂), 3.26-3.12 (m, 4 H; CH₂), 3.11-2.96 (m, 8 H; ArCH₂Ar, NCH₂), 2.44-2.29 (m, 4 H; SCH₂), 1.93-1.73 (m, 8 H; OCH₂CH₂), 1.56 (br s, 4 H; CH₂), 1.02 (t, $^3J(\text{H,H})=7.2$ Hz, 6 H; OCH₂CH₂CH₃), 0.83 (m, 6 H; OCH₂CH₂CH₃). MALDI-TOF-MS Calcd for C₁₂₆H₁₂₈N₁₆O₁₀S₂ m/z = 2088.9, Found m/z = 2091.1 [M+H].

Calix[4]arene dimelamine 4j was prepared from calix[4]arene dimelamine **1a** (0.15 g, 0.15 mmol) and Fmoc-*L*-Cys(Trt)-OH (0.35 g, 0.59 mmol) and obtained as a white solid in 37% yield. M.p. 165-169 °C. ^1H NMR (300 MHz, DMSO- d_6 , 298 K) δ = 8.6, 8.5, 7.9 (br s, 4 H; NH), 7.83 (d, $^3J(\text{H,H})=6.9$ Hz, 4 H; Fmoc), 7.7 (br s, 2 H; NH), 7.67 (d, $^3J(\text{H,H})=6.4$ Hz, 4 H; Fmoc), 7.57-7.11 (m, 42 H; ArH, NH), 6.8-6.5 (br m, 2 H; NH), 6.3-6.0 (m, 10 H; ArH, NH), 4.31-4.19 (m, 10 H; ArCH₂Ar, CH(Fmoc), CH₂(Fmoc)), 4.03 (br s, 2 H; CH(Cys)), 3.86 (br t, 4 H; OCH₂), 3.55 (br s, 4 H; OCH₂), 3.28-2.68 (m, 12 H; ArCH₂Ar, NCH₂), 2.46-2.45 (m, 4 H; SCH₂), 1.99-1.70 (m, 8 H; OCH₂CH₂), 1.02

(t, $^3J(\text{H,H})=7.2$ Hz, 6 H; $\text{OCH}_2\text{CH}_2\text{CH}_3$), 0.83 (br t, 6 H; $\text{OCH}_2\text{CH}_2\text{CH}_3$), 0.77-0.65 (m, 12 H; CCH_3). MALDI-TOF-MS Calcd for $\text{C}_{130}\text{H}_{136}\text{N}_{16}\text{O}_{10}\text{S}_2$ $m/z = 2145.0$, Found $m/z = 2147.7$ [M+H].

Calix[4]arene dimelamine 4k was prepared from calix[4]arene dimelamine **1d** (0.104 g, 0.11 mmol) and Fmoc-*L*-Ser(tBu)-OH (0.088 g, 0.23 mmol) and obtained as a white solid in 75% yield. M.p. 136-139 °C. FAB-MS Calcd for $\text{C}_96\text{H}_{118}\text{N}_{16}\text{O}_{12}$ $m/z = 1688.1$, Found $m/z = 1685.8$ [M+H].

Assembly 4k₃•(DEB)₆: ^1H NMR (300 MHz, CDCl_3 , 298K) $\delta = 14.07$ (s, 2 H; H_a), 13.28 (s, 2 H; H_b), 8.35 (s, 2 H; H_c), 7.67 (d, $^3J(\text{H,H})= 7.2$ Hz, 4 H; Fmoc), 7.53-7.40 (m, 6 H; Fmoc, H_d), 7.31 (t, $^3J(\text{H,H})= 7.2$ Hz, 4 H; Fmoc), 7.26-7.14 (m, 4 H; Fmoc), 7.13-6.97 (m, 6 H; ArH, H_g), 6.84 (s, 2H; H_f), 6.79 (t, $^3J(\text{H,H})= 7.5$ Hz, 2 H; ArH), 6.61 (s, 2 H; H_e), 6.52 (br s, 2 H; NH), 5.98 (s, 2 H; H_h), 5.67 (m, 2 H; NH), 4.42 (ABq, $^2J(\text{H,H})= 15.0$ Hz, 4 H; ArCH_2Ar), 4.31 (d, $^3J(\text{H,H})= 7.2$ Hz, 4 H; $\text{CH}_2(\text{Fmoc})$), 4.18-3.85 (br m, 10 H; OCH_2 , $\text{CH}(\text{Fmoc})$, NCH), 3.80-3.50 (br m, 10 H; OCH_2 , $\text{CH}_2(\text{Ser})$, NCH), 3.34-3.18 (m, 6 H; $\text{CH}(\text{Ser})$, CH_2), 3.18-3.00 (m, 6 H; ArCH_2Ar , NCH), 2.08-1.7 (m, 20 H; OCH_2CH_2 , $\text{CH}_2(\text{DEB})$), 1.13-0.64 (br m, 42 H; $\text{OCH}_2\text{CH}_2\text{CH}_3$, $\text{CH}_3(\text{DEB})$, tBu).

Calix[4]arene dimelamine 4l. Calix[4]arene dimelamine **4k** (0.044 g, 0.026 mmol) was dissolved in TFA (4 mL) and stirred overnight. The TFA was evaporated and the solid was dissolved in CH_2Cl_2 and washed with NaHCO_3 , H_2O , and brine and dried (Na_2SO_4). Evaporation of the solvent and purification by column chromatography (CH_2Cl_2 : MeOH: NH_4OH (aq) (95:4.5:0.5)) gave the product as a white solid in 61% yield. FAB-MS Calcd for $\text{C}_{88}\text{H}_{102}\text{N}_{16}\text{O}_{12}$ $m/z = 1574.8$, Found $m/z = 1573.5$ [M+H].

Assembly 4l₃•(DEB)₆: ^1H NMR (300 MHz, CDCl_3 , 298K) $\delta = 14.07$ (s, 2 H; H_a), 13.27 (s, 2 H; H_b), 8.32 (s, 2 H; H_c), 7.67 (d, $^3J(\text{H,H})= 7.2$ Hz, 4 H; Fmoc), 7.53-7.47 (m, 6 H; Fmoc, H_d), 7.30 (t, $^3J(\text{H,H})= 7.2$ Hz, 4 H; Fmoc), 7.21 (t, $^3J(\text{H,H})= 7.2$ Hz, 4 H; Fmoc), 7.12-6.96 (m, 6 H; ArH, H_g), 6.87 (s, 2H; H_f), 6.80 (t, $^3J(\text{H,H})= 7.5$ Hz, 2 H; ArH), 6.62 (s, 4H; H_e , NH), 5.97 (s, 2 H; H_h), 5.77 (m, 2 H; NH), 4.47-4.31 (m, 8 H; ArCH_2Ar , $\text{CH}_2(\text{Fmoc})$), 4.14-3.73 (br m, 14 H; OCH_2 , $\text{CH}(\text{Fmoc})$, $\text{CH}(\text{Ser})$, $\text{CH}_2(\text{Ser})$, NCH), 3.65-3.42 (m, 6 H; OCH_2 , NCH), 3.34-3.04 (br m, 10 H; ArCH_2Ar , NCH , CH_2), 2.06-1.68 (m, 18 H; OCH_2CH_2 , $\text{CH}_2(\text{DEB})$), 1.02 (t, $^3J(\text{H,H})= 7.5$ Hz, 6 H; $\text{OCH}_2\text{CH}_2\text{CH}_3$), 0.96-0.66

(m, 18 H; OCH₂CH₂CH₃, CH₃(DEB)). (Due to broad and overlapping signals, the OH signal could not be interpreted)

Calix[4]arene dimelamine 4m was prepared from calix[4]arene dimelamine **1d** (0.11 g, 0.11 mmol) and Fmoc-*L*-Met-OH (0.093 g, 0.24 mmol) and obtained as a white solid in 62% yield. FAB-MS Calcd for C₉₂H₁₀₈N₁₆O₁₀ $m/z = 1660.9$, Found $m/z = 1661.9$ [M+H].

Assembly 4m₃•(DEB)₆: ¹H NMR (300 MHz, CDCl₃, 298K) $\delta = 14.05$ (s, 2 H; H_a), 13.26 (s, 2 H; H_b), 8.3d (d, ³ J (H,H)= 6.6 Hz, 2 H; H_c), 7.66 (d, ³ J (H,H)= 7.2 Hz, 4 H; Fmoc), 7.58-7.40 (m, 6 H; Fmoc, H_d), 7.30 (t, ³ J (H,H)= 7.2 Hz, 4 H; Fmoc), 7.21 (t, ³ J (H,H)= 7.2 Hz, 4 H; Fmoc), 7.12-6.95 (m, 6 H; ArH, H_e), 6.85 (s, 2H; H_f), 6.80 (t, ³ J (H,H)= 7.2 Hz, 2 H; ArH), 6.63 (s, 2 H; H_e), 6.25 (s, 2 H; NH), 5.98 (s, 2 H; H_h), 4.42 (ABq, ² J (H,H)= 14.1 Hz, 4 H; NH), 4.34-4.24 (m, 6 H; CH₂(Fmoc), NCH), 4.16-3.86 (m, 8 H; CH(Fmoc), NCH, OCH₂), 3.84-6.66 (m, 2 H; NCH) 3.57 (br t, 4 H; OCH₂), 3.36-2.78 (m, 10 H; CH (Met), NCH, ArCH₂Ar, CH₂), 2.46-2.24 (m, 4 H; SCH₂), 2.10-2.66 (m, 26 H; OCH₂CH₂, CH₂(DEB), CH₂(Met), SCH₃), 1.10-0.68 (m, 24 H; OCH₂CH₂CH₃, CH₃(DEB)).

Calix[4]arene dimelamine 4n was prepared from calix[4]arene dimelamine **1a** (0.11 g, 0.11 mmol) and Fmoc-*L*-His(Trt)-OH (0.14 g, 0.22 mmol) and obtained as a white solid in 40% yield. FAB-MS Calcd for C₁₃₂H₁₃₄N₂₀O₁₀ $m/z = 2159.1$, Found $m/z = 2159.3$ [M+H].

Calix[4]arene dimelamine 4o was prepared from calix[4]arene dimelamine **1d** (0.15 g, 0.15 mmol) and Fmoc-*L*-Arg(Pbf)-OH (0.39 g, 0.59 mmol) and obtained as a white solid in 65% yield. ¹H NMR in CDCl₃ is too broad for accurate interpretation. MALDI-TOF-MS Calcd for C₁₂₀H₁₄₆N₂₂O₁₆S₂ $m/z = 2215.1$, Found $m/z = 2217.8$ [M+H].

Calix[4]arene dimelamine 4p was prepared from calix[4]arene dimelamine **1a** (0.075 g, 0.078 mmol) and Fmoc-*L*-Arg(Pbf)-OH (0.20 g, 0.31 mmol) and obtained as a white solid in 54% yield. ¹H NMR (300 MHz, DMSO-*d*₆, 298 K) $\delta = 8.6, 8.5, 7.9$ (br s, 4 H; NH), 7.86 (d, ³ J (H,H)=7.8 Hz, 4 H; Fmoc), 7.76-7.20 (m, 18 H; ArH, NH), 6.8-6.1 (m, 16 H; ArH, NH), 4.38-4.14 (m, 10 H; ArCH₂Ar, CH(Fmoc), CH₂(Fmoc)), 3.40 (br s, 2 H; CH(Arg)), 3.88 (t, ³ J (H,H)=8 Hz, 4 H; OCH₂), 3.57 (br s, 4 H; OCH₂), 3.20-2.98 (m, 12

H; ArCH₂Ar, NCH₂), 2.91 (s, 6 H; CH₃(Pbf)), 2.47 (s, 6 H; CH₃(Pbf)), 2.41 (s, 6 H; CH₃(Pbf)), 1.98 (s, 6 H; CH₃(Pbf)), 1.94-1.71 (m, 8 H; OCH₂CH₂), 1.70-1.31 (m, 12 H; CH₂), 1.37 (s, 6 H; CH₃(Pbf)), 1.04 (t, ³J(H,H)=7.5 Hz, 6 H; OCH₂CH₂CH₃), 0.86 (t, ³J(H,H)=7.8 Hz 6 H; OCH₂CH₂CH₃), 0.79 (s, 12 H; CCH₃). MALDI-TOF-MS Calcd for C₁₂₄H₁₅₄N₂₂O₁₆S₂ *m/z* = 2272.8, Found *m/z* = 2273.3 [M+H].

Loading of the ArgoGel-OH. ArgoGel-OH (10 g) and Fmoc-Gly-OH (5.11 g, 17.2 mmol) were dried over P₂O₅ in a desiccator connected to a vacuum pump overnight and DMF (50 mL) was added. Pyridine (2.3 mL, 28.3 mmol) and 2,6-dichlorobenzoylchloride (2.48 mL, 17.2 mmol) were added to the “mixture” and the mixture was shaken overnight. The resin was filtered and washed with DMF (3x), MeOH (3x), CH₂Cl₂ (3x), and Et₂O (3x) and dried over P₂O₅ in a vacuum desiccator. The loading of the resin was determined by measuring the UV absorbance at 301 nm after deprotection of the Fmoc group by piperidine. A loading of 0.34 mmol/g was determined.

Synthesis of pentapeptides. the peptide chemistry was carried out according to the following protocol by using an automated system (Syro Robot Synthesizer, MultisynTech, Witten, Germany, software: Syro 2000):

1. Fmoc-deprotection

The resin was treated with a 40 % solution of piperidine in NMP (2.2 mL, 6 min), followed by treatment with a 20 % solution of piperidine in NMP (2.0 mL, 6 min). This solution was removed by filtration, followed by washing with NMP (5 x 2.2 mL, 1 min).

2. Coupling Fmoc-protected amino acid

Fmoc-X-OH (4 equiv; 0.55 M in NMP), HBTU (4 equiv; 0.37 M in NMP), and DIPEA (8 equiv; 1.37 M in NMP) were added to the resin. The mixture was allowed to react for 75 min. at rt. Subsequently, the solution was removed by filtration, followed by washing with NMP (3 x 2.2 mL, 2 min).

3. Cleavage and purification

The resin was treated with a 10 % solution of Et₃N in MeOH (3.5 mL, 3.5 h). The resin was removed by filtration and washed with MeOH (2 x 2.5 mL, 3min) and CH₂Cl₂ (2 x 2.5 mL, 3min). The filtrate was evaporated to dryness and the solid was triturated in an appropriate solvent.

N-t-Boc-Gly-L-Lys(Boc)-L-Tyr(tBu)-L-Ala-Gly-OMe: Purity HPLC (35% H₂O, 65% MeCN (containing 0.1% TFA) > 95%. MALDI-TOF-MS Calcd for C₃₇H₇₀N₆O₁₁ *m/z* = 774.5, Found *m/z* = 787.4 [M+Na].

N-t-Boc-Gly-L-Lys(Boc)-Gly-L-Asn(Trt)-Gly-OMe: Purity HPLC (35% H₂O, 65% MeCN (containing 0.1% TFA) > 92%. MALDI-TOF-MS Calcd for C₄₆H₆₁N₇O₁₁ *m/z* = 887.4, Found *m/z* = 910 [M+Na].

Deprotection of the methyl ester: the protected peptide was dissolved in a mixture of THF/MeOH (6 mL, 1:1) and cooled at 0-5 °C. LiOH (5 equiv.) in H₂O (2 mL) was added and the mixture was stirred for 3 h at 0-5 °C. The mixture was acidified with HCl to pH 4 and the solvent was evaporated. The solid was redissolved in EtOAc and washed with HCl (1 M), H₂O, and brine and dried (Na₂SO₄).

N-t-Boc-Gly-L-Lys(Boc)-L-Tyr(tBu)-L-Ala-Gly-OH was obtained in 89% yield. Purity HPLC (35% H₂O, 65% MeCN (containing 0.1% TFA) ~ 95%. MALDI-TOF-MS Calcd for C₃₆H₆₈N₆O₁₁ *m/z* = 760.5, Found *m/z* = 773.6 [M+Na].

N-t-Boc-Gly-L-Lys(Boc)-Gly-L-Asn(Trt)-Gly-OH was obtained in 77% yield. Purity HPLC (35% H₂O, 65% MeCN (containing 0.1% TFA) > 90%. MALDI-TOF-MS Calcd for C₄₅H₅₉N₇O₁₁ *m/z* = 873.4, Found *m/z* = 896.5 [M+Na].

Calix[4]arene dimelamine 5a. Calix[4]arene dimelamine **1d** (0.039 g, 0.041 mmol) was dissolved in CH₂Cl₂ (15 mL) and N-t-Boc-L-Phe-Gly-Gly-OH (0.062 g, 0.16 mmol), HATU (0.062 g, 0.16 mmol), HOBT (0.022 g, 0.16 mmol) and DIPEA (0.14 mL, 0.082 mmol) were added and the mixture was stirred at room temperature for 1 week. The organic layer was washed with HCl (1N), H₂O and brine and dried (Na₂SO₄). Evaporation of the solvent and purification by column chromatography (CH₂Cl₂ : MeOH : NH₄OH (aq) (90 : 9.5 : 0.5)) gave the product in 63 % yield (0.043 g, 0.026 mmol). M.p. 152-154 °C. ¹H NMR (300 MHz, DMSO-*d*₆, 298K) δ = 8.6 (br s, 1 H; NH), 8.4 (br s, 1 H; NH), 8.3 (br t, 2 H; NH), 8.1 (br t, 2H; NH), 7.8-7.6 (br s, 2 H; NH), 7.5-7.4 (br m, 4 H; NH) 7.3-7.0 (m, 12 H; ArH), 6.9-6.6 (br m, 2 H; NH), 6.4-6.0 (m, 10 H; ArH, NH), 4.33 (ABq, ²J(H,H)= 12.9 Hz, 4 H; ArCH₂Ar), 4.24-4.16 (m, 2 H; CH (Phe)), 3.90 (t, ³J(H,H)= 7.8 Hz, 4 H; OCH₂), 3.7 (br m, 4 H; CH₂ (Gly)), 3.72-3.57 (m, 8 H; OCH₂, CH₂ (Gly)), 3.4 (m, 4 H; NCH₂), 3.19-2.99 (m, 12 H; ArCH₂Ar, NCH₂, CHH (Phe)), 2.74 (t,

$^2J(\text{H,H}) = 13.5$ Hz, 2 H; CHH (Phe)), 2.0-1.8 (m, 8 H; OCH_2CH_2), 1.28 (s, 18 H; Boc), 1.08 (t, $^3J(\text{H,H}) = 7.5$ Hz, 6 H; $\text{OCH}_2\text{CH}_2\text{CH}_3$), 0.89 (t, $^3J(\text{H,H}) = 7.5$ Hz, 6 H; $\text{OCH}_2\text{CH}_2\text{CH}_3$). MALDI-TOF-MS Calcd for $\text{C}_{88}\text{H}_{118}\text{N}_{20}\text{O}_{14}$ $m/z = 1678.9$, Found $m/z = 1680.2$ [M+H].

Calix[4]arene dimelamine 5b. Calix[4]arene dimelamine **1d** (0.028 g, 0.029 mmol) was dissolved in CH_2Cl_2 (10 mL) and N-t-Boc-Gly-L-Lys(Boc)-L-Tyr(tBu)-L-Ala-Gly-OH (0.059 g, 0.064 mmol), HATU (0.025 g, 0.064 mmol), HOBt (0.009 g, 0.064 mmol) and DIPEA (0.076 mL, 0.59 mmol) were added and the mixture was stirred at room temperature for 1 week. The organic layer was washed with HCl (1N) and brine and dried (Na_2SO_4). Evaporation of the solvent and purification by preparative TLC (CH_2Cl_2 : MeOH : NH_4OH (aq) (90 : 9.5 : 0.5)) gave the product in 27 % yield (0.019 g, 0.0078 mmol). M.p. 159-163 °C. MALDI-TOF-MS Calcd for $\text{C}_{122}\text{H}_{206}\text{N}_{26}\text{O}_{24}$ $m/z = 2419.6$, Found $m/z = 2422.9$ [M+H]. ^1H NMR spectrum is too complicated for interpretation.

Calix[4]arene dimelamine 5c. Calix[4]arene dimelamine **5b** (0.012 g, 0.0050 mmol) was dissolved in a TFA : H_2O (9 : 1) (1 mL) mixture and stirred for 2 hours at room temperature. Evaporation of the solvent and addition and subsequent evaporation of toluene (2x) gave the product in quantitative yield.). M.p. 127-129 °C. MALDI-TOF-MS Calcd for $\text{C}_{92}\text{H}_{154}\text{N}_{28}\text{O}_{16}$ $m/z = 1907.2$, Found $m/z = 1908.6$ [M+H]. ^1H NMR spectrum is too complicated for interpretation.

Calix[4]arene dimelamine 5d. Calix[4]arene dimelamine **1d** (0.010 g, 0.010 mmol) was dissolved in CH_2Cl_2 (10 mL) and N-t-Boc-Gly-L-Lys(Boc)-Gly-L-Asn(Trt)-Gly-OH (0.037 g, 0.042 mmol), HATU (0.016 g, 0.042 mmol), HOBt (0.006 g, 0.16 mmol) and DIPEA (0.035 mL, 0.20 mmol) were added and the mixture was stirred at room temperature for 1 week. N-t-Boc-Gly-L-Lys(Boc)-Gly-L-Asn(Trt)-Gly-OH (0.018 g, 0.022 mmol), HATU (0.008 g, 0.022 mmol), HOBt (0.003 g, 0.08 mmol) and DIPEA (0.035 mL, 0.20 mmol) were added for the second time and stirred for another 2 days at room temperature. The organic layer was washed with 1M HCl, H_2O and brine and dried (Na_2SO_4). Evaporation of the solvent and purification by column chromatography (CH_2Cl_2 : MeOH : NH_4OH (aq) (90 : 9.5 : 0.5)) gave the product 41 % yield (0.011 g,

0.0042 mmol). M.p. 167-170 °C. MALDI-TOF-MS Calcd for C₁₄₂H₁₈₄N₂₈O₂₄ m/z = 2665.4, Found m/z = 2667.6 [M+H]. ¹H NMR spectrum is too complicated for interpretation.

Calix[4]arene dimelamine 5e. Calix[4]arene dimelamine **1a** (0.014 g, 0.014 mmol) was dissolved in CH₂Cl₂ (10 mL) and N-t-Boc-Gly-*L*-Lys(Boc)-Gly-*L*-Asn(Trt)-Gly-OH (0.05 g, 0.057 mmol), HATU (0.022 g, 0.057 mmol), HOBt (0.008 g, 0.057 mmol) and DIPEA (0.0505 mL, 0.28 mmol) were added and the mixture was stirred at room temperature for 2 weeks. The solvent was evaporated and the product redissolved in EtOAc. The organic layer was washed with HCl (1N), H₂O, and brine and dried (Na₂SO₄). Evaporation of the solvent and purification by column chromatography (CH₂Cl₂ : MeOH : NH₄OH (aq) (95 : 4.5 : 0.5)) gave the product 52 % yield (0.02 g, 0.007 mmol). M.p. 165-167 °C. MALDI-TOF-MS Calcd for C₁₄₆H₁₉₂N₂₈O₂₄ m/z = 2721.4, Found m/z = 2726 [M+H]. ¹H NMR spectrum is too complicated for interpretation.

3,5-diaminobenzyl ester. 3,5-diaminobenzoic acid (5.0 g, 33 mmol) was dissolved in MeOH (50 mL) and *p*-toluenesulfonic acid (12.5 g, 66 mmol) was added. The mixture was refluxed for 24h and was evaporated to dryness and EtOAc was added. The solution was washed with NaHCO₃, H₂O, and brine and dried (Na₂SO₄). Evaporation of the solvent gave the crude product, which was suspended in NaHCO₃ (aq) and washed with CHCl₃. The organic layers were combined and washed with H₂O and brine and dried (Na₂SO₄). The crude product was obtained in 37% yield. M.p. 130-132 °C. ¹H NMR (300 MHz, DMSO-*d*₆, 298K) δ = 6.63 (s, 2 H; ArH), 5.62 (s, 1 H; ArH), 4.58 (s, 3 H; OMe). ¹³C NMR (75 MHz, DMSO-*d*₆, 298K) δ = 167.2, 149.3, 130.5, 103.6, 51.4. FAB-MS Calcd for C₈H₁₀O₂ m/z = 166.2, Found m/z = 168.1 [M+D].

3,5-di-(*D*-Ala-Boc)benzyl ester 6. 3,5-diaminobenzyl ester (0.10 g, 0.6 mmol) was dissolved in CH₂Cl₂ (10 mL) and HO-*D*-Ala-Boc (0.34 g, 1.8 mmol), HBTU (0.68 g, 1.8 mmol), HOBt (0.24 g, 1.8 mmol), and DIPEA (1.0 mL, 6.0 mmol) were added. The mixture was stirred at room temperature overnight and washed with citric acid, HCl (1 M), H₂O, and brine and dried (Na₂SO₄). Evaporation of the solvent gave the crude product, which was purified by column chromatography (EtOAc:hexane (1:1)) to give the

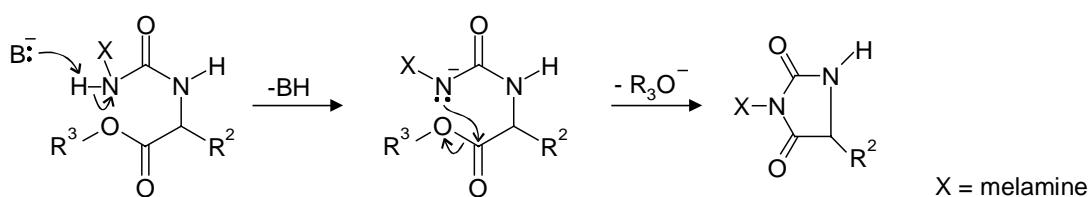
crude product in quantitative yield. M.p. 104-105 °C. ^1H NMR (300 MHz, CD_3OD , 298K) δ = 8.08 (s, 1 H; ArH), 7.95 (m, 2 H; ArH), 4.02-4.18 (m, 2 H; CH(Ala)), 3.85 (s, 3 H; OMe), 1.28-1.40 (m, 24 H; Boc, $\text{CH}_3(\text{Ala})$). ^{13}C NMR (75 MHz, CD_3OD , 298K) δ = 172.5, 166.0, 155.8, 138.5, 130.5, 115.8, 115.2, 78.8, 50.8, 50.3, 26.8, 16.4. FAB-MS Calcd for $\text{C}_{24}\text{H}_{36}\text{N}_4\text{O}_8$ m/z = 508.3, Found m/z = 508.2 [M^+].

3,5-di-(D-Ala-Boc)benzoic acid 7. 3,5 di-(D-Ala-Boc)benzyl ester **6** (0.26 g, 0.52 mmol) was dissolved in a mixture of THF/MeOH (6 mL, 1:1) and cooled to 0-5 °C. LiOH (0.087 g, 2.1 mmol) in H_2O (2 mL) was added and the mixture was stirred for 5 h at 0-5 °C. The mixture was acidified with HCl to pH 4 and the solvent was evaporated. The solid was redissolved in EtOAc and washed with HCl (1 M), H_2O , and brine and dried (Na_2SO_4). Evaporation of the solvent gave the product in 60 % yield. M.p. 155-157 °C. ^1H NMR (300 MHz, CD_3OD , 298K) δ = 8.08 (s, 1 H; ArH), 7.88 (m, 2 H; ArH), 4.01-4.20 (m, 2 H; CH(Ala)), 1.23-1.42 (m, 24 H; Boc, $\text{CH}_3(\text{Ala})$). ^{13}C NMR (75 MHz, CD_3OD , 298K) δ = 172.5, 167.2, 155.2, 138.8, 131.1, 116.2, 115.2, 78.8, 50.3, 26.8, 16.5. FAB-MS Calcd for $\text{C}_{23}\text{H}_{34}\text{N}_4\text{O}_8$ m/z = 494.2, Found m/z = 495.1 [$\text{M}+\text{H}$].

Calix[4]arene dimelamine 5f. Calix[4]arene dimelamine **1d** (0.025 g, 0.026 mmol) was dissolved in CH_2Cl_2 (3 mL) and 3,5 di-(D-Ala-Boc)benzoic acid **7** (0.05 g, 0.10 mmol), HBTU (0.035 g, 0.10 mmol), HOBT (0.015 g, 0.10 mmol), and DIPEA (0.1 mL, 0.53 mmol) were added. The mixture was stirred at rt overnight. Evaporation of the solvent gave the crude product, which was purified by column chromatography (CH_2Cl_2 :MeOH: NH_4OH (90:9.5:0.5)) to give the pure product in 48 % yield. M.p. 178-179 °C. ^1H NMR (300 MHz, $\text{DMSO}-d_6$, 298K) δ = 10.02 (s, 4 H; NH), 8.6 (br s, 1 H; NH), 8.5-8.3 (br m, 3 H; NH), 8.07 (s, 2 H; ArH), 7.67 (s, 4 H; ArH), 7.5-7.4 (m, 4 H; NH/ArH), 7.05(d, $^3J(\text{H,H})$ = 5.7 Hz, 4 H; NH), 6.8-6.0 (br m, 12 H; NH, ArH), 4.31 (ABq, $^2J(\text{H,H})$ = 12.3 Hz, 4 H; ArCH_2Ar), 4.11 (t, $^3J(\text{H,H})$ =7.5 Hz, 4 H; CH(Ala)), 3.84 (t, $^3J(\text{H,H})$ =7.5 Hz, 4 H; OCH_2), 3.60 (br t, 4 H; OCH_2), 3.4-3.3 (m, 8 H; NCH_2), 3.15-2.97(m, 4 H; ArCH_2Ar), 2.0-1.7 (m, 12 H; OCH_2CH_2 , $\text{CH}_2(\text{spacer})$), 1.4-1.1 (m, 52 H; Boc, $\text{CH}_3(\text{Ala})$), 1.05 (t, $^3J(\text{H,H})$ = 7.2 Hz, 6 H; $\text{OCH}_2\text{CH}_2\text{CH}_3$), 0.87 (t, $^3J(\text{H,H})$ =7.5 Hz, 6 H; $\text{OCH}_2\text{CH}_2\text{CH}_3$). MALDI-TOF-MS Calcd for $\text{C}_{98}\text{H}_{130}\text{N}_{22}\text{O}_{18}$ m/z = 1907.0, Found m/z = 1909.5 [$\text{M}+\text{H}$].

4.5 References

- ¹ a) Akerfeldt, K.S.; Kim, R.M.; Camac, D.; Groves, J.T.; Lear, J.D.; DeGrado, W.F. *J. Am. Chem. Soc.* **1992**, *114*, 9656-9657; b) Mutter, M.; Tuchscherer, G.G.; Miller, C. Altmann, K.H.; Carey, R.I.; Wyss, D.F.; Labhardt, A.M.; Rivier, J.E. *J. Am. Chem. Soc.* **1992**, *114*, 1463-1470; c) Cheng, Y.; Suenaga, T.; Still, W. C. *J. Am. Chem. Soc.* **1996**, *118*, 1813-1814.
- ² a) Park, H.S.; Lin, Q.; Hamilton, A.D. *J. Am. Chem. Soc.* **1999**, *121*, 8-13; b) Hamuro, Y.; Crego-Calama, M.; Park, H.S.; Hamilton, A.D. *Angew. Chem. Int. Ed.* **1997**, *36*, 2680-2683.
- ³ Crego-Calama, M.; Hulst, R.; Fokkens, R.; Nibbering, N.M.M.; Timmerman, P.; Reinhoudt, D.N. *Chem. Commun.* **1998**, 1021-1022.
- ⁴ Prins, L.J.; Huskens, J.; de Jong, F.; Timmerman, P.; Reinhoudt, D.N. *Nature (London)* **1999**, *398*, 498-502.
- ⁵ a) Kerckhoffs, J.M.C.A.; Crego-Calama, M.; Luyten, I.; Timmerman, P.; Reinhoudt, D.N. *Org. Lett.* **2000**, *2*, 4121-4124; Chapter 3 of this thesis.
- ⁶ The first attempt for the synthesis of calix[4]arene dimelamines **3** was the activation of calix[4]arene dimelamine **1a** or **1d** by 4-nitrophenol chloroformate and DIPEA as a base. Unfortunately, the desired product could not be isolated due to the base-catalyzed reaction of a carbamate to an isocyanate, liberating free 4-nitrophenol during evaporation of the solvent, even after acidification of the crude mixture. The isocyanate immediately reacted with the basic groups present the solution (for instance NH₂ protons of the calix[4]arene dimelamines). Similar synthesis reported in Matthews, S.E.; Pouton, C.W.; Threadgill, M.D. *New J. Chem.* **1999**, *23*, 1087-1096.
- ⁷ The formed product is base labile; upon washing with NaOH (1 M) a side product with a mass of the desired product minus 32 was formed. The loss of 32 mass units can be explained by the formation of a hydantoin (Boeijen, A.; Liskamp, R.J.M. *Eur. J. Org. Chem.* **1999**, *9*, 2127-2135)



- ⁸ Pope, B.M.; Sheu, J.-M.; Stanley, R.L.; Tarbell, D.S.; Yamamoto, Y. *J. Org. Chem.* **1978**, *43*, 2410-2414.
- ⁹ Unfortunately sometimes the Fmoc-signal overlaps with other signals in the ¹H NMR spectrum.
- ¹⁰ Mammen, M.; Simanek, E.E.; Whitesides, G.M. *J. Am. Chem. Soc.* **1996**, *118*, 12614-12623.
- ¹¹ Bielejewska, A.G.; Marjo, C.E.; Prins, L.J.; Timmerman, P.; de Jong, F.; Reinhoudt, D.N. *J. Am. Chem. Soc.* **2001**, *123*, 7518-7533.
- ¹² “Syro” provided by Multisynthetech, Witten, Germany. Software version: Syro 2000.
- ¹³ Due to overlapping signals of the peptide and the calix[4]arene, the exact yield of the assembly formation could not be determined.

Appendix

Abbreviations

Boc	Butoxycarbonyl
Fmoc	9-Fluorenylmethoxycarbonyl
tBu	t-Butyl
Trt	Tryl
Pbf	2,2,4,6,7-Pentamethyldihydrobenzofuran-5-sulfonyl
Cbz	Benzyloxycarbonyl
EDC	1-[3-(Dimethylamino)propyl]-3-ethylcarbodiimide hydrochloride
HBTU	2-(1H-Benzotriazole-1-yl)-1,1,3,3-tetramethyluronium hexafluorophosphate
HATU	2-(1H-9-Azabenzotriazole-1-yl)-1,1,3,3-tetramethyluronium hexafluorophosphate
HOBt	<i>N</i> -Hydroxybenzotriazole
DIPEA	Diisopropylethylamine
DMAP	4-Dimethylaminopyridine
NMP	<i>N</i> -Methylpyrrolidine

Chapter 5

Complexation of Phenolic Guests by *Endo-* and *Exo-Hydrogen-Bonded Receptors**

*In this chapter the complexation of small, neutral phenols by hydrogen-bonded receptors is described. The phenol receptors are formed by the self-assembly of calix[4]arene dimelamines or tetramelamines with 5,5-diethylbarbiturate (DEB) or cyanurate derivatives (CYA). The double rosette assemblies have their phenol-binding functionalities (ureido groups) both at the top and bottom of the double rosette. These double rosettes can be considered as *exo-receptors*. The tetrarosette assemblies form a cavity with binding sites between the two double rosettes for guest encapsulation. The tetrarosettes function as *endo-receptors*.*

* This work has been submitted for publication: Kerckhoffs, J.M.C.A.; Ishi-I, T.; Parachiv, V.; Timmerman, P.; Crego-Calama, M.; Shinkai, S.; Reinhoudt, D.N.

5.1 Introduction

Molecular recognition of substrates (guests) by receptors is a topic studied intensively in (bio)chemistry.¹ Compared to natural systems, most synthetic receptors² described in the literature support only a limited number of weak interactions. These synthetic receptors are usually capable of binding a single guest, be it a cation,³ an anion,⁴ or a small neutral molecule.⁵ Furthermore, the labor-intensive synthesis of these covalent receptors has been for decades based on rational design, where the focus is on optimization of the electronic and steric complementarity between the synthetic host and the targeted guest molecule.¹ However, natural receptors can selectively bind much larger and more structurally complex substrates than the smaller synthetic receptors. This is possible because natural receptors use multiple interactions to enhance the binding strength and selectivity,⁶ simple by combination of the basic set of natural “tools” such as amino acids and nucleotides.⁷ In proteins, the binding strength of a molecule to a target is increased when the target displays multiple sites for binding and the protein contains several discrete binding sites.⁸

In attempts to mimic Nature, interest is now focused more on diversity generation of synthetic multivalent receptors (and ligands) rather than on their rational design.⁹ For example, Still and co-workers¹⁰ have reported the synthesis of 10^4 receptors for N-acylated ⁵Leu enkephalin methyl ester from an A,B-cis cholic core by variations in the tripeptidic arms. Also, recently our group showed that the binding affinity for caffeine in water varies significantly upon random combinations of the side chains of a tetracationic porphyrin receptor.¹¹ Hamilton et al.¹² showed a nice example of functional diversity in developing a multivalent calix[4]arene based ligand bearing four peptidic loops that is able to bind to the surface of cytochrome c. Although the covalent approach has led to the synthesis of many effective receptors, our group¹³ and others^{14,15} have recently focused their effort on the creation of diversity in receptor molecules by using noncovalent synthesis. Noncovalent synthesis allows chemical diversity to be achieved much more readily by the simple combination of molecular building blocks.

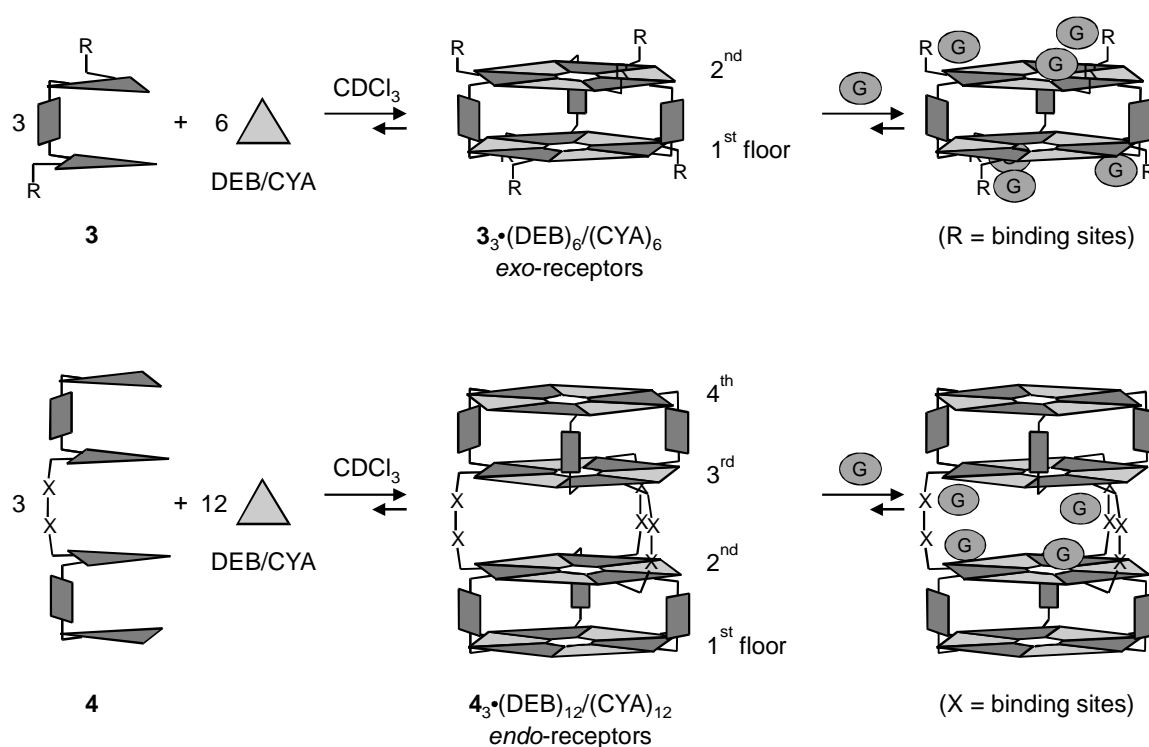
Our group has previously reported the noncovalent synthesis of a great variety of hydrogen-bonded double¹⁶ and tetra-roses,¹⁷ consisting of 9 or 15 building blocks held together by 36 or 72 cooperative hydrogen bonds, respectively (Scheme 5.1). The assemblies are formed by mixing calix[4]arene dimelamines with 2 or 4 equivalents of DEB (5,5-diethylbarbiturate) or CYA (cyanurate derivatives) in apolar solvents. These

rosette assemblies are used as a simple platform to bring together multiple ligand binding sites, that are attached to the melamine units. The approach can be used even with polar hydrogen bond donor and acceptor groups, such as small peptides.¹⁸ The main advantage of this noncovalent approach is that a library of potential receptors can be easily generated in solution by simply mixing different calix[4]arene dimelamines with 2 or 4 equivalents of DEB or CYA under conditions that allow for the reversible exchange of the melamine derivatives.¹³

These noncovalent receptors are mainly designed for the complexation of a single guest. In this chapter the objective was to use the noncovalent synthesis for the generation of multivalent receptors,¹⁹ and results are presented of the complexation ability of the functionalized double and tetra-rosette assemblies as *exo*- and *endo*-receptors for multiple phenolic guests, respectively. The interest in phenol moieties resides in the fact that they are important parts of different biomolecules such as adrenergic receptors²⁰ and flavones.²¹ Furthermore, phenols have been widely studied in physical-organic research and for their binding to natural receptors,²² and are therefore excellent model compounds. Despite the fact of their importance for biochemical purposes, there are few examples of synthetic receptors for phenolic guests.²³

5.2 Results and Discussion

Assemblies $3_3 \cdot (\text{DEB})_6 / (\text{CYA})_6$ are *exo*-receptors in which guest recognition occurs at the bottom of the first floor and at the top of the second floor. Assemblies $4_3 \cdot (\text{DEB})_{12} / (\text{CYA})_{12}$ can be seen as *endo*-receptors in which recognition occurs in the cavity between the two double rosettes (between the second and third floors) (Scheme 5.1).¹⁷



Scheme 5.1. Formation of exo- and endo-hydrogen-bonded receptors $3_3 \bullet (\text{DEB})_6 / (\text{CYA})_6$ and $4_3 \bullet (\text{DEB})_{12} / (\text{CYA})_{12}$.

In the double rosette $3_3 \bullet (\text{DEB})_6 / (\text{CYA})_6$, and tetrarosette $4_3 \bullet (\text{DEB})_{12} / (\text{CYA})_{12}$, the multiple phenol binding sites are brought together by simply mixing the corresponding building blocks in apolar solvents, such as chloroform or toluene.¹⁸ (Scheme 5.1). Specifically, exo-receptors $3_3 \bullet (\text{DEB})_6 / (\text{CYA})_6$ are formed by mixing the corresponding calix[4]arene dimelamine **3** bearing the phenol recognition sites R, with 2 equivalents of DEB or CYA. Similarly, endo-receptors $4_3 \bullet (\text{DEB})_{12} / (\text{CYA})_{12}$ are formed by mixing the corresponding tetramelamine **4** (containing two calix[4]arene dimelamine units covalently connected by a flexible linker bearing the phenol binding sites X) with 4 equivalents of DEB or CYA. These assemblies have a high thermodynamic stability due to the formation of 36 (double rosette) and 72 (tetrarosette) cooperative hydrogen bonds, which renders these assemblies stable in CDCl_3 even at concentrations of 10^{-4} M.

5.2.1 Synthesis of Double- and Tetrarosette Assemblies

Calix[4]arene dimelamines **2**^{16b} and **3a**¹⁸ were synthesized by reaction of bis(chlorotriazine) **1a** with an excess of butylamine and 2,2-dimethyl-1,3-propane diamine, respectively. Compounds **3b-f**¹⁸ were synthesized by reaction of **3a** with the

corresponding isocyanate or acid chloride derivative. Calix[4]arene tetramelamine **4a**^{17b} was synthesized by a reaction of **3g**^{17b} with 0.5 equiv of 1,4-diaminobutane bis(*p*-nitrophenyl dicarbamate). Compound **4b**^{17b} was synthesized by reaction of **1b** first with an excess of 2,2-dimethyl-1,3-propane diamine, followed by reaction of the intermediate with 0.5 equiv of 1,4-diaminobutane bis(*p*-nitrophenyl dicarbamate). All compounds were fully characterized by ¹H NMR, FAB MS, and elemental analysis or ¹³C NMR.

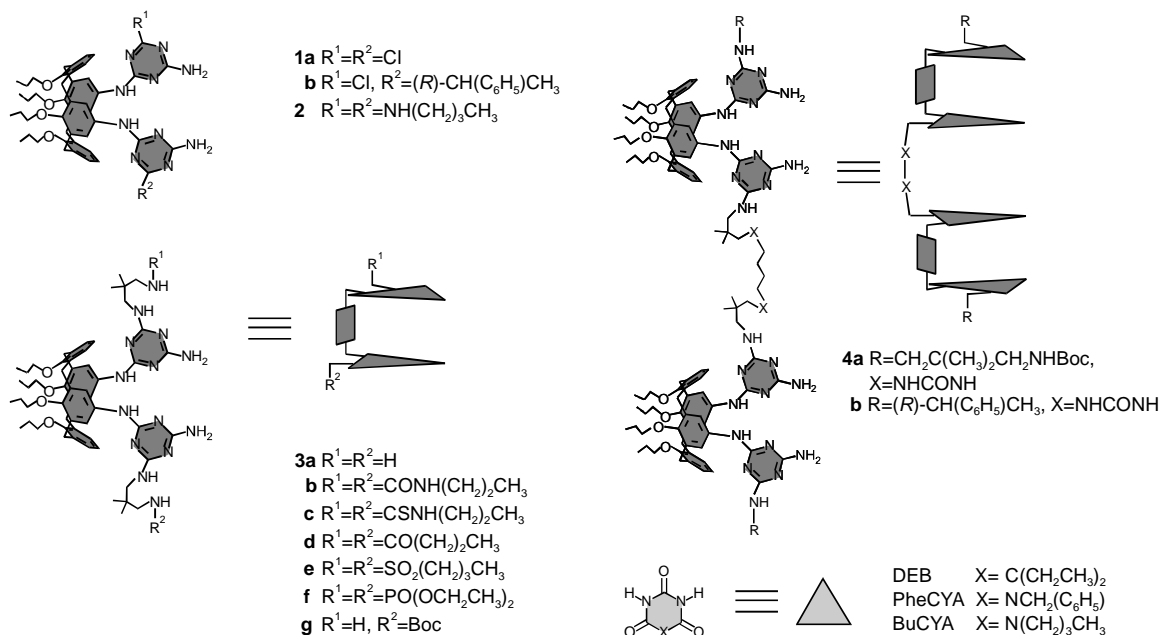


Chart 5.1. Molecular structures and schematic representations of molecular compounds 1-4.

5.2.2 Complexation Studies with Exo-Receptors

The detailed structural analysis of the assembly **3b**₃•(DEB)₆ by ¹H NMR spectroscopy showed that the 2,2-dimethylpropyl side chain adopts a rigid conformation (see Chapter 3). As previously explained, in the assembly this ureido side chain is folded back over the calix[4]arene aromatic rings due to hydrogen bond formation between one of the urea NH protons (H_m) and one of the nitrogen atoms of the triazine ring (Figure 5.1).¹⁸ This back-folding of the ureido side chains results in the formation of potential binding pockets for the phenol guests at the top and bottom of the double rosette.

Complexation of 4-nitrophenol (**5a**, see Figure 5.1 for molecular structure) by the double rosette assembly **3b**₃•(DEB)₆ (in CDCl₃ at 293 K) was studied by ¹H NMR spectroscopy. Upon addition of **5a**, (ca. 60 equiv) to **3b**₃•(DEB)₆ (1 mM), a ~ 0.45 ppm downfield shift of one of the two ureido protons (H_m) was observed (Figure 5.1), while

the downfield shift of the other ureido proton (H_n) was smaller but still significant (~ 0.2 ppm). The shifts of the other rosette signals were much smaller (< 0.08 ppm). Furthermore, upon addition of 1 equiv of **5a** to $3b_3 \cdot (DEB)_6$, the ArH signal (ArH next to Ar-NO₂) of this guest showed an upfield shift of 0.085 ppm. This upfield shift is probably due to the expected formation of the hydrogen bond between the hydroxyl of **5a** and the urea carbonyls of $3b_3 \cdot (DEB)_6$.

As a control experiment, 7 equiv of 4-nitroanisole (**6**, see Chart 5.2) were added to assembly $3b_3 \cdot (DEB)_6$ (1 mM). No significant changes in the ¹H NMR spectrum of assembly $3b_3 \cdot (DEB)_6$ were observed. This experiment indicates that the hydroxyl group of **5a** is important for the binding of **5a** to $3b_3 \cdot (DEB)_6$, supporting the hypothesis that the complexation occurs via the hydrogen bond formation between the carbonyl of the ureido functionality of **3b** and the hydroxyl of the phenol **5a**.

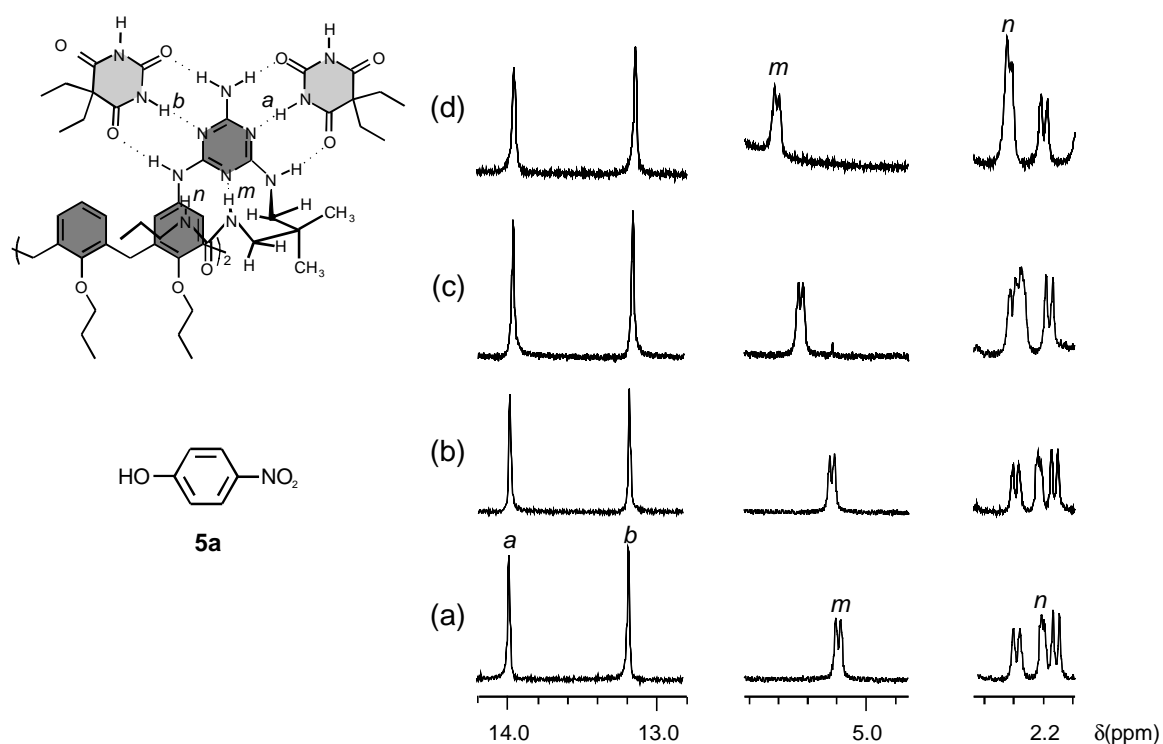


Figure 5.1. Parts of the ¹H NMR spectra of $3b_3 \cdot (DEB)_6$ (1 mM) in CDCl₃ at 293K: (a) 0, (b) 1, (c) 10, and (d) 60 equivalents of **5a**.

The binding affinity of **5a** to the assembly $3b_3 \cdot (DEB)_6$ was determined by a ¹H NMR titration experiment in CDCl₃ (1 mM, 293 K). The chemical shift of the urea NH proton H_m was monitored during the titration (Figure 5.2). Several binding models for the

binding of **5a** to $\mathbf{3b}_3\bullet(\text{DEB})_6$ can be envisioned. Two binding models will be discussed in detail: (i) a 1:2 ($\mathbf{3b}_3\bullet(\text{DEB})_6$: **5a**) binding model, where phenol complexation occurs in the binding pockets above and beneath the double rosette, and (ii) a multivalent 1:6 binding model due to the presence of the 6 ureido groups in the assembly (3 at the top and 3 at the bottom of the double rosette). An intrinsic K_a of 134 M^{-1} was estimated by using a non-cooperative 1:2 binding model, and an intrinsic K_a of 202 M^{-1} was estimated by using a non-cooperative 1:6 binding model (Table 5.1, see also Appendix).²⁴ The calculated K_a values are on the same order as reported K_a values for the complexation of phenol derivatives to urea carbonyl groups.²⁵ Thus, no significant cooperativity is observed for the complexation of **5a** to $\mathbf{3b}_3\bullet(\text{DEB})_6$. Nevertheless, assembly $\mathbf{3b}_3\bullet(\text{DEB})_6$ has an advantage when compared with the phenol complexation to a single urea molecule. Assembly $\mathbf{3b}_3\bullet(\text{DEB})_6$ has six independent binding sites that are well oriented and preorganized. They are arranged in such a way that they might bind to adjacent sites of larger guest molecules.^{8a}

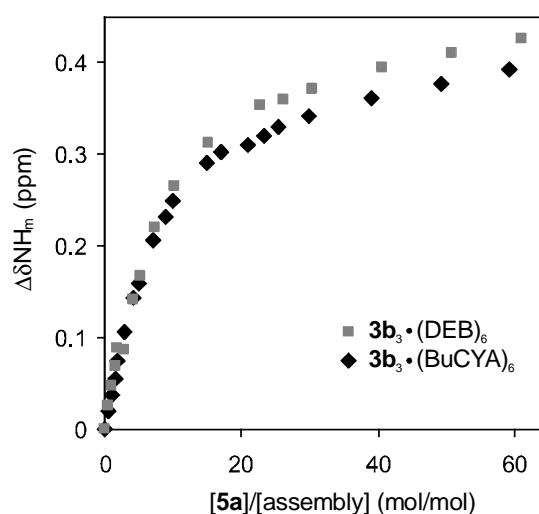


Figure 5.2. Plot of the induced shifts ($\Delta\delta\text{NH}_m$) of the ^1H NMR signal NH_m versus $[\mathbf{5a}]/[\mathbf{3b}_3\bullet(\text{DEB})_6]$ (■) and versus $[\mathbf{5a}]/[\mathbf{3b}_3\bullet(\text{BuCYA})_6]$ (◆) in CDCl_3 (1 mM for assembly).

Further confirmation of the complex stoichiometry was provided by Ag^+ labeling MALDI-TOF Mass Spectrometry.²⁶ This is a relatively soft ionization method that provides a nondestructive way to generate charged species for the estimation of the stoichiometry of a complex. In carrying out the MALDI-TOF experiments, different concentrations of rosette assembly, ranging from 10 mM to 0.1 mM of $\mathbf{3b}_3\bullet(\text{DEB})_6$, and different equivalents of phenol guest **5a** (10, 30, and 60 equiv) were used.²⁷ As shown in

Figure 5.3a, the mass spectrum of the sample containing $3\mathbf{b}_3\cdot(\text{DEB})_6$ (10 mM) and $5\mathbf{a}$ (10 equiv) showed a relatively intense signal at m/z 5589.2 (calcd for $3\mathbf{b}_3\cdot(\text{DEB})_6\cdot5\mathbf{a}_6\cdot\text{Ag}^+ = 5587.8$) and a smaller signal at m/z 5452 (calcd for $3\mathbf{b}_3\cdot(\text{DEB})_6\cdot5\mathbf{a}_5\cdot\text{Ag}^+ = 5448.8$). The mass spectrum of the sample containing 1.0 mM of the complex and 10 equiv of $5\mathbf{a}$ showed two signals of similar intensity at m/z 5310 (calcd for $3\mathbf{b}_3\cdot(\text{DEB})_6\cdot5\mathbf{a}_4\cdot\text{Ag}^+ = 5309.7$) and m/z 5171 (calcd for $3\mathbf{b}_3\cdot(\text{DEB})_6\cdot5\mathbf{a}_3\cdot\text{Ag}^+ = 5170.7$). Also, among other signals, three smaller signals at m/z 5034, 5451, and 5588 corresponding to the complexation of 2, 5, and 6 equiv of $5\mathbf{a}$, respectively, were present. The mass spectrum of the most dilute sample (0.1 mM, 10 equiv $5\mathbf{a}$) showed a relatively intense signal at m/z 4894 (calcd for $3\mathbf{b}_3\cdot(\text{DEB})_6\cdot5\mathbf{a}\cdot\text{Ag}^+ = 4892.6$) and smaller signals at m/z 4753 and 5033, corresponding to the free host ($3\mathbf{b}_3\cdot(\text{DEB})_6\cdot\text{Ag}^+$) and the complexation of 2 molecules of $5\mathbf{a}$ ($3\mathbf{b}_3\cdot(\text{DEB})_6\cdot5\mathbf{a}_2\cdot\text{Ag}^+$) respectively (Figure 5.3b).

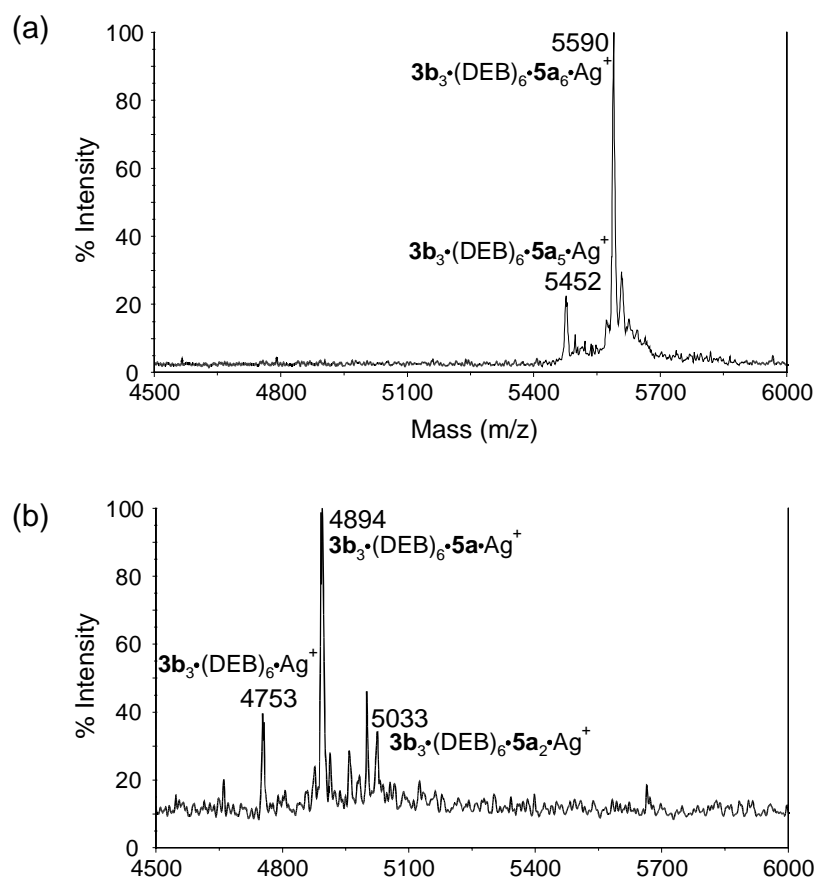


Figure 5.3. MALDI-TOF mass spectra by using Ag^+ -labeling technique for the complexations of (a) $3\mathbf{b}_3\cdot(\text{DEB})_6$ with $5\mathbf{a}$ (10 mM, 10 equiv $5\mathbf{a}$), and (b) $3\mathbf{b}_3\cdot(\text{DEB})_6$ with $5\mathbf{a}$ (0.1 mM, 10 equiv $5\mathbf{a}$), in CH_2Cl_2 .

In summary, these results showed that at higher concentrations of double rosette more guest molecules are complexed. The distribution of the different complexes found in the MALDI-TOF MS experiments is in agreement with the expectations based on the non-cooperative 1:6 binding model using an intrinsic K_a of 202 M^{-1} obtained experimentally from the ^1H NMR titration (Figure 5.4). Furthermore, MALDI-TOF MS experiments where the concentration of $3\mathbf{b}_3\cdot(\text{DEB})_6$ was kept constant and the number of equiv of phenol $5\mathbf{a}$ (30 and 60 equiv) was increased, have been performed. In these experiments, formation of the higher molecular weight complexes were observed upon addition of more equiv of $5\mathbf{a}$.

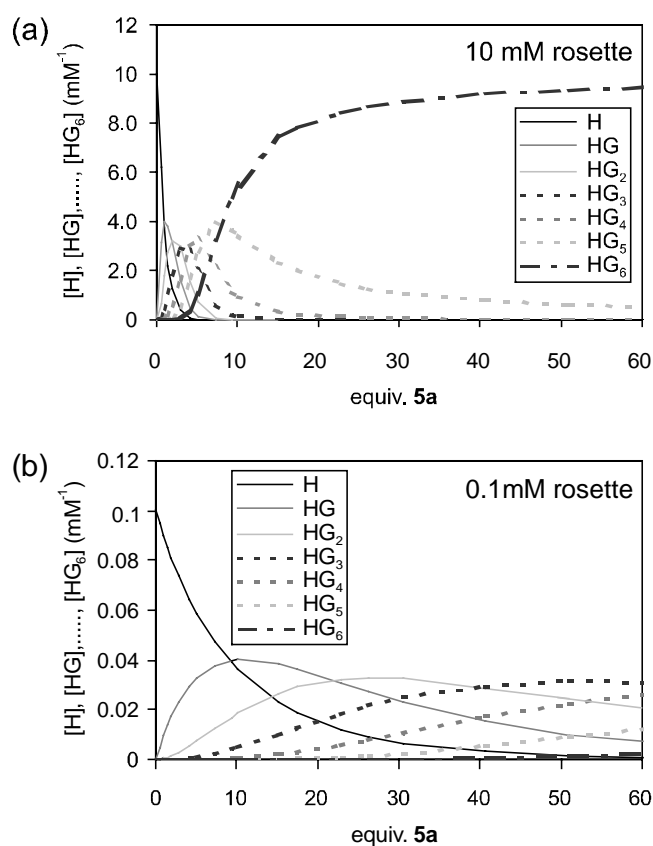


Figure 5.4. Distribution of the different complexes $3\mathbf{b}_3\cdot(\text{DEB})_6\cdot 5\mathbf{a}_n$ at different concentrations of total host, (a) 10 mM, (b) 0.1 mM, and 10 equiv of $5\mathbf{a}$ using a non-cooperative 1:6 binding model with a K_a of 202 M^{-1} . $H = 3\mathbf{b}_3\cdot(\text{DEB})_6$ and $G = 5\mathbf{a}$.

To determine the effect of a possible change in the geometry of the complex due to the substitution of CYA for DEB on the complexation of phenol $5\mathbf{a}$, the complexation of $5\mathbf{a}$ to assembly $3\mathbf{b}_3\cdot(\text{BuCYA})_6$ was also studied by ^1H NMR. The geometry of the double

rosette plane is different when DEB or CYA are part of the assembly due to the different electron distributions. We also observed a downfield shift of H_m after addition of **5a** to $\mathbf{3b}_3\bullet(\text{BuCYA})_6$ ($\Delta\delta$ 0.25 ppm; 10 equiv **5a**). The data obtained from the titration (1 mM rosette in CDCl_3 , 293 K) were fitted using the 1:6 binding model described above to give an intrinsic K_a of 239 M^{-1} . Thus, no significant difference between the complexation of **5a** to $\mathbf{3b}_3\bullet(\text{DEB})_6$ or to $\mathbf{3b}_3\bullet(\text{BuCYA})_6$ was observed. This result showed that the effect of the geometry of the rosette plane on the complexation is minimal.

The data that have been presented above indicate that hydrogen bond formation between the guest's hydroxyl group and the receptor's ureido carbonyl groups are the driving force for phenol complexation by $\mathbf{3b}_3\bullet(\text{DEB})_6$. To confirm the importance of this ureido side chain in promoting phenol recognition by the assembly, the interaction of **5a** with $\mathbf{2}_3\bullet(\text{DEB})_6$, an assembly that lacks the ureido groups, was studied. A ^1H NMR titration of double rosette $\mathbf{2}_3\bullet(\text{DEB})_6$ (1 mM, 293 K) with **5a** showed no significant changes in the chemical shifts for the ^1H NMR signals of either **5a** or $\mathbf{2}_3\bullet(\text{DEB})_6$. Because assembly $\mathbf{2}_3\bullet(\text{DEB})_6$ lacks the ureido protons H_m , one of the aromatic signals of **5a** (ArH next to Ar- NO_2) and proton H_d (one of the NH protons of the melamine unit, see Figure 5.1 for similar description) were monitored to compare $\mathbf{3b}_3\bullet(\text{DEB})_6$ and $\mathbf{2}_3\bullet(\text{DEB})_6$. No significant change in the chemical shift of the aromatic protons of **5a** is observed upon addition to $\mathbf{2}_3\bullet(\text{DEB})_6$, while in the case of assembly $\mathbf{3b}_3\bullet(\text{DEB})_6$ a $\Delta\delta$ value of -0.085 ppm was observed. Also when proton H_d is followed, only small shifts (< 0.025 ppm upfield) are visible during the titration with $\mathbf{2}_3\bullet(\text{DEB})_6$, while larger shifts ($\Delta\delta$ 0.05 ppm, 10 equiv **5a**) were observed in the case of $\mathbf{3b}_3\bullet(\text{DEB})_6$.

Furthermore, the intensities of the diagnostic NH_{DEB} -protons, H_a and H_b (see Figure 5.1 for similar H description), for the assembly $\mathbf{2}_3\bullet(\text{DEB})_6$ decrease after addition of 10 equiv of phenol **5a**, suggesting that assembly dissociation occurs upon phenol addition.²⁸ The dissociation as revealed by ^1H NMR spectroscopy is accompanied by a color change of the solution from colorless to yellow, consistent with deprotonation of phenol **5a**.²⁹ In sharp contrast, when up to 60 equiv of **5a** is added to $\mathbf{3b}_3\bullet(\text{DEB})_6$, no color change or change in the ^1H NMR of the H_a or H_b signals is observed, indicating that dissociation of the assembly does not occur. Therefore, it seems likely that assembly $\mathbf{2}_3\bullet(\text{DEB})_6$ is less stable and dissociates more readily than $\mathbf{3b}_3\bullet(\text{DEB})_6$, thereby liberating the free calix[4]arene dimelamine in solution, that can deprotonate **5a**.

The complexation of **5a** by several functionalized double rosettes has also been studied. Addition of **5a** to the thioureido assembly (**3c**₃•(DEB)₆) showed only a small shift of H_m ($\Delta\delta$ 0.06 ppm, 10 equiv). This observed shift is much smaller than the shift of H_m for assembly **3b**₃•(DEB)₆ ($\Delta\delta$ 0.26 ppm) upon addition of 10 equiv **5a**. Addition of ~ 10 equiv **5a** to **3e**₃•(DEB)₆ (sulfonamide) and **3f**₃•(DEB)₆ (phosphoramidate) did not shift any signals in the ¹H NMR spectrum. The NMR data suggest that there is no complexation of **5a** by **3e**₃•(DEB)₆ or **3f**₃•(DEB)₆. This could be because the hydrogen bond acceptor ability (or electron density) of the phosphoramidate and sulfonamide oxygens and the sulfur of the thiourea³⁰ is too low to enable detectable complexation by phenol **5a**. Addition of **5a** to assembly **3d**₃•(DEB)₆, containing an amide in the side chain, showed a similar shift ($\Delta\delta$ 0.25 ppm, 10 equiv) as was seen for the ureido-containing assembly **3b**₃•(DEB)₆. The ¹H NMR titration of the addition of **5a** to assembly **3d**₃•(DEB)₆ yielded an intrinsic K_a of 155 M⁻¹, a value that is on the same order of magnitude as the K_a for binding of **5a** by **3b**₃•(DEB)₆.

5.2.3 Complexation Studies with Endo-Receptors

To assess the difference between *exo*- and *endo*-receptors, recognition studies of **5a** by tetra-rosette assemblies **4a**₃•(DEB)₁₂ were performed under the same experimental conditions as for **3b**₃•(DEB)₆. For **4a**₃•(DEB)₁₂, the urea NH_α proton signal at 5.20 ppm (Figure 5.5) showed a significant downfield shift upon addition of **5a** ($\Delta\delta$ 0.375 ppm, 10 equiv **5a**). On the other hand, the induced shift of the NH_β signal of the terminal carbamate moiety is much smaller ($\Delta\delta$ 0.02 ppm, 10 equiv **5a**). These results indicate that the hydroxyl group of **5a** interacts predominantly with the internal ureido carbonyl groups that are positioned within the cavity formed by **4a**₃•(DEB)₁₂.³¹

To demonstrate that the phenol guest complexation occurs in the cavity between the two double rosettes, the signals of the H_a and H_b protons were monitored in a typical NMR titration experiment (Figure 5.5). Interestingly, upon addition of 10 equiv of **5a** the only significant shifts were for the NH_{a2} ($\Delta\delta$ -0.095 ppm) and NH_{b2} signals ($\Delta\delta$ -0.05 ppm) of the second and third floors of the tetra-rosette. In contrast, the corresponding guest-induced shifts for the first and fourth rosette floors were much smaller ($\Delta\delta$ +0.01 ppm for NH_{a1} and -0.02 ppm for NH_{b1}, 10 equiv **5a**). These data clearly indicate that phenol **5a** is complexed within the assembly's cavity, between the second and the third

floors of the tetra-rosette. Similar results were also found for $4\mathbf{a}_3\cdot(\text{BuCYA})_{12}$, $4\mathbf{b}_3\cdot(\text{DEB})_{12}$, and $4\mathbf{b}_3\cdot(\text{BuCYA})_{12}$ assemblies. This is to be expected since the ureido carbonyls in the linker are positioned between the 2nd and 3rd floors.

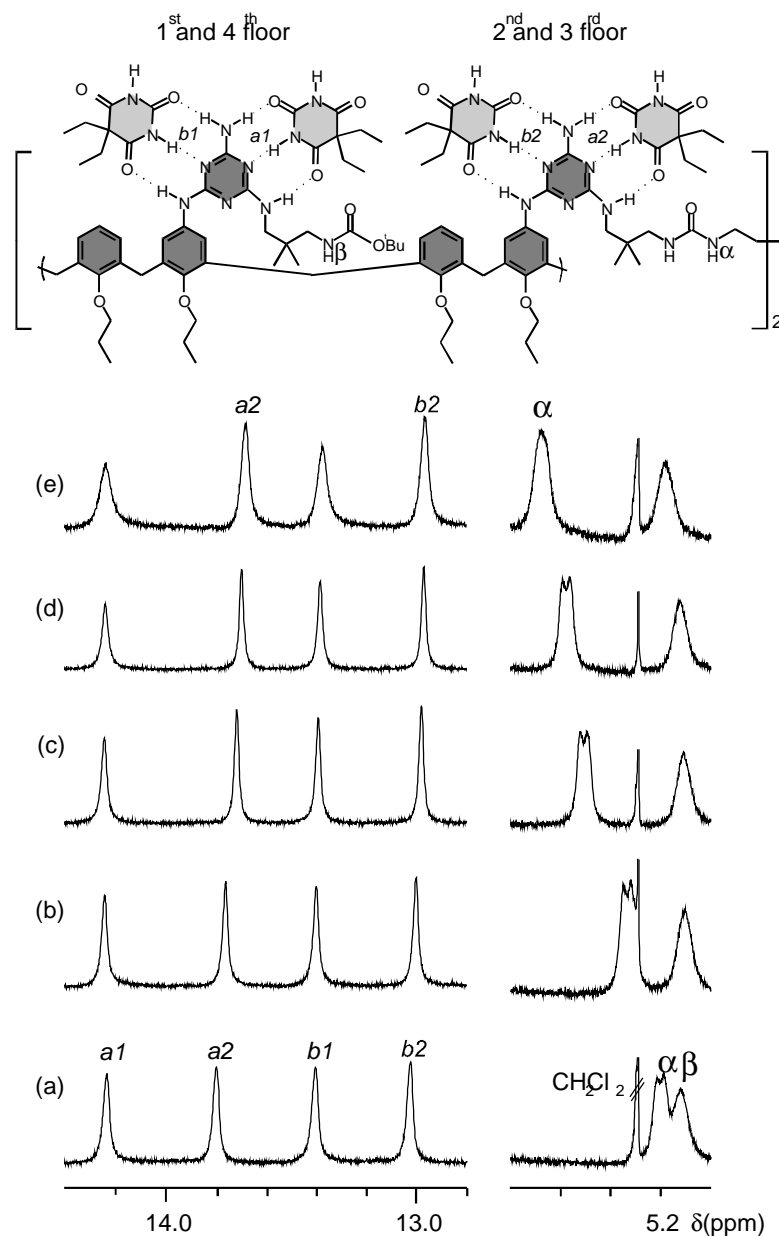


Figure 5.5. Parts of the ^1H NMR spectra of $4\mathbf{a}_3\cdot(\text{DEB})_{12}$ (1 mM) in CDCl_3 at 293K: (a) 0, (b) 2, (c) 6, (d) 10, and (e) 20 equivalents of $5\mathbf{a}$.

Generally, for barbituric acid-based assemblies ($4\mathbf{a}_3\cdot(\text{DEB})_{12}$ and $4\mathbf{b}_3\cdot(\text{DEB})_{12}$) the $\text{NH}_{\text{a}1}$ and $\text{NH}_{\text{b}1}$ peaks on the first and fourth floors tended to broaden upon the addition of $5\mathbf{a}$ (Figure 5.5). This peak broadening is ascribed to proton exchange between the OH of

5a and the $\text{NH}_{\text{a1}}/\text{NH}_{\text{b1}}$.³² The peak broadening, indicative of significant proton exchange in the barbituric acid-based chiral assembly $\mathbf{4b}_3\cdot(\text{DEB})_{12}$, is consistent with the lower stability of this DEB-based assembly. Additional proof of the lability of the tetra-rosette assembly $\mathbf{4b}_3\cdot(\text{DEB})_{12}$ was gathered by the disassociation of the assembly upon the addition of excess **5a**.³³ The more stable cyanuric acid-based³⁴ assembly $\mathbf{4b}_3\cdot(\text{BuCYA})_{12}$ did not show the broadening of the NH_{a1} and NH_{b1} signals, indicating the inhibition of the amide NH - phenol OH proton exchange due to the larger stability of the rosette's hydrogen bonding network.³⁴

In contrast to the double rosette system, a 1:4 stoichiometry of the tetra-rosette $\mathbf{4a}_3\cdot(\text{DEB})_{12}$ complexation with **5a** was estimated. A Job plot³⁵ indicates a maximum at a 1:4 molar ratio of $\mathbf{4a}_3\cdot(\text{DEB})_{12}$ and **5a** (Figure 5.6).

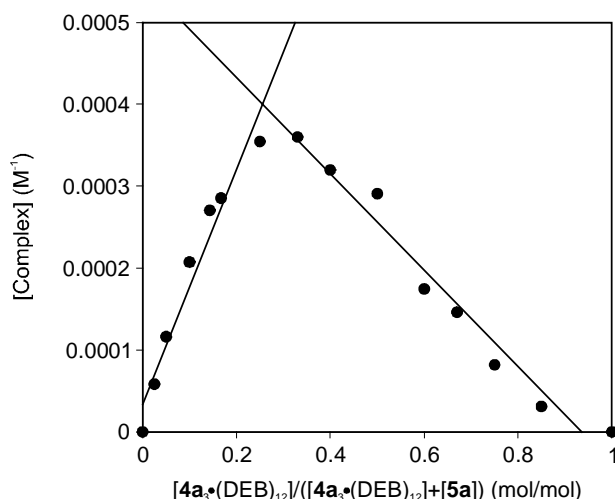


Figure 5.6. Job plot for the complexation of $\mathbf{4a}_3\cdot(\text{DEB})_{12}$ with **5a**: the sum of $[\mathbf{4a}_3\cdot(\text{DEB})_{12}]$ and $[\mathbf{5a}]$ was maintained constant (4 mM) in CDCl_3 at 293K.

Only four **5a** guest molecules could be complexed within the cavity³¹ rather than six, probably due to space limitations. The intrinsic K_a was estimated from ^1H NMR titration data (Figure 5.7) by using a non-cooperative 1:4 complex model. The estimated values are summarized in Table 5.1.

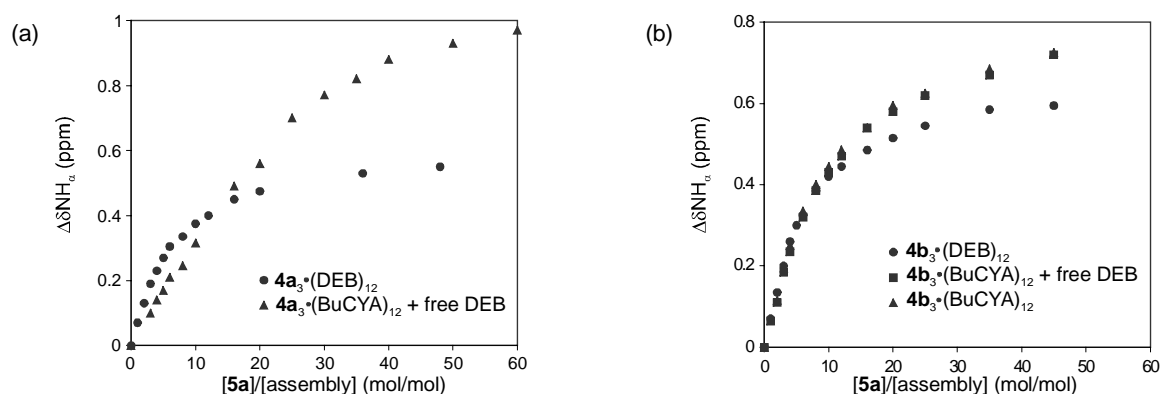


Figure 5.7. Plots of the induced shifts ($\Delta\delta\text{NH}_\alpha$) of the NMR signal NH_α versus $[\mathbf{5a}]/[\text{assembly}]$ in CDCl_3 (1 mM for assembly) for: (a) $\mathbf{4a}_3\bullet(\text{DEB})_{12}$ (●) and $\mathbf{4a}_3\bullet(\text{BuCYA})_{12} + \text{free DEB}$ (▲), (b) $\mathbf{4b}_3\bullet(\text{DEB})_{12}$ (●), $\mathbf{4b}_3\bullet(\text{BuCYA})_{12}$ (▲), and $\mathbf{4b}_3\bullet(\text{BuCYA})_{12} + \text{free DEB}$ (■).

Table 5.1. Intrinsic binding constants (K_a)^[a] for the complexations of double and tetra rosette assemblies (1 mM) with $\mathbf{5a}$ in CDCl_3 at 293K.^[b]

Assembly	K_a (M^{-1})	
	1:4 model	1:6 model
$\mathbf{3b}_3\bullet(\text{DEB})_6$	-	202 (195) ^[c]
$\mathbf{3b}_3\bullet(\text{BuCYA})_6$	-	239
$\mathbf{3d}_3\bullet(\text{DEB})_6$	-	155
$\mathbf{4a}_3\bullet(\text{DEB})_{12}$	286	-
$\mathbf{4a}_3\bullet(\text{BuCYA})_{12}$	116	-
$\mathbf{4b}_3\bullet(\text{DEB})_{12}$	299 ^[d]	-
$\mathbf{4b}_3\bullet(\text{BuCYA})_{12}$	137 –150	-

[a] Numbers of binding constants are not measured precisely.

[b] K_a values were estimated by nonlinear least-square method using non-cooperative 1:4 and 1:6 complex models.

[c] $\mathbf{5c}$ was used as a guest molecule.

[d] ref 36.

Guest encapsulation in tetra-rosette assemblies was also supported by MALDI-TOF mass spectrometry using the Ag^+ -labeling technique. For $\mathbf{4b}_3\bullet(\text{DEB})_{12}$, in the presence of 12 equiv of $\mathbf{5a}$, the ion peak for the parent assembly $\mathbf{4b}_3\bullet(\text{DEB})_{12}$ (calcd. for $\mathbf{4b}_3\bullet(\text{DEB})_{12}\bullet\text{Ag}^+ = 8913.7$) was observed as the major species. Under the same experimental conditions $\mathbf{4b}_3\bullet(\text{BuCYA})_{12}$ afforded the ion peaks for the 1:2 and 1:3

complexes with **5a** (calcd. for $\mathbf{4b}_3 \cdot (\text{BuCYA})_{12} \cdot \mathbf{5a}_2 \cdot \text{Ag}^+ = 9203.7$ and $\mathbf{4b}_3 \cdot (\text{BuCYA})_{12} \cdot \mathbf{5a}_3 \cdot \text{Ag}^+ = 9342.8$, respectively). No peak of the parent assembly $\mathbf{4b}_3 \cdot (\text{BuCYA})_{12}$ was observed (calcd. for $\mathbf{4b}_3 \cdot (\text{BuCYA})_{12} \cdot \text{Ag}^+ = 8925.7$). More interestingly, upon the addition of a large excess of **5a** (45 equiv) the 1:4 complex (calcd. for $\mathbf{4b}_3 \cdot (\text{BuCYA})_{12} \cdot \mathbf{5a}_4 \cdot \text{Ag}^+ = 9481.8$) was detected as the main species, a stoichiometry that coincides with the results from the Job plot.

Generally, the K_a values (286-299 M^{-1}) for the barbituric acid-based $\mathbf{4}_3 \cdot (\text{DEB})_{12}$ tetra-rosettes are larger compared to those for the cyanuric acid-based tetra-rosettes $\mathbf{4}_3 \cdot (\text{BuCYA})_{12}$ (116-150 M^{-1}).³⁶ This observed difference in phenol binding strengths may be attributed to structural differences between barbituric- and cyanuric acid-based assemblies. Somehow, the structure of DEB, with its tetrahedral sp^3 -carbon in the 6-membered ring in host $\mathbf{4}_3 \cdot (\text{DEB})_{12}$ shows better complementarity for guest **5a** than host $\mathbf{4}_3 \cdot (\text{BuCYA})_{12}$, containing CYA with its flatter sp^3 -nitrogen. In contrast, the K_a values obtained for the complexation of **5a** to *exo*-receptors $\mathbf{3b}_3 \cdot (\text{DEB})_6$ and $\mathbf{3b}_3 \cdot (\text{BuCYA})_6$ are similar (see above), providing another indication that binding of **5a** to assembly $\mathbf{4a}_3 \cdot (\text{DEB})_{12}$ does not occur on the outer rosette platforms (1st and 4th floors).

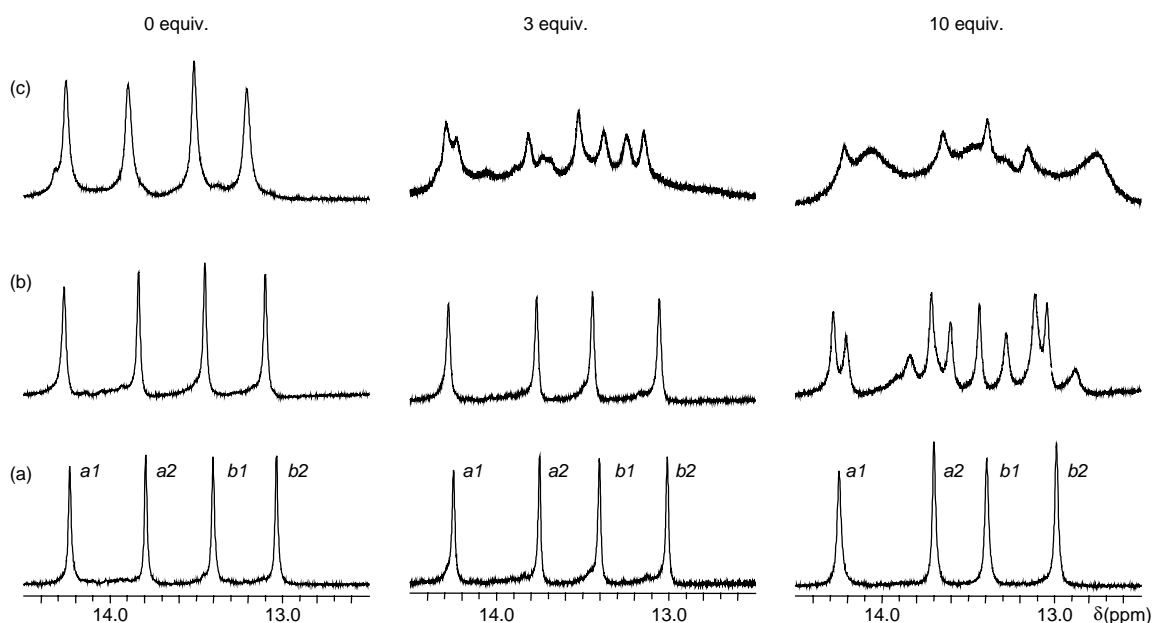


Figure 5.8. Parts of the ^1H NMR spectra of $\mathbf{4a}_3 \cdot (\text{DEB})_{12}$ (1 mM) in CDCl_3 in the presence of **5a** (0, 3, and 10 equiv): (a) 293, (b) 273, and (c) 233 K (For assignment, see structure in Figure 5.5).

Strong evidence for the encapsulation of guest **5a** within the 2nd and 3rd floors of tetra-rosette **4a₃•(DEB)₁₂** was gathered from variable temperature (VT) NMR measurements. For tetra-rosette assembly **4a₃•(DEB)₁₂**, splittings of ¹H NMR signals H_{a1}, H_{a2}, H_{b1}, H_{b2}, and NH_α were observed in the presence of **5a** (3 and 10 equiv) at low temperature (< 273K, Figure 5.8). This signal splitting is ascribed to the presence of more than one species in solution on the NMR time-scale, namely the different complexed **4a₃•(DEB)₁₂•5a_n** (n = 1-4) and uncomplexed **4b₃•(DEB)₁₂** assemblies in solution. In the absence of phenol guest **5a** no splitting of the NMR signals is found (Figure 5.8). Similar phenomena were also observed in **4a₃•(BuCYA)₁₂** and **4b₃•(DEB)₁₂** systems. In contrast to these VT results with the tetra-rosette, the VT ¹H NMR spectra of **3b₃•(DEB)₆** with either 3 or 10 equiv of **5a** (between 243K and 333K) did not show splitting of the H_a and H_b signals. For the double rosette fast exchange between the complexed guest and the free guest occurs at an even lower temperature (243K), and only averaged NMR signals are observed.

5.2.4 Selectivity Studies with *Exo*- and *Endo*-Receptors

Various substituted phenol derivatives **5** (Chart 5.2) were selected as possible guest molecules and the induced shifts of the NH_{m/α} signal ($\Delta\delta\text{NH}_{m/\alpha}$) for **3b₃•(DEB)₆** (Table 5.2) and **4a₃•(DEB)₁₂** were carefully checked.

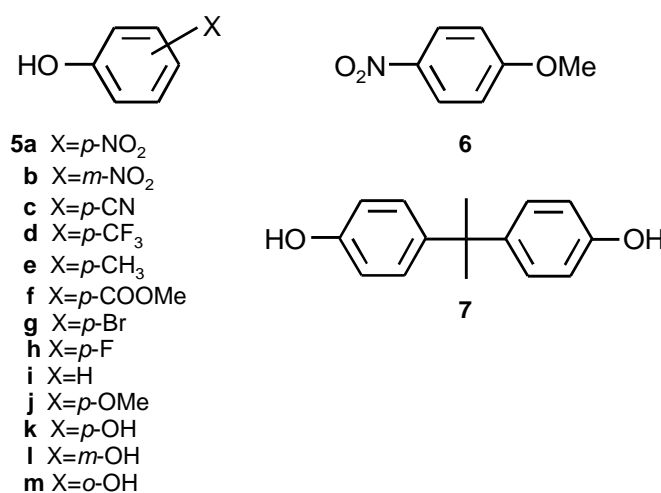


Chart 5.2. Molecular structures of compounds 5-7.

The $\Delta\delta\text{NH}_{m/\alpha}$ values (in experiments with 1.0 mM and 10 equiv of **5**) were plotted against Hammett parameters σ_p or σ_m (Figure 5.9).³⁷ The σ_p or σ_m parameters are

quantified descriptors of the ability of an organic functional group to affect the electron density distribution of an aryl group. While Hammett plots have been routinely used in physical organic chemistry, they have also found increasing use in supramolecular systems.³⁸

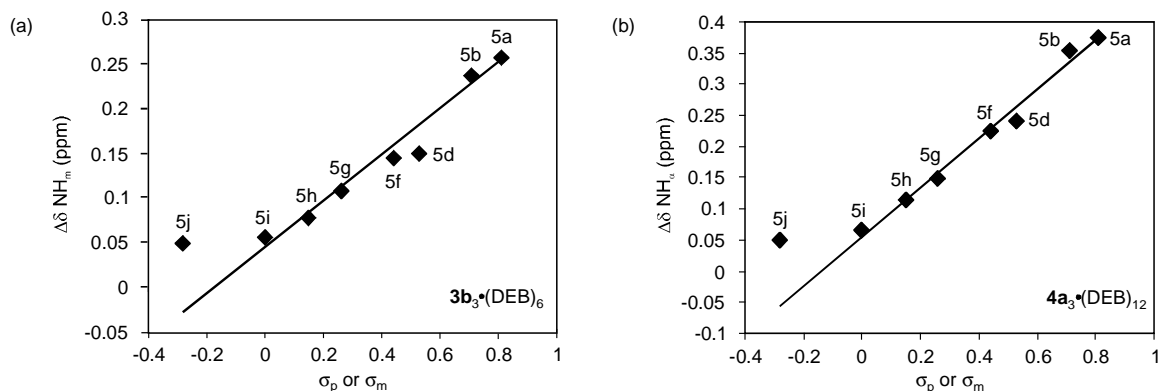


Figure 5.9. Hammett plots for the NMR signal of $NH_{m/\alpha}$ in the assemblies (a) $3b_3 \cdot (DEB)_6$ and (b) $4a_3 \cdot (DEB)_{12}$ (1 mM) in the presence of **5a-b**, **5d**, and **5f-j** (10 equiv) in $CDCl_3$ at 293K.

For both assemblies, the Hammett plot showed larger 1H NMR chemical shift changes upon addition of more acidic phenols with stronger electron withdrawing groups, like NO_2 (**5a**), CF_3 (**5d**) and $COOMe$ (**5f**). These results indicate, once again, the importance of the acidity of the OH group in interacting with the urea carbonyl groups in $3b_3 \cdot (DEB)_6$ and $4a_3 \cdot (DEB)_{12}$. Furthermore, for assembly $3b_3 \cdot (DEB)_6$ a good linear correlation between $\Delta\delta NH_m$ and σ_p/σ_m was observed for **5a**, **5b**, **5g**, **5h**, and **5i** (bearing p - NO_2 , m - NO_2 , p -Br, p -F, and H respectively). For **5j** (bearing an electron donor group p -OMe) the observed shift is larger than expected based on the Hammett parameter σ_p , suggesting that the OMe-group may interact positively with $3b_3 \cdot (DEB)_6$.

For assembly $4a_3 \cdot (DEB)_{12}$, a good linear correlation between $\Delta\delta NH_\alpha$ and σ_p/σ_m was also observed for phenols **5a**, **5b**, **5f**, **5g**, **5h** and **5i** (bearing p - NO_2 , m - NO_2 , p -COOMe, p -Br, p -F, and H substituents, respectively). Again the observed shift was larger when using **5j** (bearing p -OMe) than expected based on the Hammett parameter σ_p .

The Hammett plots in Figure 5.9 clearly show that the hydroxyl group's acidity is of great importance for phenol complexation by receptors $3b_3 \cdot (DEB)_6$ and $4a_3 \cdot (DEB)_{12}$. This importance is further emphasized by the other phenol derivatives. The addition of 10 equiv of phenol (**5i**) ($pK_a = 9.89$) showed a shift of 0.06 ppm for H_m in the 1H NMR spectrum. The addition of other less acidic phenols with pK_a values around 10, such as p -

cresol (**5e**) and 4-fluorophenol (**5h**), showed much smaller shifts for H_m . Addition of 4-cyanophenol (**5c**), with a pK_a of 7.97, showed a large downfield shift for H_m ($\Delta\delta$ 0.22 ppm, 10 equiv **5c**), comparable to the H_m shift caused by addition of *p*-nitrophenol **5a** (10 equiv, $pK_a = 7.15$). Determination of the binding constant of **5c** to assembly **3b₃•(DEB)₆** by a 1H NMR titration (1 mM, $CDCl_3$, 298 K) yielded an intrinsic K_a of $195 M^{-1}$ for formation of the 1:6 complex, a value that is on the same order as the intrinsic K_a obtained for **5a** ($202 M^{-1}$).

The complexation of guest molecules containing two hydroxyl groups was also studied. The addition of catechol (**5m**, 9-10 equiv), which has a pK_a of 9.85, showed a downfield shift of the urea NH signal H_m of 0.19 ppm. The obtained shift of H_m is larger than expected based on the pK_a value of this phenol guest. However, pK_a values are generally measured in aqueous solutions, where the intramolecular bond between the two hydroxyl groups does not occur. In apolar solutions, such as chloroform, this intramolecular hydrogen bond is formed and therefore the proton that is not involved in the hydrogen bond becomes more acidic. Catechol (**5m**) is unique in that it has two hydroxyl groups ortho to each other. Therefore in principle two hydrogen bonds to the carbonyl of the ureido functionality can be formed by **5m**. If two hydrogen bonds are formed one would expect the complex to be stronger. Because of the low solubility of **5m** in $CDCl_3$, the intrinsic K_a could not be determined by 1H NMR titration. If the two hydroxyl functionalities are further apart, as in resorcinol (**5l**, $pK_a = 9.81$), the observed shift of H_m after the addition of **5l** is much smaller ($\Delta\delta$ 0.07 ppm, 8 equiv). The formation of the second hydrogen bond is probably not possible because of the geometry of the complex. Also the intramolecular hydrogen bond acidifying the other proton cannot occur.

Upon addition of **7** (bearing 2 OH-groups, 10 equiv) to assembly **3b₃•(DEB)₆**, a 0.16 ppm downfield shift was observed for NH_m . The observed shift is larger than expected based on the acidity of **7** (pK_a estimated around 10). The two hydroxyl functionalities are too far apart to form either an intramolecular hydrogen bond or two hydrogen bonds with the same carbonyl functionality as for **5m**, therefore we suggest a two-point interaction (with two different carbonyl functionalities).

Table 5.2. Changes of chemical shifts ($\Delta\delta$) for the complexation of guest molecules to $3b_3 \cdot (DEB)_6$ (1 mM, $CDCl_3$ at 293 K).

Guest	$pK_a^{[a]}$	$\sigma_p/\sigma_m^{[b]}$	$\Delta\delta$ (ppm)	equiv	Guest	pK_a	σ_p/σ_m	$\Delta\delta$ (ppm)	equiv
5a	7.15	0.81	0.26	10	5i	9.89	0	0.06	10
5b	8.28	0.71	0.24	10	5j		-0.28	0.05	10
5c	7.97	0.70	0.22	10	5k		-0.38	0.05	5
5d		0.53	0.15	10	5l	9.81	0.13	0.07	8
5e	10.17	-0.14	0.06	14	5m	9.85		0.19	10
5f		0.44	0.15	10	6			0.0	7
5g		0.26	0.11	10	7			0.16	10

[a] values were obtained from D.R. Lide, *Handbook of Chemistry and Physics*, 83rd ed. CRC press LLC, 2002, pp 8-46 – 8-56.

[b] values were obtained from ref 37.

5.3 Conclusions

Complexation of phenol derivatives **5** is achieved by using both double and tetra-rosettes. For the *exo*-receptors $3b_3 \cdot (DEB)_6 / (CYA)_6$ and $3d_3 \cdot (DEB)_6$ a 1:6 binding stoichiometry is observed. The guest molecules are complexed on both the top and bottom of the assembly. In contrast $4_3 \cdot (DEB)_{12} / (CYA)_{12}$ are *endo*-receptors that show a 1:4 binding stoichiometry as determined by Job plot and MALDI-TOF MS. The complexation of **5a** inside the cavity between the second and third floors of the tetra-rossette is supported by VT NMR measurements. Splitting of the 1H NMR signals for the NH_{DEB} -protons was observed at low temperatures upon addition of **5a**, indicating slow exchange between the free host $4_3 \cdot (DEB)_{12}$ and different complexed hosts $4_3 \cdot (DEB)_{12} \cdot 5a_n$ ($n=1-4$).

The pK_a of the phenol derivatives is important for the complexation to the ureido carbonyls in the double and tetra-rosettes. Acidic phenol derivatives with pK_a values between 7.0-8.0 are the best guests. Phenol acidity, however, is not the only factor that influences binding to the rosette assemblies. Structural constraints in the guest can also be important. Thus catechol, a relatively poor acid with a pK_a of 9.85 is a good binder to $3b_3 \cdot (DEB)_6$, probably due to the formation of two-point hydrogen bonds to the ureido group or to an intramolecular hydrogen bond. Addition of **7** clearly shows that formation of two hydrogen bonds strengthens the binding. The pK_a of the hydrogen bond accepting

atom is also important for the binding. Acceptor atoms with a low electron density are not capable of a strong complexation of **5a**. Furthermore, it has been shown that the double rosette contains six independent and well organized binding sites and it has good potential as a noncovalent assembly for multivalent molecular recognition.

5.4 Experimental Section

¹H NMR spectra were recorded on a Varian Unity 300 spectrometer or on a Varian Unity 400 WB spectrometer. Residual solvent protons were used as an internal standard and chemical shifts are given relative to tetramethylsilane (TMS) or to the residual solvent protons. FAB-MS spectra were recorded with a Finnigan MAT 90 spectrometer with *m*-nitrobenzyl alcohol (NBA) as a matrix. Laser desorption ionization mass spectrometry was performed using a modified MALDI-TOF instrument (Voyager RP-DE, Perceptive Biosystems/Applied Biosystems, Framingham, MA, USA), equipped with delayed extraction. A 337 nm UV nitrogen laser producing 2 ns pulses and the mass spectra were obtained in the linear mode. No organic acid matrix could be used during the experiments due to instability of the assemblies. An 8-10 µl of the sample of a known concentration was deposited on the (cold) spot-well, adding a 0.5 µl of a 10⁻⁶ molar solution of AgOOCF₃. The samples were covered by a non-acidic liquid polymer-film, not interacting or mixing with the samples. In order to avoid crystallization of the samples, the pressure in the ion source was reduced drastically, keeping the pressure in the time-of-flight region under relatively high vacuum. The samples were introduced via a sample-plate insertion system at near atmospheric pressure. Threshold laser energies were used in order to avoid fragmentation due to high-energy laser power. After each experiment internal calibrations were performed using a mixture of known proteins (ACTH 1-36, Bovine Insulin B oxidized, Bovine Insulin, Myoglobin (horse heart) and Cytochrome C (horse heart)) of the selected mass range. CD spectra were measured on a JASCO J-715 spectropolarimeter in a 0.01 cm width cell. Compounds **1a**,^{16b} **1b**,^{17b} **2**^{16b}, **3a-3b**,¹⁸ and **3d-3f**,¹⁸ **3g**,^{17b} and **4a-4b**^{17b} were prepared according to methods described previously.

Formation of assemblies $2_3 \cdot (\text{DEB})_6$, $3_3 \cdot (\text{DEB})_6 / (\text{CYA})_6$, and $4_3 \cdot (\text{DEB})_{12} / (\text{CYA})_{12}$

Hydrogen-bonded assemblies $2_3 \cdot (\text{DEB})_6$, $3_3 \cdot (\text{DEB})_6$ and $4_3 \cdot (\text{DEB})_{12}$ were prepared by mixing calix[4]arene dimelamines **2** or **3** or calix[4]arene tetramelamine **4** with 2.5 and 4 equivalents of DEB, respectively, in CDCl_3 for 15 min. Similarly, assembly $3b_3 \cdot (\text{CYA})_6$ was prepared by mixing calix[4]arene dimelamine **3b** with 2.5 equivalents CYA in CDCl_3 . Assemblies $4_3 \cdot (\text{CYA})_{12}$ were either prepared from $4_3 \cdot (\text{DEB})_{12}$ by exchange of DEB with CYA or by direct mixing of calix[4]arene tetramelamine **4** with 4 equivalents CYA and heating at 328K for 1 week.

5,17-Bis({4-amino-6-[(N-propylcarbothioyl-3-amino-2,2-dimethylpropyl)amino]-1,3,5-triazine-2-yl}-amino-25,26,27,28-tetrapropoxycalix[4]arene (3c**).** Calix[4]arene dimelamine **3a** (0.150 g, 0.15 mmol) was dissolved in THF (25 mL) and propyl isothiocyanate (0.15 mL, 1.4 mmol) was added. The solution was stirred for 1 h. The solvent was evaporated and the residue redissolved in CH_2Cl_2 and washed with water (3 times) and brine and then dried on MgSO_4 . The crude product was purified by column chromatography (SiO_2 , $\text{CH}_2\text{Cl}_2/\text{MeOH}/\text{NH}_4\text{OH} = 90/9.5/0.5$). Dimelamine **3c** was obtained as a white solid (0.142 mg, 79%) MS (FAB): m/z 1213.6 ($[\text{M}+\text{H}]^+$, calcd 1212.7). ^{13}C NMR (75 MHz, CDCl_3 , 298K) δ 180.2, 166.8, 166.6, 164.1, 158.3, 151.8, 137.2, 136.6, 134.4, 133.2, 132.2, 131.8, 128.9, 121.1, 120.8, 120.3, 49.1, 48.1, 46.6, 37.2, 31.1, 23.8, 23.5, 23.0, 22.7, 11.3, 10.8, 9.8.

Assembly $3c_3 \cdot (\text{DEB})_6$: ^1H NMR (75 MHz, CDCl_3 , 298K) δ 13.96 (s, 2 H; H_a); 13.12 (s, 2 H; H_b); 8.58 (s, 2 H; H_c); 7.90-7.81 (m, 2 H; H_d); 7.09-7.04 (m, 6 H; ArH , H_g); 6.96 (s, 2 H; H_f); 6.84 (t, $^3J(\text{H},\text{H}) = 7.5$ Hz, 2 H; ArH); 6.69 (s, 2 H; H_e); 6.40 (br d, 2 H; H_m); 6.08 (s, 2 H; H_h); 4.46 (ABq, $^2J(\text{H},\text{H}) = 12.9$ Hz, 4 H; ArCH_2Ar), 4.07-3.54 (m, 14 H; OCH_2 , H_i , H_k , H_o), 3.05 (ABq, $^2J(\text{H},\text{H}) = 13.5$ Hz, 4 H; ArCH_2Ar), 2.77-2.64 (m, 4 H; H_j , H_n), 2.37-2.30 (m, 2 H; H_l), 2.22-1.75 (m, 18 H; H_p , CH_2), 1.21-0.74 (m, 40 H; $\text{NHCH}_2\text{CH}_2\text{CH}_3$, CH_3), 0.64 (t, $^3J(\text{H},\text{H}) = 6.6$ Hz, 6 H; $\text{NHCH}_2\text{CH}_2\text{CH}_3$).

5.5 References

- Ohkanda, J.; Lockman, J.W.; Kothare, M.A.; Qian, Y.; Blaskovich, M.; Sebt, S.; Hamilton, A.D. *J. Med. Chem.* **2002**, *45*, 177-188.

- ² Recent review on synthetic receptors: Hartley, J.H.; James, T.D.; Ward, C.J. *J. Chem. Soc., Perkin Trans. 1*, **2000**, 3155-3184.
- ³ a) Cram, D.J.; Kaneda, T.; Helgeson, R.C.; Brown, B.; Knobler, C.B.; Maverick, E.; Trueblood, K.N. *J. Am. Chem. Soc.* **1985**, *107*, 3645-3657; b) Bell, T.W.; Khasanov, A.B.; Drew, M.G.B.; Filikov, A.; James, T.L. *Angew. Chem. Int. Ed.* **1999**, *38*, 2543-2547; c) Chrisstoffels, L.A.J.; de Jong, F.; Reinhoudt, D.N.; Sivelli, S.; Gazzola, L.; Casnati, A.; Ungaro, R. *J. Am. Chem. Soc.* **1999**, *121*, 10142-10151.
- ⁴ a) Gale, P.A. *Coord. Chem. Rev.* **2001**, *213*, 79-128; b) Miyaji, H.; Anzenbacher Jr., P.; Sessler, J.L.; Bleasdale, E.R.; Gale, P.A. *Chem. Commun.* **1999**, 1723-1724; c) Sansone, F.; Baldini, L.; Casnati, A.; Lazzarotto, M.; Ugozzoli, F.; Ungaro, R. *Proc. Natl. Acad. Sci. USA*, **2002**, *99*, 4842-4847; d) Yamamoto, M.; Sugasaki, A.; Ikeda, M.; Takeuchi, M.; Frimat, K.; James, T.D.; Shinkai, S. *Chem. Lett.* **2001**, 520-521; e) Snellink-Ruël, B.H.M.; Antonisse, M.M.G.; Engbersen, J.F.J.; Timmerman, P.; Reinhoudt, D.N. *Eur. J. Org. Chem.* **2000**, 165-170; f) Snowden, T.S.; Bisson, A.P.; Anslyn, E.V. *J. Am. Chem. Soc.* **1999**, *121*, 6324-6325.
- ⁵ a) Middel, O.; Verboom, W.; Reinhoudt, D.N. *Eur. J. Org. Chem.* **2002**, 2587-2597; b) Droz, A.S.; Diederich, F. *J. Chem. Soc., Perkin Trans. 1*, **2000**, 4224-4226; c) Tamaru, S.; Shinkai, S.; Khasanov, A.B.; Bell, T.W. *Proc. Natl. Acad. Sci. USA*, **2002**, *99*, 4972-4976; d) Starnes, S.D.; Rudkevich, D.M.; Rebek, Jr., J. *J. Am. Chem. Soc.* **2001**, *123*, 4659-4669; e) Orner, B.P.; Salvatella, X.; Quesada, J.S.; de Mendoza, J.; Giralt, E.; Hamilton, A.D. *Angew. Chem. Int. Ed.* **2002**, *41*, 117-119; f) Almaraz, M.; Raposo, C.; Martín, M.; Caballero, M.C.; Morán, J.R. *J. Am. Chem. Soc.* **1998**, *120*, 3516, 3517.
- ⁶ a) Mammen, M.; Choi, S.-K.; Whitesides, G.M. *Angew. Chem. Int. Ed.* **1998**, *37*, 2754-2794; b) Lee, Y.C.; Lee, R.T. *Acc. Chem. Res.* **1995**, *28*, 321-327; c) Lindhorst, T.K. *Top. Curr. Chem.* **2002**, *218*, 201-235.
- ⁷ Benjamini, E.; Sunshine, G.; Leskowitz, S. *Immunology, A Short Course*, 3rd ed. Wiley, New York, **1996**.
- ⁸ a) Goodsell, D.S.; Olson, A.J. *Annu. Rev. Biophys. Biomol. Struct.* **2000**, *29*, 105-153; b) Zhang, Z.; Merritt, E.A.; Ahn, M.; Roach, C.; Hou, Z.; Verlinde, C.L.M.J.; Hol, W.G.J.; Fan, E. *J. Am. Chem. Soc.* **2002**, *124*, 12991-12998.

- ⁹ a) Löwik, D.W.P.M.; Weingarten, M.D.; Broekema, M.; Brouwer, A.J.; Still, W.C.; Liskamp, R.M.J. *Angew. Chem. Int. Ed.* **1998**, *37*, 1846-1850. Reviews about diversity generation: b) de Miguel, Y.R.; Sanders, J.K.M. *Curr. Opin. Chem. Biol.* **1998**, *2*, 417-421; c) Still, W.C. *Acc. Chem. Res.* **1996**, *29*, 155-163; d) Lavigne, J.J.; Anslyn, E.V. *Angew. Chem. Int. Ed.* **2001**, *40*, 3118-3130. Examples of the introduction of multiple binding sites: e) Rao, J.H.; Lahiri, J.; Isaacs, L.; Weis, R.M.; Whitesides, G.M. *Science*, **1998**, *280*, 708-711; f) Colonna, B.; Harding, V.D.; Nepogodiev, S.A.; Raymo, F.M.; Spencer, N.; Stoddart, J.F. *Chem. Eur. J.* **1998**, *4*, 1244-1254; g) Lindhorst, T.K. *Top. Curr. Chem.* **2002**, *218*, 201-235; h) van Wageningen, A.M.A.; Liskamp, R.M.J. *Tetrahedron Lett.* **1999**, *40*, 9347-9351; i) Rasmussen, P.H.; Rebek Jr., J. *Tetrahedron Lett.* **1999**, *40*, 3511-3514; j) Vrasidas, I.; de Mol, N.J.; Liskamp, R.J.M.; Pieters, R.J. *Eur. J. Org. Chem.* **2001**, *24*, 4685-4692; k) Davis, B.G. *J. Chem. Soc., Perkin Trans. 1*, **1999**, 3215-3237; l) Jayaraman, N.; Nepogodiev, S.A.; Stoddart, J.F. *Chem. Eur. J.* **1997**, *3*, 1193-1199; m) Dondoni, A.; Kleban, M.; Hu, X.; Marra, A.; Banks, H.D. *J. Org. Chem.* **2002**, *67*, 4722-4733.
- ¹⁰ a) Boyce, R.; Li, G.; Nestler, H.P.; Suenaga, T.; Still, W.C. *J. Am. Chem. Soc.* **1994**, *116*, 7955-7956. b) Cheng, Y.; Suenaga, T.; Still, W.C. *J. Am. Chem. Soc.* **1996**, *118*, 1813-1814.
- ¹¹ Fiammengo, R.; Crego-Calama, M.; Timmerman, P.; Reinhoudt, D.N. *Chem. Eur. J.* in press.
- ¹² Hamuro, Y.; Crego-Calama, M.; Park, H.S.; Hamilton, A.D. *Angew. Chem. Int. Ed.* **1997**, *36*, 2680-2683.
- ¹³ a) Crego-Calama, M.; Hulst, R.; Fokkens, R.; Nibbering, N.M.M.; Timmerman, P.; Reinhoudt, D.N. *Chem. Commun.* **1998**, 1021-1022; b) Crego-Calama, M.; Timmerman, P.; Reinhoudt, D.N. *Angew. Chem. Int. Ed.* **2000**, *39*, 755-758.
- ¹⁴ a) Ramström, O.; Lehn, J.-M. *Nature Reviews, Drug Discovery*, **2002**, *1*, 26-36; b) Rowan, S.J.; Cantrill, S.J.; Cousins, G.R.L.; Sanders, J.K.M.; Stoddart, J.F. *Angew. Chem. Int. Ed.* **2002**, *41*, 898-952.
- ¹⁵ a) Goodman, M.S.; Jubian, V.; Linton, B.; Hamilton, A.D. *J. Am. Chem. Soc.* **1995**, *117*, 11610-11611; b) Cousins, G.R.L.; Furlan, R.L.E., Ng, Y.-F.; Redman, J.E.; Sanders, J.K.M. *Angew. Chem. Int. Ed.* **2001**, *40*, 423-428; c) Cousins, G.R.L.;

- Poulsen, S.-A.; Sanders, J.K.M. *Chem. Commun.* **1999**, 1575-1576; Examples of diversity generation and amplification can be found in d) Goral, V.; Nelen, M.N.; Eliseev, A.V.; Lehn, J.-M. *Proc. Natl. Acad. Sci. U.S.A.* **2001**, 98, 1347-1352; e) Eliseev, A.V.; Nelen, M.N. *J. Am. Chem. Soc.* **1997**, 119, 1147-1148; f) Furlan, R.L.E.; Ng, Y.-F.; Otto, S.; Sanders, J.M.K. *J. Am. Chem. Soc.* **2001**, 123, 8876-8877; g) Huc, I.; Lehn, J.-M. *Proc. Natl. Acad. Sci. USA* **1997**, 94, 2106-2110.
- ¹⁶ a) Vreekamp, R.H.; van Duynhoven, J.P.M.; Hubert, M.; Verboom, W.; Reinhoudt, D.N. *Angew. Chem. Int. Ed.* **1996**, 35, 1215-1218; b) Timmerman, P.; Vreekamp, R.H.; Hulst, R.; Verboom, W.; Reinhoudt, D.N.; Rissanen, K.; Udachin, K.A.; Ripmeester, J. *Chem. Eur. J.* **1997**, 3, 1823-1832.
- ¹⁷ a) Jolliffe, K.A.; Timmerman, P.; Reinhoudt, D.N. *Angew. Chem. Int. Ed.* **1999**, 38, 933-937; b) Prins, L.J.; Neuteboom, E.E.; Parashiv, V.; Crego-Calama, M.; Timmerman, P.; Reinhoudt, D.N. *J. Org. Chem.* **2002**, 67, 4808-4820.
- ¹⁸ See Kerckhoffs, J.M.C.A.; Crego-Calama, M.; Luyten, I.; Timmerman, P.; Reinhoudt, D.N. *Org. Lett.* **2000**, 2, 4121-4124 and Chapter 3.
- ¹⁹ a) Matsuura, K.; Hibino, M.; Yamada, Y.; Kobayashi, K. *J. Am. Chem. Soc.* **2001**, 123, 357-358; b) Sakai, S.; Sasaki, T. *J. Am. Chem. Soc.* **1994**, 116, 1587-1588.
- ²⁰ a) Herm, M.; Molt, O.; Schrader, T. *Chem. Eur. J.* **2002**, 8, 1485-1499; b) Bernardo, A.R.; Stoddard, J.F.; Kaifer, A.E. *J. Am. Chem. Soc.* **1992**, 114, 10624-10613.
- ²¹ Harborne, J.B.; Williams, C.A. *Phytochemistry*, **2000**, 55, 481-504.
- ²² Krasowski, M.D.; Hong, X.; Hopfinger, A.J.; Harrison, N.L. *J. Med. Chem.* **2002**, 45, 3210-3221.
- ²³ Jansen, R.J.; de Gelder, J.; Rowan, A.E.; Scheeren, H.W.; Nolte, R.J.M. *J. Org. Chem.* **2001**, 66, 2643-2653.
- ²⁴ The program microsoft excel and a nonlinear least-square fitting procedure is used.
- ²⁵ Two different K_a values of 25 and 180 M⁻¹ for the formation of two hydrogen bonds between resorcinol and two urea carbonyl groups were found (see ref [23]); The obtained K_a depends also on the substituent on the phenol.
- ²⁶ a) Timmerman, P.; Jolliffe, K.A.; Crego-Calama, M.; Weindmann, J.-L.; Prins, L.J.; Cardullo, F.; Snellink-Ruel, B.H.M.; Fokkens, R.; Nibbering, N.M.M.; Shinkai, S.; Reinhoudt, D.N. *Chem. Eur. J.* **2000**, 6, 4104-4115; b) Armstrong, D.W.; Zhang, L.-K.; He, L.; Gross, M.L. *Anal. Chem.* **2001**, 73, 3679-3686, and their references

therein; c) Ring, S.; Rudich, Y. *Rapid Commun. Mass Spectrom.* **2000**, *14*, 515-519; d) Fujita, T.; Itagaki, Y.; Hisaka, M.; Naoki, H.; Nakajima, T.; Andriantsiferana, M. *Rapid Commun. Mass Spectrom.* **1997**, *11*; 1115-1119.

²⁷ Besides large intensity signals, corresponding with the protonated and Ag⁺-cationized molecules of the building blocks (at m/z 1181 and m/z 1288 respectively), clusters of ions (intensities of TIC (Total Ion Current) between < 1% and 12%) could be observed in the high mass range. Among unidentified signals in the mass range 3000-7000, the signals for the complexes of **3b**₃•(DEB)₆ with **5a** were detected, which were all in agreement with their theoretical mass assignment according to their isotopic pattern. In all experiments no quantitative observations could be made due to ion fluctuations of the clusters observed in the high mass range.

²⁸ Broadening of protons H_{a/b} (NH protons of DEB) is also observed in assembly **2**₃•(DEB)₆. This indicates that this proton is in fast exchange. This observed broadening is also an indication for the lower stability of **2**₃•(DEB)₆.

²⁹ pK_a of *N,N'*-dibutylmelamine is 5.78,^[34a] and pK_a of **5a** is 7.15.

³⁰ a) Murray, B.A.; Whelan, G.S. *Pure & Appl. Chem.* **1996**, *68*, 1561-1567; b) Gieling, G.T.W.; Scheeren, H.W.; Israël, R.; Nolte, R.J.M. *Chem. Commun.* **1996**, 241-244.

³¹ Gas-phase molecular modeling calculations (Quanta 97, CHARMM 24.0) of the empty assembly showed that the cavity between the second and third floors is completely shielded from the environment and that the six ureido carbonyl groups are pointing toward the center of this endohedral cavity.

³² In a control system, the assembly **8**₃•(DEB)₁₂, where tetramelamine **8** does not bear ureido moieties (for drawing of compound **8** see: compound **2b** in ref 17a), the broadening of the NH_{a1} and NH_{b1} peaks occurred along with no shifts upon the addition of **5a** ($\delta_{1/2}$, from 5.6 Hz to 26 Hz for NH^{a1}, 10 equiv. **5a**). On the other hand, such a broadening does not occur for the second and third floors ($\delta_{1/2}$, 5.4 Hz for NH_{a2}, 0 and 10 equiv. **5a**). The results suggest that the proton exchange occurs between the OH proton of **5a** and the NH_{a1}/NH_{b1} protons of the first and fourth floors. For **4b**₃•(DEB)₁₂, the peak broadening ($\delta_{1/2}$, from 8.4 Hz to 26 Hz for NH_{a1}, 10 equiv. **5a**) was more significant compared to that of achiral **4a**₃•(DEB)₁₂

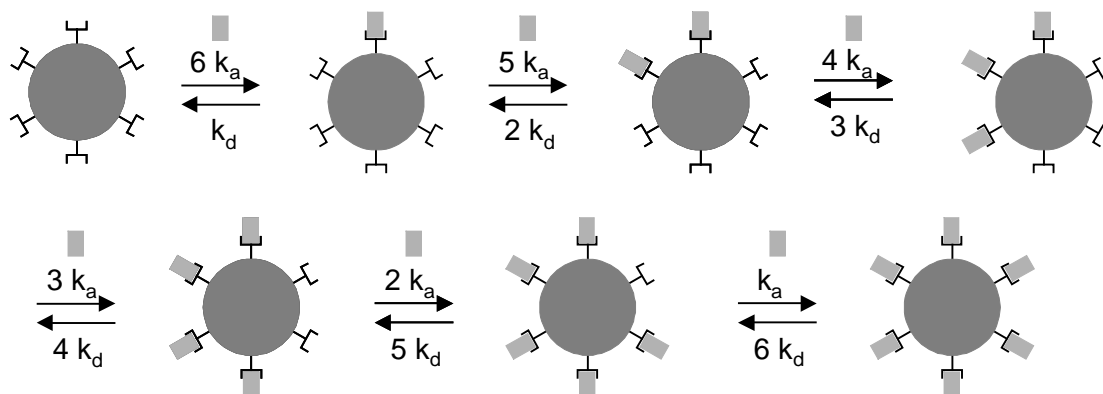
system ($\delta_{1/2}$, from 6.0 Hz to 8.4 Hz for NH_{a1} , 10 equiv. of **5a**), indicating the facilitation of the proton exchange in the chiral system. For $\mathbf{4b}_3\bullet(\text{BuCYA})_{12}$ the peak broadening of the NH_{a1} and NH_{b1} was hardly observed ($\delta_{1/2}$, from 6.4 Hz to 6.7 Hz for NH_{a1} , 10 equiv. **5a**).

- ³³ In the absence of **5a**, $\mathbf{4b}_3\bullet(\text{DEB})_{12}$ is strongly CD active due to the asymmetric arrangement of the many different chromophoric units within the assembly (Prins, L.J.; Huskens, J.; de Jong, F.; Timmerman, P.; Reinhoudt, D.N. *Nature* **1999**, 398, 498-502). The strong CD band around 290 nm decreased upon the addition of **5a**, indicating the decomposition of the tetra-rossette assembly initiated by the significant proton exchange. The CD intensity was reduced to ca. 40% (20 equiv. **5a**), which is comparable to the assembly formation of 40% estimated from the ^1H NMR method. On the other hand, for $\mathbf{4b}_3\bullet(\text{BuCYA})_{12}$, the CD intensity around 290 nm hardly decreased upon the addition of **5a**. This phenomenon is ascribed to the high stability of $\mathbf{4b}_3\bullet(\text{BuCYA})_{12}$ as suggested by the ^1H NMR study.
- ³⁴ a) Mascal, M.; Fallon, P.S.; Batsanov, A.S.; Heywood, B.R.; Champ, S.; Colclough, M. *J. Chem. Soc., Chem. Commun.* **1995**, 805-806; b) Bielejewska, A.; Marjo, C.; Prins, L.J.; Timmerman, P.; de Jong, F.; Reinhoudt, D.N. *J. Am. Chem. Soc.* **2001**, 123, 7518-7533.
- ³⁵ Connors, K.A. *Binding Constants*, Wiley, New York, **1987**.
- ³⁶ The large K_a value of $299 \text{ mol}^{-1}\text{dm}^3$ in the $\mathbf{4b}_3\bullet(\text{DEB})_{12}$ system is not very reliable because $\mathbf{4b}_3\bullet(\text{DEB})_{12}$ dissociated upon the addition of more than 10 equiv **5a**.
- ³⁷ March, J. *Advanced Organic Chemistry*, 4th ed. Wiley, New York, **1992**, pp 278-286.
- ³⁸ Ashton, P.R.; Fyfe, M.C.T.; Hickingbottom, S.K.; Stoddard, J.F.; White, A.J.P.; Williams, D.J. *J. Chem. Soc., Perkin Trans. 2* **1998**, 2117-2128.

Appendix

The 1:6 Binding model

For the calculation of K_a -values for the double rosette $3_3 \cdot (\text{DEB})_6$ a non-cooperative 1:6 binding model was used. The cartoon of this model is presented below.



The first guest molecule has six possibilities to bind to hexa-valent receptor and only one possibility to dissociate. The K_1 is therefore $6 \times K_a$ ($K_a = k_a/k_d$). All the K -values are related to the intrinsic binding constant K_a in the following way:

$$K_1 = 6 \times K_a$$

$$K_4 = 3/4 \times K_a$$

$$K_2 = 5/2 \times K_a$$

$$K_5 = 2/5 \times K_a$$

$$K_3 = 4/3 \times K_a$$

$$K_6 = 1/6 \times K_a$$

The different K values are now related to each by the following equation:

$$K_1 = 12/5 \times K_2 = 9/2 \times K_3 = 8 \times K_4 = 15 \times K_5 = 36 \times K_6$$

Chapter 6

Self-Organization of Guest Molecules in Self-Assembled Capsules: Artificial Viruses

In this chapter the encapsulation of three alizarin dye molecules by a self-assembled receptor is described. Encapsulation occurs in a highly organized manner, i.e. a noncovalent hydrogen-bonded trimer of the dye is formed. The encapsulation is highly cooperative and upon complexation the conformation of the double rosette changes from staggered to symmetrically eclipsed. The structure as determined by ^1H NMR spectroscopy of the assembly in solution is the same as the structure in the solid state, which was determined by X-ray diffraction studies. Addition of BuCYA to the rosette with the encapsulated dye trimer releases the dye from the rosette. The alizarin dye is also encapsulated in a tetra-rosette composed of two double rosettes covalently connected by a flexible linker. Two noncovalent alizarin trimers, one in between the 1st and 2nd floors and one in between the 3rd and 4th floors, are encapsulated.

6.1 Introduction

Biological systems such as cells and viruses encapsulate entities within their structure.¹ The level of self-organization and encapsulation in biological processes are still far beyond the synthetic abilities of chemists. Nevertheless, the use of self-assembling systems for encapsulation represents nowadays an ambitious goal for the synthesis of large organized structures. The advantage of these self-assembled systems is their ability to “proof-read” and correct mistakes.

In the field of self-assembly, encapsulation of guest molecules is a topic studied intensively.² The capsules can either be formed by covalent³ or noncovalent synthesis⁴ (see also Chapter 2). While capsules synthesized in a covalent manner should contain a “door” through where the guest molecule(s) can enter the capsule, the noncovalent capsules can complex the guest molecule(s) by (re-)assembling the capsule around these guest molecule(s). Thus, the noncovalent approach facilitates the synthesis of molecular capsules dramatically. Capsules have many potential applications, ranging from drug delivery and molecular recognition to molecular reaction chambers for catalysis and stabilization of reactive intermediates.⁵

As already pointed out, nature shows excellent examples of encapsulation of guest molecules. One of the most simple examples of encapsulation in nature are viruses. These consist of a nucleic acid surrounded by a protein coat, a capsid, which protects the nucleic acid (see Figure 6.12a). Some viruses have a lipid membrane that surrounds the protein coat. The protein coat is self-assembled from many copies of one or a few polypeptide chains and is highly symmetrical. The encapsulated species in these and other natural systems are highly organized. The organization and complexity found in biological systems are as yet beyond the ability of chemists. So far organization of guest molecules in synthetic capsules is mainly achieved by steric constraints, *i.e.* size-dependent encapsulation.⁶ There are not many examples known wherein the organization of the enclosure occurs via noncovalent interactions. One such instance was reported by Fujita and co-workers⁷ concerning the formation of hydrophobic dimers of *cis*-stilbene derivatives in self-assembled coordination cages.

In this chapter, the highly ordered organization of three guest molecules (via the formation of three intermolecular hydrogen bonds between the guests) within a noncovalent capsule formed by a double rosette, is described. Even though the design is very primitive, this complex shows some interesting structural similarities with the

viruses found in nature. The double rosette can be seen as a capsid, the protecting shell of the self-assembled guest molecules. The double rosette itself is also self-assembled from multiple copies of two building blocks, forming a highly symmetrical capsule. The encapsulated molecules form a noncovalent trimer by intermolecular hydrogen bonds, similar to the hydrogen-bonded double stranded DNA.

6.2 Results and Discussion

6.2.1 Synthesis and Formation of Double Rosette Assembly

In Chapter 5, the complexation of phenol derivatives by double rosettes acting as *exo*-receptors was described. The functionalities on the top and bottom of these double rosettes are used as binding sites. The X-ray crystal structure⁸ of assembly **1b**₃•(DEB)₆ described in Chapter 3 (Chart 6.1) showed that the two rosettes are tightly stacked on top of each other with a separation of 3.5 Å at the edges and 3.2 Å in the center of the rosettes. Therefore, flat (guest) molecules might be encapsulated in the cavity between the two rosette layers. In this way, the double rosette assemblies can be regarded as *endo*-receptors. The dye alizarin (**2a**) was chosen because this guest molecule has a large flat aromatic structure and additionally can be used as a probe for UV spectroscopy (UV maximum 420-430 nm).

As was reported in the previous chapters, double rosettes **1**₃•(DEB)₆/(CYA)₆ are formed by mixing the corresponding calix[4]arene dimelamine **1** with 2 equiv of 5,5-diethylbarbiturate (DEB) or cyanurate derivatives (CYA) in apolar solvents, such as chloroform, toluene, or benzene. Calix[4]arene dimelamines **1** (Chart 6.1) were synthesized according to literature procedures.^{8,9}

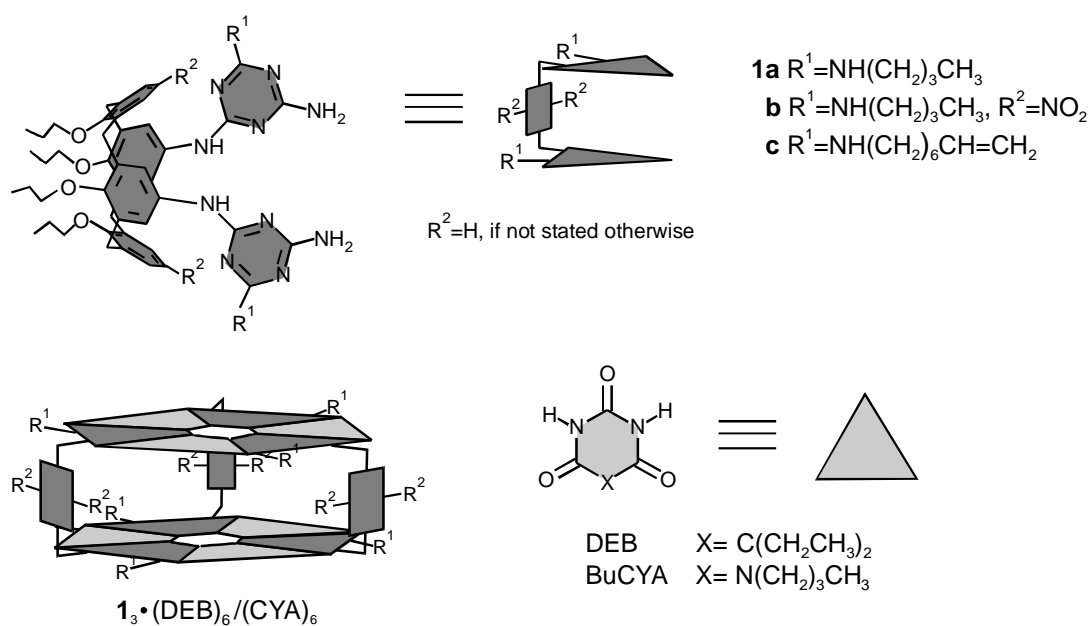


Chart 6.1. Molecular representations of compounds **1** and the corresponding hydrogen-bonded assemblies $\mathbf{1}_3 \bullet (\text{DEB})_6 / (\text{CYA})_6$.

6.2.2 Encapsulation of Alizarin (**2a**) by $\mathbf{1a}_3 \bullet (\text{DEB})_6$

Upon the addition of alizarin (**2a**, 4 equiv, Figure 6.1) to assembly $\mathbf{1a}_3 \bullet (\text{DEB})_6$ (1.0 mM in CDCl_3), remarkable shifts in the ^1H NMR signals of nearly all protons, both of assembly $\mathbf{1a}_3 \bullet (\text{DEB})_6$ and of guest **2a** (Figure 6.1), were observed. Furthermore, integration of the signals in the ^1H NMR spectrum clearly showed a 3:1 complexation of **2a** to assembly $\mathbf{1a}_3 \bullet (\text{DEB})_6$. The symmetry of the complex, reflected by the relatively simple ^1H NMR spectrum, indicated that three molecules of **2a** should be complexed in between the two rosette layers. If the three molecules of **2a** would have been complexed on top and/or bottom of the double rosette, the symmetry of the assembly would be broken, giving rise to a far more complicated ^1H NMR spectrum.

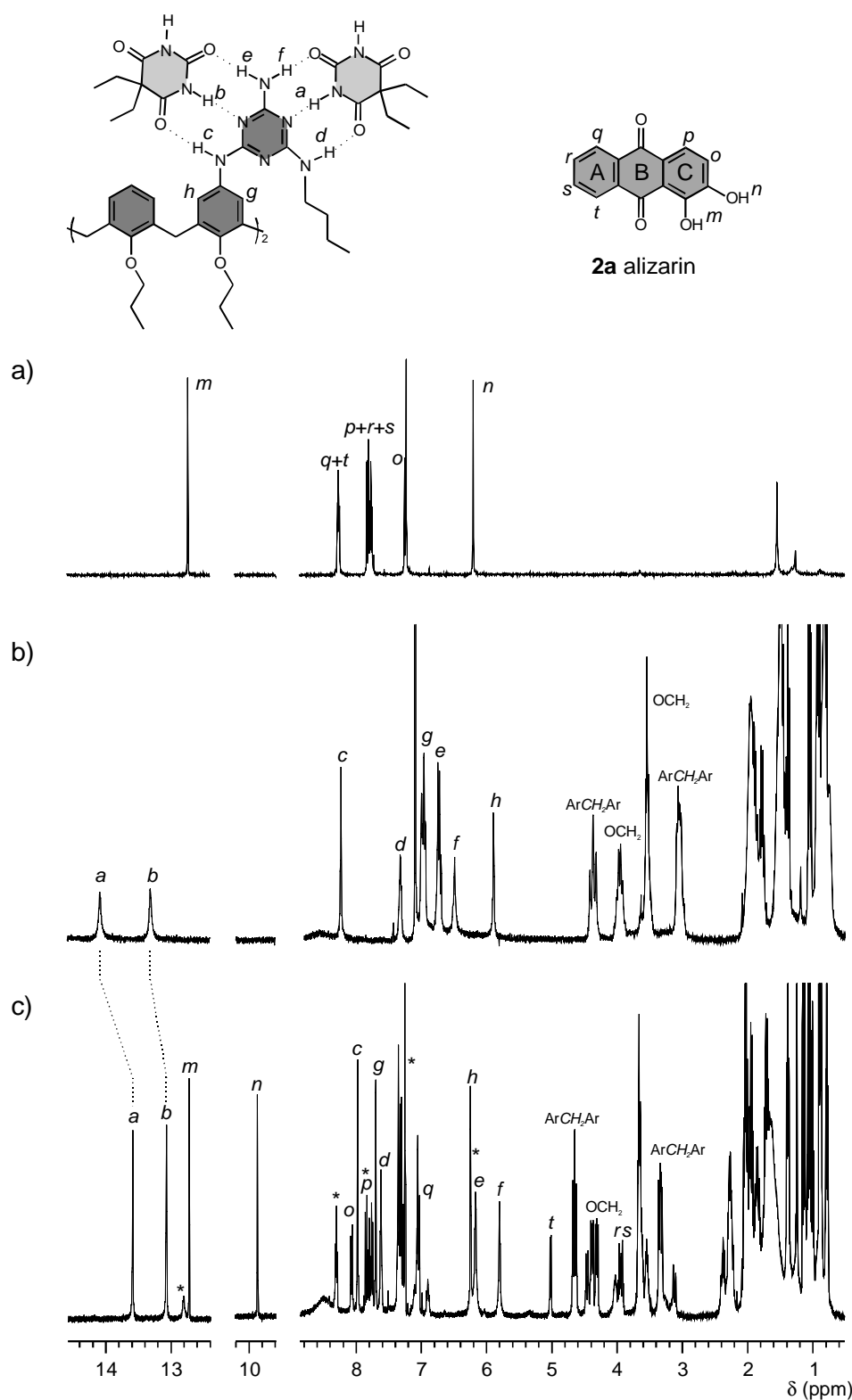


Figure 6.1. ^1H NMR spectra of (a) **2a**, (b) assembly **Ia₃•(DEB)₆**, and (c) complex **Ia₃•(DEB)₆•2a₃**. Signals marked with * belong to the free **2a**. Spectra were recorded in CDCl_3 at 400 MHz and 298 K.

Addition of 0-3 equiv of **2a** showed the ^1H NMR signals of $\mathbf{1a}_3\cdot(\text{DEB})_6\cdot\mathbf{2a}_3$ as well of $\mathbf{1a}_3\cdot(\text{DEB})_6$, indicating slow exchange between free $\mathbf{1a}_3\cdot(\text{DEB})_6$ and the complex $\mathbf{1a}_3\cdot(\text{DEB})_6\cdot\mathbf{2a}_3$ on the NMR time-scale. Heating the sample to 60 °C still showed the ^1H NMR signals for $\mathbf{1a}_3\cdot(\text{DEB})_6\cdot\mathbf{2a}_3$ and $\mathbf{1a}_3\cdot(\text{DEB})_6$ separately. Thus, the formed assembly $\mathbf{1a}_3\cdot(\text{DEB})_6\cdot\mathbf{2a}_3$ has a high kinetic stability. No other significant signals were observed, e.g. for complexes with only one or two molecules of **2a**; thus the complexation of **2a** seems to be strongly cooperative. After the addition of 4 equiv. of **2a** only the chemical shifts of the complex $\mathbf{1a}_3\cdot(\text{DEB})_6\cdot\mathbf{2a}_3$ and the free **2a** were observed in the ^1H NMR spectrum. Thus, these preliminary observations indicated that the complex has a structure of three molecules of **2a** encapsulated between the two rosette layers of assembly $\mathbf{1a}_3\cdot(\text{DEB})_6$ (see Figure 6.5).

All the signals in the ^1H NMR spectrum (Figure 6.1) of complex $\mathbf{1a}_3\cdot(\text{DEB})_6\cdot\mathbf{2a}_3$ (1 mM, CDCl_3 , 298 K) were assigned by using 2D ^1H NMR (2D DQF¹⁰, TOCSY¹¹ and NOESY¹²) experiments. The large shifts observed for the alizarin protons (> 3 ppm) clearly indicate encapsulation of the guest molecules. The aromatic protons H_r , H_s , and H_t of **2a** (ring A, see Figure 6.1) shifted 3.28-3.88 ppm upfield, indicating that ring A is partially included in the calix[4]arene cone. The observed shift is due to the anisotropy provided by the numerous aromatic rings that line the interior of the capsule.¹³ Furthermore, the NH_{DEB} -protons H_a and H_b in the complex $\mathbf{1a}_3\cdot(\text{DEB})_6\cdot\mathbf{2a}_3$ are shifted upfield in comparison with the free host $\mathbf{1a}_3\cdot(\text{DEB})_6$, 0.58 ppm for H_a and 0.30 ppm for H_b . The signals of H_c and H_d (also hydrogen-bonded) are shifted 0.44 ppm upfield and 0.13 ppm downfield, respectively. Protons H_e and H_f , situated in the internal part of the rosette cavity, show a large upfield shift of 0.71 and 0.84 ppm, respectively. In summary, all these shifts confirm the encapsulation of **2a** between the two rosette planes. All the data point to a complex of a possible trimer of alizarin ($\mathbf{2a}_3$) in between the two rosette layers.

However, if encapsulation of trimer $\mathbf{2a}_3$ occurred in the staggered conformation of the double rosette one would expect four instead of two signals because in a D_3 complex the symmetry between H_a and H_a' (or H_b and H_b') in the two planes of the rosette is broken by the nonsymmetrical trimer of alizarin. Figure 6.1 shows only two signals for the NH_{DEB} -protons (H_a and H_b) in the ^1H NMR spectrum. This suggests a conformational change of the assembly $\mathbf{1a}_3\cdot(\text{DEB})_6$ from staggered D_3 to symmetrical eclipsed C_{3h} for the

complex $\mathbf{1a}_3 \cdot (\text{DEB})_6 \cdot \mathbf{2a}_3$ (Figure 6.2). The number of signals corresponding to the NH_{DEB} -protons in the 13-15 ppm region reflects the symmetry of the assembly. In the *staggered* isomer the two melamines on each calix[4]arene are oriented anti-parallel with respect to each other. In the *eclipsed* isomers the melamines on each calix[4]arene unit are facing the same side of the calix[4]arene. (For more details about symmetry see also Section 3.2 and 6.2.3).

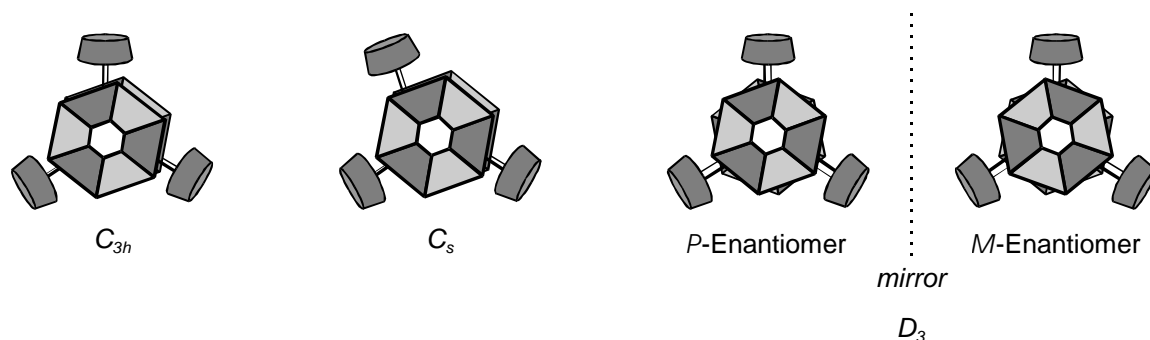


Figure 6.2. Schematic presentation of the three conformational isomers of $\mathbf{1a}_3 \cdot (\text{DEB})_6$.

6.2.3 Symmetry of the Complex $\mathbf{1a}_3 \cdot (\text{DEB})_6 \cdot \mathbf{2a}_3$

Complexation of $\mathbf{2a}_3$ to the double rosette $\mathbf{1a}_3 \cdot (\text{DEB})_6$ breaks the D_3 symmetry of the rosette in the assembly (see Figure 6.4).¹⁴ The D_3 symmetrical structure has one C_3 axis (perpendicular to the plane of the page) and three C_2 axes perpendicular to the C_3 . For the D_3 isomer two signals for the NH_{DEB} -protons H_a and H_b are expected because the three substituents on the dimelamines render these NH_{DEB} -protons nonequivalent in the assembly (Figure 6.3).

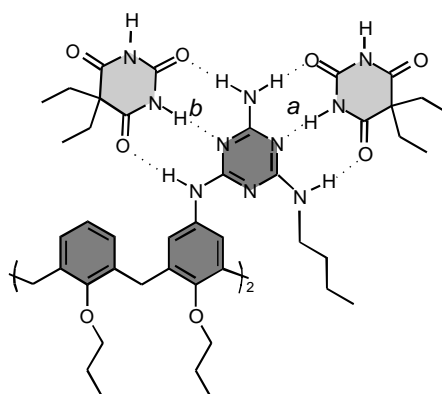


Figure 6.3. Structure of a part of assembly $\mathbf{1a}_3 \cdot (\text{DEB})_6 \cdot \mathbf{2a}_3$ showing the NH_{DEB} -protons H_a and H_b , and the three different substituents on the dimelamine.

The two rosette layers are interconverted via a C_2 -axis, rendering the protons in one rosette layer homotopic compared to the protons in the other rosette layer and giving identical resonances in the spectrum. Encapsulation of the trimer $2a_3$ in the D_3 conformation would result in a structure with the C_3 axis but without the C_2 axes. Only a C_3 axis would lead to four signals for the NH_{DEB} -protons, two for each rosette. However, only two signals for these protons were observed in the 1H NMR spectrum (Figure 6.1). This indicated that there must be another element of symmetry rendering the two rosette layers symmetrically related to each other. The presence of only two signals in the 1H NMR spectrum could only be explained by the presence of a horizontal plane of symmetry. The two rosette layers are then enantiotopic, giving the same resonances in the NMR spectrum. Consequently, the presence of the horizontal symmetry plane (σ_h) between the two rosette layers implies that upon encapsulation of $2a_3$ a conformational change of the calix[4]arene melamine from staggered to eclipsed must have occurred (Figure 6.4).

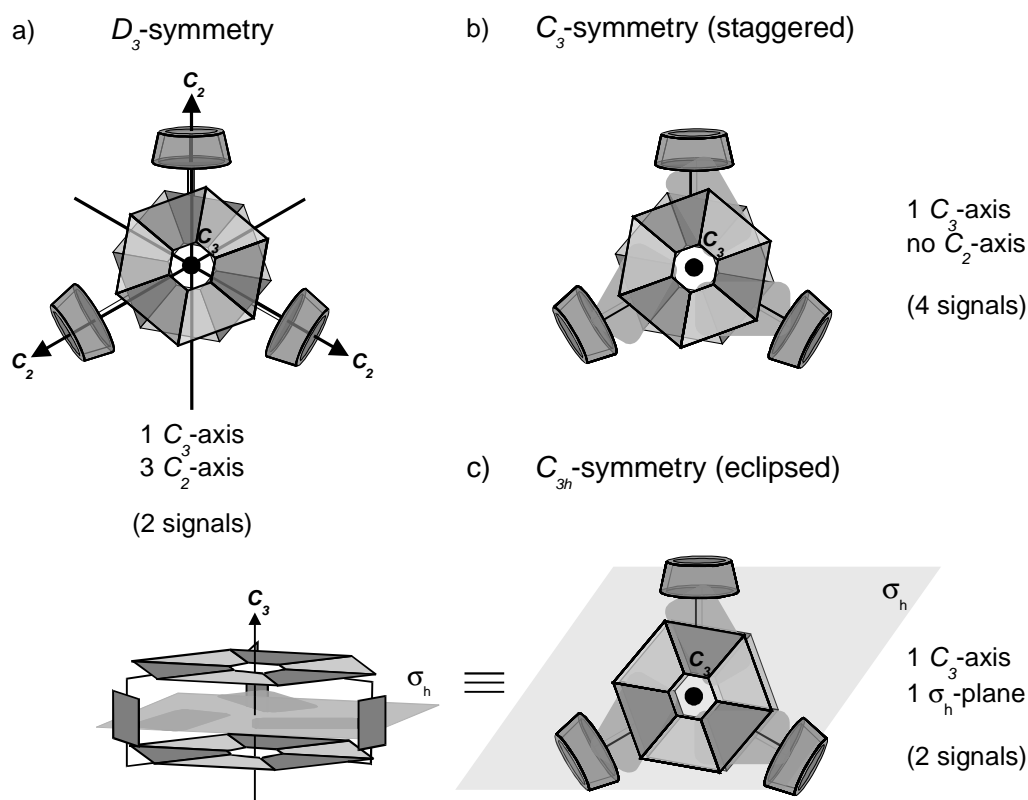


Figure 6.4. Symmetry groups for the (a) assembly $1a_3 \cdot (DEB)_6$, (b) assembly $1a_3 \cdot (DEB)_6$ after complexation of $2a$, and (c) after complexation of $2a$ and change of the conformation in the calix[4]arene dimelamines.

The eclipsed calix[4]arene dimelamine can form two rosettes, one with the melamines all in the same direction, the C_{3h} -isomer, and one in which one of the calix[4]arene dimelamines is rotated 180° , the C_s -isomer (see Figure 6.2). While both rosettes have a horizontal plane of symmetry, the C_{3h} -isomer has also a C_3 -axis and therefore only two signals for the NH_{DEB} -protons. Six signals are expected for the C_s -isomer. In summary, upon complexation of **2a** by $\mathbf{1a}_3 \cdot (\text{DEB})_6$ the conformation of the rosette changes from staggered to symmetrical eclipsed. The possible mechanism for complexation is depicted in Figure 6.5.

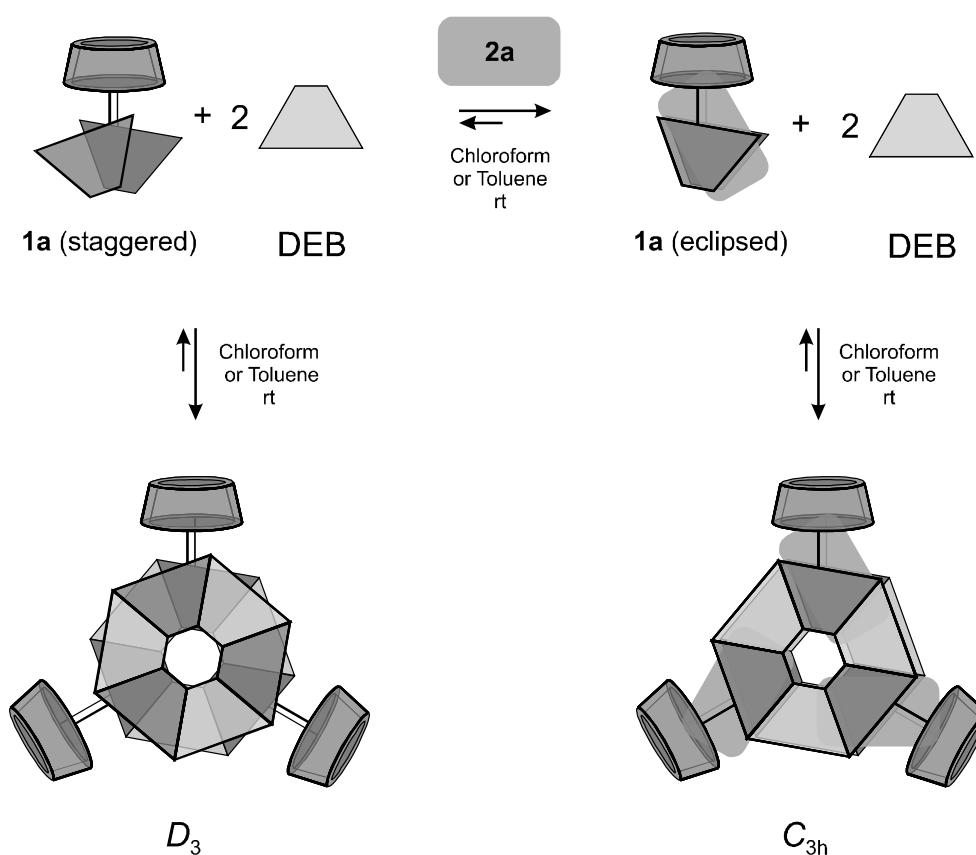


Figure 6.5. Proposed mechanism for the complexation of **2a** by $\mathbf{1a}_3 \cdot (\text{DEB})_6$.

Additional proof for the conformational change of assembly $\mathbf{1a}_3 \cdot (\text{DEB})_6$ from staggered to symmetrical eclipsed after complexation comes from a ring closure metathesis (RCM) reaction (Figure 6.6). As described previously by our group,^{9,15} assembly $\mathbf{1c}_3 \cdot (\text{DEB})_6$ (Chart 6.1), with oct-7-enyl side chain substituents on the melamine ring, forms a cyclic trimer (covalent linkage of the three calix[4]arene units) in the

presence of the Grubbs catalyst¹⁶ in CD_2Cl_2 . It was shown by ^1H NMR and modeling that assembly $\mathbf{1c}_3 \cdot (\text{DEB})_6$ is exclusively present in the staggered conformation (D_3 isomer). After the RCM reaction, the exclusive formation of the cyclic trimer (Figure 6.6) was proven by the presence of only the trimer signal at m/z 3100 (calcd for $\text{C}_{180}\text{H}_{240}\text{N}_{36}\text{O}_{12} \cdot \text{H}^+$ = 3100) in the MALDI-TOF mass spectrum. Moreover, the formation of the cyclic trimer was also proven by ^1H NMR spectroscopy. The terminal vinylic protons at δ 5.0 and δ 5.8 ppm disappeared during the reaction while a new broad signal at δ 5.5 ppm for the internal vinylic protons in assembly $\mathbf{1c}_3 \cdot (\text{DEB})_6$ appeared.

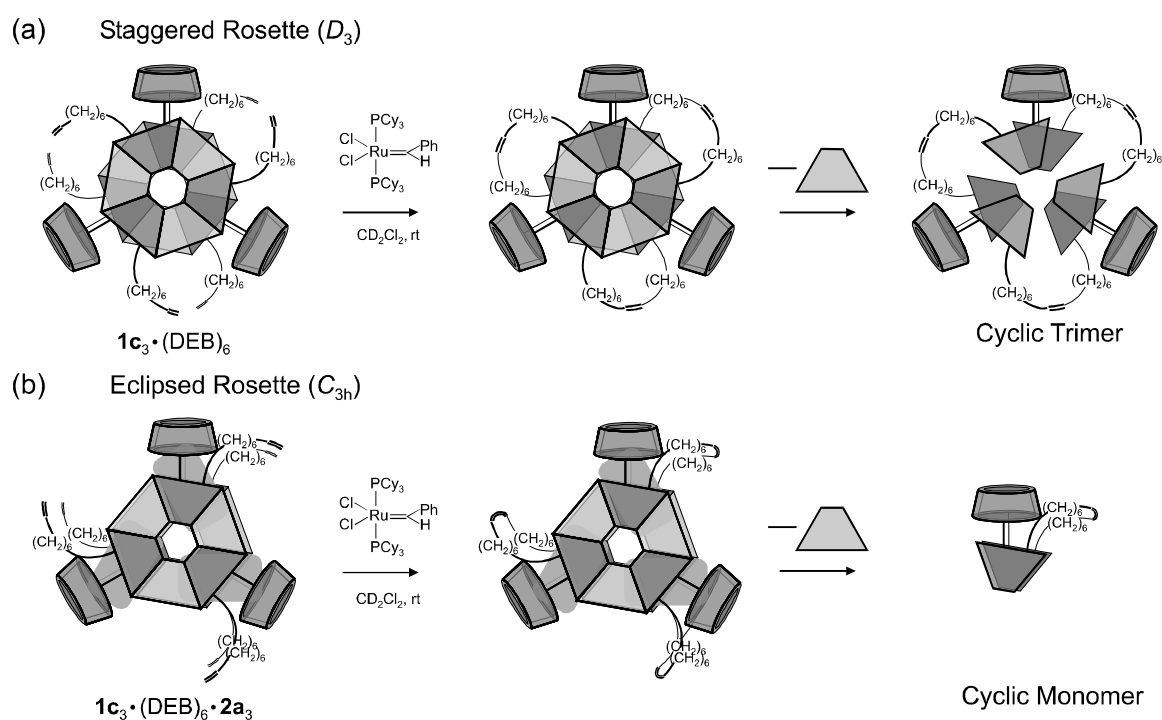


Figure 6.6. Metathesis reaction of assembly $\mathbf{1c}_3 \cdot (\text{DEB})_6$ in the (a) staggered conformation yielding the cyclic trimer, and (b) symmetrical eclipsed conformation yielding the cyclic monomer.

In the staggered D_3 conformation the two alkene chains connected to the same calix[4]arene are too far apart for an intramolecular reaction (Figure 6.7). This results in a geometry of the complex where the alkene chains connected to the melamines at different calix[4]arenes are close enough for an “intermolecular” reaction, yielding the cyclic trimer instead of the cyclic monomer. In the eclipsed conformation the two melamines on the same calix[4]arene are close enough for an “intramolecular” reaction, yielding the cyclic monomer.

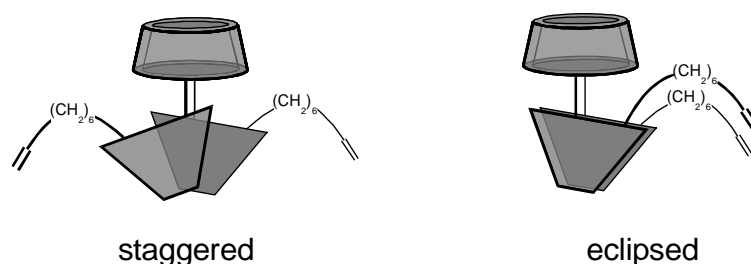


Figure 6.7. Staggered and eclipsed orientation of the two melamine units of calix[4]arene dimelamine **1c**.

Therefore, the complexation behavior of $\mathbf{1c}_3 \cdot (\text{DEB})_6$, containing oct-7-enyl side chain substituents, with **2a** was studied by ^1H NMR spectroscopy. This study showed the same complexation behaviour as $\mathbf{1a}_3 \cdot (\text{DEB})_6$. Upon complexation the two initial signals for the NH_{DEB} -protons at 14.05 and 13.25 ppm in $\mathbf{1c}_3 \cdot (\text{DEB})_6$ disappeared while two new upfield shifted signals at 13.48 and 12.99 ppm for these protons emerged (Figure 6.8). The presence of only 2 signals for the NH_{DEB} -protons suggested again that the conformation of the calix[4]arene dimelamines changes from staggered to (symmetrical) eclipsed upon complexation of **2a**. Subsequently, the ring closure metathesis (RCM) reaction with complex $\mathbf{1c}_3 \cdot (\text{DEB})_6 \cdot \mathbf{2a}_3$ was studied by ^1H NMR spectroscopy and MALDI-TOF mass spectrometry. In the ^1H NMR spectrum of the sample after the RCM reaction with $\mathbf{1c}_3 \cdot (\text{DEB})_6 \cdot \mathbf{2a}_3$, the signals for the two terminal vinylic protons at 5.8 and 4.9 ppm disappeared, and a new signal for internal vinylic protons at 5.6 ppm developed. MALDI-TOF mass spectrometry showed mainly the mass signal ($m/z = 1034.3$; calcd for $\text{C}_{60}\text{H}_{20}\text{N}_{12}\text{O}_{14} \cdot \text{H}^+ = 1033.6$) corresponding to the monomer. An almost negligible signal for the cyclic dimer ($\sim 5\%$), and the cyclic trimer ($< 1\%$) was observed, probably from some traces of assembly $\mathbf{1c}_3 \cdot (\text{DEB})_6$ without **2a**. Thus, the formation of the monomer is only possible if in $\mathbf{1c}_3 \cdot (\text{DEB})_6 \cdot \mathbf{2a}_3$ the calix[4]arene dimelamines exist in a (symmetrical) eclipsed conformation instead of in a staggered conformation. Consequently, the RCM reaction gave an indirect proof of the conformational change in assembly $\mathbf{1a}_3 \cdot (\text{DEB})_6$ from staggered (D_3) to symmetrical eclipsed (C_{3h}) upon encapsulation of **2a**.

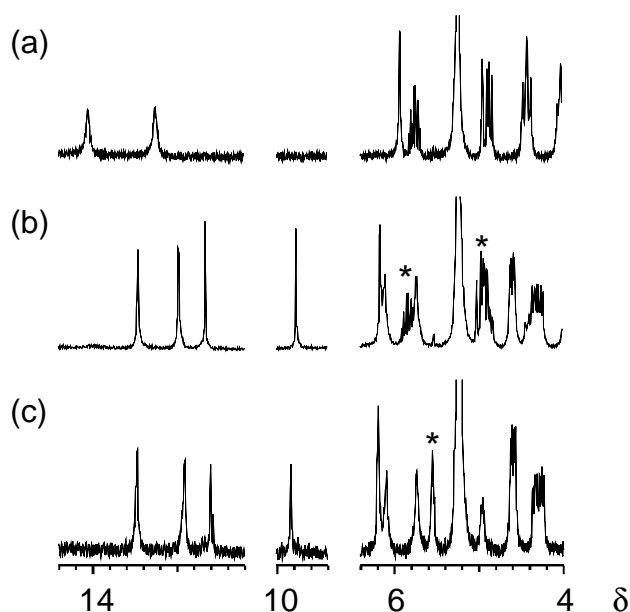


Figure 6.8. Parts of the ¹H NMR spectra of (a) assembly **1c₃•(DEB)₆**, (b) **1c₃•(DEB)₆•2a₃** before, and (c) **1c₃•(DEB)₆•2a₃** after metathesis reaction. Vinylic protons are marked with *. Spectra were recorded at 300 MHz in CD₂Cl₂ at 298K.

6.2.4 Detailed Studies on the Encapsulation of Alizarin (**2a**) by **1a₃•(DEB)₆**

Interestingly, the alizarin hydroxyl OH_n resonates at 6.24 ppm in free **2a**, while a shift to 9.87 ppm ($\Delta\delta$ 3.63 ppm) was observed upon complexation by assembly **1a₃•(DEB)₆** (Figure 6.1). This large shift suggested that OH_n is involved in hydrogen bond formation, probably with the carbonyl functionality of an adjacent **2a** molecule. The other hydroxyl OH_m which is already involved in an intramolecular hydrogen bond before complexation hardly shifted ($\Delta\delta$ -0.02 ppm). As visualized in Figure 6.9, **2a** could be complexed between the double rosette with the OH functionalities pointing either outward or inward with respect to the rosette. Further structural analysis of assembly **1a₃•(DEB)₆•2a₃** in CDCl₃, by NOESY experiments, revealed connectivities between OH_n and H_o, and between OH_n and H_q.

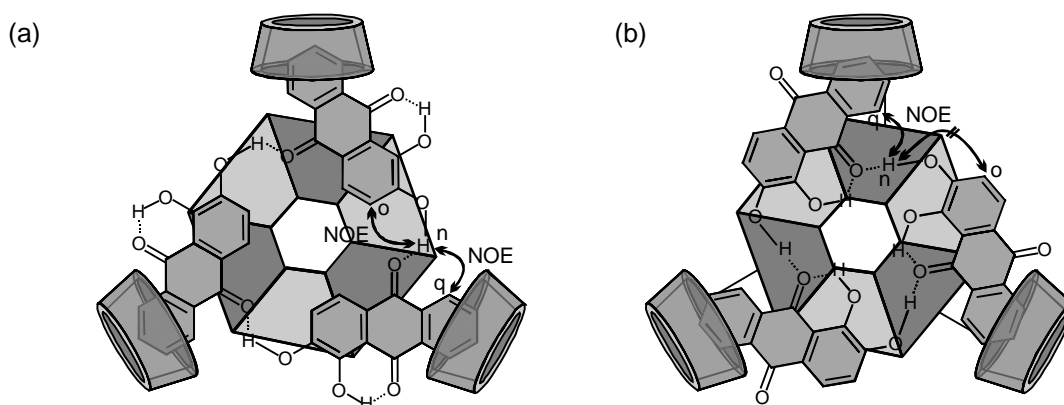


Figure 6.9. Formation of the trimer of **2a** with (a) hydroxyl functionalities pointing outwards and (b) inwards related to the rosette plane. (Only the bottom floor of the rosette is shown for clarity reasons.)

If the hydroxyl functionalities were pointing inwards, an NOE connectivity only between the OH_n and H_q would be expected. If the hydroxyl functionalities were pointing outwards, an NOE connectivity between OH_n and H_q of the same molecule **2a**, and an NOE connectivity between OH_n and H_o of the neighboring molecule **2a** would be expected. Thus, the NOESY experiment indicated that complexation of **2a** occurs with the OH functionalities pointing outwards with respect to the rosette (Figure 6.9). It thus seems that the noncovalent combination of three molecules of alizarin in the trimer is totally regioselective, i.e. only one of the two possible regioisomers is formed. To prove the templation role of the double rosette in the formation of the trimer **2a**₃, an NOESY experiment with **2a** in the absence of the capsule was performed. The NOESY experiment of **2a** did not show NOE connectivities between the hydroxyl OH_n and other protons, indicating that the hydroxyl OH_n in the absence of the template is not hydrogen-bonded, ruling out the formation of the trimer in the absence of the rosette.

Gas-phase molecular modeling calculations (Quanta 97, CHARMm 24.0) also support the formation of the alizarin trimer **2a**₃ as depicted in Figure 6.10. While the minimization of the rosette with the structure depicted in Figure 6.9b led to the capsule destruction, the minimization of the rosette with the encapsulated **2a**₃, where the hydroxyl functionalities point outwards, left the capsule intact. Thus, modeling also showed that the double rosette assembly is capable of regioselectively templating trimer **2a**₃.

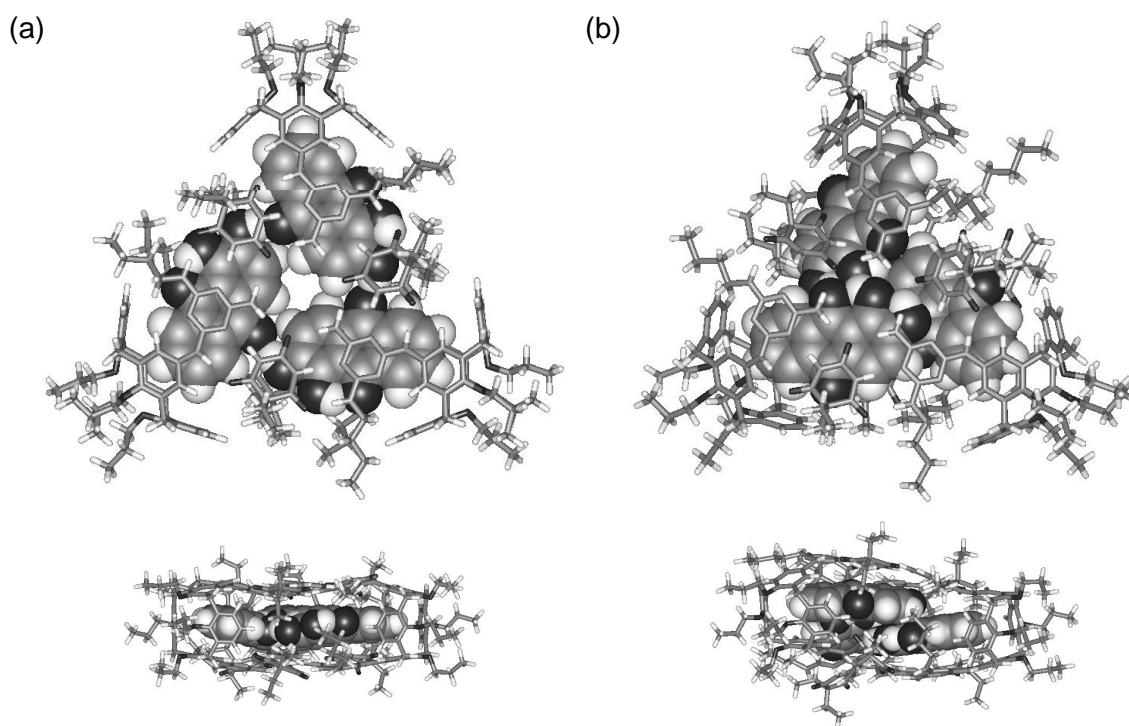


Figure 6.10. Gas-phase-minimized structure of assembly $\mathbf{1a}_3\bullet(\text{DEB})_6\bullet\mathbf{2a}_3$ with (a) hydroxyl groups pointing outwards and (b) pointing inwards the rosette plane. The $\mathbf{2a}$ molecules are presented in CPK style, assembly $\mathbf{1a}_3\bullet(\text{DEB})_6$ is presented by lines.

In summary, ^1H NMR data showed that the addition of alizarin ($\mathbf{2a}$) to $\mathbf{1a}_3\bullet(\text{DEB})_6$ results in the formation of a complex where three molecules of $\mathbf{2a}$ are encapsulated between the two rosette layers of the hydrogen-bonded assembly $\mathbf{1a}_3\bullet(\text{DEB})_6$. Thereby, the formation of a hydrogen bond network between the carbonyl functionality of one alizarin molecule and the hydroxyl of the adjacent alizarin molecule explains the strong cooperativity observed in the complexation process. Besides the formation of the three hydrogen bonds, the π - π stacking of $\mathbf{2a}$ with the triazine, barbiturate and the aromatic rings of the calix[4]arenes stabilizes the complex.

MALDI-TOF mass experiments using Ag^+ to ionize the double rosette assemblies were also used to characterize this double rosette complex.¹⁷ A sample of $\mathbf{1a}_3\bullet(\text{DEB})_6$ (1 mM) and $\mathbf{2a}$ (4 equiv.) showed an intense signal at m/z 4322 and a smaller signal at m/z 4557, indicating the formation of the 1:1 (calc. for $[\mathbf{1a}_3\bullet(\text{DEB})_6]\bullet\mathbf{2a}\bullet\text{Ag}^+ = 4313$), and the 1:2 (calc. for $[\mathbf{1a}_3\bullet(\text{DEB})_6]\bullet\mathbf{2a}_2\bullet\text{Ag}^+ = 4553$) complex. The signal for the 1:3 complex formation (m/z 4795; calc. for $\mathbf{1a}_3\bullet(\text{DEB})_6\bullet\mathbf{2a}_3\bullet\text{Ag}^+ = 4793$) was hardly observed, while

this is the only species observed by ^1H NMR spectroscopy. The influence of Ag^+ on the formation of $\mathbf{1a}_3 \cdot (\text{DEB})_6 \cdot \mathbf{2a}_3$, was studied by adding a 10^{-6} M solution of AgOOCCF_3 to an assembly of $\mathbf{1a}_3 \cdot (\text{DEB})_6 \cdot \mathbf{2a}_3$ and measuring the ^1H NMR spectra. Addition of 0.05 equiv. gave an identical spectrum as in the absence of AgOOCCF_3 , while addition of 0.15 equiv. showed new signals in the ^1H NMR spectrum. The formed complex is probably not stable in the presence of a larger amount of Ag^+ in solution. Most likely, the encapsulated guest $\mathbf{2a}$ is partially removed from the complex.

6.2.5 Selectivity Studies with Receptor $\mathbf{1a}_3 \cdot (\text{DEB})_6$

A series of anthraquinones (**2**) (Chart 6.2) was selected as potential guest molecules and the induced shifts of the proton signals of $\mathbf{1a}_3 \cdot (\text{DEB})_6$ and **2** or **3** in the ^1H NMR spectra were monitored.

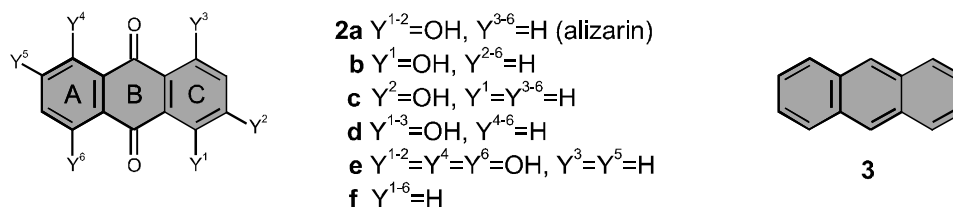


Chart 6.2. Molecular structures of compounds **2** and **3**.

Addition of anthracene (**3**), lacking both carbonyl and hydroxyl functionalities, did not shift any signal in the ^1H NMR spectrum. Thus, the main driving force for the complexation is not a simple π - π stacking between the guest molecules and the rosette plane. Even anthraquinone (**2f**), lacking only the hydroxyl groups, did not show any shift of the signals in the ^1H NMR spectrum, evidencing the importance of the hydroxyl groups for the complexation. Subsequently, to test if both hydroxyl functionalities present in alizarin are essential for the complexation, ^1H NMR studies with 1-hydroxyanthraquinone (**2b**), containing only one OH group at position-1, and 2-hydroxyanthraquinone (**2c**), containing only one OH group at position-2, were performed. Shifts of the signals are only observed upon addition of **2c**. Thus, the OH at position-2 (OH_n) in alizarin is important for the complexation, while the OH at position-1 (OH_m) is not. These observations are in agreement with the proposed complex structure, so OH_n is involved in the formation of an intermolecular hydrogen bond with the carbonyl of the adjacent

alizarin molecule, while OH_m is only involved in an intramolecular hydrogen bond with a carbonyl.

In the binding model (Figure 6.9a), ring A is partially encapsulated in the calix[4]arene cone. Therefore, substitutions in ring A (Chart 6.2) with, for instance, hydroxyl functionalities should decrease the complexation ability. After addition of 1,2,5,8-hydroxyanthraquinone (**2e**) to **1a₃•(DEB)₆**, no change in the chemical shifts of either guest or host were observed, indicating that no complexation occurred. Probably substitution of the aromatic ring A with bulkier functionalities does not enable ring A to penetrate into the calix[4]arene cone. Furthermore, when a new OH group was introduced in ring C as in purpurin (**2d**), the complexation of the guest to **1a₃•(DEB)₆** was not substantially affected in comparison with the encapsulation of **2a**.

The binding constant for the binding of **2a** to **1a₃•(DEB)₆** was determined by ¹H NMR spectroscopy. An ¹H NMR titration (1 mM rosette in CDCl₃) was performed by monitoring the percentage of **1a₃•(DEB)₆** and **1a₃•(DEB)₆•2a₃** present in solution. A binding constant *K* was estimated from ¹H NMR titration data by using the equations 1 to 4 (see below). Only two species, **1a₃•(DEB)₆** and **1a₃•(DEB)₆•2a₃**, were observed by ¹H NMR spectroscopy (see above); therefore it was assumed that complex **1a₃•(DEB)₆•2a₃** is formed in one step.



$$K = \frac{[\mathbf{1a_3\bullet(DEB)_6\bullet 2a_3}]}{[\mathbf{1a_3\bullet(DEB)_6}][\mathbf{2a}]^3} \quad (2)$$

$$[(\mathbf{1a_3\bullet(DEB)_6})_{\text{tot}}] = [\mathbf{1a_3\bullet(DEB)_6}] + [\mathbf{1a_3\bullet(DEB)_6\bullet 2a_3}] \quad (3)$$

$$[\mathbf{2a}_{\text{tot}}] = [\mathbf{2a}] + 3[\mathbf{1a_3\bullet(DEB)_6\bullet 2a_3}] \quad (4)$$

The amount of free guest **2a** is difficult to measure precisely because it is hardly present in the solution, therefore the *K* value cannot be calculated accurately. The concentration of free guest is recalculated indirectly from the concentration of the complex that is formed (**1a₃•(DEB)₆•2a₃** equation 4). A *K* ≥ 10¹⁰ M⁻³ was estimated. For a more precise calculation of the binding constant *K*, a different experiment was carried out with lower concentrations of **(1a₃•(DEB)₆)_{tot}** and **2a_{tot}**. The ¹H NMR spectrum of

assembly $\mathbf{1a}_3 \bullet (\text{DEB})_6$ (0.1 mM in CDCl_3) with 2 equiv. of $\mathbf{2a}$ clearly showed the presence of free $\mathbf{2a}$. The amount of H_2O that is present in the CDCl_3 at this concentration and the lower concentration of building blocks $\mathbf{1a}$ and DEB shifted the equilibrium to the separate building blocks. Therefore, assembly $\mathbf{1a}_3 \bullet (\text{DEB})_6$ at this concentration was not formed quantitatively. Recalculation of the total concentration of $\mathbf{1a}_3 \bullet (\text{DEB})_6$ by integration of the NH_{DEB} -protons and the ArCH_2Ar -bridge protons gave a total concentration of the host assembly of 0.043 mM. The total guest concentration is constant (0.20 mM). With these total host/guest concentrations a K -value of 10^{11} M^{-3} was estimated.

Calculation of the binding constants of $\mathbf{2b}$ and $\mathbf{2c}$ to $\mathbf{1a}_3 \bullet (\text{DEB})_6$ yielded comparable K values.

6.2.6 Stability Studies with Complex $\mathbf{1a}_3 \bullet (\text{DEB})_6 \bullet \mathbf{2a}_3$

Formation of the noncovalent trimer $\mathbf{2a}_3$ inside the self-assembled capsid might stabilize the hydrogen-bonded network of the rosette by π - π interaction between the rosette layers and the $\mathbf{2a}$ -trimer. As a consequence, the double rosette might be more stable in polar solvents ($\text{DMSO-}d_6$, CD_3OD). Therefore, the thermodynamic stabilities of uncomplexed assembly $\mathbf{1a}_3 \bullet (\text{DEB})_6$ and complex assembly $\mathbf{1a}_3 \bullet (\text{DEB})_6 \bullet \mathbf{2a}_3$ were determined by ^1H NMR titrations of $\mathbf{1a}_3 \bullet (\text{DEB})_6$ or $\mathbf{1a}_3 \bullet (\text{DEB})_6 \bullet \mathbf{2a}_3$ (CDCl_3 , 1 mM, 298 K) with $\text{DMSO-}d_6$ (using 1,4-dinitrobenzene ($\delta = 8.3$ -8.4 ppm) as an internal standard).¹⁸ The percentage assembly present in the $\text{CDCl}_3/\text{DMSO-}d_6$ mixture was determined by integration of the NH_{DEB} -protons H_a and H_b (see Figure 6.1 for assignment). No significant difference in thermodynamic stability between $\mathbf{1a}_3 \bullet (\text{DEB})_6$ and $\mathbf{1a}_3 \bullet (\text{DEB})_6 \bullet \mathbf{2a}_3$ was observed. ^1H NMR titrations of $\mathbf{1a}_3 \bullet (\text{DEB})_6$ and $\mathbf{1a}_3 \bullet (\text{DEB})_6 \bullet \mathbf{2a}_3$ (CDCl_3 , 1 mM, 298 K) with CD_3OD were carried out because CD_3OD better allows hydrophobic interactions than $\text{DMSO-}d_6$. The NH_{DEB} signals characteristic for assembly formation could not be monitored due to the exchange of these protons with the deuterium of the solvent. Therefore ArH_h at 5.97 ppm (see Figure 6.1 for assignment) in the free and 6.20 ppm in the complexed assembly were monitored. Unfortunately, the ArH_h signals are overlapping with free NH and OH protons, which made the accurate determination of the thermodynamic stability very difficult. Nevertheless, qualitatively no difference between the thermodynamic stability of $\mathbf{1a}_3 \bullet (\text{DEB})_6$ and $\mathbf{1a}_3 \bullet (\text{DEB})_6 \bullet \mathbf{2a}_3$ in

CD₃OD is observed. π - π interaction do not appear to be an important factor in the complex stabilization.

6.2.7 X-Ray Crystal Structure of **1a₃•(DEB)₆•2a₃**

Crystallization of assembly **1a₃•(DEB)₆•2a₃** from diffusion of hexane into a solution of the complex in dichloromethane gave large single crystals suitable for X-ray diffraction studies. The crystal structure (Figure 6.11) provides irrefutable solid state evidence for the encapsulation of three molecules of **2a** by assembly **1a₃•(DEB)₆**. In the crystal structure of a double rosette without the trimer **2a₃** encapsulated (Figure 3.3; assembly **1b₃•(DEB)₆** in Chapter 3), the rosette layers are stacked on top of each other with an intermolecular separation from 3.5 Å at the edges to 3.2 Å in the center of the rosette.⁸ The crystal structure of **1a₃•(DEB)₆•2a₃**, showed that upon encapsulation of **2a**, the intermolecular separation between two rosette layers increases to 6.7 Å at the edges to 6.4 - 6.9 Å in the center of the rosette. Furthermore, the crystal structure reveals that the two melamines of one calix[4]arene are in a parallel orientation, as indicated by ¹H NMR and RCM studies. In this way the electron deficient aromatic ring of **2a** is stacked in between the electron rich nitrogen atoms in the aromatic rings of the melamine. The OH groups of **2a** are pointing outwards with respect to the rosette as was also indicated by the NOE connectivities and modeling studies. The O-O distance (between the carbonyl of one **2a** and the hydroxyl of the other **2a**) in the hydrogen-bonded network forming the **2a₃** trimer is 2.7 Å, which is within the hydrogen bond formation distance.

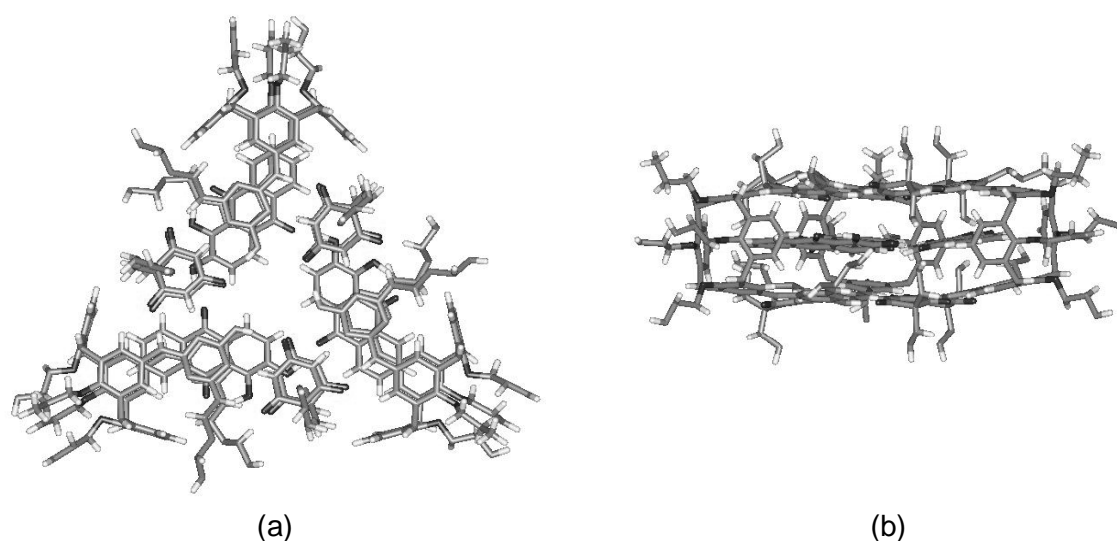


Figure 6.11. X-ray crystal structure of complex $1\mathbf{a}_3 \cdot (\text{DEB})_6 \cdot 2\mathbf{a}_3$. Both (a) top and (b) side view are shown. Only the main component of the disordered butyl and propyl groups are shown.

6.2.8 Release of Alizarin (**2a**) from the Complex $1\mathbf{a}_3 \cdot (\text{DEB})_6 \cdot 2\mathbf{a}_3$

As already discussed briefly in the introduction, complex $1\mathbf{a}_3 \cdot (\text{DEB})_6 \cdot 2\mathbf{a}_3$ shows very primitive structural similarities with viruses. The viral capsid is built in a highly symmetrical way from many copies of a few polypeptides. Double rosette $1\mathbf{a}_3 \cdot (\text{DEB})_6 \cdot 2\mathbf{a}_3$ also displays a high level of symmetry (C_{3h}) and is also spontaneously self-assembled from the individual components. Double stranded DNA, self-assembled by multiple hydrogen bonds, is encapsulated by the capsid of the virus. Also the alizarin trimer encapsulated by the double rosette is held together by multiple hydrogen bonds. Furthermore, the double rosette can be functionalized with recognition groups on the outside of the rosette (see Chapter 3), mimicking the virus' anchor points to the host cell. Besides these structural similarities, one of the initial action mechanism of the virus, *i.e.* release of the nucleic acid into the cell, was mimicked. Some of the naked viruses (*i.e.* without the lipid membrane) release the genetic material after adsorption to the host cell (Figure 6.12). In the capsules presented in this chapter, liberation of the encapsulated material can also be achieved by an external stimulus. Addition of BuCYA (for structure see Chart 6.1) to complex $1\mathbf{a}_3 \cdot (\text{DEB})_6 \cdot 2\mathbf{a}_3$ releases the guest molecules **2a** (Figure 6.12), resulting in a similar assembly $1\mathbf{a}_3 \cdot (\text{BuCYA})_6$ without the encapsulated material. The release is achieved because obviously assembly $1\mathbf{a}_3 \cdot (\text{BuCYA})_6$ (bearing cyanuric instead of barbituric derivatives) is not able to encapsulate **2a**. Moreover, cyanurates form

stronger hydrogen bonds with melamines than barbiturates, allowing DEB molecules to be substituted by BuCYA.¹⁹ The rearrangement and release was confirmed by ¹H NMR. The addition of 2.1 equiv BuCYA to complex $\mathbf{1a}_3 \bullet (\text{DEB})_6 \bullet \mathbf{2a}_3$ showed an ¹H NMR spectrum where all the signals of $\mathbf{1a}_3 \bullet (\text{DEB})_6 \bullet \mathbf{2a}_3$ have disappeared and only signals corresponding to assembly $\mathbf{1a}_3 \bullet (\text{BuCYA})_6$ and free $\mathbf{2a}$ can be seen.

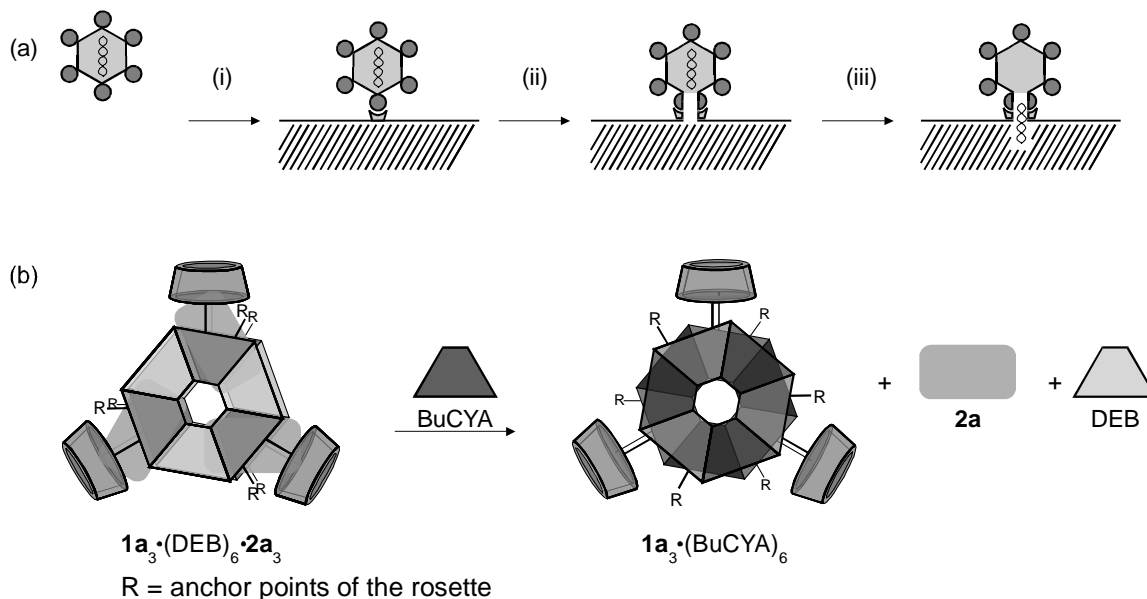


Figure 6. 12. (a) Part of the replication cycle of naked viruses: (i) adsorption of the virus to a host (cell), (ii) rearrangement of the capsid proteins, (iii) release of the encapsulated genetic material; (b) rearrangement and release of the encapsulated dye trimer by addition of BuCYA.

As a control experiment, $\mathbf{2a}$ was added directly to assembly $\mathbf{1a}_3 \bullet (\text{BuCYA})_6$ (1 mM, CDCl_3 , 298 K) and no changes in the chemical shifts of either the host $\mathbf{1a}_3 \bullet (\text{BuCYA})_6$ or the guest $\mathbf{2a}$ were observed. Also, no extra set of signals for the assembly $\mathbf{1a}_3 \bullet (\text{BuCYA})_6 \bullet \mathbf{2a}_3$ appeared. This different behavior of $\mathbf{1a}_3 \bullet (\text{BuCYA})_6$ when compared to $\mathbf{1a}_3 \bullet (\text{DEB})_6$ might be ascribed to structural differences between barbituric- and cyanuric acid. Somehow, the structure of DEB, with its tetrahedral sp^3 -carbon allows a better fit for the $\mathbf{2a}$ trimer than CYA with its flatter sp^3 -nitrogen. This results in a smaller distance between the two rosette layers for the capsule bearing CYA. Therefore, for the complexation of $\mathbf{2a}$ to occur the assembly $\mathbf{1a}_3 \bullet (\text{BuCYA})_6$ has to undergo larger structural changes than assembly $\mathbf{1a}_3 \bullet (\text{DEB})_6$, disfavoring the encapsulation of $\mathbf{2a}$. These structural effects were also supported by gas-phase molecular modeling calculations.

6.2.9 Encapsulation of Alizarin (**2a**) by Tetrarosette $4_3 \cdot (\text{DEB})_{12}$

As already discussed in Chapter 5, the tetrarosette assembly behaves as an *endo*-receptor, as evidenced by complexation of phenol derivatives in the cavity between the 2nd and 3rd floors. In the experiments described in this section, the tetrarosette $4_3 \cdot (\text{DEB})_{12}$ is also acting as an *endo*-receptor, but now using the cavities between the 1st and 2nd as well as between the 3rd and 4th floors.

Tetrarosette $4_3 \cdot (\text{DEB})_{12}$ is formed by mixing tetramelamine **4** (two calix[4]arene dimelamine units covalently connected through a flexible linker) with 4 equiv of DEB (Chart 6.3).

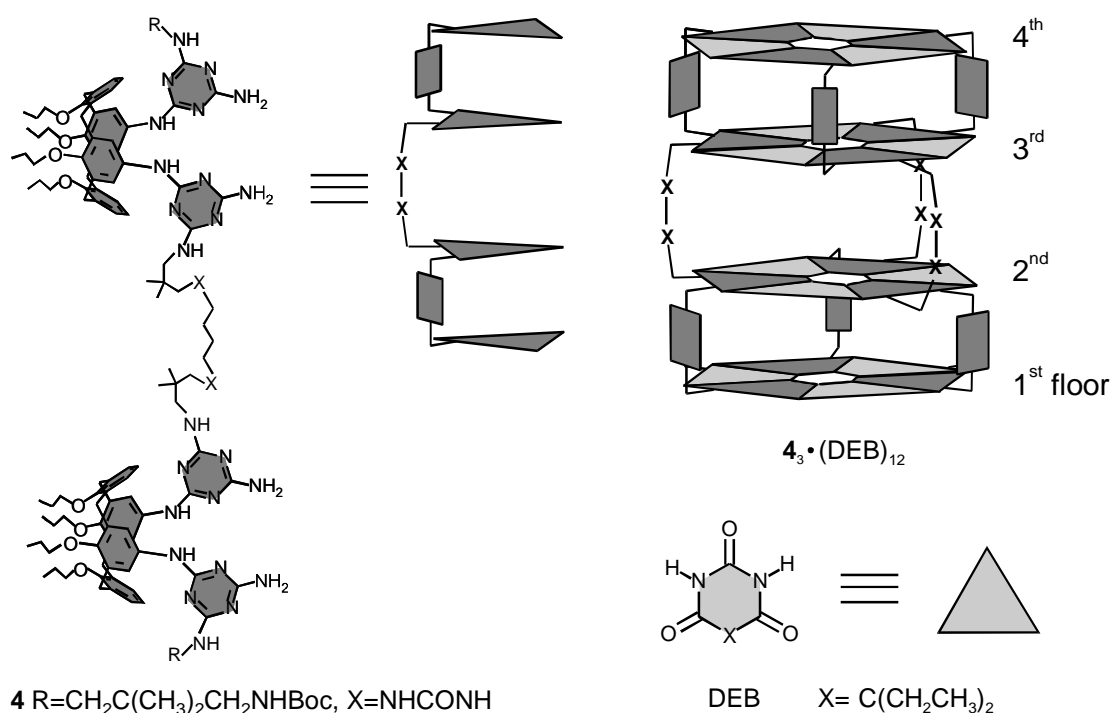


Chart 6.3. Molecular representations of compound **4** and DEB and hydrogen-bonded assembly $4_3 \cdot (\text{DEB})_{12}$.

The formation of a complex of **2a** with tetrarosette $4_3 \cdot (\text{DEB})_{12}$ was studied by ^1H NMR spectroscopy. Upon addition of **2a** to $4_3 \cdot (\text{DEB})_{12}$ most of the signals showed remarkable shifts in the ^1H NMR spectrum, similar to what was observed for the double rosette $1a_3 \cdot (\text{DEB})_6$. The NH_{DEB} -protons (H_a and H_b) showed upfield shifts from 14.17, 13.73, 13.33, and 12.96 ppm to 13.11, 12.93, 12.84, and 12.66 ppm (Figure 6.13).

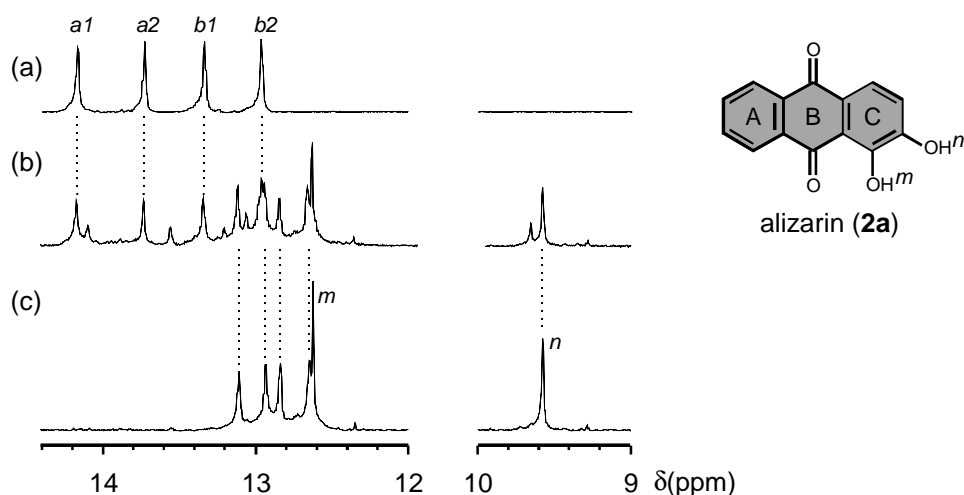


Figure 6.13. ^1H NMR spectra of assembly $4_3\bullet(\text{DEB})_{12}$ with (a) 0 equiv. **2a**, (b) 3 equiv. **2a**, and (c) 6 equiv. **2a**.

Also in this case the OH_n of **2a** (see Figure 6.13 for proton assignment) was shifted downfield to 9.58 ppm ($\Delta\delta$ 3.34 ppm), which indicated the formation of a hydrogen bond with the carbonyl of the adjacent **2a** molecule. As was expected for an assembly with two double rosettes, the integration of the ^1H NMR signals yielded a 6:1 ratio for the complexation (**2a**: $4_3\bullet(\text{DEB})_{12}$). Thus, two trimers of **2a** were encapsulated by the tetra-rosette, one in between the 1st and the 2nd and one in between the 3rd and the 4th rosette floors (Figure 6.14).

^1H NMR titration of the encapsulation of **2a** (up to approximately 6 equiv²⁰) by $4_3\bullet(\text{DEB})_{12}$ (1.0 mM in CDCl_3) showed two sets of new signals in the 14.4 – 12.4 ppm region, as well as 2 signals around 9.7-9.5 ppm, after the addition of 3 equiv. **2a**. One of the sets corresponds to the formation of the assembly $4_3\bullet(\text{DEB})_{12}\bullet 2a_6$. The other set of signals corresponds to the formation of a complex with only one **2a**₃ trimer, $4_3\bullet(\text{DEB})_{12}\bullet 2a_3$. Based on the intensities observed for the NH_{DEB} -protons, the relative concentrations of the three different assemblies are 1:1:1 ($6_3\bullet(\text{DEB})_{12}$) : ($6_3\bullet(\text{DEB})_{12}\bullet 2a_3$) : ($6_3\bullet(\text{DEB})_{12}\bullet 2a_6$). These relative concentrations indicated that only the complexation of **2a** within the trimer is strongly cooperative, while complexation of the first **2a**₃ trimer does not significantly influence the complexation of the second **2a**₃ trimer.

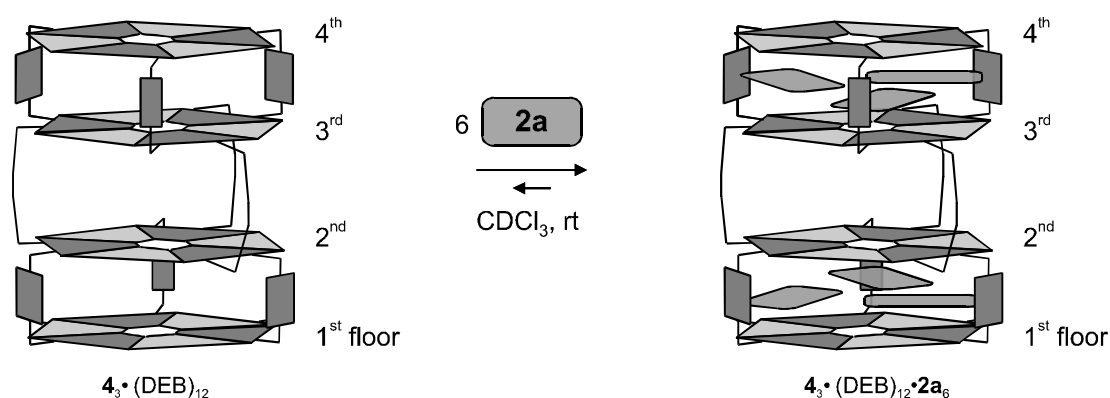


Figure 6.14. Encapsulation of two **2a** trimers by tetrarosette $4_3 \cdot (\text{DEB})_{12}$.

For complex $4_3 \cdot (\text{DEB})_{12} \cdot 2\mathbf{a}_6$, four signals were observed in the ^1H NMR spectrum. Earlier results²¹ showed that assembly $4_3 \cdot (\text{DEB})_{12}$ exists in the *SSS* (staggered-staggered-staggered) isomer (Figure 6.15). Encapsulation of two **2a** trimers by the tetrarosette in this conformation would give 4 or 8 signals, depending on the direction in which the second **2a** trimer is encapsulated. Nevertheless, in addition to the *SSS*, different other isomers could also exist (see Figure 6.15).

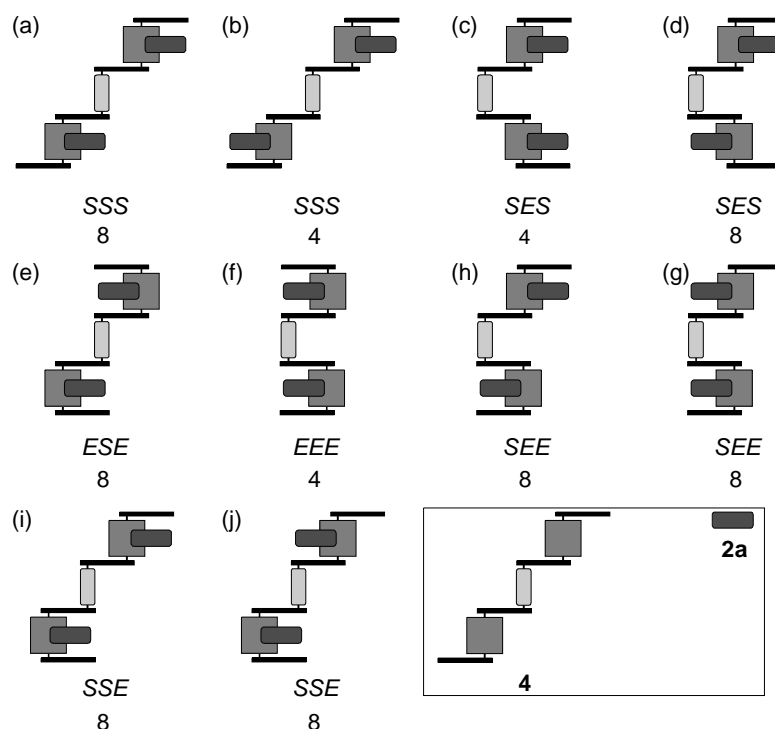


Figure 6.15. Schematic representation of all possible isomers of a tetrarosette assembly. Only assemblies with C_3 -axes are considered, which means that all 3 tetramelamines have the same orientation. The isomers are coded with 3 letters (*S* for staggered and *E* for eclipsed). The number of signals expected for the isomer are given below the schematic representations.

If a similar behavior is expected for tetra-rosette $4_3 \cdot (\text{DEB})_{12}$ as for double rosette $1a_3 \cdot (\text{DEB})_6$, encapsulation of **2a** should change the conformation from staggered to symmetrical eclipsed. Two different conformational isomers depicted in Figure 6.15 show a symmetrical eclipsed conformation for the double rosettes, *i.e.* *ESE* (e) and *EEE* (f). Based on four signals observed in the ^1H NMR spectrum, the *EEE* isomer is the most likely to be formed.

6.3 Conclusions

In this chapter a novel type of guest complexation by double rosettes is described in which guest molecules are complexed in between the two rosette layers of the double rosette $1a_3 \cdot (\text{DEB})_6$. Three molecules of alizarin were complexed in a highly organized manner (a noncovalent trimer) by the formation of a hydrogen bond network. Ring A of the alizarin is pointing inwards the calix[4]arene cone. Thus, the double rosette $1a_3 \cdot (\text{DEB})_6$ is capable of templating the regioselective synthesis of the trimer **2a₃**, that is not formed in the absence of assembly. The encapsulation process changes the conformation of the calix[4]arene dimelamines from staggered to eclipsed. This translates into a symmetry change for the self-assembled capsule from D_3 to C_{3h} in solution. This solution state conformation is supported by the X-ray of the crystal structure.

Additionally, the complex $1a_3 \cdot (\text{DEB})_6 \cdot 2a_3$ is able to release the encapsulated material upon addition of BuCYA.

Tetra-rosette $4_3 \cdot (\text{DEB})_{12}$ forms a 1:6 complex with **2a**. In the complex $4_3 \cdot (\text{DEB})_{12} \cdot 2a_6$, two trimers are encapsulated in the two cavities between the 1st and 2nd floors and between the 3rd and 4th floors of the tetra-rosette. The trimer formation is strongly cooperative as revealed by the absence of encapsulation of only one or two molecules of **2a**. However, the encapsulation of the second **2a** trimer occurs independently from the encapsulation of the first trimer.

6.4 Experimental Section

^1H NMR spectra were recorded at 300 or 400 MHz on a Varian Unity 300, or a Varian Unity 400 WB spectrometer with tetramethylsilane (TMS) as an internal reference in CDCl_3 solutions or with CDCl_3 as the internal reference. The 2D DQF-COSY consisted of 2048 datapoints in t_2 and 276 increments in t_1 . For the TOCSY experiment,

the total TOCSY mixing time was set to 65 ms. The spectrum was acquired with 2048 data points in t_2 and 276 FIDs in t_1 . The NOESY experiments were acquired with a mixing time of 100ms, 2048 datapoints in t_2 and 276 increments in t_1 . FAB-MS spectra were recorded with a Finnigan MAT 90 spectrometer with *m*-nitrobenzyl alcohol (NBA) as a matrix. MALDI-TOF mass spectra were recorded on a PerSpective Biosystems Voyager-De-RP spectrometer. A 337 nm UV nitrogen laser producing 3 ns pulses was used in the linear and reflectron modes.

Compounds **1a-1b**,⁸ **1c**⁹, and **4**²¹ were prepared according to methods described previously.

Formation of assemblies **1₃•(DEB)₆/(CYA)₆** and **4₃•(DEB)₁₂**

Hydrogen-bonded assemblies **1₃•(DEB)₆** and **4₃•(DEB)₆** were prepared by mixing calix[4]arene dimelamines **1** or tetramelamine **4** with 2.5 and 4.0 equivalents of DEB, respectively, in CDCl₃ and toluene-*d*₈ for 15 min. Similarly, assembly **1a₃•(CYA)₆** was prepared by mixing the calix[4]arene dimelamine **1a** with 2.1 equivalents of CYA in CDCl₃ for 15 min.

Ring Closure Metathesis reaction

Calix[4]arene dimelamine **1c** (0.020 g, 0.019 mmol) and DEB (0.0086 g, 0.038 mmol) were dissolved in CD₂Cl₂ (2 mL) and **2a** (0.0060 g, 0.025 mmol) was added. The Grubbs catalyst (0.0031 g, 0.0038 mmol) was added to the assembly. The mixture was stirred at rt for 16h, and an additional amount of Grubbs catalyst (0.0016 g, 0.0019 mmol) was added. The mixture was stirred at rt for 24h before quenched by extensive bubbling with oxygen.

Single Crystal X-Ray Diffraction

Crystal data and structure refinement for 3[C₅₄H₇₂N₁₂O₄]·6[C₈H₁₂N₂O₃]·3[C₁₄H₈O₄]·4.5[C₆H₁₄] (**1a₃•(DEB)₆•2a₃•(hexane)_{4.5}**, Mr=5193.44. Red, cube-shaped crystals were obtained from diffusion of hexane into a solution of the complex in dichloromethane. A crystal of dimensions 0.25 x 0.25 x 0.25 mm was selected for measurement. This crystal was cubic, space group *Pa* $\bar{3}$ (no. 205) with a=41.043(6), V=69139.1(18) Å³, Z=8, D_x=1.00 g cm⁻³, F(000)=22248, μ(Mo Kα)=0.06 mm⁻¹. Where

relevant, the contribution of the disordered solvent molecules has been included in the reported data (*vide infra*). 186112 Reflections were measured ($R_{\sigma}=0.1117$), 12481 of which are independent ($R_{int}=0.1886$, $1.0^{\circ} < \theta < 21.05^{\circ}$, $-37 \leq h \leq 41$, $-41 \leq k \leq 28$, $-41 \leq l \leq 39$, $T=150$ K, Mo $K\alpha$ radiation, graphite monochromator, $\lambda=0.71073$ Å). Data were collected on an Enraf-Nonius KappaCCD area detector on rotating anode. Data were not corrected for absorption effects. The structure was solved by direct methods (SHELXS-97), and refined on F^2 using SHELXL-97-2. A number of alkyl side chains displayed disorder. For severely disordered side chains a two site disorder model with refined occupancy was introduced. The remaining side chains were more satisfactorily described with large anisotropic displacement parameters. Mild distance restraints were applied to the disordered regions, ensuring equal bond lengths and angles within an alkyl chain. 35% of the unit cell volume is filled with severely disordered solvent. Atomic positions could not be recognized. The contribution of this disordered density to the scattered intensity was taken into account with the squeeze procedure, as implemented in platon. A total electron count of 5360 e per unit cell was found in a region with a volume of 24257 Å³. These values suggest that the disordered solvent is hexane rather than dichloromethane. Hydrogen atoms, including those involved in hydrogen bonding, were included in the refinement on calculated positions riding on their carrier atoms. Ordered non-hydrogen atoms were refined with anisotropic displacement parameters. Disordered non-hydrogen atoms were refined with a single isotropic displacement parameter for each pair of major and minor component atoms. Hydrogen atoms were refined with a fixed isotropic displacement parameter related to the value of the equivalent isotropic displacement parameter of their carrier atoms. Final $wR2=0.2551$, $w=1/[\sigma^2(F^2)+(0.1250 P)^2]$, where $P=(\max(F_o^2,0)+2F_c^2)/3$, $R1=0.0899$ (for 5649 $I>2\sigma(I)$), $S=1.053$, 1009 refined parameters, $-0.30 < \Delta\rho < 0.43$ e Å⁻³.

Complex 1a₃•(DEB)₆•2a₃: ¹H NMR (400 MHz, CDCl₃ (7.255), 298K) δ = 13.59 (s, 2 H; H_a), 13.08 (s, 2 H; H_b), 12.73 (s, 1 H; OH guest), 9.87(s, 1 H; OH guest), 8.07 (d, ³ J (H,H)= 8.4 Hz, 2 H; ArH guest), 7.98 (s, 2 H; H_c), 7.60 (d, ³ J (H,H)= 8.0 Hz, 2 H; ArH guest), 7.71 (d, ⁴ J (H,H)= 2.4 Hz, 2 H; H_g) 7.65-7.59 (m, 2 H; H_d), 7.40-7.30(m, 4 H; ArH), 7.07-7.04 (m, 3 H; ArH, ArH guest), 6.24 (d ⁴ J (H,H)= 2.0 Hz, 2 H; H_h), 6.17 (s, 2 H; H_e), 5.80 (s, 2H; H_f), 5.02 (d, ³ J (H,H)= 7.2 Hz, 1 H; ArH guest), 4.65 (ABq, ² J (H,H)=

12.4 Hz, 4 H; ArCH₂Ar), 4.39 (t, ³J(H,H)= 8.6 Hz, 2 H; OCH₂), 4.32 (t, ³J(H,H)=8.4 Hz, 2 H; OCH₂), 3.99-3.91 (m, 2 H; ArH guest), 3.72-3.50 (m, 8 H; OCH₂, CH₂ butyl), 3.34 (ABq, ²J(H,H)= 12.6 Hz, 4 H; ArCH₂Ar), 2.44-2.20 (m, 8 H; CH₂(DEB), OCH₂CH₂), 2.10-1.69 (m, 16 H; CH₂(DEB), OCH₂CH₂, CH₂ butyl), 1.39 (t, ³J(H,H)= 7.4 Hz, 6 H; CH₃ (DEB)), 1.14 (t, ³J(H,H)= 7.2 Hz, 6 H; CH₃ butyl), 1.10-0.99 (m, 12 H; OCH₂CH₂CH₃), 0.79 (t, ³J(H,H)= 7.4 Hz, 6 H; CH₃ (DEB)).

6.5 References

- ¹ Avers, C.J. *Molecular Cell Biology*, Addison-Wesley, Reading, **1986**, pp.768-770.
- ² Recent review about Molecular Capsules: Hof, F.; Craig, S.L.; Nuckolls, C.; Rebek Jr., J. *Angew. Chem. Int. Ed.* **2002**, *41*, 1488-1508.
- ³ a) Chopra, N.; Sherman, J.C. *Angew. Chem. Int. Ed.* **1999**, *38*, 1955-1957; b) Cram, D.J.; Karbach, S.; Kim, Y.H.; Baczynskyj, L.; Kallemeyn, G.W. *J. Am. Chem. Soc.* **1985**, *107*, 2575-2576.
- ⁴ a) Shivanyuk, A.; Rebek, Jr., J. *Chem. Commun.* **2001**, 2374-2375; b) Corbellini, F.; Fiammengo, R.; Timmerman, P.; Crego-Calama, M.; Versluis, K. Heck, A.J.R.; Luyten, I.; Reinhoudt, D.N. *J. Am. Chem. Soc.* **2002**, *124*, 6569-6575; b) Takeda, N.; Umemoto, K.; Yamaguchi, K.; Fujita, M. *Nature* **1999**, *398*, 794-799.
- ⁵ a) Kang, J.; Rebek, J., Jr. *Nature* **1997**, *385*, 50-52; b) Kang, J.; Santamaría, J.; Hilmersson, G.; Rebek, J., Jr. *J. Am. Chem. Soc.* **1998**, *120*, 7389-7390; c) Kang, J.; Hilmersson, G.; Santamaría, J.; Rebek, J., Jr. *J. Am. Chem. Soc.* **1998**, *120*, 3650-3656; d) Schalley, C.A. *Adv. Mater.* **1999**, *11*, 1535-1537.
- ⁶ Heinz, T.; Rudkevich, D.M.; Rebek, Jr., J. *Nature*, **1998**, *394*, 764-766.
- ⁷ Kusukawa, T.; Fujita, M. *J. Am. Chem. Soc.* **1999**, *121*, 1397-1398.
- ⁸ Timmerman, P.; Vreekamp, R.H.; Hulst, R.; Verboom, W.; Reinhoudt, D.N.; Rissanen, K.; Udachin, K.A.; Ripmeester, J. *Chem. Eur. J.* **1997**, *3*, 1823-1832.
- ⁹ Cardullo, F.; Crego-Calama, M.; Snellink-Ruël, B.H.M.; Weidmann, J.-L.; Bielejewska, A.; Fokkens, R. Nibbering, N.M.M.; Timmerman, P.; Reinhoudt, D.N. *Chem. Commun.* **2000**, 367-368.
- ¹⁰ Rance, M.; Sørensen, O.W.; Bodenhausen, G.; Wagner, G.; Ernst, R.R.; Wütrich, K. *Biochem. Biophys. Res. Commun.* **1983**, *117*, 479-485.
- ¹¹ Bax, A.; Davis, D.G. *J. Magn. Reson.* **1985**, *65*, 355-360.

- ¹² Jeener, J.; Meier, B.H.; Bachman, P.; Ernst, R.R. *J. Chem. Phys.* **1979**, *71*, 4546-4569.
- ¹³ Saito, S.; Nuckolls, C.; Rebek, Jr., J. *J. Am. Chem. Soc.* **2000**, *122*, 9628-9630.
- ¹⁴ Prins, L.J.; Timmerman, P.; Reinhoudt, D.N. *Pure & Appl. Chem.* **1998**, *70*, 1459-1468.
- ¹⁵ Prins, L.J.; Jolliffe, K.A.; Hulst, R.; Timmerman, P.; Reinhoudt, D.N. *J. Am. Chem. Soc.* **2000**, *122*, 3617-3627.
- ¹⁶ Grubbs, R.H.; Chang, S. *Tetrahedron* **1998**, *54*, 4413-4450.
- ¹⁷ Timmerman, P.; Jolliffe, K.A.; Crego-Calama, M.; Weindmann, J.-L.; Prins, L.J.; Cardullo, F.; Snellink-Ruel, B.H.M.; Fokkens, R.; Nibbering, N.M.M.; Shinkai, S.; Reinhoudt, D.N. *Chem. Eur. J.* **2000**, *6*, 4104-4115.
- ¹⁸ a) Mammen, M.; Simanek, E.E.; Whitesides, G.M. *J. Am. Chem. Soc.* **1996**, *118*, 12614-12623; b) Chapter 3 in this thesis.
- ¹⁹ Bielejewska, A.G.; Marjo, C.E.; Prins, L.J.; Timmerman, P.; de Jong, F.; Reinhoudt, D.N. *J. Am. Chem. Soc.* **2001**, *123*, 7518-7533.
- ²⁰ Due to the low solubility of **2a**, only a titration up to 6 equiv. is carried out.
- ²¹ Prins, L.J.; Neuteboom, E.E.; Parashiv, V.; Crego-Calama, M.; Timmerman, P.; Reinhoudt, D.N. *J. Org. Chem.* **2002**, *67*, 4808-4820.

Chapter 7

Towards Artificial Antibodies: Small Dynamic Combinatorial Libraries

In the first part of this chapter the encapsulation of the alizarin trimer $2a_3$ by dynamic mixtures of up to 20 different self-assembled receptors is described. The relative concentration of the best receptor in the mixture is amplified by the template effect exerted by $2a_3$. In the second part, a library of different alizarin-like dye molecules was added to the nonchiral self-assembled receptor $1a_3 \cdot (DEB)_6$. This receptor is able to template the formation of the best fitting trimer. The highly organized encapsulation of the alizarin trimer $2a_3$ by chiral self-assembled receptors R- or S- $3_3 \cdot (DEB)_6$ is reported. The encapsulation of the alizarin trimer $2a_3$ by the racemic mixture of R- and S- $3_3 \cdot (DEB)_6$ is also investigated. Upon addition of $2a$ the R- and S- $3_3 \cdot (DEB)_6$ form heteromeric double rosettes, which is not the case in the absence of $2a$.

7.1 Introduction

Natural antibodies consist of an assembly of peptide chains that are built up from the 20 natural amino acids. The diversity in these antibodies is generated by random genetic recombinant processes. By using a self-assembled scaffold to bring together multiple binding sites, the diversity generation process of the antibodies can be mimicked. In the research described in this thesis, double rosettes are used as the self-assembled platform. By attaching oligopeptides (see Chapter 4) to the individual building blocks it is possible to create hydrogen-bonded assemblies containing a potential binding site. The diversity of these assemblies can be generated, as in the natural antibodies, at the covalent level (by variation in amino acid sequence of the polypeptides) and at the noncovalent level (by combination of the different individual building blocks).

Combinatorial chemistry (CC) can be seen as the process of diversity generation. CC is now widely used in the search for biologically active compounds, new materials and catalysts. Its combination with supramolecular chemistry (self-assembly directed by molecular recognition) has led to a new research field of dynamic combinatorial chemistry (DCC).¹ In DCC, the building blocks are connected to each other by reversible linkages. These reversible linkages can be covalent,² such as the imines reported by Lehn et al.,³ or the hydrazones that were described by Sanders and co-workers.⁴ Alternatively, the links can be noncovalent as was shown by Fujita et al.⁵ who used metal-ligand coordination, and by our group⁶ through the use of hydrogen bonds. (see Section 2.4).

The large advantage of DCC over CC is the template effect. When a guest molecule is added to the dynamic combinatorial library (DCL), some of the building blocks present in the library bind to it more strongly and these will be removed from the pool of interconverting building blocks. In this way the thermodynamic equilibrium of the library will shift, amplifying the good receptors.

The use of hydrogen bonds for the preparation of dynamic combinatorial libraries (DCL) has not attracted much attention, probably because it is not very easy to find a system that is self-assembled by hydrogen bonds and is able to recognize molecular guests by noncovalent interactions. In this chapter, DCLs generated by the formation of hydrogen bonds are described. In general, the hydrogen bonds have the advantages of directionality, high selectivity, and comparable strength to one another. In Section 7.2.1 small DCLs of nonchiral double rosette assemblies are described of which the template ability of an added guest (alizarin) is investigated. Nevertheless, with the final goal of

synthesizing noncovalent receptors that mimic antibodies, peptides (amino acids) should be attached to the rosette platform (Chapter 4). Because peptides are chiral, the complexation behavior of double rosette assemblies bearing model chiral groups was studied first (Section 7.2.2).

7.2 Results and Discussion

7.2.1 Small Dynamic Combinatorial Libraries of Hydrogen-Bonded Receptors

Structural diversity in calix[4]arene double rosette assemblies is generated simply by mixing the appropriate number of components $\mathbf{1x}$ ($\mathbf{x}=\mathbf{a},\mathbf{b}\dots\mathbf{N}$) under thermodynamically controlled conditions.⁶ Since these hydrogen-bonded assemblies are kinetically labile, there is a continuous exchange of components $\mathbf{1x}$ between the different assemblies present. In this way, a number of M heteromeric assemblies are formed in addition to N homomeric assemblies. The total number of assemblies P (i.e., $N + M$) present in such a library rapidly increases with an increasing number of components N and is given by the following formula (Eq.1; see also Figure 7.1).

$$P = N^2 + \frac{N(N-1)(N-2)}{6} \quad (1)$$

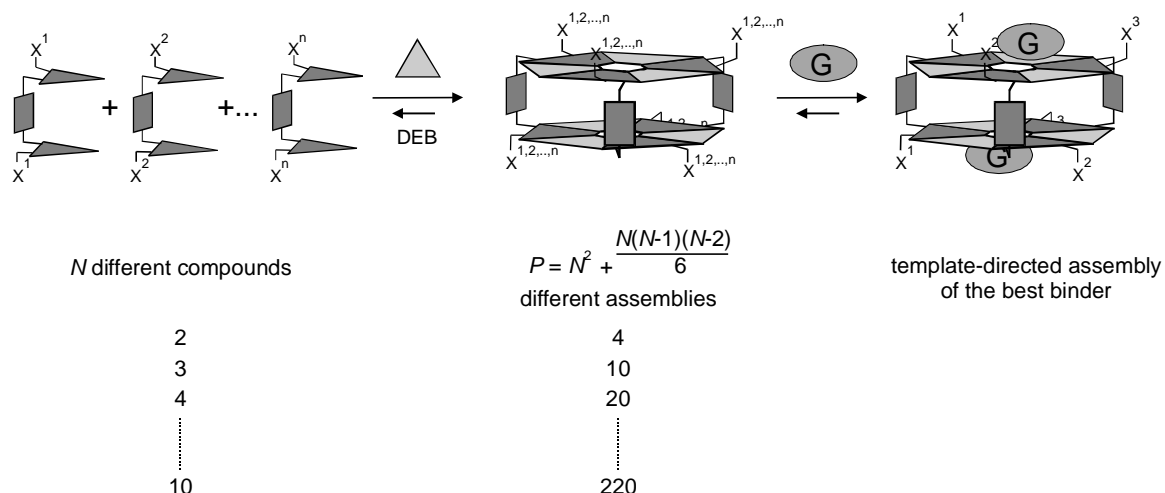


Figure 7.1. The spontaneous generation of supramolecular diversity and templated synthesis of the best binder.

Previous results in our group showed that by mixing the homomeric assemblies $\mathbf{1a}_3 \cdot (\text{DEB})_6$ and $\mathbf{1b}_3 \cdot (\text{DEB})_6$ (for chemical structures see Chart 7.1), additional heteromeric

assemblies $\mathbf{1a}_2\cdot\mathbf{1b}_1\cdot(\text{DEB})_6$ and $\mathbf{1a}_1\cdot\mathbf{1b}_2\cdot(\text{DEB})_6$ are formed spontaneously as a result of the continuous exchange of the individual components in CDCl_3 or $\text{toluene-}d_8$ (Figure 7.2).⁶ The mixing process can be clearly followed by ^1H NMR spectroscopy in CDCl_3 . The newly formed heteromeric assemblies give rise to different signals for the NH_{DEB} -protons that have been fully assigned by 2D NMR spectroscopy. It has been shown that the calix[4]arene dimelamines $\mathbf{1a}$ and $\mathbf{1b}$ are statistically distributed over the four assemblies. The statistical ratio is 1:3:3:1 for $\mathbf{1a}_3\cdot(\text{DEB})_6$, $\mathbf{1a}_2\cdot\mathbf{1b}_1\cdot(\text{DEB})_6$, $\mathbf{1a}_1\cdot\mathbf{1b}_2\cdot(\text{DEB})_6$, and $\mathbf{1b}_3\cdot(\text{DEB})_6$, respectively.

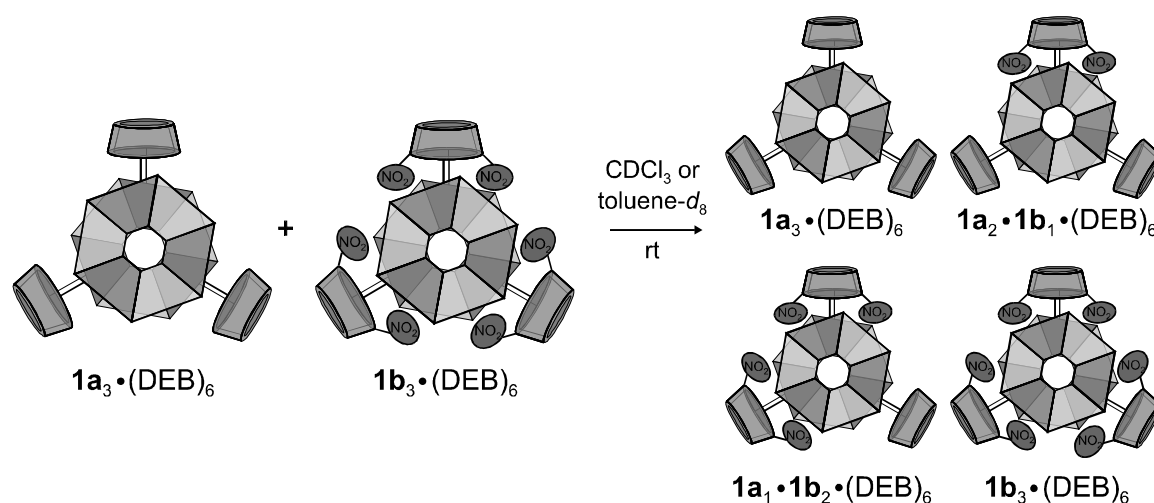


Figure 7.2. Mixing the homomeric assemblies $\mathbf{1a}_3\cdot(\text{DEB})_6$ and $\mathbf{1b}_3\cdot(\text{DEB})_6$ yielded also the heteromeric assemblies $\mathbf{1a}_2\cdot\mathbf{1b}_1\cdot(\text{DEB})_6$ and $\mathbf{1a}_1\cdot\mathbf{1b}_2\cdot(\text{DEB})_6$.

Furthermore, our group showed the first example of guest-templated selection of a hydrogen-bonded receptor in a dynamic noncovalent combinatorial library.⁷ Mixing equimolar solutions of the individual assemblies $\mathbf{1a}_3\cdot(\text{DEB})_6$ and $\mathbf{4}_3\cdot(\text{DEB})_6$ (bearing two zinc porphyrin moieties, see Figure 7.3a) in CDCl_3 at room temperature gave an almost statistical composition of the mixture (30 % homomeric; 70 % heteromeric) $\mathbf{4}_{(3-n)}\cdot\mathbf{1a}_n\cdot(\text{DEB})_6$ ($n = 0-3$, see Figure 7.3b). Addition of the tripyridyl guest $\mathbf{5}$ to this dynamic mixture shifted the equilibrium towards the maximum formation of the best receptor $\mathbf{4}_3\cdot(\text{DEB})_6$. The amplification of this receptor is a factor of 3.3 ($[\mathbf{4}_3\cdot(\text{DEB})_6]$ ~50 % after addition and ~15 % before addition of $\mathbf{5}$).

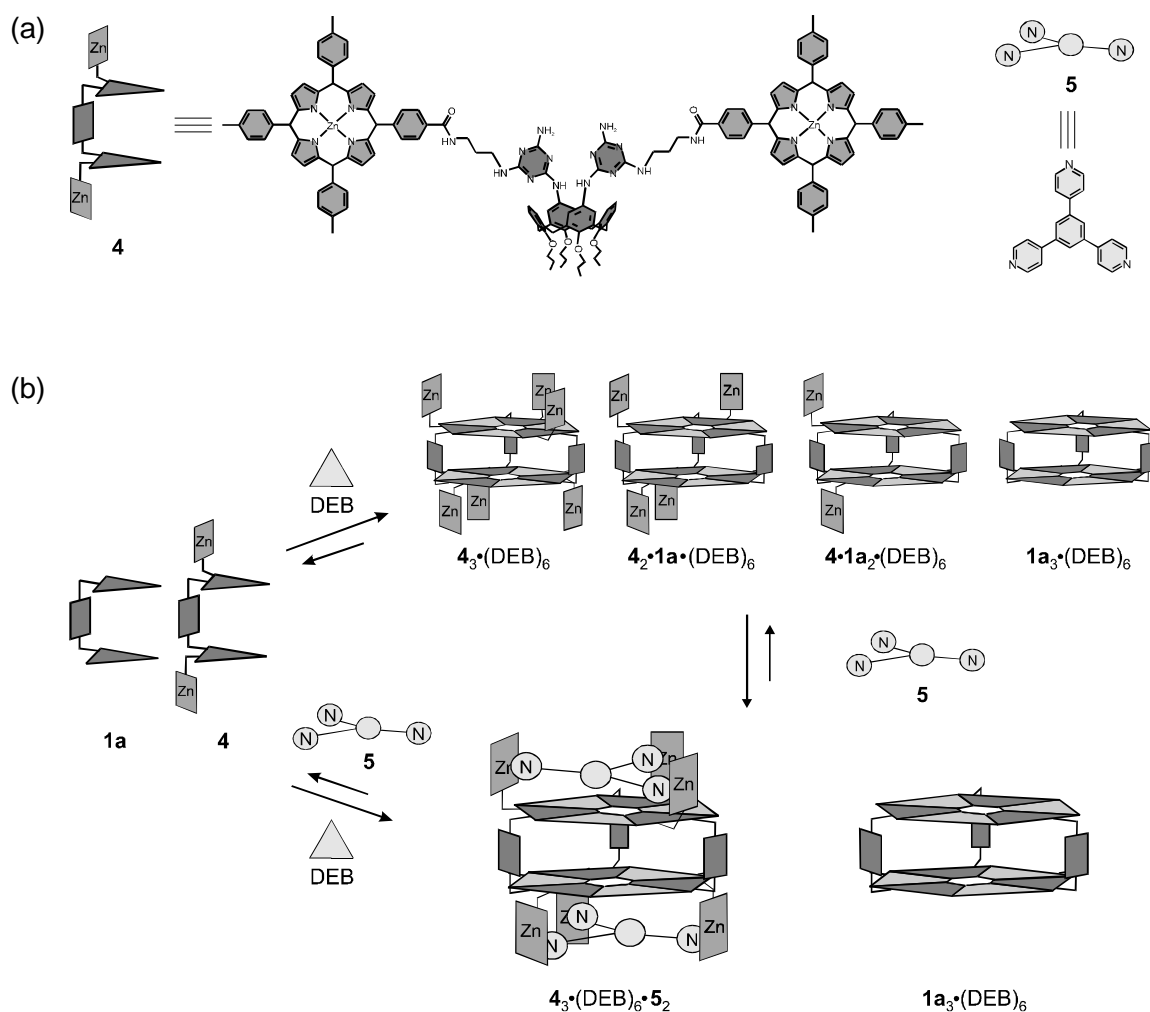


Figure 7.3. (a) Molecular and schematic representations of compounds **4** and **5**; (b) Schematic representation of the 4-component library $4_{(3-n)} \cdot 1a_n \cdot (DEB)_6$ ($n = 0-3$) and templated selection of the best receptor upon addition of guest molecule **5**.

7.2.1.1 Dynamic Libraries from Functionalized Double Rosettes

The above example describes the selection of the best binder in a mixture of *exo*-receptors, while in this section the amplification of an *endo*-receptor will be described (see also Chapter 5 for *exo*- and *endo*-receptors). As described in Chapter 6, assembly $1a_3 \cdot (DEB)_6$ templates the regioselective synthesis of the different guest trimers.

In contrast to the encapsulation of trimers by assembly $1a_3 \cdot (DEB)_6$ described in Chapter 6, the libraries described in this section are generated in toluene- d_8 . In general, the signals observed in this solvent are sharper than in $CDCl_3$. The shifts of the 1H NMR signals for the encapsulation of **2a** by $1a_3 \cdot (DEB)_6$ in toluene- d_8 differ slightly from those observed in $CDCl_3$ (see Chapter 6).

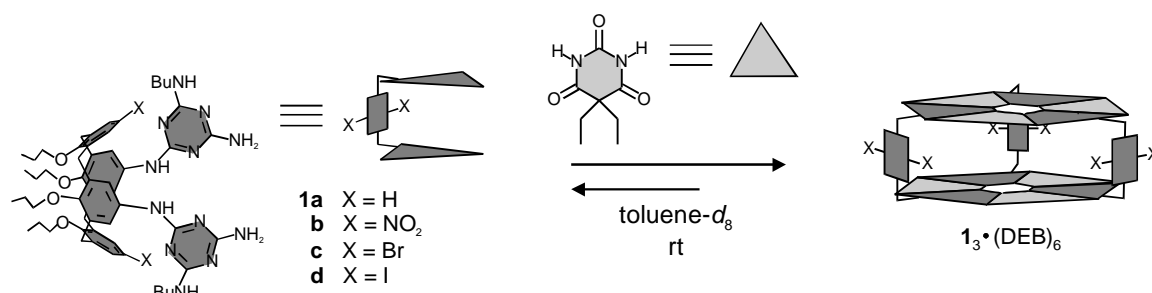


Chart 7.1. Molecular structures and schematic representations of compounds **1** and the assembly formations **1₃•(DEB)₆**.

*Encapsulation of **2a** by assemblies **1a₃•(DEB)₆** and **1b₃•(DEB)₆***

The ¹H NMR spectrum of the encapsulation of **2a** (3.7 equiv) by assembly **1a₃•(DEB)₆** (2 mM in toluene-*d*₈) showed for the OH_m signal a downfield shift from 12.51 to 12.90 ppm (Δδ 0.39 ppm). The signal of OH_n appears at 10.00 ppm (downfield shift of 4.57 ppm). The NH_{DEB}-protons H_a and H_b shifted upfield after encapsulation of **2a** to 13.78 (Δδ 0.53 ppm) and 13.22 ppm (Δδ 0.31 ppm), respectively (Figure 7.4).

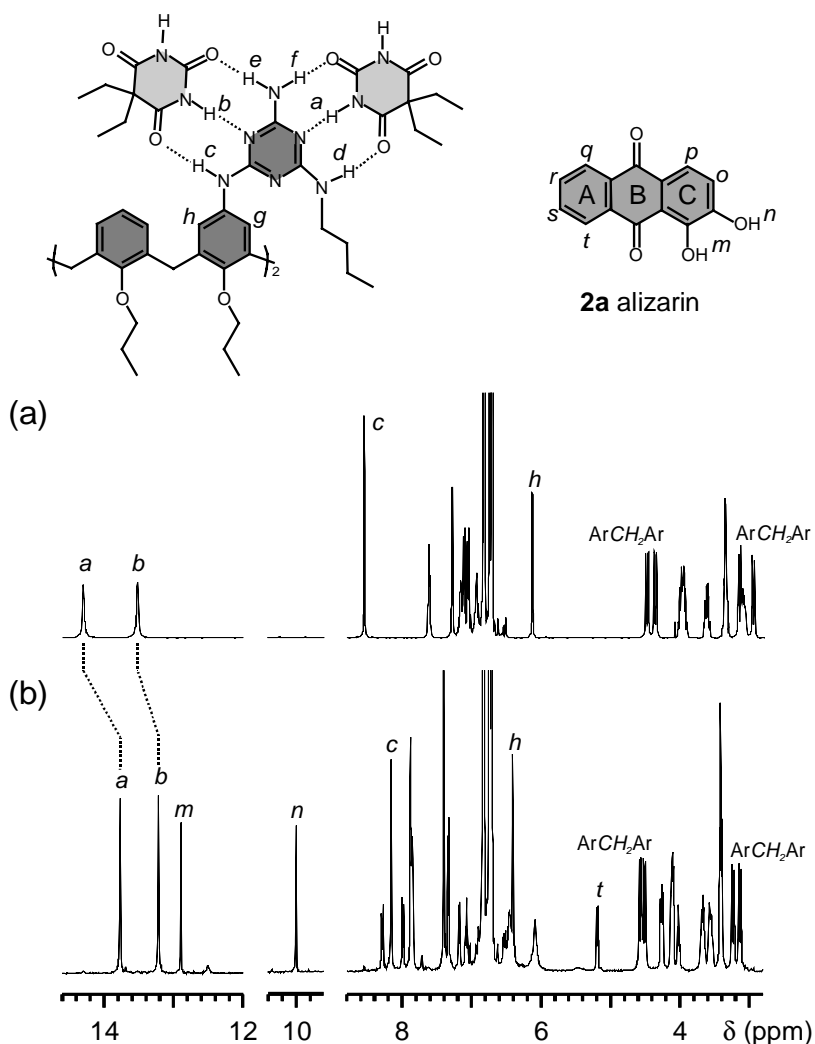


Figure 7.4. ^1H NMR spectrum of (a) assembly $\mathbf{1a}_3\cdot(\text{DEB})_6$, and (b) complex $\mathbf{1a}_3\cdot(\text{DEB})_6\cdot\mathbf{2a}_3$. Spectra were recorded in toluene- d_8 at 400 MHz and 298 K.

Addition of the dye alizarin **2a** (3 equiv) to assembly $\mathbf{1b}_3\cdot(\text{DEB})_6$ (1.6 mM in toluene- d_8) showed similar shifts in the ^1H NMR spectrum as observed for $\mathbf{1a}_3\cdot(\text{DEB})_6$. An upfield shift occurred for the NH_{DEB} -protons H_a and H_b to 13.62 ($\Delta\delta$ 0.45 ppm) and 13.26 ppm ($\Delta\delta$ 0.09 ppm), respectively. The OH_n proton was downfield shifted to 9.33 ppm ($\Delta\delta$ 3.90 ppm), while OH_m was shifted downfield to 12.81 ppm ($\Delta\delta$ 0.30 ppm). The main difference is that in the ^1H NMR spectrum of assembly $\mathbf{1a}_3\cdot(\text{DEB})_6$ after addition of 3.7 equiv of **2a**, only the signals for the complex $\mathbf{1a}_3\cdot(\text{DEB})_6\cdot\mathbf{2a}_3$ were observed, while the addition of **2a** (3 equiv) to $\mathbf{1b}_3\cdot(\text{DEB})_6$ showed the formation of only 8 % $\mathbf{1b}_3\cdot(\text{DEB})_6\cdot\mathbf{2a}_3$ in addition to 92 % free assembly $\mathbf{1b}_3\cdot(\text{DEB})_6$. Presumably, the bulky NO_2 substituents on $\mathbf{1b}_3\cdot(\text{DEB})_6$ inhibit the alizarin guests from entering the cavity.

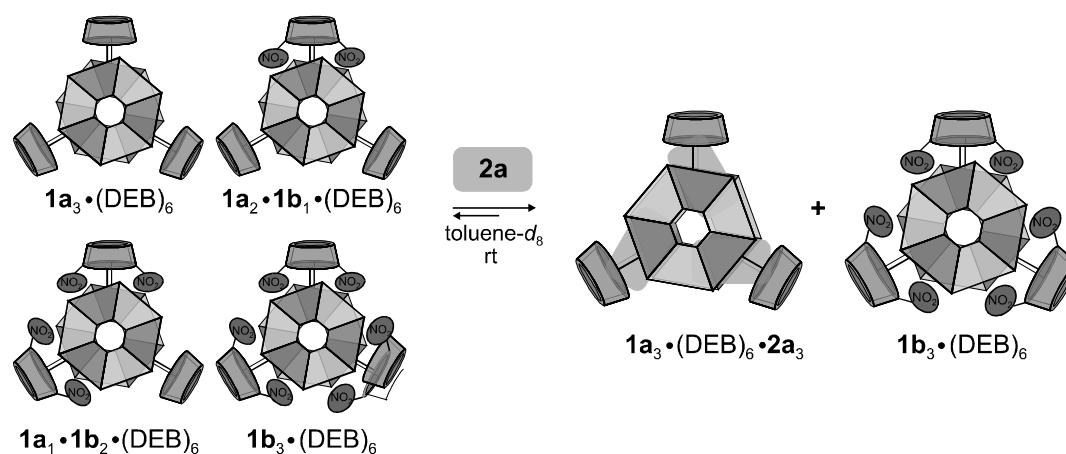


Figure 7.5. Schematic representation of the complete amplification of the best receptor $1a_3 \bullet (DEB)_6$ upon addition of guest molecule $2a$ from dynamic library $1a_n \bullet 1b_{(3-n)} \bullet (DEB)_6$ ($n = 0-3$).

Dynamic library of four components $1a_n \bullet 1b_{(3-n)} \bullet (DEB)_6$ ($n=0-3$)

The difference in encapsulation ability between $1a_3 \bullet (DEB)_6$ and $1b_3 \bullet (DEB)_6$ allows the study of the possible template effect of $2a_3$ (Figure 7.5). As described in Section 7.2.1, mixing double rosettes $1a_3 \bullet (DEB)_6$ and $1b_3 \bullet (DEB)_6$ yielded, in addition to these homomeric assemblies, the heteromeric assemblies $1a_2 \bullet 1b_1 \bullet (DEB)_6$ and $1a_1 \bullet 1b_2 \bullet (DEB)_6$ as a result of the continuous exchange of the individual components (Figure 7.2).⁶ In toluene- d_8 , the formation of the heteromeric assemblies is also clearly reflected in the 1H NMR spectrum by new signals in addition to the resonances of the homomeric assemblies. The mixing is clearly seen following protons H_a , H_b , and H_c (Figure 7.6).

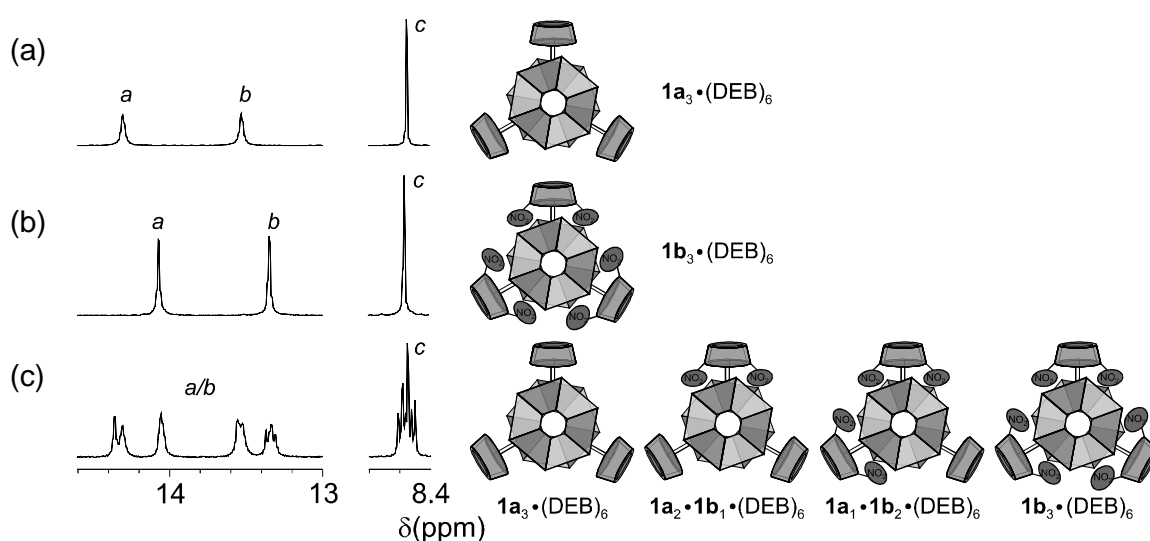


Figure 7.6. ^1H NMR spectra of (a) assembly $\mathbf{1a}_3\bullet(\text{DEB})_6$, (b) assembly $\mathbf{1b}_3\bullet(\text{DEB})_6$, and (c) the dynamic mixture $\mathbf{1a}_n\bullet\mathbf{1b}_{(3-n)}\bullet(\text{DEB})_6$ ($n=0-3$). The spectra were recorded at 400 MHz at 298 K in toluene- d_8 .

The addition of **2a** (1.2 equiv) to the dynamic mixture $\mathbf{1a}_n\bullet\mathbf{1b}_{(3-n)}\bullet(\text{DEB})_6$ ($n=0-3$) in toluene- d_8 shifted the equilibrium to the best binder $\mathbf{1a}_3\bullet(\text{DEB})_6$, which is expected from the complexation experiments performed with the individual assemblies. The appearance of one signal for the OH_n proton at 10.00 ppm in the ^1H NMR spectrum clearly demonstrates that only one complex is formed (Figure 7.7b). The resonance at 10.00 ppm corresponds to complex $\mathbf{1a}_3\bullet(\text{DEB})_6\bullet\mathbf{2a}_3$ (Figure 7.7c). No resonances are evident between 9.0-10.5 ppm, which would correspond to a complex of **2a** with either $\mathbf{1b}_3\bullet(\text{DEB})_6$ (9.33 ppm) or the two heteromeric assemblies $\mathbf{1a}_n\bullet\mathbf{1b}_{(3-n)}\bullet(\text{DEB})_6$ ($n=1,2$). Also, the NH_{DEB} -protons H_a and H_b show the amplification of the receptor $\mathbf{1a}_3\bullet(\text{DEB})_6$ in the mixture. Integration of the NH_{DEB} -protons H_a and H_b showed that the complex $\mathbf{1a}_3\bullet(\text{DEB})_6\bullet\mathbf{2a}_3$ represents ~35 % of all the present assemblies. The enrichment of the best binder $\mathbf{1a}_3\bullet(\text{DEB})_6$ in the mixture is therefore a factor of 2.8 (from ~12.5 % before to ~35 % after addition of **2a**).

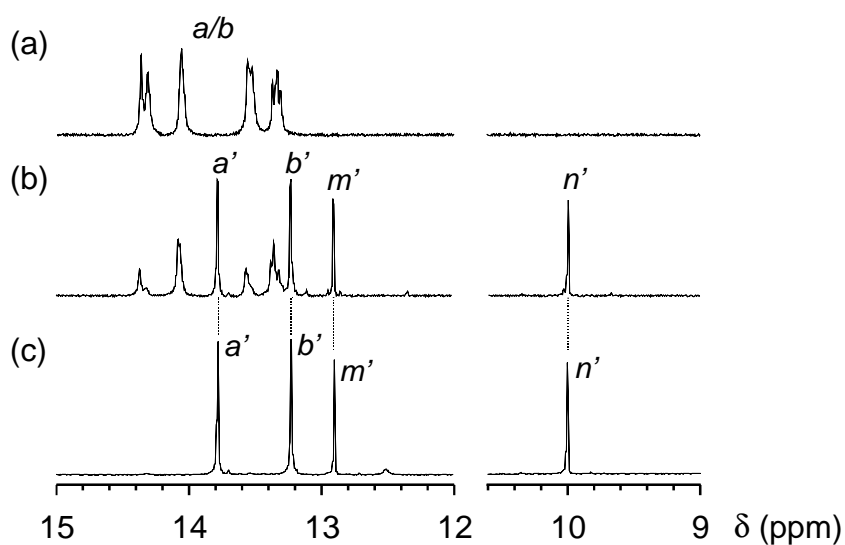


Figure 7.7. ^1H NMR spectra of dynamic mixture $\mathbf{1a}_n\cdot\mathbf{1b}_{(3-n)}\cdot(\text{DEB})_6$ ($n=0-3$) (a) in the absence of $\mathbf{2a}$ and (b) in the presence 1.2 equiv. $\mathbf{2a}$; (c) complex $\mathbf{1a}_3\cdot(\text{DEB})_6\cdot\mathbf{2a}_3$. The spectra were recorded at 400 MHz at 298 K in toluene- d_8 .

To verify that free assembly $\mathbf{1a}_3\cdot(\text{DEB})_6$ was not present in the mixture, the signal of proton H_c was monitored (Figure 7.8). This proton resonates at 8.55 ppm in the free assembly (Figure 7.8a), while it resonates at 8.16 ppm in the complex $\mathbf{1a}_3\cdot(\text{DEB})_6\cdot\mathbf{2a}_3$. Therefore, the disappearance of the resonance at 8.55 ppm would prove that there is no free assembly $\mathbf{1a}_3\cdot(\text{DEB})_6$ present in solution. Unfortunately, this signal overlaps with the resonance for H_c in $\mathbf{1a}_1\cdot\mathbf{1b}_2\cdot(\text{DEB})_6$.⁶ However, integration of the different proton signals for H_c indicated that free assembly $\mathbf{1a}_3\cdot(\text{DEB})_6$ was not present in solution in significant amounts.

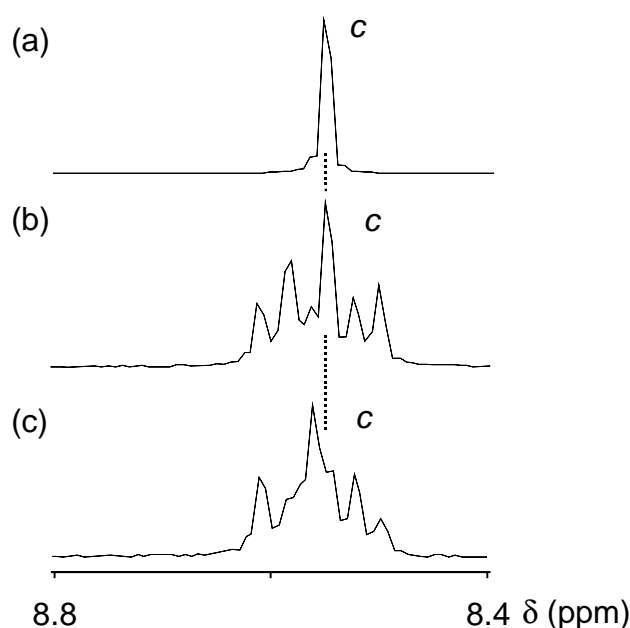


Figure 7.8. ¹H NMR spectra of (a) assembly $\mathbf{1a}_3 \cdot (\text{DEB})_6$, (b) dynamic mixture $\mathbf{1a}_n \cdot \mathbf{1b}_{(3-n)} \cdot (\text{DEB})_6$ ($n = 0-3$) in the absence of $\mathbf{2a}$ and (c) in the presence 1.2 equiv. $\mathbf{2a}$. The spectra were recorded at 400 MHz at 298 K in toluene- d_8 .

Encapsulation of $\mathbf{2a}$ by assemblies $\mathbf{1c}_3 \cdot (\text{DEB})_6$ and $\mathbf{1d}_3 \cdot (\text{DEB})_6$

To study the possible template effect of $\mathbf{2a}_3$ in larger hydrogen-bonded libraries, first the encapsulation of $\mathbf{2a}$ by assemblies $\mathbf{1c}_3 \cdot (\text{DEB})_6$ and $\mathbf{1d}_3 \cdot (\text{DEB})_6$ bearing bromo and iodo substituents, respectively, at the calix[4]arene moiety (see Chart 7.1) were studied individually. In contrast to what occurred with $\mathbf{1a}_3 \cdot (\text{DEB})_6$ and $\mathbf{1b}_3 \cdot (\text{DEB})_6$, upon addition of $\mathbf{2a}$ (3.2 equiv for $\mathbf{1c}_3 \cdot (\text{DEB})_6$ and 2.7 equiv for $\mathbf{1d}_3 \cdot (\text{DEB})_6$), two new different sets of signals (instead of one) appeared in the ¹H NMR spectrum for each assembly (2 mM in toluene- d_8). Each set of signals corresponds to two different 3:1 ($\mathbf{1c}_3 \cdot (\text{DEB})_6 \cdot \mathbf{2a}_3$) complexes (complex-1 and complex-2). Furthermore, the free assembly is observed in both cases.

As revealed by the intensities of the ¹H NMR signals for assembly $\mathbf{1c}_3 \cdot (\text{DEB})_6$, 38 % of complex-1, 12 % of complex-2, and 50 % of the free assembly were observed after addition of $\mathbf{2a}$ (Figure 7.9b). The ¹H NMR spectrum of the encapsulation of $\mathbf{2a}_3$ by $\mathbf{1c}_3 \cdot (\text{DEB})_6$ shows a large downfield shift for hydroxyl OH_n to 9.46 ($\Delta\delta$ 4.03; complex-1) and to 9.88 ppm ($\Delta\delta$ 4.45; complex-2). The observed downfield shifts for OH_m were smaller (0.42 ppm for complex-1 and 0.47 ppm for complex-2). The shifts for the NH_{DEB} -

protons H_a and H_b for complex-2 are also larger ($\Delta\delta$ 0.48 for H_a and 0.20 for H_b) than for complex-1 ($\Delta\delta$ 0.38 for H_a and 0.10 for H_b ; Figure 7.9b).

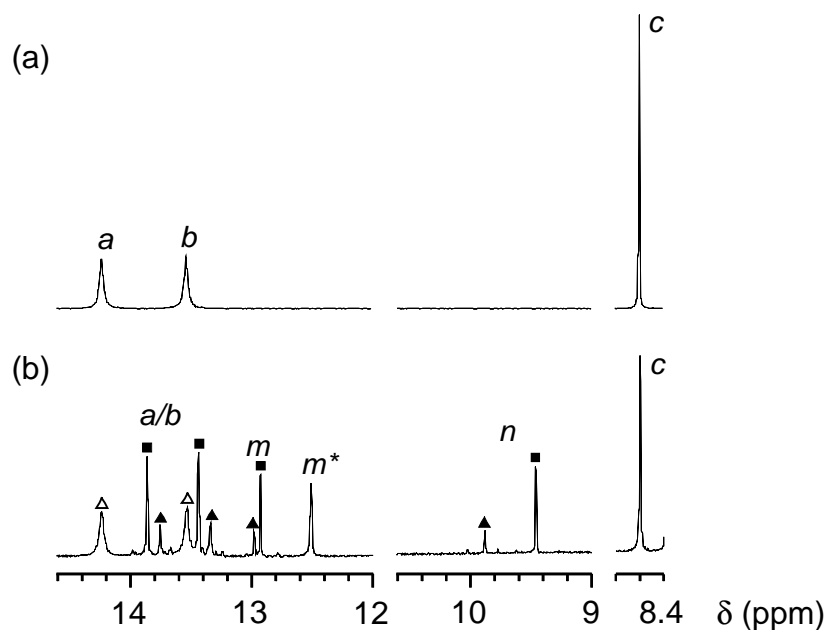


Figure 7.9. ^1H NMR spectrum of (a) assembly $1\mathbf{c}_3\cdot(\text{DEB})_6$ (2 mM) and (b) $1\mathbf{c}_3\cdot(\text{DEB})_6 + 4$ equiv. $2\mathbf{a}$. Δ represents the free assembly $1\mathbf{c}_3\cdot(\text{DEB})_6$, \blacksquare complex-1, and \blacktriangle complex-2. The signal marked with * belongs to OH_m of noncomplexed $2\mathbf{a}$. Spectra were recorded at 400 MHz in $\text{toluene-}d_8$ at 298K.

Judging from the number of signals (two) in the ^1H NMR spectrum for the NH_{DEB} -protons in both complexes, the three $2\mathbf{a}$ molecules are encapsulated by assembly $1\mathbf{c}_3\cdot(\text{DEB})_6$ in a similar fashion as $1\mathbf{a}_3\cdot(\text{DEB})_6\cdot 2\mathbf{a}_3$. Thus, the calix[4]arene dimelamines are in a symmetrical eclipsed conformation respect to each other (see Section 6.2.3).

The structural difference between complex-1 and complex-2 could not be derived from the 1D ^1H NMR spectrum. A possible difference could be that in one of the complexes the $2\mathbf{a}_3$ trimer is complexed with the hydroxyls pointing outwards (related to the rosette plane), while in the other the hydroxyls are pointing inwards (see Section 6.2.1). Another possibility is that the $2\mathbf{a}_3$ trimer is encapsulated in two different directions, i.e. clockwise and counter-clockwise, giving two constitutional isomers (Figure 7.10). Thus, the complex formation is not totally regioselective.

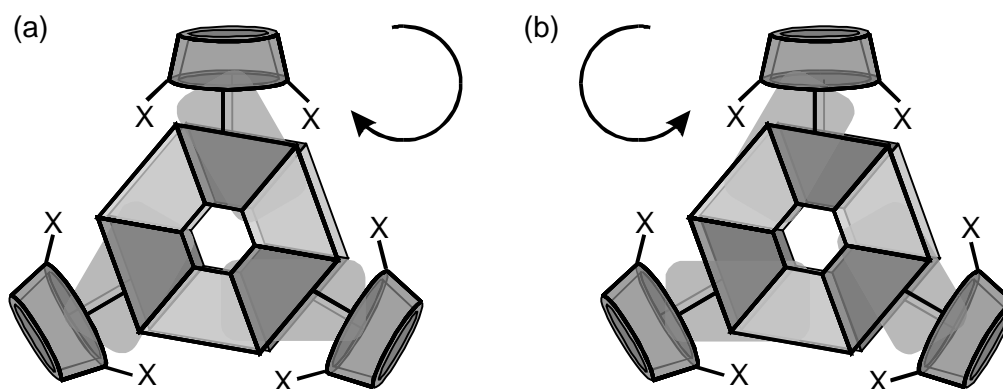


Figure 7.10. (a) Clockwise and (b) counter-clockwise encapsulation of **2a** by symmetrical eclipsed rosettes $I_3 \bullet (DEB)_6$.

For assembly $I_{d3} \bullet (DEB)_6$, 37 % of complex-1, 22 % of complex-2, and 49% of the free assembly $I_{d3} \bullet (DEB)_6$ was present after the addition of **2a** (2.7 equiv). Also for this assembly a large downfield shift for OH_n ($\Delta\delta$ 4.06 ppm for complex-1 and 4.50 ppm for complex-2) was observed. The other observed chemical shifts are comparable to the ones observed for assembly $I_{c3} \bullet (DEB)_6$.

Dynamic library of four components $I_{a_n} \bullet I_{c_{(3-n)}} \bullet (DEB)_6$ ($n=0-3$)

Subsequently, the dynamic library $I_{a_n} \bullet I_{c_{(3-n)}} \bullet (DEB)_6$ ($n = 0-3$) was prepared by mixing equimolar solutions of the individual double rosettes $I_{a_3} \bullet (DEB)_6$ and $I_{c_3} \bullet (DEB)_6$ in toluene- d_8 at room temperature. The formation of the heteromeric assemblies $I_{a_n} \bullet I_{c_{(3-n)}} \bullet (DEB)_6$ ($n = 1,2$) could be concluded from the multiple (at least 7) signals observed for H_c ($\delta = 8.67-8.50$) in the 1H NMR spectrum (Figure 7.11c). This proton resonates as a singlet at 8.55 and 8.60 ppm for both homomeric assemblies $I_{a_3} \bullet (DEB)_6$ and $I_{c_3} \bullet (DEB)_6$, respectively (Figure 7.11a-b). Similar multiple resonances for other protons in the rosette were observed. Integration of the signals observed for H_c pointed to a more or less statistical composition of the mixture $[1:3:3:1 [(I_{a_3} \bullet (DEB)_6) : (I_{a_2} \bullet I_{c_1} \bullet (DEB)_6) : (I_{a_1} \bullet I_{c_2} \bullet (DEB)_6) : (I_{c_3} \bullet (DEB)_6)]]$.

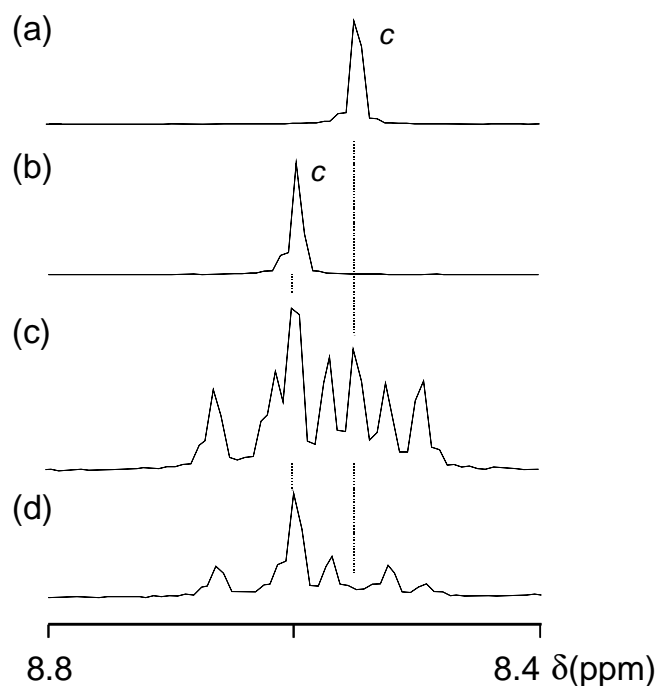


Figure 7.11. Part of the ^1H NMR spectra of assembly (a) $\mathbf{1a}_3\cdot(\text{DEB})_6$, (b) $\mathbf{1c}_3\cdot(\text{DEB})_6$, (c) dynamic mixture $\mathbf{1a}_n\cdot\mathbf{1c}_{(3-n)}\cdot(\text{DEB})_6$ ($n= 0-3$) and (d) dynamic mixture $\mathbf{1a}_n\cdot\mathbf{1c}_{(3-n)}\cdot(\text{DEB})_6$ ($n= 0-3$) plus 2 equiv of $\mathbf{2a}$. The spectra were recorded at 400 MHz at 298 K in toluene- d_8 .

Addition of $\mathbf{2a}$ (2 equiv) to the dynamic mixture $\mathbf{1a}_n\cdot\mathbf{1c}_{(3-n)}\cdot(\text{DEB})_6$ ($n= 0-3$) shifted the equilibrium to the best binder $\mathbf{1a}_3\cdot(\text{DEB})_6$. Integration of the signals in the ^1H NMR spectrum of the rosette NH_{DEB} -protons H_a and H_b and of the guest $\mathbf{2a}$ OH_m and OH_n protons showed the formation of $\sim 48\%$ complex. The signals for the OH_n (Figure 7.12b) indicated which complexes were formed with $\mathbf{2a}$.⁸ Integration of the OH_n signals showed that $\sim 43\%$ of the complexes formed is the homomeric complex $\mathbf{1a}_3\cdot(\text{DEB})_6\cdot\mathbf{2a}_3$. The heteromeric complex $\mathbf{1a}_2\cdot\mathbf{1c}_1\cdot(\text{DEB})_6\cdot\mathbf{2a}_3$ is formed in $\sim 47\%$ yield and complex $\mathbf{1a}_1\cdot\mathbf{1c}_2\cdot(\text{DEB})_6\cdot\mathbf{2a}_3$ in $\sim 10\%$ yield, while the formation of the homomeric complex $\mathbf{1c}_3\cdot(\text{DEB})_6\cdot\mathbf{2a}_3$ is negligible. In the dynamic mixture $\mathbf{1a}_n\cdot\mathbf{1c}_{(3-n)}\cdot(\text{DEB})_6$ ($n=0-3$) before the addition of $\mathbf{2a}$, assembly $\mathbf{1a}_3\cdot(\text{DEB})_6$ is present in $\sim 13\%$ yield, while, after addition of $\mathbf{2a}$, complex $\mathbf{1a}_3\cdot(\text{DEB})_6\cdot\mathbf{2a}_3$ is present in $\sim 21\%$ yield. Figure 7.11d shows that the signal for proton H_c in the homomeric assembly $\mathbf{1a}_3\cdot(\text{DEB})_6$ completely disappears, which means that no free assembly $\mathbf{1a}_3\cdot(\text{DEB})_6$ is present in solution. Thus, the amplification of $\mathbf{1a}_3\cdot(\text{DEB})_6$ in the dynamic library is a factor 1.6. The observed enrichment of $\mathbf{1a}_3\cdot(\text{DEB})_6$ in the dynamic library $\mathbf{1a}_n\cdot\mathbf{1c}_{(3-n)}\cdot(\text{DEB})_6$ ($n=0-3$) is smaller

than the enrichment in the dynamic library $\mathbf{1a}_n \cdot \mathbf{1b}_{(3-n)} \cdot (\text{DEB})_6$ ($n=0-3$), indicating that the difference in binding affinity between $\mathbf{1a}$ and $\mathbf{1c}$ is smaller than between $\mathbf{1a}$ and $\mathbf{1b}$.

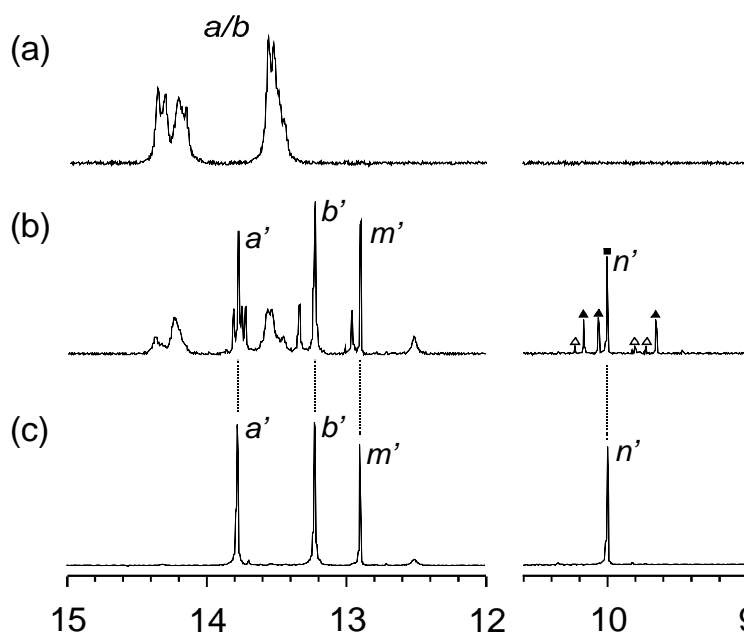


Figure 7.12. ^1H NMR spectra of dynamic mixture $\mathbf{1a}_n \cdot \mathbf{1c}_{(3-n)} \cdot (\text{DEB})_6$ ($n = 0-3$) (a) in the absence and (b) in the presence of $\mathbf{2a}$ (2 equiv.) and (c) of complex $\mathbf{1a}_3 \cdot (\text{DEB})_6 \cdot \mathbf{2a}_3$. The spectra were recorded at 400 MHz at 298 K in toluene- d_8 . ■ represents the complex $\mathbf{1a}_3 \cdot (\text{DEB})_6 \cdot \mathbf{2a}_3$, ▲ complex $\mathbf{1a}_2 \cdot \mathbf{1c}_1 \cdot (\text{DEB})_6 \cdot \mathbf{2a}_3$, and Δ complex $\mathbf{1a}_1 \cdot \mathbf{1c}_2 \cdot (\text{DEB})_6 \cdot \mathbf{2a}_3$.

Dynamic library of four components $\mathbf{1a}_n \cdot \mathbf{1d}_{(3-n)} \cdot (\text{DEB})_6$ ($n=0-3$)

The dynamic mixture $\mathbf{1a}_n \cdot \mathbf{1d}_{(3-n)} \cdot (\text{DEB})_6$ ($n = 0-3$) (total concentration 2 mM in toluene- d_8) showed the same behavior after addition of $\mathbf{2a}$ as that of library $\mathbf{1a}_n \cdot \mathbf{1c}_{(3-n)} \cdot (\text{DEB})_6$ ($n=0-3$). Prior to the guest addition, at least 5 signals were visible for proton H_c , and integration of these signals indicated a mixture close to the statistical distribution of $\mathbf{1a}$ and $\mathbf{1d}$ over the different assemblies. After the addition of $\mathbf{2a}$ (1.4 equiv) to $\mathbf{1a}_n \cdot \mathbf{1d}_{(3-n)} \cdot (\text{DEB})_6$ ($n = 0-3$), the ^1H NMR spectrum showed a total of ~ 40 % formation of complexes. Also here the resonances for the hydroxyl OH_n indicate which complexes were formed with $\mathbf{2a}$. Complex $\mathbf{1a}_3 \cdot (\text{DEB})_6 \cdot \mathbf{2a}_3$ is present in 54 % yield, the heteromeric complex $\mathbf{1a}_2 \cdot \mathbf{1d}_1 \cdot (\text{DEB})_6 \cdot \mathbf{2a}_3$ in 40 % yield, while the other heteromeric complex $\mathbf{1a}_1 \cdot \mathbf{1d}_2 \cdot (\text{DEB})_6 \cdot \mathbf{2a}_3$ is only present in 10 % yield of the total complexes formed. Assembly $\mathbf{1a}_3 \cdot (\text{DEB})_6 \cdot \mathbf{2a}_3$ is present in ~ 22 % yield in the dynamic library after the addition of $\mathbf{2a}$, indicating the enrichment of assembly $\mathbf{1a}_3 \cdot (\text{DEB})_6$ in the mixture by a factor of 1.8.

Dynamic library of ten components $\mathbf{1a}_n \cdot \mathbf{1c}_m \cdot \mathbf{1d}_{[3-(n+m)]} \cdot (\text{DEB})_6$ ($n = 0-3$; $m = 0-3$; $(n+m) \leq 3$)

Subsequently, the behavior of a 10-component dynamic library was investigated. The dynamic mixture $\mathbf{1a}_n \cdot \mathbf{1c}_m \cdot \mathbf{1d}_{[3-(n+m)]} \cdot (\text{DEB})_6$ ($n = 0-3$; $m = 0-3$; $(n+m) \leq 3$) was prepared by mixing equimolar solutions of the individual double rosettes $\mathbf{1a}_3 \cdot (\text{DEB})_6$, $\mathbf{1c}_3 \cdot (\text{DEB})_6$, and $\mathbf{1d}_3 \cdot (\text{DEB})_6$ in toluene- d_8 at room temperature. The ^1H NMR spectrum becomes too complex for the calculation of the distribution of $\mathbf{1a}$, $\mathbf{1c}$, and $\mathbf{1d}$ over the different assemblies (Figure 7.13a). However, after the addition of $\mathbf{2a}$ (0.7 equiv), the resonances of OH_n indicate the different complexes formed (Figure 7.13b). The total complex formation is $\sim 20\%$. The homomeric complex $\mathbf{1a}_3 \cdot (\text{DEB})_6 \cdot \mathbf{2a}_3$ (\blacksquare) is present in $\sim 39\%$ yield, while the two heteromeric complexes $\mathbf{1a}_2 \cdot \mathbf{1c}_1 \cdot (\text{DEB})_6 \cdot \mathbf{2a}_3$ (Δ) and $\mathbf{1a}_2 \cdot \mathbf{1d}_1 \cdot (\text{DEB})_6 \cdot \mathbf{2a}_3$ (\blacktriangle) are both present in $\sim 28\%$ yield of the total complexes (Figure 7.13b). If the distribution of the $\mathbf{1a}$, $\mathbf{1c}$, and $\mathbf{1d}$ over the assemblies would be statistical,⁹ assembly $\mathbf{1a}_3 \cdot (\text{DEB})_6$ would only be present in 3.7% yield. After the addition of $\mathbf{2a}$, complex $\mathbf{1a}_3 \cdot (\text{DEB})_6 \cdot \mathbf{2a}_3$ is present in $\sim 7.8\%$ yield, showing an enrichment factor of ~ 2 .

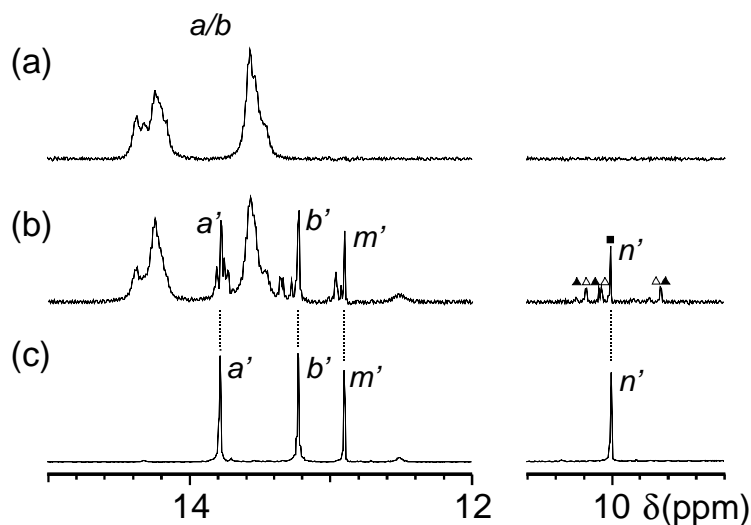


Figure 7.13. ^1H NMR spectra of dynamic mixture $\mathbf{1a}_n \cdot \mathbf{1c}_m \cdot \mathbf{1d}_{[3-(n+m)]} \cdot (\text{DEB})_6$ ($n = 0-3$; $m = 0-3$; $(n+m) \leq 3$) (a) in the absence and (b) in the presence of $\mathbf{2a}$ (2 equiv) and (c) of complex $\mathbf{1a}_3 \cdot (\text{DEB})_6 \cdot \mathbf{2a}_3$. The spectra were recorded at 400 MHz at 298 K in toluene- d_8 . \blacksquare represents the complex $\mathbf{1a}_3 \cdot (\text{DEB})_6 \cdot \mathbf{2a}_3$, \blacktriangle complex $\mathbf{1a}_2 \cdot \mathbf{1d}_1 \cdot (\text{DEB})_6 \cdot \mathbf{2a}_3$, and Δ complex $\mathbf{1a}_2 \cdot \mathbf{1c}_1 \cdot (\text{DEB})_6 \cdot \mathbf{2a}_3$.

Dynamic library of twenty components $\mathbf{1a}_n \cdot \mathbf{1b}_m \cdot \mathbf{1c}_o \cdot \mathbf{1d}_{[3-(n+m+o)]} \cdot (\text{DEB})_6$ ($n = 0-3$; $m = 0-3$; $o = 0-3$; $(n+m+o) \leq 3$)

Finally, the amplification in a 20-component dynamic library effected by trimer $\mathbf{2a}_3$ was investigated. Statistically, assembly $\mathbf{1a}_3 \cdot (\text{DEB})_6$ would only be present for 1.7 %¹⁰ in the dynamic mixture $\mathbf{1a}_n \cdot \mathbf{1b}_m \cdot \mathbf{1c}_o \cdot \mathbf{1d}_{[3-(n+m+o)]} \cdot (\text{DEB})_6$ ($n = 0-3$; $m = 0-3$; $o = 0-3$; $(n+m+o) \leq 3$) as the individual assemblies are mixed in equal amounts (Figure 7.14a). After addition of $\mathbf{2a}$ (0.5 equiv.) to the dynamic mixture, the resonances for hydroxyl OH_n indicate which complexes are formed. In total ~ 10 % of the all assemblies encapsulated the $\mathbf{2a}_3$ trimer. The homomeric complex $\mathbf{1a}_3 \cdot (\text{DEB})_6 \cdot \mathbf{2a}_3$ (■) is present in ~ 49 % yield and the two heteromeric complexes $\mathbf{1a}_2 \cdot \mathbf{1c}_1 \cdot (\text{DEB})_6 \cdot \mathbf{2a}_3$ (Δ) and $\mathbf{1a}_2 \cdot \mathbf{1d}_1 \cdot (\text{DEB})_6 \cdot \mathbf{2a}_3$ (▲) are both present in ~ 25 % yield of the total amount of complexes (Figure 7.14b). Thus, complex $\mathbf{1a}_3 \cdot (\text{DEB})_6 \cdot \mathbf{2a}_3$ is present in ~ 4.7 % yield in the dynamic mixture after the addition of $\mathbf{2a}$, showing an enrichment factor of ~ 2.8. Thus, trimer $\mathbf{2a}_3$ is even capable of selecting the best binder $\mathbf{1a}_3 \cdot (\text{DEB})_6$ in a 20-component library.

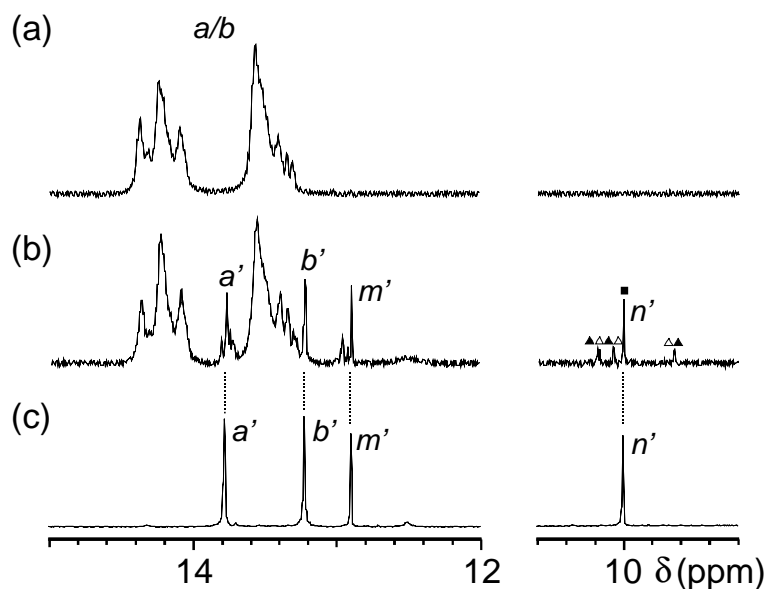


Figure 7.14. ^1H NMR spectra of dynamic mixture $\mathbf{1a}_n \cdot \mathbf{1b}_m \cdot \mathbf{1c}_o \cdot \mathbf{1d}_{[3-(n+m+o)]} \cdot (\text{DEB})_6$ ($n = 0-3$; $m = 0-3$; $o = 1-3$; $(n+m+o) \leq 3$) (a) in the absence and (b) in the presence of $\mathbf{2a}$ (2 equiv) and (c) of complex $\mathbf{1a}_3 \cdot (\text{DEB})_6 \cdot \mathbf{2a}_3$. The spectra were recorded at 400 MHz at 298 K in toluene- d_8 . ■ represents the complex $\mathbf{1a}_3 \cdot (\text{DEB})_6 \cdot \mathbf{2a}_3$, ▲ complex $\mathbf{1a}_2 \cdot \mathbf{1d}_1 \cdot (\text{DEB})_6 \cdot \mathbf{2a}_3$, and Δ complex $\mathbf{1a}_2 \cdot \mathbf{1c}_1 \cdot (\text{DEB})_6 \cdot \mathbf{2a}_3$.

7.2.1.2 Selective Noncovalent Synthesis by Receptor $1a_3 \cdot (DEB)_6$ in a “Virtual Library” of Self-Assembled Guest Trimers 2_3

Subsequently, the complex formation between one hydrogen-bonded receptor ($1a_3 \cdot (DEB)_6$) and a mixture of dye molecules **2a-2d** was studied. The four different molecules **2a-2d** chosen for this study are depicted in Chart 7.2.

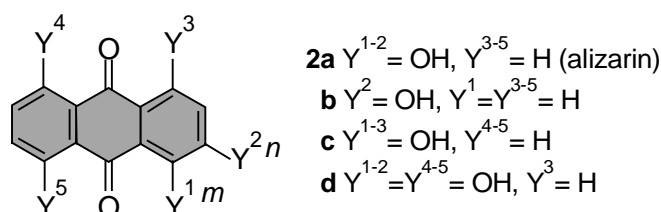


Chart 7.2. Molecular structures of compounds **2a-d**.

First, a mixture of only two guest molecules **2a** and **2b** and self-assembled receptor $1a_3 \cdot (DEB)_6$ was studied. In Chapter 6, it was reported that this receptor can template the formation of the noncovalent trimers $2a_3$ and $2b_3$ with similar affinity. Thus, after the addition of **2a** and **2b** four different complexes can be expected, two homomeric ($1a_3 \cdot (DEB)_6 \cdot 2a_3$ and $1a_3 \cdot (DEB)_6 \cdot 2b_3$), and two heteromeric ($1a_3 \cdot (DEB)_6 \cdot 2a_2 \cdot 2b$ and $1a_3 \cdot (DEB)_6 \cdot 2a \cdot 2b_2$).

The library was obtained by mixing in a 1:1 ratio two previously prepared complex solutions (1mM rosette in $CDCl_3$, $1a_3 \cdot (DEB)_6$ + **2a** (4 equiv) and $1a_3 \cdot (DEB)_6$ + **2b** (3.8 equiv)). The 1H NMR spectrum of this mixture showed additional signals in comparison to the 1H NMR spectrum of the two individual complexes (Figure 7.15), revealing the formation of the heteromeric complexes $1a_3 \cdot (DEB)_6 \cdot 2a_n \cdot 2b_{(3-n)}$ ($n=1,2$). The hydroxyl OH_m , present only in **2a**, gave four different signals in the 1H NMR spectrum of the library (Figure 7.15c). One of the signals clearly comes from the homomeric complex $1a_3 \cdot (DEB)_6 \cdot 2a_3$. The other three signals arise from the two heteromeric complexes, i.e. one signal for complex $1a_3 \cdot (DEB)_6 \cdot 2a_1 \cdot 2b_2$ (only containing one molecule of **2a**) and two broader signals for $1a_3 \cdot (DEB)_6 \cdot 2a_2 \cdot 2b_1$ (containing two molecules **2a**). The intensities of all four signals are comparable. The signal derived from the homomeric complex $1a_3 \cdot (DEB)_6 \cdot 2a_3$ accounts for three **2a** molecules, and therefore its abundance is three times smaller than the heteromeric complex. From the integration, it seems that the relative concentrations of the four different complexes $1a_3 \cdot (DEB)_6 \cdot 2a_n \cdot 2b_{(3-n)}$ ($n=0-3$) in the mixture is 1:3:3:X ($[2a]_3$) : ($[2a]_2 \cdot [2b]$) : ($[2a] \cdot [2b]_2$) : ($[2b]_3$), in agreement with the

statistical distribution of the guest molecules **2a** and **2b** over the various assemblies (if $X = 1$).¹¹ Thus, there is no preference for the encapsulation of exclusively **2a** or **2b**. The OH_n proton was expected to result in eight different signals, one for each homomeric complex and three for each heteromeric complex. The expected signals partially overlap with each other, resulting in a set of signals that is difficult to analyze. Additionally around 10 different signals for the NH_{DEB}-protons H_a and H_b were observed.

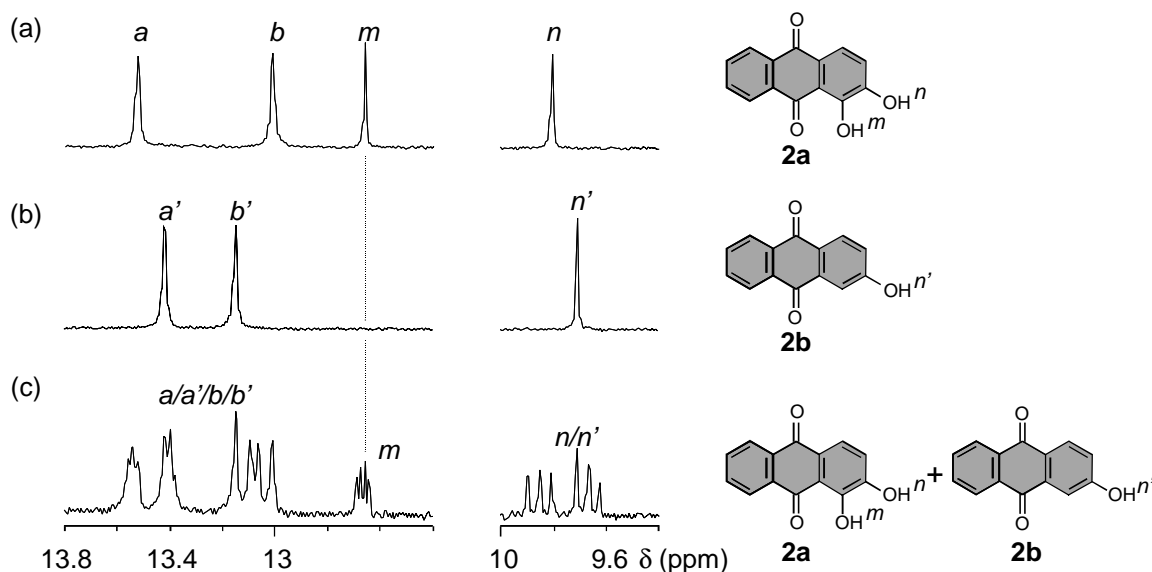


Figure 7.15. Part of the ¹H NMR spectrum for the complexation of **1a₃•(DEB)₆** and (a) **2a**, (b) **2b** to and (c) 1:1 mixture of **2a** and **2b**.

Due to the complexity of the ¹H NMR spectra, MALDI-TOF mass experiments using Ag⁺ to ionize the double rosette assemblies were also used to characterize the different double rosette complexes.¹² As already discussed in Chapter 6, the MALDI-TOF spectrum of a sample containing complex **1a₃•(DEB)₆•2a₃** showed an intense signal corresponding to the 1:1 (**1a₃•(DEB)₆:2a**) complex and a smaller signal corresponding to the 1:2 (**1a₃•(DEB)₆:2a**) complex, while the signal for the 1:3 (**1a₃•(DEB)₆:2a**) complex was hardly observed. Also, for the sample containing complex **1a₃•(DEB)₆•2b₃** a similar signal distribution was found in the MALDI-TOF mass spectrum.

When the sample containing assembly **1a₃•(DEB)₆** (0.25 mM), **2a** (3.8 equiv.), and **2b** (2.6 equiv) was measured by MALDI-TOF MS, only signals corresponding to the different combinations (homo- and heteromeric) of the 1:3 complexes (**1a₃•(DEB)₆•2a_n•2b_(3-n)** (n=0-3)) were observed in the *m/z* spectrum. No signals corresponding to 1:1 and 1:2 complexes were found. Two different signals corresponding

to the two homomeric complexes were observed at m/z 4798 (calcd for $\mathbf{1a}_3 \cdot (\text{DEB})_6 \cdot \mathbf{2a}_3 \cdot \text{Ag}^+ = 4799$) and at m/z 4753 (calcd for $\mathbf{1a}_3 \cdot (\text{DEB})_6 \cdot \mathbf{2b}_3 \cdot \text{Ag}^+ = 4751$), and another two signals corresponding to the heteromeric complexes at m/z 4781 (calcd for $\mathbf{1a}_3 \cdot (\text{DEB})_6 \cdot \mathbf{2a}_2 \cdot \mathbf{2b}_1 \cdot \text{Ag}^+ = 4783$) and at m/z 4764 (calcd for $\mathbf{1a}_3 \cdot (\text{DEB})_6 \cdot \mathbf{2a}_1 \cdot \mathbf{2b}_2 \cdot \text{Ag}^+ = 4767$). The different behavior observed between the complexes with one assembly and only one type of guest molecule versus multiple guest molecules is still unclear.

A similar mixture of guest molecules **2a** and **2d** was also investigated. A 1:1 mixture of assembly $\mathbf{1a}_3 \cdot (\text{DEB})_6$ (1 mM in CDCl_3) + 4 equiv **2a** and of assembly $\mathbf{1a}_3 \cdot (\text{DEB})_6$ (1 mM in CDCl_3) + 3.8 equiv¹³ **2d** was prepared. The ^1H NMR spectrum of this mixture showed only signals for the encapsulation of the $\mathbf{2a}_3$ trimer by assembly $\mathbf{1a}_3 \cdot (\text{DEB})_6$, and no signals for either the other homomeric complex $\mathbf{1a}_3 \cdot (\text{DEB})_6 \cdot \mathbf{2d}_3$ or the two heteromeric complexes $\mathbf{1a}_3 \cdot (\text{DEB})_6 \cdot \mathbf{2a}_2 \cdot \mathbf{2d}_1$ and $\mathbf{1a}_3 \cdot (\text{DEB})_6 \cdot \mathbf{2a}_1 \cdot \mathbf{2d}_2$ were observed (Figure 7.16). Thus, guest **2d** is not complexed by assembly $\mathbf{1a}_3 \cdot (\text{DEB})_6$. Additionally, the signals for the free assembly are visible in the ^1H NMR spectrum as a consequence of the equivalents of **2a** (2 equiv) compared to the total amount of double rosette $\mathbf{1a}_3 \cdot (\text{DEB})_6$ present. In conclusion, it is the first time that the selective noncovalent synthesis by a receptor in a virtual library of self-assembled guests is achieved.

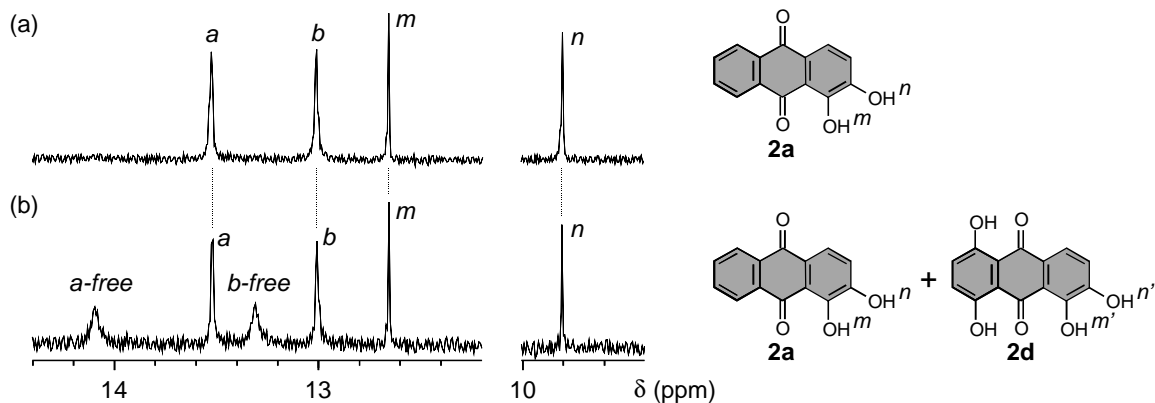


Figure 7.16. Part of the ^1H NMR spectrum for the complexation of (a) **2a** to $\mathbf{1a}_3 \cdot (\text{DEB})_6$ and (b) a mixture of **2a** and **2d** to $\mathbf{1a}_3 \cdot (\text{DEB})_6$.

Unfortunately, the ^1H NMR spectrum and the MALDI-TOF spectrum for the sample in which assembly $\mathbf{1a}_3 \cdot (\text{DEB})_6$ and the four guest molecules **2a-2d** were present was too complicated to provide relevant information.

7.2.2 Complexation of Alizarin **2a** by Chiral Assemblies $R\text{-3a}_3\bullet(\text{DEB})_6$ and $S\text{-3b}_3\bullet(\text{DEB})_6$

As described in the introduction, the final aim is to prepare libraries of noncovalent receptor molecules mimicking the selective processes encountered in antibodies. Therefore, the effect of chirality of the receptor libraries on the complexation behavior of rosettes bearing simple chiral groups was studied.

^1H NMR spectroscopy

As has already been described, the double rosette $\mathbf{1a}_3\bullet(\text{DEB})_6$ in the staggered conformation (D_3 symmetry) displays supramolecular chirality (see Section 3.2).¹⁴ The chirality is caused by the antiparallel orientation of the two melamines, which can either be oriented clockwise (P) or counterclockwise (M). In the absence of any other source of chirality, the assemblies exist as a racemic mixture of the P - and M -enantiomeric helices (showing only two signals in the 15-13 ppm region). The introduction of chiral substituents at the periphery of the rosette leads to the formation of diastereomeric instead of enantiomeric helices (in the case of diastereomers, four signals should then appear in the low field region, 13-15ppm).¹⁴

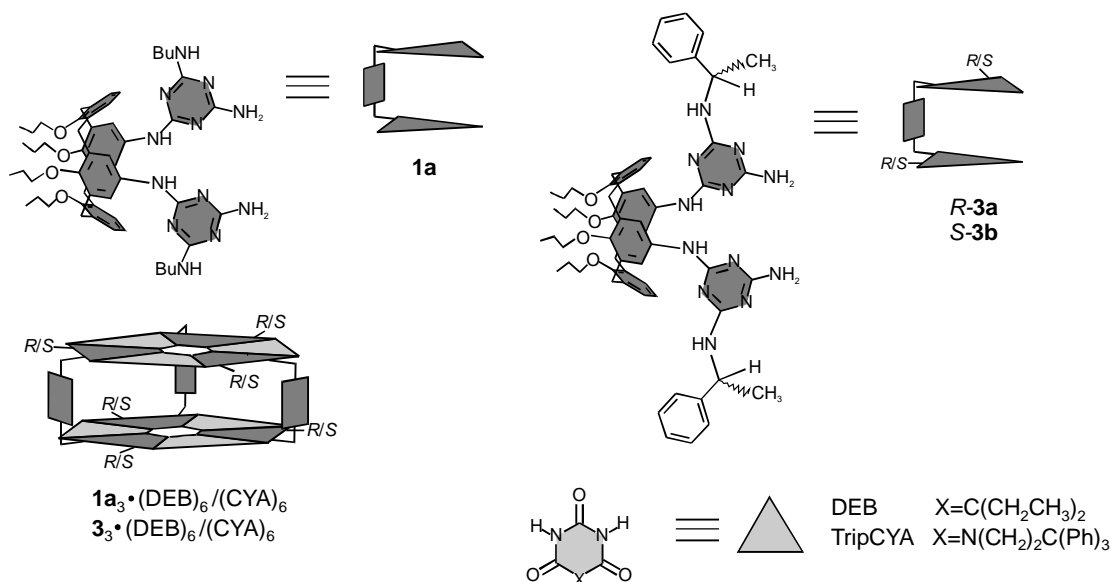


Chart 7.3. Molecular representations of compounds **1** and **3** and the corresponding hydrogen-bonded assemblies $\mathbf{1}_3\bullet(\text{DEB})_6/(\text{CYA})_6$ and $\mathbf{3}_3\bullet(\text{DEB})_6/(\text{CYA})_6$.

To study the effect of a chiral environment on the encapsulation of alizarin **2a**, the addition of **2a** to chiral rosettes $\mathbf{3}_3\bullet(\text{DEB})_6$ (Chart 7.3), containing either an (R)-1-

phenylethyl (**R-3a**) or an (*S*)-1-phenylethyl group (**S-3b**), was investigated. Both rosette assemblies form quantitatively in chloroform, toluene, and benzene as could be confirmed by integration of the signals in the ^1H NMR spectra. The presence of only two signals in the 15-13 ppm region (instead of four as expected for the diastereomeric mixture) proves that both double rosettes are present exclusively as one of the two possible diastereomers (complete chiral induction). Assembly **R-3a₃**•(DEB)₆ exists only in the *M*-configuration and assembly **S-3b₃**•(DEB)₆ only in the *P*-configuration.¹⁴ Therefore, due to the fact that dimelamine derivatives **R-3a** and **S-3b** are enantiomers, the two assemblies are also enantiomers. Upon addition of **2a** (3-4 equiv) to either **R-3a₃**•(DEB)₆ or **S-3b₃**•(DEB)₆ (1.0 mM in CDCl₃ at 298 K), the initial two signals of the NH_{DEB}-protons between 12-15 ppm disappeared, and four new signals in this area appeared (Figure 7.17). The NH_{DEB}-protons H_a and H_b resonated after complexation of **2a** at 13.66, 13.42, 12.93, and 12.89 ppm. Additionally, a downfield shift of 3.79 ppm was observed for the OH_n proton of **2a**. Also, the changes in chemical shifts for the other protons of the guest **2a** and the assemblies **3₃**•(DEB)₆ are comparable to the shifts obtained for the protons in the complexation of **2a** with the achiral assembly **1a₃**•(DEB)₆ (see Chapter 6).

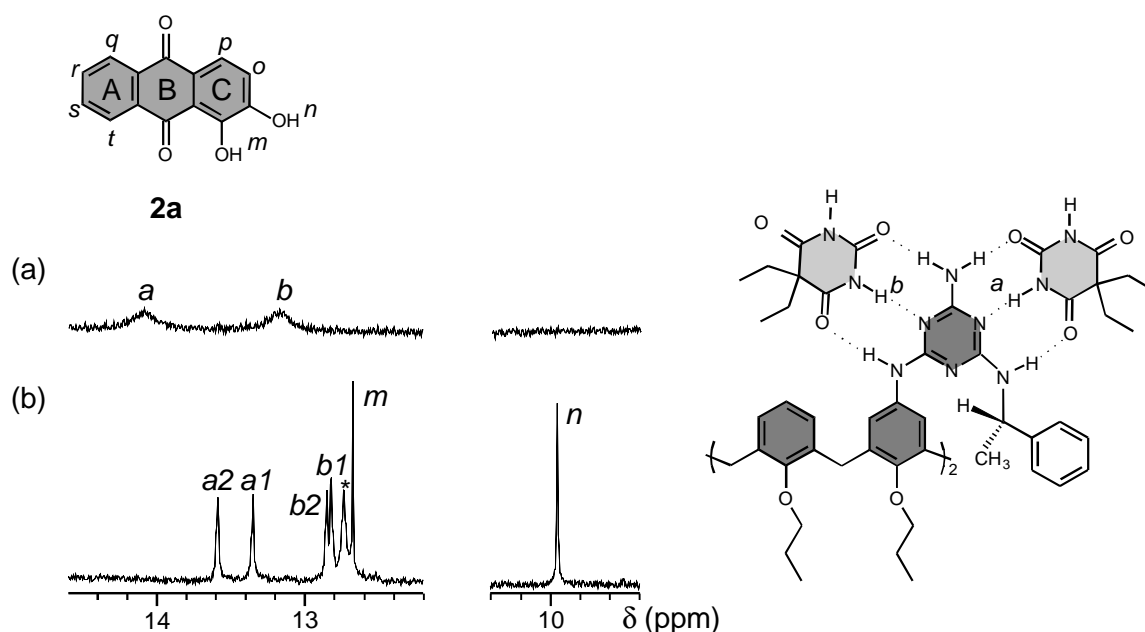


Figure 7.17. ^1H NMR spectra of (a) assembly **S-3b₃**•(DEB)₆, and (b) complex **S-3b₃**•(DEB)₆•**2a₃**. The signal marked with * belongs to OH_m of free **2a**. Spectra were recorded in CDCl₃ at 300 MHz at 298 K.

The presence of four signals in the ^1H NMR spectrum potentially indicates that two different symmetrical eclipsed complexes (C_{3h}) with **2a** are formed (two sets of two different signals) or that one staggered complex (C_3) is formed (four different signals, see Chapter 6).

The symmetrical eclipsed rosette might complex clockwise and counter-clockwise the trimer of **2a**, which would give two constitutional isomers (for drawing see Figure 7.10). If two different constitutional isomers with C_{3h} -symmetry (symmetrical eclipsed) are formed with **2a**, the π - π stacking between **2a** and **3** would probably stabilize one constitutional isomer more than the other (partial regioselectivity). Nevertheless, all four signals for NH_{DEB} -protons H_a and H_b have the same intensity, which would mean that both constitutional isomers have the same free energy (zero regioselectivity) at the thermodynamic equilibrium, which is not very likely. Furthermore, for the nonchiral complex $\mathbf{1a}_3 \cdot (\text{DEB})_6 \cdot \mathbf{2a}_3$ (Chapter 6) only one of the two possible constitutional isomers was formed. More importantly, only one set of signals for the guest **2a** is observed. In the case that two constitutional isomers would be present in solution, also two sets of signals for **2a** should be expected. Therefore, it seems that only one complex is formed, with the calix[4]arene dimelamines in a staggered conformation, and thus C_3 -symmetry. Because there is no horizontal symmetry plane σ_h that converts one rosette layer into the other rosette layer, the protons in the two rosette floors resonate at different chemical shifts. This explains the four signals in the ^1H NMR spectra. For this staggered conformation the direction (clockwise or counter-clockwise) of the complexation of three **2a** molecules would result in the formation of identical assemblies (Figure 7.18).

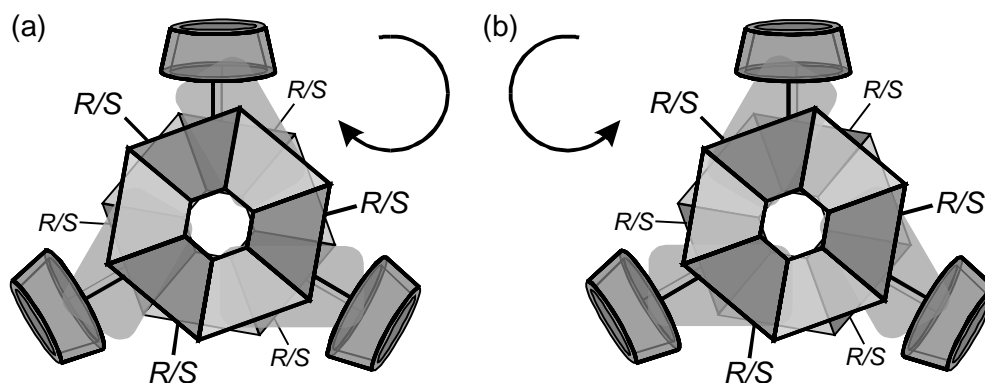


Figure 7.18. (a) clockwise and (b) counter-clockwise encapsulation of the $\mathbf{2a}_3$ trimer by $\mathbf{3}_3 \cdot (\text{DEB})_6$, bearing the calix[4]arene dimelamines in the staggered conformation.

Additionally, total induction for complexes $\mathbf{3}_3 \cdot (\text{DEB})_6 \cdot \mathbf{2a}_3$ is observed because the formed complexes are only present as one diastereomer, as was proven by ^1H NMR spectroscopy (only one set of four different signals). The ^1H NMR spectra of assembly $R\text{-}\mathbf{3a}_3 \cdot (\text{DEB})_6 \cdot \mathbf{2a}_3$ and $S\text{-}\mathbf{3b}_3 \cdot (\text{DEB})_6 \cdot \mathbf{2a}_3$ are identical, indicating that the two complexes are indeed enantiomers. CD spectroscopy provided information about the rotation of the diastereomers (a positive signal for the *M*-diastereomer ($R\text{-}\mathbf{3a}_3 \cdot (\text{DEB})_6 \cdot \mathbf{2a}_3$) and a negative signal for the *P*-diastereomer ($S\text{-}\mathbf{3b}_3 \cdot (\text{DEB})_6 \cdot \mathbf{2a}_3$).

Furthermore, in 2D ^1H NMR spectroscopy, an NOE connectivity is observed between OH_m and one of the chiral CH_3 -groups of calix[4]arene dimelamine, which also indicates that $\mathbf{2a}$ is complexed with the hydroxyl functionalities pointing outwards with respect to the rosette plane, as is the case for complex $\mathbf{1a}_3 \cdot (\text{DEB})_6 \cdot \mathbf{2a}_3$ (Figure 7.19).

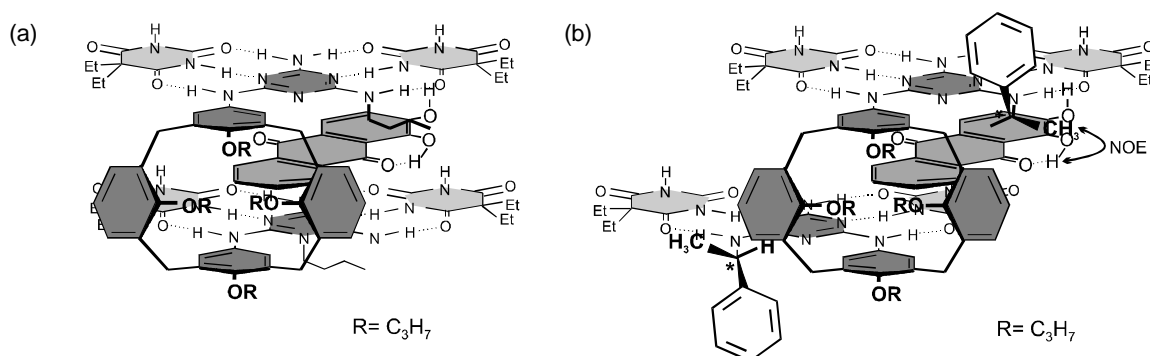


Figure 7.19. Side view of (a) complex $\mathbf{1a}_3 \cdot (\text{DEB})_6 \cdot \mathbf{2a}_3$, and (b) $R\text{-}\mathbf{3a}_3 \cdot (\text{DEB})_6 \cdot \mathbf{2a}_3$.

From these ^1H NMR studies it can be concluded that the encapsulation of $\mathbf{2a}_3$ trimer by chiral double rosettes R - or S - $\mathbf{3}_3 \cdot (\text{DEB})_6$ occurs with the hydroxyl groups pointing outwards, and that upon encapsulation the calix[4]arene dimelamines still exist in the staggered conformation, and thus do not change from staggered to eclipsed as for $\mathbf{1a}_3 \cdot (\text{DEB})_6$ (see Chapter 6).

A possible explanation for the different conformation of the calix[4]arene dimelamines in the complexes comes from earlier studies¹⁵ in our group. From these studies, it is known that assembly type $\mathbf{1}_3 \cdot (\text{DEB})_6$ and $\mathbf{3}_3 \cdot (\text{DEB})_6$ exclusively form the D_3 isomer, because steric hindrance between the 5-alkyl substituents of the barbiturate fragments in the upper and lower rosette floors prevents the formation of the C_{3h} and C_s isomers (see Figure 6.2). However, the assembly formed by calix[4]arene dimelamine $\mathbf{1a}$ with TripCYA (for molecular structure see Chart 7.3) exists 90% in the symmetrical

eclipsed conformation (C_{3h}), while the chiral calix[4]arene dimelamines *R*- or *S*-**3** with TripCYA form exclusively the D_3 isomer. The chiral substituents have a strongly preferred orientation with respect to the rosette core and are unable to rotate as was revealed by 2D ^1H NMR ROESY experiments. This preferred orientation can only be adopted in the D_3 isomer and therefore the calix[4]arene dimelamines in the assembly *R*- or *S*-**3** $\cdot(\text{DEB})_6$ will not change to an eclipsed conformation upon complexation of **2a**. Therefore a different complexation behavior is observed for the achiral assembly **1a** $\cdot(\text{DEB})_6$ and the chiral assemblies *R*- or *S*-**3** $\cdot(\text{DEB})_6$. The different encapsulation behavior is visualized in Figure 7.20, wherein gas-phase molecular modeling calculations (Quanta 97, CHARMM 24.0) were used to obtain the minimized structure for both complexes **1a** $\cdot(\text{DEB})_6\cdot\mathbf{2a}_3$ and *R*-**3a** $\cdot\text{DEB}_6\cdot\mathbf{2a}_3$.

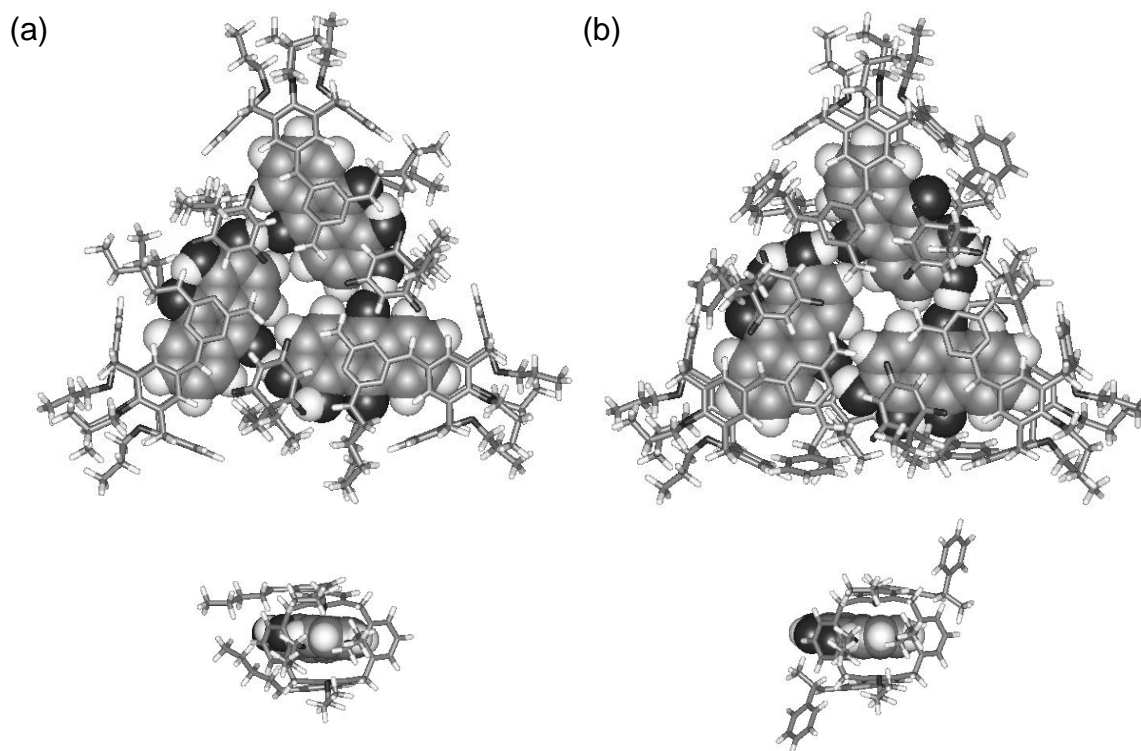


Figure 7.20. Gas-phase-minimized structure of assemblies (a) **1a** $\cdot(\text{DEB})_6\cdot\mathbf{2a}_3$ with the calix[4]arene dimelamines in the eclipsed conformation (C_{3h} -symmetry) and (b) *R*-**3a** $\cdot(\text{DEB})_6\cdot\mathbf{2a}_3$ with the calix[4]arene dimelamines in the staggered conformation (C_3 -symmetry). The **2a** molecules are drawn in CPK style, the assemblies are represented by lines.

CD spectroscopy

CD spectroscopy performed with the samples containing complexes *R*- or *S*-**3** $\cdot(\text{DEB})_6\cdot\mathbf{2a}_3$ (1 mM assembly in CHCl_3 or benzene- d_6 at 298 K) is in agreement with

the proposed staggered conformation of the dimelamines. When a fixed amount of **2a** (4 equiv) is added to assemblies *R*- or *S*-**3₃**•(DEB)₆, a CD signal is observed for complexed assemblies *R*- or *S*-**3₃**•(DEB)₆•**2a**₃ (Figure 7.21). This means that the complexes *R*- or *S*-**3₃**•(DEB)₆•**2a**₃ are still chiral. Thus, it can be concluded that the melamines are in a staggered conformation, because assemblies in the eclipsed conformation are not chiral due to the horizontal plane and would be therefore CD silent.

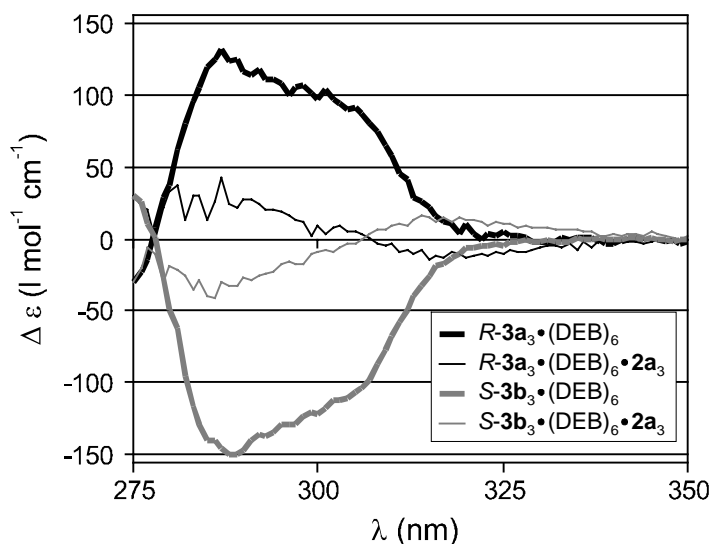


Figure 7.21. CD spectra of assemblies $3_3\cdot(\text{DEB})_6\cdot 2a_n$ ($n=0$ or 3). All spectra were recorded in benzene- d_6 (1.0 mM for the assemblies) at 298 K.

Intriguingly, the subsequent addition of **2a** to assemblies *R*- or *S*-**3₃**•(DEB)₆ shows a decrease in the CD signal. The CD signal of both assemblies is almost silent after addition of 4 equiv **2a** (Figure 7.21). The observed decrease in CD intensity is not due to the destruction of the assemblies because ¹H NMR spectroscopy showed by integration of the NH_{DEB}-protons that the assemblies were still quantitatively present after alizarin complexation. Furthermore, ¹H NMR spectroscopy showed that only one diastereomer is formed (only four instead of eight signals observed), so the decrease cannot be due to racemization. Thus, upon addition of **2a**, the calix[4]arene cone in the double rosette *R*- or *S*-**3₃**•(DEB)₆ probably has to widen to allow the complexation. Consequently, the two melamine units must become further apart, decreasing the turn in the helix and therefore decreasing the intensity of the CD signal.¹⁶ Gas-phase molecular modeling calculations (Quanta 97, CHARMM 24.0) of assemblies *R*- or *S*-**3₃**•(DEB)₆ and complexes *R*- or *S*-

$3_3 \bullet (\text{DEB})_6 \bullet 2\mathbf{a}_3$ supported this hypothesis, showing also a structure with a widened calix[4]arene cone (Figure 7.22).

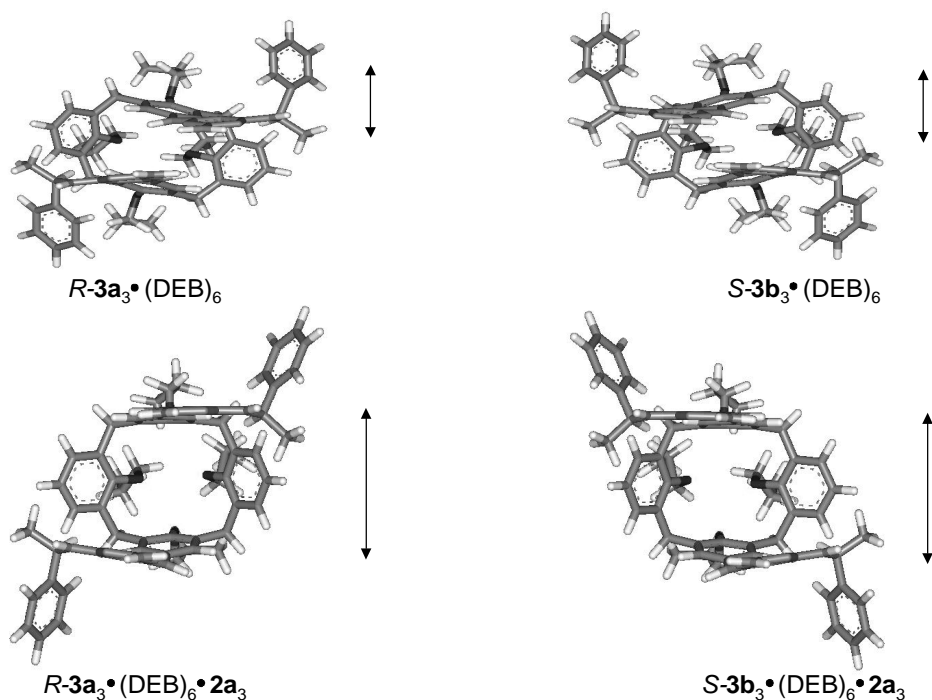


Figure 7.22. Structure of calix[4]arene dimelamines $R-3\mathbf{a}$ (*M*-diastereomer) and $S-3\mathbf{b}$ (*S*-diastereomer) (from the side view), generated by gas-phase molecular modeling calculations, showing the widening of the calix[4]arene cone.

The binding affinity of $2\mathbf{a}$ to assemblies R - or $S-3_3 \bullet (\text{DEB})_6$ (1 mM in either CHCl_3 or benzene- d_6) was determined by a CD titration experiment. The decrease in the CD intensity was monitored during the titration (Figure 7.23) and a binding constant K_a of $1.1 \times 10^{12} \text{ M}^{-3}$ for $2\mathbf{a}$ to assembly $R-3\mathbf{a}_3 \bullet (\text{DEB})_6$ in CHCl_3 was estimated using the same binding model as in Chapter 6 (formation of the complex in one step). In a similar experiment, a K_a of $7.5 \times 10^{10} \text{ M}^{-3}$ for the encapsulation of $2\mathbf{a}$ by assembly $S-3\mathbf{b}_3 \bullet (\text{DEB})_6$ in CHCl_3 was calculated. In benzene- d_6 , K_a values on the same order of magnitude were observed.

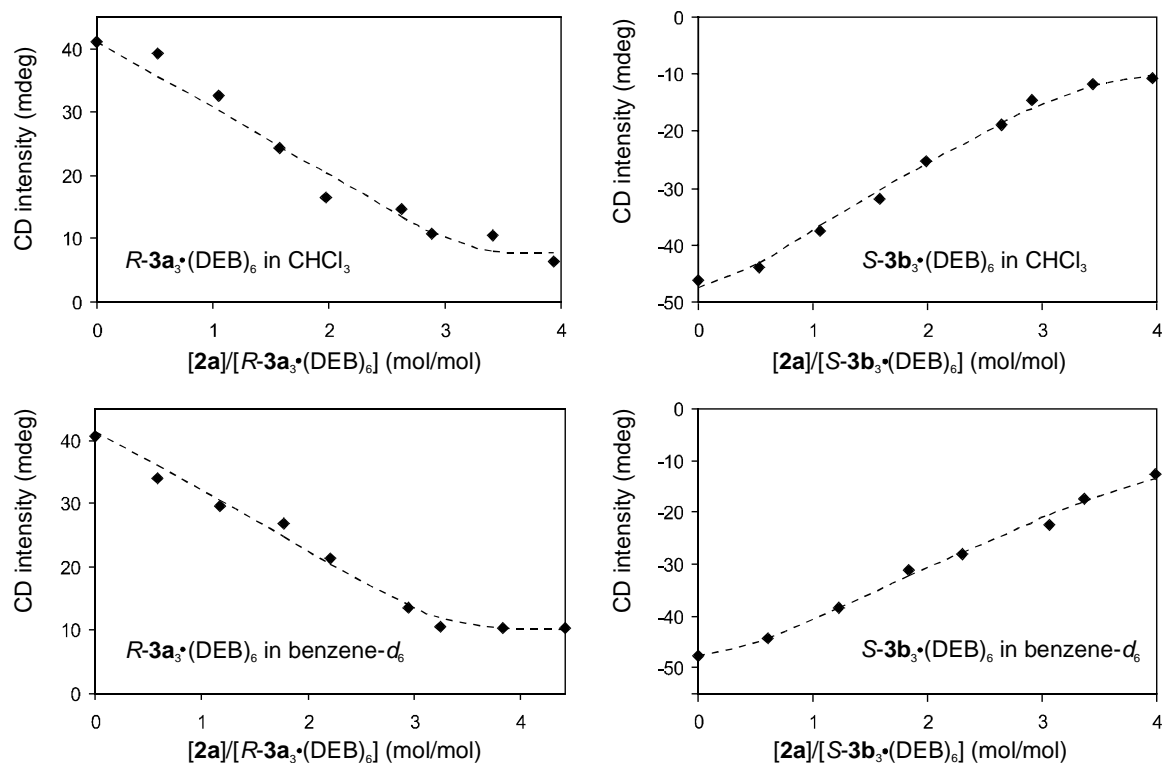


Figure 7.23. Plots of the observed CD intensity of assemblies $3_3\bullet(\text{DEB})_6$ versus $[2\mathbf{a}]/[3_3\bullet(\text{DEB})_6]$ in CHCl_3 and benzene- d_6 .

7.2.2.1 Dynamic Libraries from Chiral Rosettes $R\text{-}3\mathbf{a}_3\bullet(\text{DEB})_6$ and $S\text{-}3\mathbf{b}_3\bullet(\text{DEB})_6$

Suprisingly, mixing assemblies $R\text{-}3\mathbf{a}_3\bullet(\text{DEB})_6$ and $S\text{-}3\mathbf{b}_3\bullet(\text{DEB})_6$ in a 1:1 ratio showed a ^1H NMR spectrum that is identical to spectra of the separate assemblies, i.e. only one set of signals for the NH_{DEB} -protons H_a and H_b . No additional signals were observed, indicating that the heteromeric assemblies $R\text{-}3\mathbf{a}_n\bullet S\text{-}3\mathbf{b}_{(3-n)}\bullet(\text{DEB})_6$ ($n=1,2$) are not formed.¹⁵ The preference for either the *M*- or *P*-helix of the chiral calix[4]arene dimelamine is too strong to form rosette assemblies containing both $R\text{-}3\mathbf{a}$ and $S\text{-}3\mathbf{b}$, with opposite chirality (*R* and *S*). However, addition of $2\mathbf{a}$ (3-4 equiv) to the mixture of assemblies *R*- and *S*- $3_3\bullet(\text{DEB})_6$ showed an additional set of signals in the ^1H NMR spectrum when compared to the ^1H NMR spectra of the isolated complexes $R\text{-}3\mathbf{a}_3\bullet(\text{DEB})_6\bullet 2\mathbf{a}_3$ and $S\text{-}3\mathbf{b}_3\bullet(\text{DEB})_6\bullet 2\mathbf{a}_3$ (Figure 7.24). The additional signals are from the heteromeric complexes $R\text{-}3\mathbf{a}_2\bullet S\text{-}3\mathbf{b}_1\bullet(\text{DEB})_6\bullet 2\mathbf{a}_3$ and $R\text{-}3\mathbf{a}_1\bullet S\text{-}3\mathbf{b}_2\bullet(\text{DEB})_6\bullet 2\mathbf{a}_3$, which are formed after the addition of $2\mathbf{a}$. The strong preference for either the *M*- or the *P*-helicity is decreased upon encapsulation of $2\mathbf{a}_3$, probably due to the decrease in the helix turn as described in Section 7.2.2.

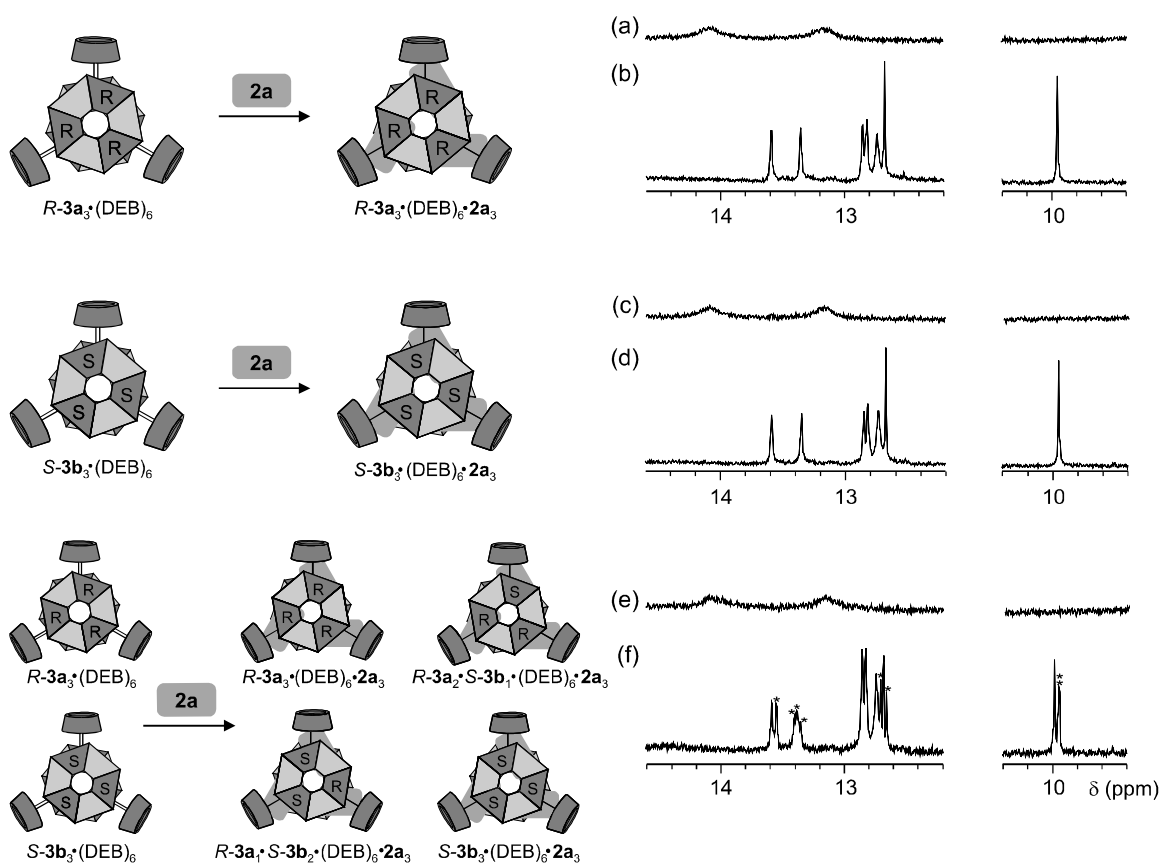


Figure 7.24. ^1H NMR spectra of assemblies (a) $R\text{-}3a_3\bullet(\text{DEB})_6$, (b) $R\text{-}3a_3\bullet(\text{DEB})_6\bullet 2a_3$, (c) $S\text{-}3b_3\bullet(\text{DEB})_6$, (d) $S\text{-}3b_3\bullet(\text{DEB})_6\bullet 2a_3$, (e) $R\text{-}3a_3\bullet(\text{DEB})_6 + S\text{-}3b_3\bullet(\text{DEB})_6$, and (f) homomeric assemblies $R\text{-}3a_3\bullet(\text{DEB})_6\bullet 2a_3$ and $S\text{-}3b_3\bullet(\text{DEB})_6\bullet 2a_3$, and heteromeric assemblies $R\text{-}3a_n\bullet S\text{-}3b_{(3-n)}\bullet(\text{DEB})_6\bullet 2a_3$; ($n=1,2$). Some of the signals for the heteromeric assemblies are marked with *. Spectra were recorded in CDCl_3 at 300 MHz at 298 K.

Thus, contrary to our expectations, instead of the template effect, after addition of the guest to a dynamic mixture of chiral host assemblies selecting the formation of the strongest receptor (see Section 2.4.2). The addition of a guest molecule to the “static” mixture of chiral receptor molecules templated the formation of the “virtual” heteromeric assemblies.¹⁷

7.3 Conclusions and Outlook

In small dynamic combinatorial libraries from calix[4]arene dimelamines **1a-1d** and DEB, the selection of the best binder after guest addition is achieved. The largest amplification factor (2.8) is observed after the addition of **2a** to the four component

library $\mathbf{1a}_n \cdot \mathbf{1b}_{(3-n)} \cdot (\text{DEB})_6$ ($n = 0-3$). Addition of $\mathbf{2a}$ to the twenty component library of $\mathbf{1a}_n \cdot \mathbf{1b}_m \cdot \mathbf{1c}_o \cdot \mathbf{1d}_{[3-(n+m+o)]} \cdot (\text{DEB})_6$ ($n = 0-3$; $m = 0-3$; $o = 0-3$; $(n+m+o) \leq 3$) also showed amplification of the best binder $\mathbf{1a}_3 \cdot (\text{DEB})_6$. Furthermore, the best receptor $\mathbf{1a}_3 \cdot (\text{DEB})_6$ allows the selective noncovalent synthesis of the best fitted guest from a library of “virtual” self-assembled trimers. It was shown that characterization of the libraries by ^1H NMR spectroscopy becomes very complex as the libraries become larger. Also, MALDI-TOF mass spectrometry is not an appropriate technique because the distribution of the different assemblies in the spectra do not correspond to the abundance of the mixture in solution, probably because the assemblies have a different energy of ionization.

Encapsulation of the $\mathbf{2a}_3$ trimer also occurs by chiral double rosettes *R*- or *S*- $\mathbf{3}_3 \cdot (\text{DEB})_6$. In contrast to the encapsulation of the $\mathbf{2a}_3$ trimer by the nonchiral assembly $\mathbf{1a}_3 \cdot (\text{DEB})_6$, the encapsulation process did not change the conformation of calix[4]arene dimelamines from the staggered to eclipsed for assemblies *R*- or *S*- $\mathbf{3}_3 \cdot (\text{DEB})_6$. The symmetry of the assembly is therefore changed from D_3 to C_3 . The addition of $\mathbf{2a}$ to the mixture of chiral homomeric assemblies *R*- $\mathbf{3a}_3 \cdot (\text{DEB})_6$ and *S*- $\mathbf{3b}_3 \cdot (\text{DEB})_6$ surprisingly templated the formation of the “virtual” heteromeric assemblies *R*- $\mathbf{3a}_2 \cdot \mathbf{S-3b}_1 \cdot (\text{DEB})_6$ and *R*- $\mathbf{3a}_1 \cdot \mathbf{S-3b}_2 \cdot (\text{DEB})_6$.

From the results presented in this thesis, it is concluded that hydrogen-bonded assemblies can be functionalized with different polar and nonpolar functional groups (Chapter 3 and 4). These functionalized hydrogen-bonded assemblies can act as *endo*- and *exo*-receptors for the complexation of guest molecules (Chapter 5 and 6). Libraries of hydrogen-bonded receptors can be prepared and addition of a guest molecule can template the formation of the best receptor, thus mimicking the selection process of antibodies.

7.4 Experimental Section

^1H NMR spectra were recorded at 300 or 400 MHz on a Varian Unity 300, or a Varian Unity 400 WB spectrometer with either tetramethylsilane (TMS) or the solvent as internal reference. The 2D DQF-COSY consisted of 2048 datapoints in t_2 and 267 increments in t_1 . For the TOCSY experiment, the total TOCSY mixing time was set to 65 ms. The spectrum was acquired with 2048 data points in t_2 and 267 FIDs in t_1 . The

NOESY experiments were acquired with a mixing time of 90 ms, 2048 datapoints in t_2 and 267 increments in t_1 . MALDI-TOF mass spectra were recorded on a PerSeptive Biosystems Voyager-De-RP spectrometer. A 337 nm UV nitrogen laser producing 3 ns pulses was used in the linear and reflectron modes.

Compounds (**1a-1b**, and **1d**)¹⁸ **1c**¹⁹, and **3**¹⁴ were prepared according to methods described previously.

Formation of assemblies **1₃•(DEB)₆** and **3₃•(DEB)₆**

Hydrogen-bonded assemblies **1₃•(DEB)₆** and **3₃•(DEB)₆** were prepared by mixing calix[4]arene dimelamines **1** or **3** with 2.5 equivalents of DEB, respectively in CDCl₃, toluene-*d*₈ or benzene-*d*₆ for 15 min.

Formation of the libraries of **1_n•1_b_m•1_c_o•1_d_[3-(n+m+o)]•(DEB)₆** and the addition of **2a**

Separate assemblies (**1a-d**)₃•(DEB)₆ were prepared as described above. The appropriate amount of the different assemblies was mixed and left overnight to reach the thermodynamic equilibrium. The correct number of equiv of **2a** were directly added to the NMR tubes and left overnight at 373 K to avoid crystallization of the assemblies. In all the cases some solid **2a** was still present in the tubes when the NMR spectra were measured.

Complex 3₃•(DEB)₆•2a₃: ¹H NMR (400 MHz, CDCl₃ (7.255), 298K) δ = 13.66 (s, 1 H; H_{a2}), 13.42 (s, 1 H; H_{a1}), 12.93 (s, 1 H; H_{b2}), 12.89 (s, 1 H; H_{b1}), 12.75 (s, 1 H; OH_m), 10.03 (s, 1 H; OH_n), 8.32-8.29 (m, 1 H; H_{d1}), 8.02 (d, ³J(H,H)= 8.4 Hz, 1 H; H_o), 7.97-7.95 (m, 3 H; H_{c1}, H_{c2}, ArH), 7.86-7.78 (m, 3 H; H_{d2}, H_{g1}, H_p), 7.68 (m, 1H; H_{g2}), 7.60-7.52 (m, 4 H; ArH), 7.48-7.41 (m, 2 H; ArH), 7.32 (t, ³J(H,H)= 6.8 Hz, 3 H; ArH), 7.14 (m, 2 H, ArH), 7.06-7.01 (m, 2 H; H_q, ArH), 6.90 (t, ³J(H,H)= 7.6 Hz, 1 H; ArH), 6.30-6.25 (m, 3 H; H_{h2}, H_{h1}, H_{f2}), 6.11 (s, 1 H, H_{f1}), 5.95 (s, 1 H, H_{e2}), 5.72 (s, 1 H, H_{e1}), 5.48 (t, ³J(H,H)= 7.6 Hz, 1 H, H_{i2}), 5.42 (t, ³J(H,H)= 6.8 Hz, 1 H, H_{i1}), 5.07 (t, ³J(H,H)= 4.4 Hz, 1 H, H_i), 4.64 (ABq, ²J(H,H)= 12.4 Hz, 4 H; ArCH₂Ar), 4.42-4.15 (m, 4 H; OCH₂), 3.96-3.84 (m, 2 H; H_r, H_s), 3.68 (t, ³J(H,H)= 7.2 Hz, 4 H, OCH₂), 3.26 (ABq, ²J(H,H)= 12.6 Hz, 4 H; ArCH₂Ar), 2.61-1.88 (m, 19 H; H_{j2} CH₂(DEB), OCH₂CH₂), 1.69 (d, ³J(H,H)= 6.4 Hz, 3 H; H_{j1}), 1.09 (m, 12 H; OCH₂CH₂CH₃), 0.88 (t, ³J(H,H)= 7.2 Hz, 6

H; CH₃ (DEB)), 0.75 (q, ³J(H,H)=7.6 Hz, 6 H; CH₃ (DEB)). (Due to broad and overlapping signals, two ArH signals are not visible)

7.5 References

- Recent reviews in the field of dynamic combinatorial chemistry: a) Otto, S.; Furlan, R.L.E.; Sanders, J.K.M. *Curr. Opin. Chem. Biol.* **2002**, *6*, 321-327; b) Lehn, J.-M.; Eliseev, A.V. *Science*, **2001**, *291*, 2331-2332; c) Otto, S.; Furlan, R.L.E.; Sanders, J.K.M. *Drug Discov. Today*, **2002**, *7*, 117-125; d) Ramstrom, O.; Lehn, J.-M. *Nat. Rev. Drug. Disc.* **2002**, *1*, 26-36; e) Rowan, S.J.; Cantrill, S.J.; Cousins, G.R.L.; Sanders, J.K.M.; Stoddart, J.F. *Angew. Chem. Int. Ed. Engl.* **2002**, *41*, 898-952.
- Rowan, S.J.; Cantrill, S.J.; Cousins, G.R.L.; Sanders, J.K.M.; Stoddart, J.F. *Angew. Chem. Int. Ed.* **2002**, *41*, 898-952.
- Huc, I.; Lehn, J.-M. *Proc. Natl. Acad. Sci. U.S.A.* **1997**, *94*, 2106-2110.
- Farlan, R.L.E.; Ng, Y.-F.; Otto, S.; Sanders, J.M.K. *J. Am. Chem. Soc.* **2001**, *123*, 8876-8877.
- Hiraoka, S.; Kubota, Y.; Fujita, M. *Chem. Commun.* **2000**, 1509-1510.
- Crego-Calama, M.; Hulst, R.; Fokkens, R.; Nibbering, N.M.M.; Timmerman, P.; Reinhoudt, D.N. *Chem. Commun.* **1998**, 1021-1022.
- Crego-Calama, M.; Timmerman, P.; Reinhoudt, D.N. *Angew. Chem. Int. Ed.* **2000**, *39*, 755-758.
- The signal marked with ■ (Figure 7.12b) is clearly coming from the homomeric complex **1a**₃•(DEB)₆•**2a**₃ as can be seen from the ¹H NMR spectrum of the individual assembly (Figure 7.12c). The integration of the signals reveals that the signals marked with a ▲ belong to one complex and that the signals marked with Δ belong to another complex. The fact that three signals belong to one complex mean that these are heteromeric assemblies, giving separate signals for each OH_n. The signals marked with ▲ probably belong to the complex **1a**₂•**1c**₁•(DEB)₆•**2a**₃, considering that OH_n protons closer to calix[4]arene melamine **1a** resonate at > 10.0 ppm and the that OH_n protons closer to calix[4]arene melamine **1c** resonate at < 9.9 ppm. Following the same consideration, the signals marked with Δ belong to complex **1a**₁•**1c**₂•(DEB)₆•**2a**₃. Consequently, it seems that calix[4]arene dimelamine

1c in the dynamic mixture forms heteromeric complexes that are similar to the complex **1a₃•(DEB)₆•2a₃**.

- ⁹ For the ten component library, wherein the different components are mixed in equimolar amounts, the statistical composition is as followed:

Assemblies	Relative concentration of each assembly
1a₃•(DEB)₆, 1c₃•(DEB)₆, 1d₃•(DEB)₆	1/27
1a₂•1c₁•(DEB)₆, 1a₁•1c₂•(DEB)₆, 1a₂•1d₁•(DEB)₆, 1a₁•1d₂•(DEB)₆, 1c₂•1d₁•(DEB)₆, 1c₁•1d₂•(DEB)₆.	3/27
1a₁•1c₁•1d₁•(DEB)₆,	6/27

- ¹⁰ For the twenty component library, wherein the different components are mixed in equimolar amounts, the statistical composition is as followed:

Assemblies	Relative concentration of each assembly
1a₃•(DEB)₆, 1b₃•(DEB)₆, 1c₃•(DEB)₆, 1d₃•(DEB)₆	1/64
1a₂•1b₁•(DEB)₆, 1a₁•1b₂•(DEB)₆, 1a₂•1c₁•(DEB)₆, 1a₁•1c₂•(DEB)₆, 1a₂•1d₁•(DEB)₆, 1a₁•1d₂•(DEB)₆, 1b₂•1c₁•(DEB)₆, 1b₁•1c₂•(DEB)₆, 1b₂•1d₁•(DEB)₆, 1b₁•1d₂•(DEB)₆, 1c₂•1d₁•(DEB)₆, 1c₁•1d₂•(DEB)₆,	3/64
1a₁•1b₁•1c₁•(DEB)₆, 1a₁•1b₁•1d₁•(DEB)₆,	6/64
1a₁•1c₁•1d₁•(DEB)₆, 1b₁•1c₁•1d₁•(DEB)₆,	

- ¹¹ Complex **1a₃•(DEB)₆•2b₃** does not contain the OH_m proton and therefore the abundance of this complex could not be determined by the integration of this signal. Integration of the OH_n signals is difficult because these signals are partially overlapping.

- ¹² a) Jolliffe, K.A.; Crego-Calama, M.; Fokkens, R.; Nibbering, N.M.M.; Timmerman, P.; Reinhoudt, D.N.; *Angew. Chem. Int. Ed.* **1998**, *37*, 1247-1251; b) Timmerman, P.; Jolliffe, K.A.; Crego-Calama, M.; Weindmann, J.-L.; Prins, L.J.; Cardullo, F.; Snellink-Ruel, B.H.M.; Fokkens, R.; Nibbering, N.M.M.; Shinkai, S.; Reinhoudt,

D.N. *Chem. Eur. J.* **2000**, *6*, 4104-4115; c) see Chapter 5 for a description of the MALDI-TOF measurements.

- ¹³ 3.8 equiv of **2d** is the weighed amount. Not all material is dissolved in CDCl₃.
- ¹⁴ Prins, L.J.; Huskens, J.; De Jong, F.; Timmerman, P.; Reinhoudt, D.N. *Nature*, **1999**, *398*, 498-502.
- ¹⁵ Prins, L.J.; Jolliffe, K.A.; Hulst, R.; Timmerman, P.; Reinhoudt, D.N. *J. Am. Chem. Soc.* **2000**, *122*, 3617-3627.
- ¹⁶ Berova, N.; Nakanishi, K.; Wood, R.W. *Circular Dichroism, Principles and Applications*, 2nd ed. Wiley, **2000**, pp 604-605.
- ¹⁷ Virtual is used in the sense that these assemblies are not present before addition of the guest **2a**, while they are formed after addition. Virtual libraries were mentioned earlier in Lehn, J.-M. *Chem. Eur. J.* **1999**, *5*, 2455-2463.
- ¹⁸ Timmerman, P.; Vreekamp, R.H.; Hulst, R.; Verboom, W.; Reinhoudt, D.N.; Rissanen, K.; Udachin, K.A.; Ripmeester, J. *Chem. Eur. J.* **1997**, *3*, 1823-1832.
- ¹⁹ Cardullo, F.; Crego-Calama, M.; Snellink-Ruël, B.H.M.; Weidmann, J.-L.; Bielejewska, A.; Fokkens, R. Nibbering, N.M.M.; Timmerman, P.; Reinhoudt, D.N. *Chem. Commun.* **2000**, 367-368.

Summary

This thesis deals with the noncovalent synthesis of hydrogen-bonded assemblies and their ability to function as synthetic receptors. The assemblies are formed spontaneously by mixing calix[4]arene dimelamines with two equivalents of barbiturates (DEB) or cyanurates (CYA) in apolar solvents. The assemblies have a high thermodynamic stability as a result of the formation of 36 hydrogen bonds that bring together the 9 different components.

In Chapter 2, the literature concerning the development of synthetic receptors is described. The chapter starts with a general view of the most representative classes of covalent receptors, followed by an overview of noncovalent receptors assembled either by metal-coordination, ionic interactions or hydrogen bonds. The chapter ends with an overview of the generation of synthetic receptors using combinatorial chemistry. Both static and dynamic combinatorial libraries of potential receptors are described.

The synthesis of functionalized hydrogen-bonded assemblies is described in Chapters 3 and 4. Chapter 3 deals with the formation and stability of noncovalent assemblies functionalized with polar groups, while Chapter 4 deals with amino acid functionalized assemblies. Thermodynamic stability studies by ^1H NMR titrations with $\text{DMSO-}d_6$ and CD titrations with THF showed that assemblies bearing six ureido or amido functionalities have a significantly higher stability than the non-functionalized assembly. This higher stability is the result of the formation of an extra hydrogen bond between the NH proton of the ureido or amide group and one of the nitrogens (N-1) of the triazine ring. The synthesis of assemblies with different spacers between the melamine and the polar functionality was performed to evaluate their influence on the assembly formation. When the 2,2-dimethylpropyl spacer is used the side chains fold back over the calix[4]arene aromatic rings. A similar structural organization is observed for the propyl spacer, although the side chains contain more rotational freedom.

Thermodynamic stability studies of the amino acid functionalized assemblies (Chapter 4) showed that steric strain is an important factor in the formation of the hydrogen-bonded aggregates. The amino acids are introduced onto the rosette platform either via an ureido or amide bond. Introduction of bulky amino acids via an amide linker partially or completely inhibited the formation of the double rosette assemblies, while

assemblies bearing amino acids attached to the melamine via an ureido linker are formed in quantitative yield, due to a different orientation of the bulky R-group of the amino acids. Furthermore, the nature of the spacer plays also an important role in the assembly formation. The synthesis of assemblies bearing peptides is also influenced by similar factors, i.e. bulkiness of the amino acids and nature of the spacers.

Chapters 5 and 6 deal with the complexation abilities of these hydrogen-bonded assemblies. The complexation of phenol derivatives by double and tetra-rosettes is described in Chapter 5. The encapsulation of alizarin molecules (1,2-dihydroxyanthraquinone) is discussed in Chapter 6. Double rosettes functionalized at the top and the bottom with ureido functionalities complex six small, neutral phenols. For instance, 4-nitrophenol is complexed by the ureido functionalized assembly with an intrinsic binding constant K_a of 202 M^{-1} . The complexation takes place on the top and bottom of the rosette and therefore this assembly can be considered to be an *exo*-receptor. Phenol complexation by tetra-rosettes (two double rosettes connected to each other via a flexible spacer) occur in 1:4 stoichiometry as determined from a Job plot and MALDI-TOF MS. An intrinsic binding constant K_a of 299 M^{-1} for the complexation of 4-nitrophenol by an ureido functionalized tetra-rosette was obtained. Binding occurs within the cavity between the 2nd and 3rd floor of the tetra-rosette and thus these assemblies behave as *endo*-receptors. The complexation studies with different substituted phenols demonstrated that the acidity of the phenol derivative is important for the complexation. Also the acidity of the hydrogen accepting atom was found to be significant.

Not only tetra-rosettes but also the double rosette assemblies showed *endo*-receptor abilities as reported in Chapter 6. Three alizarin molecules are encapsulated by the self-assembled double rosette receptor in a highly organized and cooperative manner. As a result a hydrogen-bonded trimer of alizarin molecules between the 1st and the 2nd floor of the double rosette is formed. Upon the encapsulation, the hydrogen-bonded receptor adopts a conformation (by changing from staggered to symmetrical eclipsed) that optimizes the complementarity with the guest. The structure of the complex in solution as determined by ^1H NMR studies is identical to the solid state structure obtained from X-ray diffraction studies. Upon addition of BuCYA, which replaces the DEB fragments in the rosette, the alizarin trimer is released from the hydrogen-bonded receptor giving an empty assembly. Additionally, two trimers of alizarin, one in between the 1st and 2nd and

one in between the 3rd and 4th rosette layer, are encapsulated in the tetrarosette assembly. This encapsulation is also highly cooperative.

Encapsulation of guests by small dynamic libraries of the hydrogen-bonded receptors is discussed in Chapter 7. Addition of alizarin to a four-component library of host molecules, created by mixing two different rosette assemblies under thermodynamic conditions, gave an amplification factor for the best receptor of 2.8. Similarly, the addition of alizarin to a twenty-component library (mixing four different rosettes) showed in the library enrichment of the best binder. Addition of a library of different alizarin-like molecules to the best receptor was studied and showed that the receptor is able to select the best fitting guest.

Samenvatting

Dit proefschrift beschrijft de niet-covalente synthese van waterstofgebrugde assemblages en hun eigenschappen als synthetische receptoren. Deze assemblages vormen spontaan na menging van calix[4]areen dimelamines met twee equivalenten barbituraten (DEB) of cyanuraten (CYA) in apolaire oplosmiddelen. De assemblages hebben een hoge thermodynamische stabiliteit als gevolg van de vorming van 36 waterstofbruggen die in totaal 9 verschillende componenten samenbrengen.

In Hoofdstuk 2 is een literatuur overzicht gegeven over de ontwikkeling van synthetische receptoren. Het hoofdstuk begint met een algemeen overzicht van de meest representatieve categorieën van covalente receptoren. Vervolgens wordt een overzicht van niet-covalente receptoren, geassembleerd hetzij via metaal-coördinatie, ionische interacties of waterstofbruggen gegeven. Het hoofdstuk besluit met een overzicht van de ontwikkeling van synthetische receptoren via combinatoriële chemie. Zowel statische als dynamische combinatoriële bibliotheken van mogelijke receptoren zijn beschreven.

In de Hoofdstukken 3 en 4 worden de synthese van gefunctionaliseerde, waterstofgebrugde assemblages beschreven. Hoofdstuk 3 behandelt de vorming en stabiliteit van niet-covalente assemblages gefunctionaliseerd met polaire groepen, terwijl in Hoofdstuk 4 aminozuur-gefunctionaliseerde assemblages worden beschreven. Studies van de thermodynamische stabiliteit met behulp van ^1H NMR titraties met $\text{DMSO-}d_6$ en CD titraties met THF laten zien dat assemblages die zes ureido- of amidofunctionaliteiten bezitten, een significant hogere stabiliteit vertonen dan de niet-gefunctionaliseerde assemblage. Deze hogere stabiliteit is het gevolg van de vorming van een extra waterstofbrug tussen het NH proton van de ureido of amido groep en één van de stikstof atomen (N-1) van de triazine ring. De synthese van de assemblages met verschillende spacers tussen het melamine en de polaire functionaliteit werd uitgevoerd om de invloed op de vorming van de assemblages te bepalen. Wanneer de 2,2-dimethylpropyl spacer wordt gebruikt, zijn de zijketens teruggevouwen over de calix[4]areen aromaatringen. Een overeenkomstige structurele organisatie werd waargenomen voor de propyl spacer, alhoewel de zijketens wel vrijer kunnen roteren.

Studies naar de thermodynamische stabiliteit, uitgevoerd met de aminozuur-gefunctionaliseerde assemblages (Hoofdstuk 4) laten zien dat sterische beperking een

belangrijke factor is voor de vorming van de waterstofgebrugde assemblages. De aminozuren zijn via een urea- of amidebinding aan het rozetplatform gekoppeld. De koppeling van volumineuze aminozuren via een amidebinding verhindert de dubbele rozetvorming gedeeltelijk of geheel, terwijl assemblages waarin aminozuren gekoppeld zijn via een ureabinding in kwantitatieve opbrengst gevormd worden. Dit laatste door een verschillende oriëntatie van de volumineuze R-groep van de aminozuren. Het karakter van de spacer speelt ook een belangrijke rol in de vorming van de assemblages. De synthese van assemblages met peptiden wordt beïnvloed door dezelfde factoren, de omvangrijkheid van de aminozuren en het karakter van de spacer.

Hoofdstuk 5 en 6 behandelen het complexerend vermogen van deze waterstofgebrugde assemblages. De complexering van fenol derivaten door dubbele en tetrazettes is beschreven in Hoofdstuk 5, terwijl het onderzoek in Hoofdstuk 6 zich bezighoudt met het insluiten van alizarine moleculen (1,2-dihydroxyanthrachinon). Dubbele rozettes aan de boven- en onderkant gefunctionaliseerd met ureidofunctionaliteiten kunnen kleine, neutrale fenolen complexeren. Zo wordt 4-nitrofenol bijvoorbeeld gecomplexed door de ureido-gefunctionaliseerde rozet met een intrinsieke bindingsconstante K_a van 202 M^{-1} . De complexering vindt plaats aan de boven- en onderkant van de rozet en daarom kan deze assemblage gezien worden als *exo*-receptor. Complexering van fenol door tetrazettes (twee dubbele rozettes aan elkaar verbonden door een flexibele spacer) vindt plaats in een 1:4 stoichiometrie zoals blijkt uit een Job plot en MALDI-TOF MS. De intrinsieke bindingsconstante voor de complexering van 4-nitrofenol door een ureido-gefunctionaliseerde tetrazet is 299 M^{-1} . De binding vindt plaats in de holte tussen de 2^e en 3^e verdieping van het tetrazet en daarom zijn deze assemblages ook als *endo*-receptoren te beschouwen. Complexeringsstudies met verschillend gesubstitueerde fenolen hebben laten zien dat de zuurheid van het fenol derivaat belangrijk is voor de complexering. Tevens is de zuurheid van het waterstof acceptierend atoom van belang.

Zoals beschreven staat in Hoofdstuk 6 kunnen niet alleen tetrazettes maar ook dubbele rozet assemblages als *endo*-receptor fungeren. Drie alizarine moleculen worden door de zelf-assemblerende dubbele rozet receptor in een zeer georganiseerde en coöperatieve wijze ingesloten. Als resultaat wordt een waterstofgebrugd trimeer van alizarine moleculen tussen de 1^{ste} en 2^e verdieping van de dubbele rozet gevormd. Tijdens de insluiting, neemt de waterstofgebrugde receptor een conformatie aan waarin de

complementariteit met de gast optimaal is (verandering van de melamines van anti-parallelle naar parallelle oriëntatie ten opzichte van elkaar). De structuur van het complex zoals bepaald in oplossing met behulp van ^1H NMR studies is gelijk aan de vaste fase structuur verkregen met behulp van röntgenstraling diffractie. Na toevoeging van BuCYA, welke de DEB-fragmenten in de rozet vervangt, wordt de alizarine trimeer door de waterstofgebrugde receptor vrijgelaten. Bovendien worden twee alizarine trimeren, één tussen de 1^{ste} en 2^e en één tussen de 3^e en 4^e rozetlaag, in een tetrazet ingesloten. Deze insluiting is ook hier zeer coöperatief.

Insluiting van gasten door kleine dynamische bibliotheken van waterstofbruggende receptoren wordt besproken in Hoofdstuk 7. De toevoeging van alizarine aan een 4-componenten bibliotheek van receptoren, verkregen na menging van twee verschillende rozet assemblages onder thermodynamische condities, gaf een versterkingsfactor van 2.8 voor de beste receptor. Overeenkomstig gaf de toevoeging van alizarine aan een 20-componenten bibliotheek (menging van vier verschillende rozettes) een verrijking van de beste receptor in de bibliotheek. Tevens werd de toevoeging van een bibliotheek van verschillende alizarine-achtige moleculen aan de beste receptor bestudeerd. Het bleek dat de receptor het vermogen heeft om de beste complementaire gast te selecteren.

Dankwoord

Nu ik de laatste letters van mijn proefschrift aan het schrijven ben, realiseer ik me dat de afgelopen vier en een half jaar voorbij gevlogen zijn. Toen ik vrienden vertelde dat ik vanuit Leiden naar het Oosten van het land zou verhuizen, keken ze me aan of ik niet goed bij mijn hoofd was. Na al die jaren is gebleken dat het toch niet zo'n slechte stap is geweest. Het was een leerzame tijd en ik heb met veel plezier gewerkt. Natuurlijk heb ik niet al het werk alleen gedaan. Het proefschrift zoals het nu voor U ligt zou nooit tot stand zijn gekomen zonder de bijdrage van een aantal mensen. Therefore, I would like to thank everyone from the SMCT-group that I met over these four years and with whom I had a wonderful time here in Enschede. Thank you all. I'm sorry I cannot mention you all individually. There are a few people in particular that I would like to thank.

Mijn promotor David Reinhoudt wil ik bedanken dat hij het aandurfde om een vrouw uit Leiden in zijn groep een promotieonderzoek uit te laten voeren. Ik heb er nooit een moment spijt van gehad dat ik het aanbod geaccepteerd heb en denk met plezier terug aan de werkbijeenkomsten die we hebben gehad. Het tempo waarmee jij de verschillende versies van mijn proefschrift nakeek, verbaast mij nog steeds.

Peter Timmerman, de enthousiaste begeleiding gedurende de eerste helft van mijn promotie periode heeft mij zeker gestimuleerd om steeds op zoek te gaan naar nieuwe, interessante aspecten binnen het onderzoek. Mercedes Crego-Calama, you had to take over the daily supervision and I think you did it perfectly. The work discussions we had made the project develop in an extremely nice and fast manner. I will never forget your enthusiasm when we got the crystal structure of the complex. I also really appreciated the effort you made to make, especially the text, in my thesis more clear and fluent.

De Technologiestichting STW wil ik bedanken voor de financiële ondersteuning van het onderzoek en de leden van de gebruikerscommissie STW voor hun bijdrage in de ontwikkeling van het project. Mattijs ten Cate, nu sta je er alleen voor om al die bladzijden in het STW verslag te vullen. Succes ermee.

Rob Liskamp en John Kruijtzter (Universiteit van Utrecht) wil ik bedanken voor de mogelijkheid die zij mij gegeven hebben om de beginselen van de peptiden chemie in hun groep te leren kennen. Ingrid Luyten bedank ik voor het uitvoeren van de 2D ¹H NMR experimenten in het begin van het onderzoek en later voor het altijd bereid zijn te helpen

met problemen rondom NMR-spectroscopie. Roel Fokkens en Nico Nibbering hebben een grote bijdrage aan het onderzoek geleverd door het meten van MALDI-TOF MS van de rozet assemblages. Tieme Stevens, Hannie Visser en Annemarie Montanaro ben ik erkentelijk voor de analyse van nieuwe verbindingen. Joop Toevank, Irene Wolbers, Mark Brouwer, en Marcel de Bruine, jullie deden altijd je best om chemicaliën, glaswerk en dergelijke zo snel mogelijk naar Enschede te krijgen, vooral als ik na een foute planning weer iets met spoed nodig had. Carla Weber-van de Ploeg dank je wel dat je altijd klaar stond om administratieve zaken af te handelen. Richard Egberink bedankt voor alle hulp bij computer problemen. Jij hebt er toch maar voor gezorgd dat ik kon blijven typen aan mijn proefschrift.

Afstudeerder Christiaan Wikkerink, jij hebt samen met mij aan de aminozuur gefunctionaliseerde assemblages die in Hoofdstuk 4 terug te vinden zijn gewerkt. Mijn dank hiervoor. Without the collaboration with Tsutomu Ishi-I in the work (tetra-rosettes) described in Chapter 5, this would never have been such a nice story. Zonder de magische handen van Fijs van Leeuwen zou Huub Kooijman (Bijvoet Centrum in Utrecht) nooit de bruikbare kristallen gekregen hebben voor het oplossen van de kristalstructuur in Hoofdstuk 6. Jullie beide bedankt voor het vele werk dat jullie hierin hebben gestoken.

Becky Zimmerman and Bart-Jan Ravoo thanks for reading my concept thesis and giving suggestions to improve the final version. Ik ben Jurriaan Huskens dankbaar voor zijn hulp bij het gebruik van de verschillende bindingsmodellen. I'm grateful to Juanjo Garcia-Lopez, Leonard Prins, and Jeffery Davis for the fruitful discussions dealing with the amazing chemistry of hydrogen-bonded assemblies. Miguel, next to our discussions about encapsulation and the collaboration on the encapsulation of alizarin by chiral rosettes (Chapter 7), you were there to support me in finishing the thesis, muchas gracias.

Bianca Snellink-Ruël, het was altijd prettig om de nodige frustraties rond de peptide robot met je te delen. Het is ons uiteindelijk toch gelukt om er peptides mee te maken. Bedankt voor alle hulp tijdens de afgelopen vier jaar. Ik ben dan ook heel blij dat je me tijdens de laatste minuten van mijn promotie periode als paranimf wilt bijstaan. Pauline van Meurs, mijn andere paranimf, we hebben het proces van een promotieonderzoek tegelijkertijd, hoewel ergens anders, doorstaan. Daardoor waren we perfect in staat om de ups en downs te delen. Ik ben daarom ook zeer blij dat je deze up (hopelijk) ook met me wilt delen.

Uiteindelijk, pap en mam bedankt voor jullie vertrouwen in mij en voor de aanmoedigen om niet voortijdig op te geven. Renate en Vanessa, ik weet dat jullie als mijn zusjes ook graag in het dankwoord willen, bedankt voor de gezelligheid als ik weer eens een weekend thuis was.

Jessica

Curriculum Vitae

Jessica Kerckhoffs werd geboren op 13 december 1974 te Breda. Na het behalen van het VWO-diploma in 1993 aan het Newman College in Breda begon zij aan de studie Scheikunde aan de Universiteit van Leiden. Haar afstudeerwerk betrof de synthese van ruthenium complexen met tetradentaat liganden, onder leiding van Prof. J. Reedijk en Dr. J.G. Haasnoot. Van september 1997 tot en met februari 1998 verbleef zij als Erasmus/Socrates studente aan de University of Poitiers, France, onder leiding van Prof. J.P. Gesson. Vanaf 15 oktober 1998 verrichtte zij haar promotieonderzoek in de vakgroep Supramoleculaire Chemie en technologie onder de supervisie van Prof. dr. ir. D.N. Reinhoudt, Dr. M. Crego-Calama en Dr. P. Timmerman. De resultaten van het promotieonderzoek zijn beschreven in dit proefschrift. Vanaf 1 mei zal zij werkzaam zijn als post-doc aan de University of Warwick, UK, onder leiding van Dr. M.J. Hannon.